

WL-TR-95-3061



**QUANTITATIVE FEEDBACK THEORY (QFT) FOR THE ENGINEER**  
**A Paradigm for the Design of Control Systems for Uncertain**  
**Nonlinear Plants**

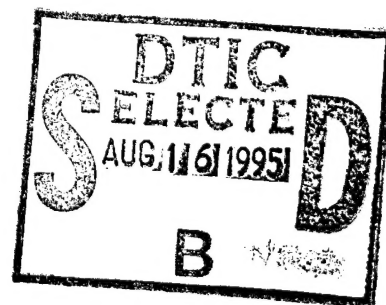
Dr. C. H. Houppis, Editor  
Professor of Electrical Engineering  
Air Force Institute of Technology  
&  
Senior Research Associate  
Control Systems Development Branch  
Flight Control Division

June 1995

Approved for Public Release; Distribution Unlimited

19950814 069

FLIGHT DYNAMICS DIRECTORATE  
WRIGHT LABORATORY  
AIR FORCE MATERIEL COMMAND  
WRIGHT-PATTERSON AIR FORCE BASE, OHIO 45433-7521



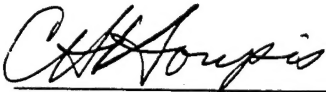
DTIC QUALITY INSPECTED 1

NOTICE

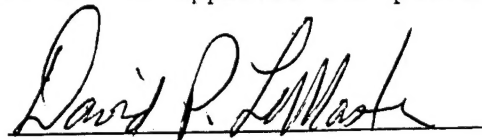
When Government drawings, specifications, or other data are used for any purpose other than in connection with a definitely Government-related procurement, the United States Government incurs no responsibility or any obligation whatsoever. The fact that the government may have formulated or in any way supplied the said drawings, specifications, or other data, is not to be regarded by implication, or otherwise in any manner construed, as licensing the holder, or any other person or corporation; or as conveying any rights or permission to manufacture, use, or sell any patented invention that may in any way be related thereto.

This report is releasable to the National Technical Information Service (NTIS). At NTIS, it will be available to the general public, including foreign nations.

This technical report has been reviewed and is approved for publication.



Dr. C.H. HOUPIS  
Senior Research Associate



DAVID P. LEMASTER  
Chief, Flight Control Division  
Flight Dynamics Directorate



JAMES K. RAMAGE  
Chief, Control Systems Development Branch  
Flight Control Division

Accession For	
NTIS GRA&I	<input checked="checked" type="checkbox"/>
DTIC TAB	<input type="checkbox"/>
Unannounced	<input type="checkbox"/>
Justification	
By	
Distribution/	
Availability Codes	
Dist	Avail and/or Special
A-1	

If your address has changed, if you wish to be removed from our mailing list, or if the addressee is no longer employed by your organization please notify WL/FIGS, WPAFB, OH 45433-7521 to help us maintain a current mailing list.

Copies of this report should not be returned unless return is required by security considerations, contractual obligations, or notice on a specific document.

REPORT DOCUMENTATION PAGE			Form Approved OMB No. 0704-0188	
Public reporting burden for this collection of information is estimated to average 1 hour per response, including the time for reviewing instructions, searching existing data sources, gathering and maintaining the data needed, and completing and reviewing the collection of information. Send comments regarding this burden estimate or any other aspect of this collection of information, including suggestions for reducing this burden, to Washington Headquarters Services, Directorate for Information Operations and Reports, 1215 Jefferson Davis Highway, Suite 1204, Arlington, VA 22202-4302, and to the Office of Management and Budget, Paperwork Reduction Project (0704-0188), Washington, DC 20503.				
1. AGENCY USE ONLY (Leave blank)		2. REPORT DATE JUNE 1995		3. REPORT TYPE AND DATES COVERED
4. TITLE AND SUBTITLE QUANTITATIVE FEEDBACK THEORY (QFT) FOR THE ENGINEER A Paradigm for the Design of Control Systems for Uncertain Nonlinear Plants			5. FUNDING NUMBERS PE 62201 PR 2403 TA 06 WU 65	
6. AUTHOR(S) Dr. C.H. Houppis Other Authors: Dr. M. Pachter, Capt S. Rasmussen, Capt D. Trosen, R. Sating				
7. PERFORMING ORGANIZATION NAME(S) AND ADDRESS(ES) Flight Dynamics Directorate Wright Laboratory Air Force Materiel Command Wright Patterson AFB OH 45433-7625			8. PERFORMING ORGANIZATION REPORT NUMBER	
9. SPONSORING/MONITORING AGENCY NAME(S) AND ADDRESS(ES) Flight Dynamics Directorate Wright Laboratory Air Force Materiel Command Wright Patterson AFB OH 45433-7625			10. SPONSORING/MONITORING AGENCY REPORT NUMBER  WL-TR-95-3061	
11. SUPPLEMENTARY NOTES				
12a. DISTRIBUTION / AVAILABILITY STATEMENT  APPROVED FOR PUBLIC RELEASE: DISTRIBUTION UNLIMITED			12b. DISTRIBUTION CODE	
13. ABSTRACT (Maximum 200 words) The report brings the Quantitative Feedback Theory (QFT) material up to the state-of-the-art level and aims to provide students and practicing engineers a document that presents QFT in a unified and logical manner and which addresses the real-world control problems. QFT is a unified theory using the available measurable states that is applied to the design of multiple-input multiple-output (MIMO) systems. It incorporates the multivariable nature of control systems' structured plant uncertainties, variation, robustness performance requirements, cross-coupling and external disturbance attenuation requirements, nonlinearities in the plant model, and requirements for decoupled outputs. The document also presents the fundamentals of system identification and discusses the vital MIMO QFT CAD package.				
14. SUBJECT TERMS QUANTITATIVE FEEDBACK THEORY (QFT) CROSS-COUPLING MULTIPLE-INPUT MULTIPLE-OUTPUT (MIMO) SYSTEMS STATE-OF-THE-ART LEVEL AND AIMS			15. NUMBER OF PAGES 307	
			16. PRICE CODE	
17. SECURITY CLASSIFICATION OF REPORT Unclassified		18. SECURITY CLASSIFICATION OF THIS PAGE UNCLASSIFIED		19. SECURITY CLASSIFICATION OF ABSTRACT UNCLASSIFIED
				20. LIMITATION OF ABSTRACT UL

# QUANTITATIVE FEEDBACK THEORY (QFT) FOR THE ENGINEER

## A Paradigm for the Design of Control Systems for Uncertain Nonlinear Plants

2nd Edition

### PREFACE

Since the publication in 1987 of the 1st edition of this technical report, great strides have been made in exploiting the full potential of the Quantitative Feedback Theory (QFT) technique. The catalyst that has propelled QFT to the level of being a major multiple-input multiple-output (MIMO) control system design method has been the development and availability of viable QFT CAD packages. Through the close collaboration of Professor Isaac M. Horowitz, the developer of the QFT technique, with Professor C. H. Houppis and his graduate students during the 1980's and the early part of the '90s, successful QFT designs involving structured parameter uncertainty have been completed and published by AFIT MS thesis students. During this period the first multiple-input single-output (MISO) and MIMO QFT CAD packages were developed at AFIT. Another major accomplishment was the successful implementation and flight test of two QFT designed flight control systems, by Captain S. J. Rasmussen, for the LAMBDA unmanned research vehicle in 1992 and 1993. Also, Dr. Charles Hall of North Carolina State University, on April 28, 1995 announced that four successful flight tests of QFT flight controllers have been accomplished. Based upon these solid accomplishments, Lockheed Advanced Development Co. and British Aerospace Ltd have begun applying the QFT design method.

This second edition brings the material up to the state-of-the-art level, and, like the first edition, aims to provide students and practicing engineers a document that presents QFT in a unified and logical manner. Refinements based upon the class testing of the first edition, are incorporated. The material in Chapters II through V and Appendix A is based upon the numerous articles written by Professor Horowitz and the numerous lectures that he presented at the Air Force Institute of Technology.

The Editor would like to express his appreciation for the support and encouragement of Professor Pachter during the preparation of this technical report. His wealth of knowledge of the flight control area has enhanced the value of this revision.

Acknowledgement is made of the support and encouragement, during the 1980's, of Mr. Evard Flinn, Branch Chief, AFWAL/FIGL, and his colleagues Mr. James Morris and Mr. Duane Rubertus. This support and encouragement was maintained by Mr. Max Davis, WL/FIG, and Mr. James Ramage and Mr. Rubertus, WL/FIGS. Further acknowledgement must be made of the support given by AFOSR/EOARD during these past many years.



## TABLE OF CONTENTS

Preface .....	ii
QFT Standard Symbols & Terminology .....	x

<u>CHAPTER</u>	<u>PAGE NO.</u>
I. Introduction .....	1
I.1 Quantitative Feedback Theory.....	1
I.1.1 Why Feedback?.....	1
I.1.2 What Can QFT Do.....	2
I.1.3 Benefits of QFT.....	3
I.2 The MISO Analog System.....	4
I.2.1 MISO Analog Control System.....	5
I.2.2 Synthesize Tracking Models.....	6
I.2.3 Disturbance Model.....	7
I.2.4 J LTI Plant Models.....	8
I.2.5 Plant Templates of $P_i(s)$ , $\mathcal{S}P(j\omega_i)$ .....	8
I.2.6 Nominal Plant.....	10
I.2.7 U-Contour (Stability bound).....	10
I.2.8 Optimal Bounds $B_o(j\omega)$ on $L_o(j\omega)$ .....	11
I.2.8.1 Tracking Bounds.....	11
I.2.8.2 Disturbance Bounds.....	12
I.2.8.3 Optimal Bounds.....	12
I.2.9 Synthesizing (or Loop Shaping) $L_o(s)$ and $F(s)$ .....	14
I.2.10 Prefilter Design.....	15
I.2.11 Simulation.....	15
I.3 The MISO Discrete Control System.....	16
I.3.1 Introduction.....	16
I.3.2 The MISO Sampled-data Control System....	17
I.3.3 $w'$ -Domain.....	17
I.3.4 Assumptions.....	18
I.3.5 Nonminimum Phase $L_o(w)$ .....	18
I.3.6 Plant Templates $\mathcal{S}P(jv)$ .....	21
I.3.7 Synthesizing $L_{mo}(w)$ .....	21
I.3.8 Prefilter Design.....	24
I.3.9 $w$ -Domain Simulation.....	25
I.3.10 $z$ -Domain.....	25

I.3.10.1	Comparison of the Controller's w- and z-Domain Bode Plots.....	25
I.3.10.2	Accuracy.....	25
I.3.10.3	Analysis of Characteristic Equation $Q_c(z)$ .....	26
I.3.10.4	Simulation and CAD Packages.....	26
I.4.	Summary.....	26
<b>II.</b>	<b>Basics of System Identification.....</b>	<b>27</b>
II.1	Introduction.....	27
II.2	Classical Route to Identification.....	28
II.3	Linear Regression.....	29
II.4	SID Approaches.....	30
II.5	Linear Regression (LR).....	31
II.6	Linear Regression for System Identification 1.....	33
II.7	Linear Regression for System Identification 2.....	36
II.8	Identification of Dynamic Systems with Process Noise Only.....	39
II.8.1	Discussion.....	41
II.9	Example.....	41
II.9.1	Identification Experiment.....	48
II.10	"Crimes" of System Identification (SID).....	51
II.10.1	Theory.....	51
II.10.2	Experimental.....	54
II.11	Static Identification.....	56
II.12	Summary.....	59
<b>III.</b>	<b>Multiple-Input Multiple-Output (MIMO) Plants: Structured Plant Parameter Uncertainty.....</b>	<b>60</b>
III.1	Intoduction.....	60
III.2	The MIMO Plant.....	61
III.3	Introduction to MIMO Compensation.....	67
III.4	MIMO Compensation.....	69
III.5	Introduction to MISO Equivalents.....	71
III.5.1	Effective MISO Equivalents.....	71

III.6	Effective MISO Loops of the MIMO System.....	76
III.6.1	Example: The 2x2 plant.....	77
III.6.2	Performance Bounds.....	80
III.6.3	QFT Design Method 2.....	85
III.6.4	Summary.....	87
III.7	Constraints on the Plant Matrix.....	88
III.8	Basically Non-Interacting (BNIC) Loops.....	93
III.9	Summary.....	94
III.10	Problems.....	95
<b>IV.</b>	<b>Design Method - The Single-Loop (MISO) Equivalents...</b>	<b>98</b>
IV.1	Introduction.....	98
IV.2	Design Example.....	99
IV.2.1	Performance Tolerance.....	100
IV.2.2	Sensitivity Analysis.....	100
IV.2.3	Simplification of the Single-loop Structures.....	104
IV.3	High Frequency Range Analysis.....	107
IV.4	Stability Analysis.....	108
IV.5	Equilibrium and Trade-offs.....	110
IV.5.1	Trade-off in High Frequency Range.....	115
IV.5.2	Some Universal Design Features.....	118
IV.5.3	Examples--Bounds Determination.....	120
IV.6	Summary.....	128
IV.7	Problems.....	128
<b>V.</b>	<b>MIMO System Design Method Two-Modified Single-Loop Equivalent.....</b>	<b>131</b>
V.1	Introduction.....	131
V.2	Design Equations for the 2x2 System.....	132
V.3	Design Guidelines.....	134
V.4	Reduced Overdesign.....	136
V.5	3x3 Design Equations.....	136
V.6	Example V.1 -- 3x3 System Design Equations...	139
V.7	m x m System, $m > 3$ .....	140
V.8	Conditions for Existence of a Solution.....	141
V.8.1	Conditions for Existence of a Solution..	142
V.8.2	Applications of Sec. V.8.1 to Design Method 2.....	145
V.8.3	Inherent Constraints.....	147

V.9	Nondiagonal $G$ .....	149
V.10	Achievability of a m.p. Effective Plant det $P$ .....	150
V.11	Summary.....	157
<b>VI.</b>	<b>MIMO System With External Disturbance Inputs.....</b>	<b>159</b>
VI.1	Introduction.....	159
VI.1.1	Aerial Refueling Background.....	159
VI.1.2	Problem Statement.....	160
VI.1.3	Assumptions.....	160
VI.1.4	Research Objectives.....	161
VI.1.5	Scope.....	161
VI.1.6	Methodology.....	162
VI.1.7	Overview of Chapter.....	162
VI.2	Air-to-Air Refueling FCS Design Concept.....	162
VI.2.1	C-135B Modeling.....	163
VI.2.2	Disturbance Modeling.....	164
VI.3	Plant and Disturbance Matrices.....	165
VI.4	Control Problem Approach.....	165
VI.5	MIMO QFT with External Output Disturbance....	169
VI.6	AFCS Design.....	177
VI.6.1	Introduction.....	177
VI.6.2	Disturbance Rejection Specification.....	177
VI.6.3	Loop Shaping.....	178
VI.6.4	Channel 2 Loop Design.....	179
VI.6.5	Channel 1 Loop Design.....	180
VI.6.6	Channel 3 Loop Design.....	185
VI.6.7	Closed Loop Lm Plots.....	185
VI.7.	Air-to-Air Refueling Simulations.....	188
VI.7.1	Linear Simulations.....	189
VI.7.2	Nonlinear Simulations.....	191
VI.8	Summary.....	194
<b>VII</b>	<b>Now the "Practicing Engineer Takes Over".....</b>	<b>195</b>
VII.1	Introduction.....	195
VII.2	Transparency of QFT.....	196
VII.3	Body of Engineering QFT Knowledge.....	198
VII.4	Nonlinearities -- The Engineering Approach...	202
VII.5	Plant Inversion.....	203
VII.6	Invertibility.....	205

VII.7	Psuedo-Continuous-Time (PCT) System.....	206
VII.8	Summary.....	207
<b>VIII</b>	<b>MIMO QFT CAD Package (Version 3).....</b>	<b>208</b>
VIII.1	Introduction.....	208
VIII.2	Introduction: Overview of Multivariable Control .....	210
VIII.3	Continuous-Time vs Discrete-Time Design.....	210
VIII.4	Overview of the Multivariable External Disturbance Rejection Problem.....	211
VIII.5	Open-loop Structure.....	212
VIII.6	Formation of Plant Models for Tracking Control Problems.....	215
VIII.7	Inverse of P.....	216
VIII.8	MISO Loops of the Tracking Control Problem..	217
VIII.9	MISO Loops of External Disturbance Rejection Problems.....	218
VIII.10	Q Matrix Validation Checks.....	219
VIII.11	Improved Method.....	220
VIII.12	Specifications.....	221
VIII.12.1	Stability Specifications.....	221
VIII.12.2	Tracking Performance Specifications..	221
VIII.12.3	External Disturbance Rejection Performance Specifications.....	222
VIII.12.4	Gamma Bound Specifications.....	222
VIII.13	Bounds on the NC.....	223
VIII.13.1	Stability Bounds.....	223
VIII.13.2	Cross-Coupling Bounds.....	223
VIII.13.3	Gamma Bounds.....	225
VIII.13.4	Allocated Tracking Bounds.....	225
VIII.13.5	External Disturbance Rejection Bounds.....	226
VIII.13.6	Composite Bounds.....	227
VIII.14	Compensator Design.....	227
VIII.15	Prefilter Design.....	228
VIII.16	Design Validation.....	229
VIII.17	Summary.....	230
<b>IX.</b>	<b>Development Implementation &amp; Flight Test of a MIMO Digital Flight Control System foran Unmanned Research Vehicle.....</b>	<b>232</b>
IX.1	Introduction.....	232
IX.2	Objective.....	233
IX.3	First Design Cycle.....	234

IX.3.1	Requirements.....	234
IX.3.2	Specifications.....	234
IX.3.3	Aircraft Model.....	234
IX.3.4	FCS Design.....	235
IX.3.5	Linear Simulations.....	235
IX.3.6	Nonlinear Simulations.....	235
IX.3.7	Hardware-in-the-Loop Simulation.....	235
IX.3.8	Flight Test.....	236
IX.4	Second Design Cycle.....	236
IX.4.1	Requirements.....	236
IX.4.2	Specifications.....	236
IX.4.3	Aircraft Model.....	237
IX.4.4	FCS Design.....	237
IX.4.5	Linear, Nonlinear, and Hardware- in-the-Loop Simulation.....	237
IX.4.6	Flight Test.....	237
IX.5	Third Design Cycle.....	239
IX.5.1	Requirements.....	239
IX.5.2	Specifications.....	239
IX.5.3	Aircraft Model.....	239
IX.5.4	FCS Design.....	240
IX.5.5	Linear, Nonlinear, and Hardware-in- the-Loop Simulations.....	240
IX.5.6	Flight Test.....	240
IX.6	Fourth Design Cycle.....	241
IX.6.1	Requirements.....	241
IX.6.2	Specifications.....	241
IX.6.3	Aircraft Model.....	241
IX.6.4	FCS Design.....	242
IX.6.5	Linear, Nonlinear, and Hardware-in- the-Loop Simulation.....	242
IX.6.6	Flight Test.....	242
IX.7	Conclusion.....	243
<b>Appendix A</b>	<b>Design Examples.....</b>	<b>244</b>
A.1	MISO Design Problem.....	244
A.2	MIMO Design Problem.....	249

<b>Appendix B</b>	<b>Longitudinal Handling Qualities</b>	
	<b>Approximations &amp; Bandwidth Minimization.....</b>	<b>269</b>
B.1	Introduction.....	269
B.2	Background.....	269
B.3	Desired Handling Qualities.....	271
B.4	Modification of the QFT Design Procedure...	274
B.5	Remarks by Dr. I. M. Horowitz.....	278
B.6	Summary.....	281
<b>References.....</b>		<b>282</b>
R.1	References for the TR.....	282
R.2	References for Other Pertinent Articles....	288
R.3	Additional References.....	290



## OFT Standard Symbols & Terminolgy

### Symbol

$\alpha_p$	-- The specified peak magnitude of the disturbance response for the MISO system
a.l.	-- Arbitrarily large
a.s.	-- Arbitrarily small
$a_{ij} = Lm \tau_{ij}$	-- The desired lower tracking bounds for the MIMO system
$b_{ij} = Lm \tau_{ij}$	-- The desired upper tracking bounds for the MIMO system
$a'_{ii}$	-- The desired modified lower tracking bound for the MIMO system: $a'_{ii} = a_{ii} + \tau_{c_{ii}}$
$b'_{ii}$	-- The desired modified upper tracking bounds for the MIMO system $b'_{ii} = b_{ii} - \tau_{c_{ii}}$
$B_D(j\omega_i), B_R(j\omega_i), B_o(j\omega_i)$	-- The disturbance, tracking, and otimal bounds on $Lm L(j\omega_i)$ for the MISO system
$B_h$	-- Ultra high frequency boundary (UHFB) for analog design
$B'_h$	-- Ultra high frequency boundary (UHFB) for discrete design
$B_u = Lm T_{R_u}$	-- The Lm of the desired tracking control ratio for the upper bound of the MISO system
$B_L = Lm T_{R_L}$	-- The Lm of the desired tracking control ratio for the lower bound of the MISO system
$B_s$	-- Stability bounds for the discrete design
BW	-- Bandwidth

$\tau_{c_{ij}}$	-- Allotted portion of the $ij$ output due to a cross-coupling effect for a MIMO system
$\delta_D(j\omega_i)$	-- The (upper) value of $Lm T_D(j\omega_i)$ for MISO system
$\delta_{hf}(j\omega_i)$	-- The dB difference between the augmented bounds of $B_U$ and $B_L$ in the high frequency range for a MISO system
$\delta_R(j\omega_i)$	-- The dB difference between $B_U$ and $B_L$ for a given $\omega_i$ for a MISO system
$\Delta\tau$	-- The difference between $b_{ii}$ and $a_{ii}$ , i.e., $\Delta\tau = b_{ii} - a_{ii}$
$c_{ij}$	-- The interaction or cross-coupling effect of a MIMO system
$D$	-- MISO and MIMO system external disturbance input
$D = \{D\}$	-- Script cap dee to denote the set of external disturbance inputs for a MIMO system $D = \{D\}$
$F, F = \{f_{ij}\}$	-- The prefilter for a MISO system and the $\ell X \ell$ prefilter matrix for a MIMO system respectively
FOM	-- Figures of merit (see Reference 15)
$G, G = \{g_{ij}\}$	-- The compensator or controller for a MISO system and the $\ell X \ell$ compensator or controller matrix for a MIMO system, respectively. For a diagonal matrix $G = \{g_i\}$
h.f.	-- High frequency
h.g.	-- High gain
$\gamma, \gamma_i$	-- The phase margin angle for the MISO system and for the $i^{th}$ loop of the MIMO system, respectively
$\gamma_{ij}$	-- A function only of the elements of a square plant matrix $P$ (or $P_d$ )
$k$	-- A running index for sampled-data systems where $k = 0, 1, 2, \dots$
$KT$	-- The sampled time
$\lambda$	-- The excess of poles over zeros of a transfer function

$L_o, L_{o_i}$	-- The optimal loop transmission function for the MISO system and the $i^{\text{th}}$ loop of the MIMO system, respectively
LHP	-- Left-half-plane
LTI	-- Linear-time-invariant
MIMO	-- Multiple-input multiple-output; more than one tracking and/or external disturbance inputs and more than one output
MISO	-- Multiple-input single-output; a system having one tracking input, one or more external disturbance inputs, and a single output
$M_L, M_{L_i}$	-- The specified closed-loop frequency domain overshoot constraint for the MISO system and for the $i^{\text{th}}$ loop of a MIMO system, respectively. This overshoot constraint may be dictated by the phase margin angle for the specified loop transmission function
m.p.	-- Minimum-phase
n.m.p.	-- Nonminimum-phase
NC	-- Nichols chart
J	-- The number of plant transfer functions for a MISO system or plant matrix for a MIMO system that describes the region of plant parameter uncertainty where $\iota = 1, 2, \dots, J$ denotes the particular plant case in the region of plant parameter uncertainty
$\omega_b$	-- the symbol for bandwidth frequency of the models for $T_{R_U}, T_{R_L}$ , and $T = \{t_{ij}\}$
$\omega_\phi, \omega_{\phi_i}$	-- phase margin frequency for a MISO system and for the $i^{\text{th}}$ loop of a MIMO system, respectively
$\omega_s$	-- Sampling frequency
P	-- MISO plant with uncertainty
$P_\iota = \{(p_{ij})_\iota\}$	-- $m \times \ell$ MIMO plant matrix where $(p_{ij})_\iota$ is the transfer function relating the $i^{\text{th}}$ output to the $j^{\text{th}}$ input for plant case $\iota$

$\mathcal{P}$	-- Script cap pee to denote a set that represents the plant uncertainty for $J$ cases in the region of plant uncertainty, i.e., $\mathcal{P} = \{\mathbf{P}_i\}$ for a MIMO system
$\mathbf{P}_d$	-- $m_d \times m$ MIMO external disturbance matrix
$\mathbf{P}_F$	-- Plant model for a tracking and external disturbance input system which is partitioned to yield $\mathbf{P}_e$ and $\mathbf{P}_d$
$\mathbf{P}_i^{-1} = \{(p_{ij}^*)_{i,j}\}$	-- The inverted plant matrix for plant case $i$ where $\ell = m$
$\mathbf{P}_{e_i} = \mathbf{P}_i \mathbf{W}$	-- The $m \times m$ effective plant matrix when $\mathbf{P}_i$ is not a square plant matrix and $\mathbf{W}$ is an $\ell \times m$ weighting or a squaring-down matrix
QFD	-- Quantitative feedback design based on quantitative feedback theory
$\mathbf{Q}_i = \{(q_{ij})_{i,j}\}$	-- An $\ell \times \ell$ matrix whose elements are given by $(q_{ij}) = 1/(q_{ij})_i$
$\mathcal{Q}$	-- Script cap que to denote a set that represents the plant uncertainty for a MIMO system, i.e., $\mathcal{Q} = \{\mathbf{Q}_i\}$
$\mathbf{R}, \mathbf{R} = \{\mathbf{r}_i\}$	-- The tracking input for a MISO system and the tracking input vector for a MIMO system, respectively
RHP	-- Right-half-plane
$T$	-- Sampling time
$\mathfrak{P}(j\omega_i)$	-- Script cap tee inconjunction with $\mathbf{P}$ or $(q_{ii})$ denotes a template, i.e., $\mathfrak{P}(j\omega_i)$ and $\mathfrak{Q}(j\omega_i)$ frequency, for a MISO and MIMO plants respectively
$T_{R_U}$	-- The desired MISO tracking control ratio that satisfies the specified upper bound FOM
$T_{R_L}$	-- The desired MISO tracking control ratio that satisfies the specified lower bound FOM
$T_D$	-- The desired MISO disturbance control ratio which satisfies the specified FOM
$T_{R_i}, T_{D_i}$	-- The MISO tracking and disturbance control ratios for case $i$
$\mathbf{T}_i = \{(t_{ij})_{i,j}\}$	-- The $m \times m$ MIMO tracking control ratio matrix for plant case $i$

$T_d = \{(t_d)_i\}$	-- The mxm MIMO external disturbance control ratio matrix
$\mathfrak{S}_R$	-- The script cap tee denotes the set that represents the tracking control ratios for J cases, i.e $\mathfrak{S}_R = \{T_R\}$ for the MISO system and $\mathfrak{S}_{R_u} = \{(T_{R_u})_i\}$ for the MIMO system
$\mathfrak{S}_D$	-- The script cap tee denotes the set that represents the disturbance control ratios for J cases. i.e., $\mathfrak{S}_D = \{T_D\}$ for the MISO system and $\mathfrak{S}_c = \{(T_{c_u})_i\}$ for the MIMO system
$\tau_{ij}$	-- A set of assigned tolerances on $t_{ij}$ where $a'_{ii}$ and $b'_{ii}$ and $\tau_{c_{ij}}$ are the assigned tolerances for tracking and cross-coupling rejection, respectively
U	-- The mx1 controller input vector
UHFB	-- The ultra high frequency boundary
$v, \mathbf{v}$	-- The MISO prefilter output and the mx1 MIMO prefilter output vector, respectively
V	-- $\lim_{\omega \rightarrow \infty} \{Lm P_{max} - Lm P_{min}\}$ is the dB limiting value for a MISO plant
$V_i$	-- $\lim_{\omega \rightarrow \infty} \{Lm (q_{ii})_{max} - Lm (q_{ii})_{min}\}$ is the $i^{th}$ loop template dB limiting value for a MIMO plant
$W = \{w_{ij}\}$	-- The weighting or squaring-down or mixer matrix
$w' = u + jv$	-- <i>w'-domain variable</i> ; the use of u and v must be interpreted in context
$Y, \mathbf{Y} = \{y_{ij}\}$	-- The output of a MISO system and the output matrix of a MIMO system, respectively, where $y_{ij} = y_{r_i} + y_{c_{ij}}$
y	-- The mx1 plant output vector
$y_{r_i}$	-- Is that portion of the $i^{th}$ output due to the $i^{th}$ input
$y_{c_{ij}}$	-- Is that portion of the $i^{th}$ output due to $c_{ij}$ (cross-coupling effect or interaction of the other loops)

## **EDITOR and COLLABORATOR**

Dr. Constantine H. Houpis  
Professor of Electrical Engineering  
Air Force Institute of Technology

&

Senior Research Associate  
Control Systems Development Branch  
Flight Control Division (WL/FIGS)  
Wright Laboratory

## **COLLABORATORS**

- |                     |                                                                                                                            |
|---------------------|----------------------------------------------------------------------------------------------------------------------------|
| Chapter I           | Dr. C. H. Houpis                                                                                                           |
| Chapter II          | Dr. Meir Pachter, Associate Professor of Electrical Engineering, Air Force Institute of Technology                         |
| Chapters III thru V | Dr. C. H. Houpis                                                                                                           |
| Chapter VI          | Dr. C. H. Houpis and Captain Dennis W. Trosen, Control System Development Branch (WL/FIGS)                                 |
| Chapter VII         | Dr. C. H. Houpis & Dr. M. Pachter                                                                                          |
| Chapter VIII        | Mr. Richard Sating, Research Associate, Department of Electrical & Computer Engineering, Air Force Institute of Technology |
| Chapter IX          | Captain Steven J. Rasmussen, Control System Development Branch (WL/FIGS)                                                   |

## **ACKNOWLEDGEMENT**

The illustrations which enhanced the technical report were produced by the tireless and professional efforts of

Mr. Jim Coughlin  
Industrial Graphic Designer  
UNC-Lear Siegler MSC

## Chapter I Introduction

### I.1 Quantitative Feedback Theory

QFT has achieved the status<sup>46</sup> as a very powerful design technique for the achievement of assigned performance tolerances over specified ranges of structured plant parameter uncertainties without and with control effector failures. It is a frequency domain design technique utilizing the Nichols chart (NC) to achieve a desired robust design over the specified region of plant parameter uncertainty. This chapter presents an overview to QFT analog and discrete design techniques for both multiple-input single-output (MISO)<sup>15,19,47</sup> control systems. For an in-depth presentation of the MISO QFT design technique the reader is referred to References 15 and 47. QFT CAD packages are readily available to expedite the design process. The purposes of this technical report are: (1) to provide a basic understanding of the MIMO QFT design technique, (2) to provide the minimum amount of mathematics necessary to achieve this understanding, (3) to discuss the basic design steps, and (4) to present two practical examples. The list of references is divided into two sections: the first section are listed the QFT articles referenced in this Technical Report (TR), and the second section is a partial list of other individuals who have published articles in the QFT area. The reader is encouraged to review the articles in both sections.

#### I.1.1 Why Feedback?

For the answer to the question of "Why do you need QFT?" consider the following system. The plant  $P$  of Fig. I.1 responds to the input  $r(t)$  with the output  $y(t)$  in the face of disturbances  $d_1(t)$  and  $d_2(t)$ . If it is desired to achieve a specified system transfer function  $T(s)$  [ $= Y(s)/R(s)$ ] then it is necessary to insert a prefilter, whose transfer function is  $T(s)/P(s)$ , as shown in Fig. I.2. This compensated system produces the desired output as long as the plant does not change and there are no disturbances. This type of system is sensitive to changes in the plant (or uncertainty in the plant), and the disturbances are reflected directly into the output. Thus, it is necessary to feed back



the information in the output in order to reduce the output sensitivity to parameter variation and attenuate the effect of disturbances on the plant output.

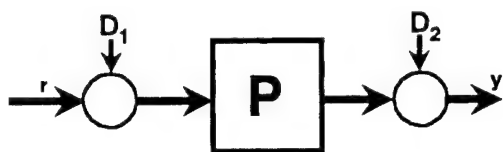


Fig. 1 An open-loop system (basic plant).

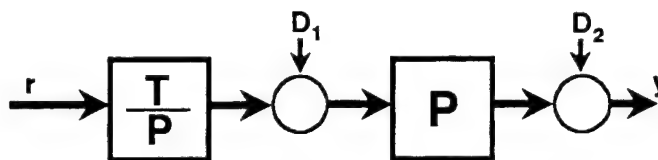


Fig. I.2 A compensated open-loop system.

In designing a feedback control system, it is desired to utilize a technique that:

- a. Addresses all known plant variations up front.
- b. Incorporates information on the desired output tolerances.
- c. Maintains reasonably low loop gain (reduce the "cost of feedback").

This last item is important in order to avoid the problems associated with high loop gains such as sensor noise amplification, saturation, and high frequency uncertainties.

### I.1.2 What Can QFT Do

Assume that the characteristics of a plant, that is to be controlled over a specified region of operation, vary, that is, a plant with plant parameter uncertainty. This plant parameter uncertainty may be described by the Bode plots of Fig. I.3. This figure represents the range of variation of plant magnitude (dB) and phase over a specified frequency range. The bounds of this variation, for this example, can be described by six LTI plant transfer functions. By the application of QFT, for a MISO control system containing this plant, a single compensator and a prefilter may be designed to achieve a specified robust design.

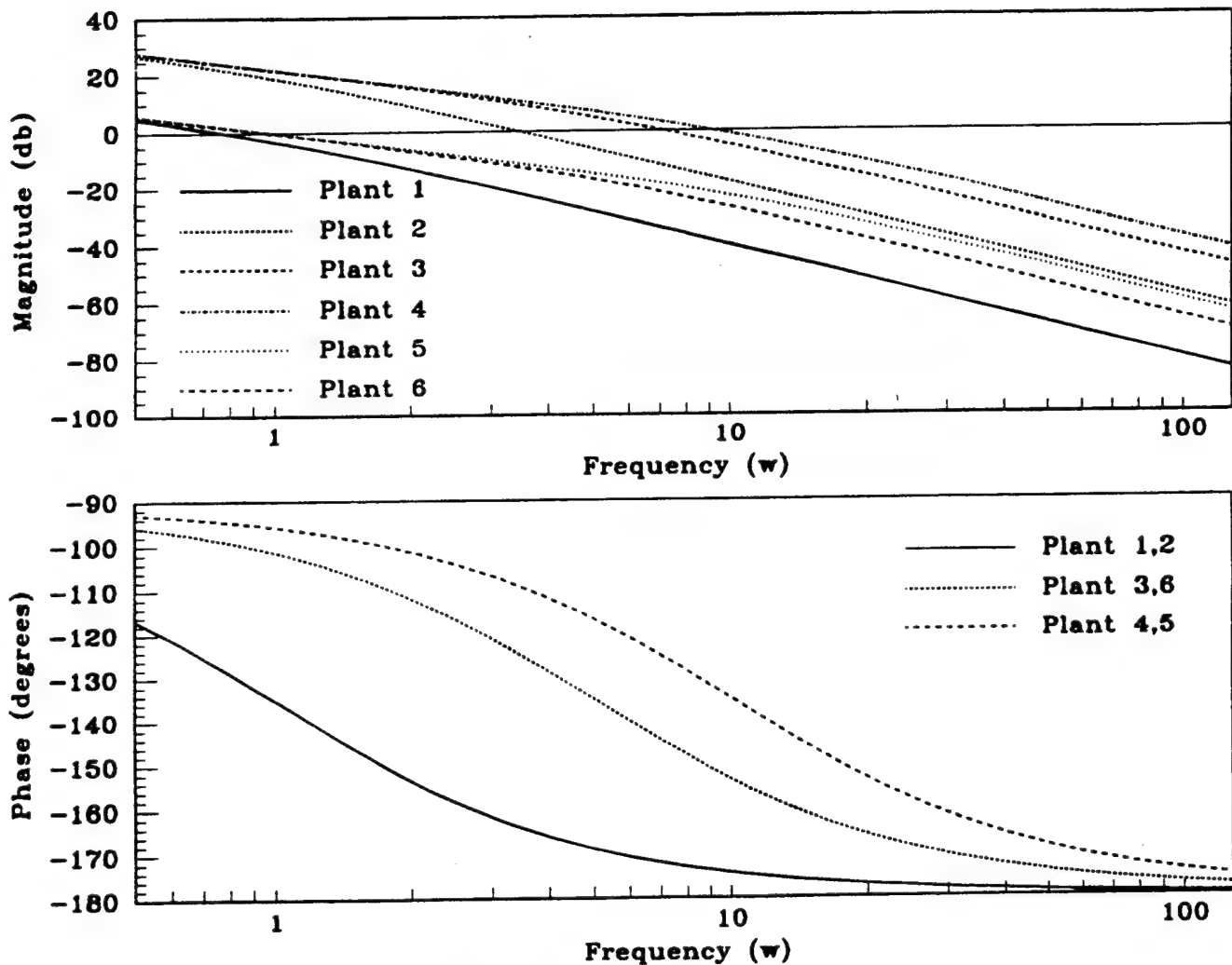


Fig. I.3 The bode plots of six LTI plants that represent the range of the plant's parameter uncertainty.

### I.1.3 Benefits of QFT

The benefits of QFT may be summarized as follows:

- a. The result is a robust design which is insensitive to plant variation.
- b. There is one design for the full envelope (no need to verify plants inside templates).
- c. Any design limitations are apparent up front.

- d. There is less development time for a full envelope design.
- e. One can determine what specifications are achievable up early in the design process.
- f. One can redesign for changes in the specifications quickly.
- g. The structure of compensator (controller) is determined up front.

## I.2 The MISO Analog Control System<sup>15</sup>

As is discussed in Chap. III, an  $m \times m$  feedback control system can be represented by an equivalent  $m^2$  MISO feedback control systems shown in Fig. I.4. Reference 15 and 47 present an in-depth presentation of the MISO QFT design technique for analog and discrete-time systems, respectively. Thus, this chapter presents an overview of the QFT technique for MISO feedback control system. It is assumed that the reader has the QFT background presented in these references.

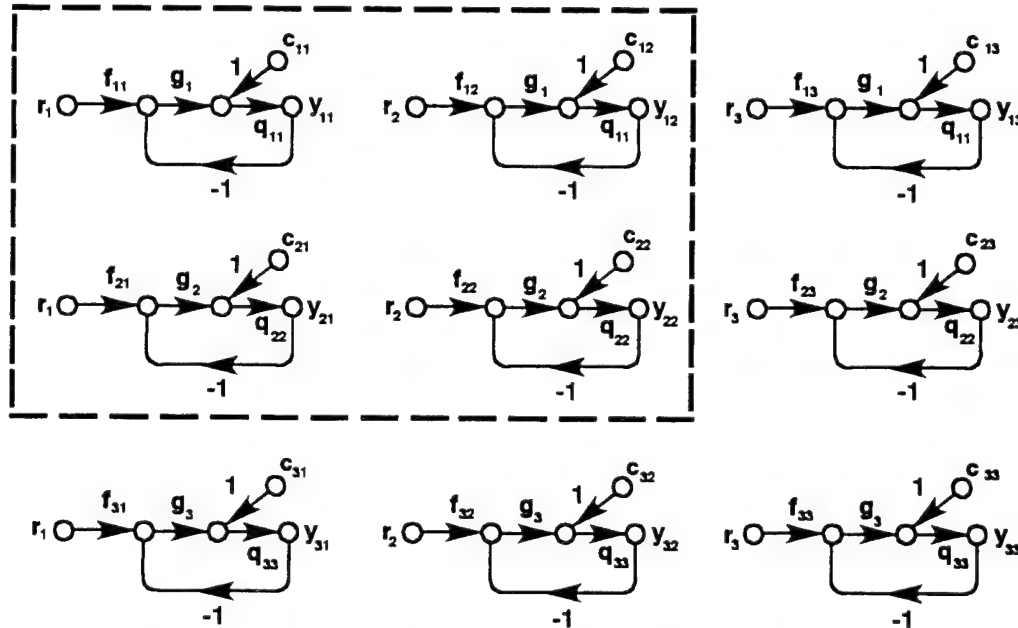


Fig. I.4  $m^2$  MISO equivalent of a 3x3 MIMO feedback control system.

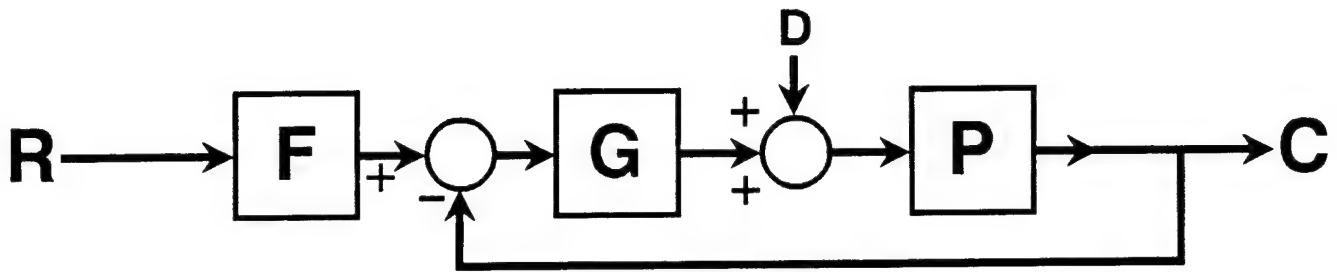


Fig. I.5 A MISO plant.

### I.2.1 MISO Analog Control System<sup>15</sup>

The overview of the MISO QFT design technique is presented in terms of the minimum-phase (m.p.) linear time-invariant (LTI) MISO system of Fig. I.5. The control ratios for tracking ( $D = 0$ ) and for disturbance rejection ( $R = 0$ ) are, respectively,

$$T_r = \frac{F(s)G(s)P(s)}{1 + G(s)P(s)} = \frac{F(s)L(s)}{1 + L(s)} \quad (I.1)$$

$$T_D = \frac{P(s)}{1 + G(s)P(s)} = \frac{P(s)}{1 + L(s)} \quad (I.2)$$

The design objective is to design the prefilter  $F(s)$  and the compensator  $G(s)$  so the specified robust design is achieved for the given region of plant parameter uncertainty. The design procedure to accomplish this objective is as follows:

- Step 1:      Synthesize the desired tracking model.
- Step 2:      Synthesize the desired disturbance model.
- Step 3:      Specify the  $J$  LTI plant models that define the boundary of the region of plant structured parameter uncertainty.
- Step 4:      Obtain plant templates, at specified frequencies, that

pictorial described the region of plant parameter uncertainty on the NC.

Step 5: Select the nominal plant transfer function  $P_o(s)$ .

Step 6: Determine the stability contour (U-contour) on the NC.

Steps 7-9: Determine the disturbance, tracking, and optimal bounds on the NC.

Step 10: Synthesize the nominal loop transmission function  $L_o(s) = G(s)P_o(s)$  that satisfies all the bounds and the stability contour.

Step 11: Based upon Steps 1 through 10 synthesize the prefilter  $F(s)$ .

Step 12: Simulate the system in order to obtain the time response data for each of the  $J$  plants.

The following sub-sections illustrate this design procedure.

### I.2.2 Synthesize Tracking Models

The tracking thumbprint specifications, based upon satisfying some or all of the step forcing function figures of merit for underdamped ( $M_p$ ,  $t_p$ ,  $t_s$ ,  $t_r$ ,  $K_m$ ) and overdamped ( $t_s$ ,  $t_r$ ,  $K_m$ ) responses, respectively, for a simple-second system, are depicted in Fig. I.6(a). The Bode plots corresponding to the time responses  $y(t)_U$  [Eq. (I.3)] and  $y(t)_L$  [Eq. (I.4)] in Fig. I.6(b) represent the upper bound  $B_U$  and lower bound  $B_L$ , respectively, of the thumbprint specifications; i.e., an acceptable response  $y(t)$  must lie between these bounds. Note that for the m.p. plants, only the tolerance on  $|T_R(j\omega_1)|$  need be satisfied for a satisfactory design. For nonminimum-phase (n.m.p.) plants, tolerances on  $\angle T_R(j\omega_1)$  must also be specified and satisfied in the design process.<sup>19,32</sup> It is desirable to synthesize the tracking control ratios

$$T_{Rv} = \frac{(\omega_n^2/a)(s+a)}{s^2 + 2\zeta\omega_n s + \omega_n^2} \quad (I.3)$$

$$T_{R_L} = \frac{K}{(s - \sigma_1)(s - \sigma_2)(s - \sigma_3)} \quad (I.4)$$

corresponding to the upper and lower bounds  $T_{RU}$  and  $T_{RL}$ , respectively, so that  $\delta_R(j\omega_1)$  increases as  $\omega_1$  increases above the 0 dB crossing frequency of  $T_{RU}$ . This characteristic of  $\delta_R$  simplifies the process of synthesizing a loop transmission  $L_o(s) = G(s)P_o(s)$  that requires the determination of the tracking bounds  $B_R(j\omega_1)$  which are obtained based upon  $\delta_R(j\omega_1)$ . The achievement of the desired performance specification is based upon the frequency bandwidth BW,  $0 < \omega \leq \omega_h$ , which is determined by the intersection of the -12 dB line and the  $B_U$  curve in Fig. I.6(b).

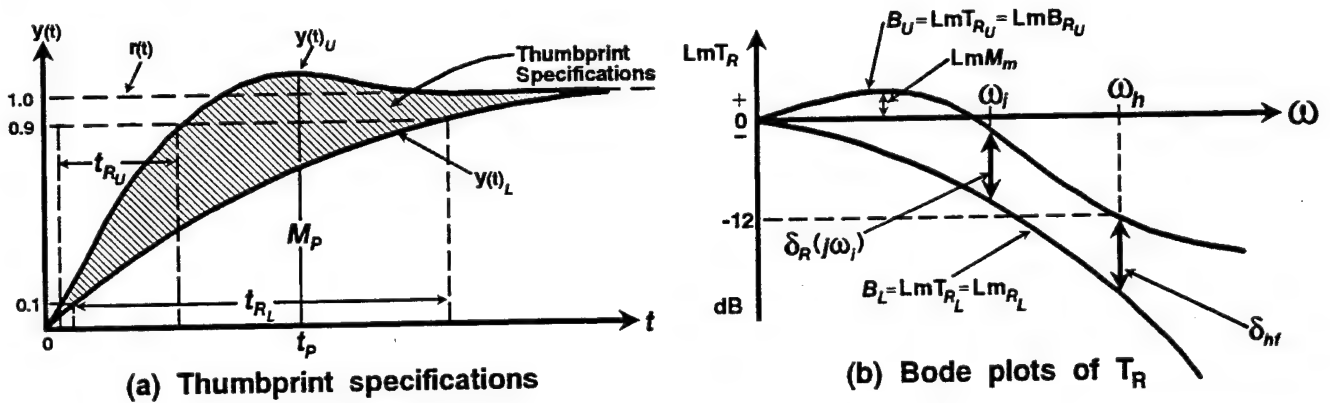


Fig. I.6 Desired response characteristics: (a) Thumbprint specifications, (b) Bode plot of  $T_R$ .

### I.2.3 Disturbance Model

The simplest disturbance control ratio model specification is  $|T_D(j\omega)| = |Y(j\omega)/D(j\omega)| \leq \alpha_p$  a constant [the maximum magnitude of the output based upon a unit step disturbance input ( $D_1$  of Fig. I.1)]. Thus the frequency domain disturbance specification is  $Lm T_D(j\omega) \leq Lm \alpha_p$  over the desired specified BW. Thus the disturbance specification is represented by only an upper bound on the NC over the specified BW.

#### I.2.4 J LTI Plant Models

The simple plant

$$P_j(s) = \frac{Ka}{s(s+a)} \quad (I.5)$$

where  $K \in \{1,10\}$  and  $a \in \{1,10\}$ , is used to illustrate the MISO QFT design procedure. The region of plant parameter uncertainty is illustrated by Fig. I.7. This region of uncertainty may be described by J LTI plants, where  $i = 1, 2, \dots, J$ . These plants lie on the boundary of this region of uncertainty. That is, the boundary points 1, 2, 3, 4, 5, & 6 are utilized to obtain 6 LTI plant models that adequately define the region of plant parameter uncertainty.

#### I.2.5 Plant Templates of $P_i(s)$ , $\angle P(j\omega_i)$

With  $L = GP$ , Eq. (I.1) yields

$$Lm T_R = Lm F - Lm \left[ \frac{L}{1+L} \right] \quad (I.6)$$

The change in  $T_R$  due to the uncertainty in  $P$ , since  $F$  is LTI, is

$$\Delta(Lm T_R) = Lm T_R - Lm F = Lm \left[ \frac{L}{1+L} \right] \quad (I.7)$$

By the proper design of  $L = L_0$  and  $F$ , this change in  $T_R$  is restricted so that the actual value of  $Lm T_R$  always lies between  $B_U$  and  $B_L$  of Fig. I.6. The first step in synthesizing an  $L_0$  is to make NC templates which characterize the variation of the plant uncertainty (see Fig. I.8), as described by  $i = 1, 2, \dots, J$  plant transfer functions, for various values of  $\omega_i$  over a specified frequency range. The boundary of the plant template can be obtained by mapping the boundary of the plant parameter uncertainty region,  $Lm P_i(j\omega_i)$  vs  $\angle P_i(j\omega_i)$ , as shown on the Nichols chart (NC) in Fig. I.8. A curve is drawn through the points 1, 2, 3, 4, 5, and 6 where the shaded area is labeled  $\angle P(j1)$ , which can be represented by plastic a template. Templates for other values of  $\omega_i$  are obtained in a similar manner. A characteristic of these templates is



that, starting from a "low value" of  $\omega_1$ , the templates widen (angular width becomes larger) for increasing values of  $\omega_1$  then as  $\omega_1$  takes on larger values and approaches infinity they become narrower and eventually approach a straight line of height  $V$  dB [see Eq. (I.9)]. Guidelines for template determination are given in the following sections: Sec. VII.2, Sec. VII.3 (E.L.3), and Sec. IX.5.4.

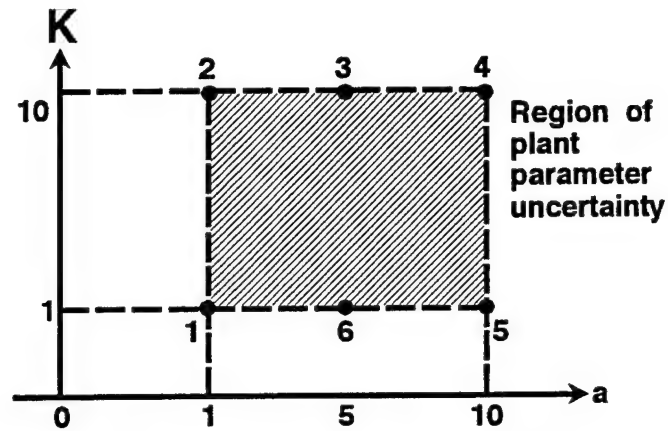


Fig. I.7 Region of plant uncertainty

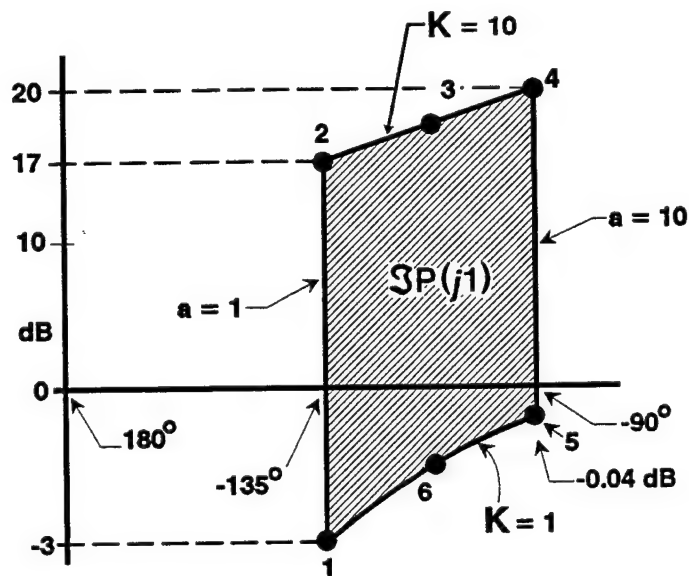


Fig. I.8 The template  $\mathcal{S}P(j1)$ .

### I.2.6 Nominal Plant

While any plant case can be chosen it is an accepted practice to select, whenever possible, a plant whose NC point is always at the lower left corner for all frequencies for which the templates are obtained.

### I.2.7 U-Contour (Stability bound)

The specifications on system performance in the frequency domain [see Fig. I.6(b)] identify a minimum damping ratio  $\zeta$  for the dominant roots of the closed-loop system which becomes a bound on the value of  $M_p \approx M_m$ . On the NC this bound on  $M_m = M_L$  [see Figs. I.6(b) and I.9] establishes a region which must not be penetrated by the templates and the loop transmission function  $L(j\omega)$  for all  $\omega$ . The boundary of this region is referred to as the universal high-frequency boundary (UHFB) or stability bound, the U-contour, because this becomes the dominating constraint on  $L(j\omega)$ . Therefore, the top portion, efa, of the  $M_L$  contour becomes part of the U-contour. For a large problem class, as  $\omega \rightarrow \infty$ , the limiting value of the plant transfer function approaches

$$\lim_{\omega \rightarrow \infty} [P(j\omega)] = \frac{K}{\omega^\lambda} \quad (\text{I.8})$$

where  $\lambda$  represents the excess of poles over zeros of  $P(s)$ . The plant template, for this problem class, approaches a vertical line of length equal to

$$\Delta \triangleq \lim_{(\omega \rightarrow \infty)} [Lm P_{\max} - Lm P_{\min}] = Lm K_{\max} - Lm K_{\min} = V \text{ dB} \quad (\text{I.9})$$

If the nominal plant is chosen at  $K = K_{\min}$ , then the constraint  $M_L$  gives a boundary which approaches the U-contour abcdefa of Fig. I.9.

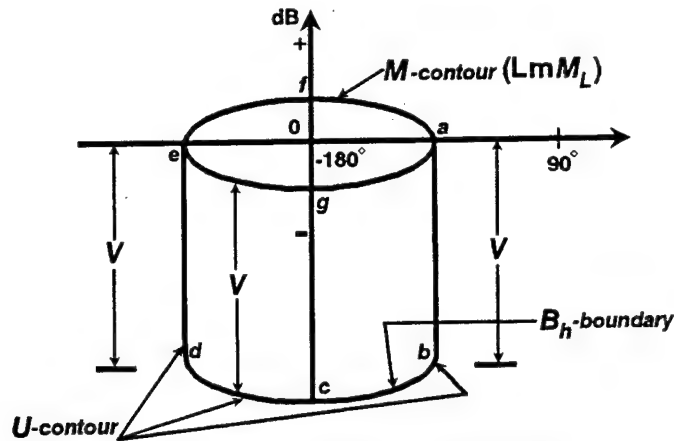


Fig. I.9 U-contour construction.

### I.2.8 Optimal Bounds $B_o(j\omega)$ on $L_o(j\omega)$

The determination of the tracking  $B_R(j\omega_i)$  and the disturbance  $B_D(j\omega_i)$  bounds are required in order to yield the optimal bounds  $B_o(j\omega_i)$  on  $L_o(j\omega_i)$ .

#### I.2.8.1 Tracking Bounds

The solution for  $B_R(j\omega_i)$  requires that the condition

$$(\text{actual}) \Delta T_R(j\omega_i) \leq \delta_R(j\omega_i) \text{ dB (see Fig. I.6(b))}$$

must be satisfied. Thus it is necessary to determine the resulting constraint, or bound  $B_R(j\omega_i)$ , on  $L(j\omega_i)$ . The procedure is to pick a nominal plant  $P_o(s)$  and to derive tracking bounds on the NC, at specified values of frequency and by use of templates or a CAD package, on the resulting nominal transfer function  $L_o(s) = G(s)P_o(s)$ . That is, along a phase angle grid line on the NC move the nominal point on the template  $\mathcal{S}P(jv_i)$  up or down, without rotating the template, until it is tangent to two M-contours whose difference in M values is essentially equal to  $\delta_R$ . When this condition has been achieved the location of the nominal point on the template becomes a point on the tracking bound  $B_R(jv_i)$  on the NC. This procedure is repeated on sufficient angle grid lines on the NC to provide sufficient points to draw  $B_R(jv_i)$  and for all values of frequency for which templates have been obtained.

### I.2.8.2 Disturbance Bounds

The general procedure for determining disturbance bounds for the MISO control system of Fig. I.5 is outlined as follows but more details are given in Reference 15. From Eq. (I.2) the following equation is obtained:

$$T_D = \frac{P_o}{\frac{P_o}{P} + L_o} = \frac{P_o}{W} \quad (\text{I.10})$$

where  $W = (P_o/P) + L_o$ . From Eq. (I.10), setting  $\text{Lm } T_D = \delta_D = \text{Lm } \alpha_p$ , the following relationship is obtained:

$$\text{Lm } W = \text{Lm } P_o - \delta_D \quad (\text{I.11})$$

For each value of frequency for which the NC templates are obtained the magnitude of  $|W(j\omega_1)|$  is obtained from Eq. (I.11). This magnitude in conjunction with the equation  $W(j\omega_1) = [P_o(j\omega_1)/P(j\omega_1)]$  are utilized to obtain a graphical solution for  $B_D(j\omega_1)$  as shown in Fig. I.10<sup>15</sup>. Note that in this figure the template is plotted in rectangular or polar coordinates.

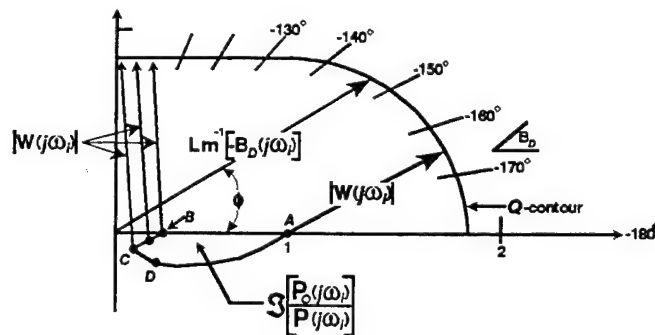


**Fig. I.10 Graphical evaluation of  $B_p(j\omega_i)$**

### I.2.8.3 Optimal Bounds

For the case shown in Fig. I.11  $B_o(j\omega_i)$  is composed of those portions of each respective bound  $B_R(j\omega_i)$  and  $B_D(j\omega_i)$  that have the largest dB values. The synthesized  $L_o(j\omega_i)$  must lie on or just above the bound  $B_o(j\omega_i)$  of Fig. I.11.

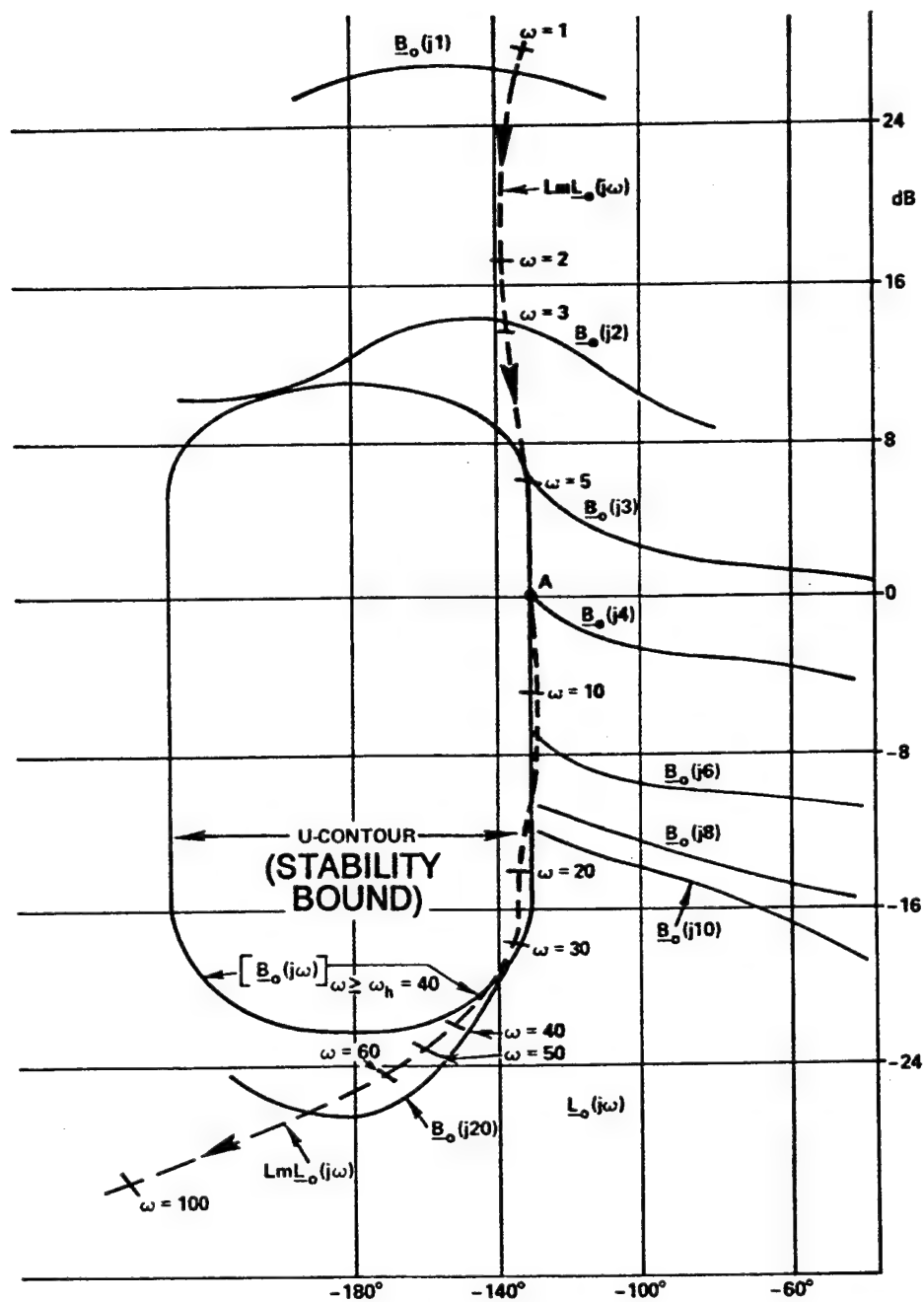


Fig. I.11 Bounds  $B_o(j\omega_i)$  and loop shaping.

### I.2.9 Synthesizing (or Loop Shaping) $L_o(s)$ and $F(s)$

The shaping of  $L_o(j\omega)$  is shown by the dashed curve in Fig. I.11. A point such as  $\text{Lm } L_o(j2)$  must be on or above  $B_o(j2)$ . Further, in order to satisfy the specifications,  $L_o(j\omega)$  cannot violate the U-contour. In this example a reasonable  $L_o(j\omega)$  closely follows the U-contour up to  $\omega = 40$  rad/sec and must stay below it above  $\omega = 40$  as shown in Fig I.11. It also must be a Type 1 function (one pole at the origin). Synthesizing a rational function  $L_o(s)$  which satisfies the above specification involves building up the function

$$L_o(j\omega) = L_{ok}(j\omega) = P_o(j\omega) \prod_{k=0}^W [K_k G_k(j\omega)] \quad (\text{I.12})$$

where for  $k = 0$ ,  $G_o = 1\angle 0^\circ$ , and  $K = \prod_{k=0}^W K_k$ . In order to minimize the order of the compensator a good starting point for "building up" the loop transmission function is to initially assume that  $L_{o0}(j\omega) = P_o(j\omega)$  as indicated in Eq. (I.12).  $L_o(j\omega)$  is built up term-by-term or by a CAD loop shaping routine,<sup>8</sup> in order (1) that the point  $L_o(j\omega_i)$  lies on or above the corresponding optimal bound  $B_o(j\omega_i)$  and (2) to stay just outside the U-contour in the NC of Fig. I.11. The design of a proper  $L_o(s)$  guarantees only that the variation in  $|T_R(j\omega_i)|$  is less than or equal to that allowed, i.e.,  $\delta_R(j\omega_i)$ . The purpose of the prefilter  $F(s)$  is to position  $\text{Lm } [T(j\omega)]$  within the frequency domain specifications, i.e., that it always lies between  $B_U$  and  $B_L$  [see Fig. I.6(b)] for all  $J$  plants. The method for determining  $F(s)$  is discussed in the next section. Once a satisfactory  $L_o(s)$  is achieved then the compensator is given by  $G(s) = L_o(s)/P_o(s)$ . Note that for this example  $L_o(j\omega)$  slightly intersects the U-contour at frequencies above  $\omega_h$ . Because of the inherent overdesign feature of the QFT technique, as a first trial design, no effort is made to fine tune the synthesis of  $L_o(s)$ . If the simulation results are not satisfactory then a fine tuning of the design can be made. The available CAD packages simplify and expedite this fine tuning.

### I.2.10 Prefilter Design<sup>15,19,32</sup>

Design of a proper  $L_o(s)$  guarantees only that the variation in  $|T_R(j\omega)|$  is less than or equal to that allowed, i.e.,  $[Lm T_R(j\omega)] \leq \delta_R(j\omega)$ . The purpose of the prefilter  $F(s)$  is to position

$$Lm T(j\omega) = Lm \frac{L(j\omega)}{1 + L(j\omega)} \quad (I.13)$$

within the frequency domain specifications. A method for determining the bounds on  $F(s)$  is as follows:

Step 1: Place the nominal point of the  $\omega_i$  plant template on the  $L_o(j\omega_i)$  point on the  $L_o(j\omega)$  curve on the NC (see Fig. I.12).

Step 2: Traversing the template, determine the maximum  $Lm T_{max}$  and the minimum  $Lm T_{min}$  values of Eq. (I.13) are obtained from the M-contours.

Step 3: Based upon obtaining sufficient data points within the desired frequency bandwidth, for various values of  $\omega_i$ , and in conjunction with the data used to obtain Fig. I.6(b) the plots of Fig. I.13 are obtained.

Step 4: Utilizing Fig. I.13, the straight-line Bode technique and the condition

$$\lim_{s \rightarrow 0} F(s) = 1 \quad (I.14)$$

for a step forcing function, an  $F(s)$  is synthesized that lies within the upper and lower plots in Fig. I.13.

### I.2.11 Simulation

The "goodness" of the synthesized  $L_o(s)$  and  $F(s)$  is determined by simulating the QFT designed control system for all J plants. MISO QFT CAD packages, as discussed in Chap. VIII, are available that expedite this simulation phase of the complete design process.



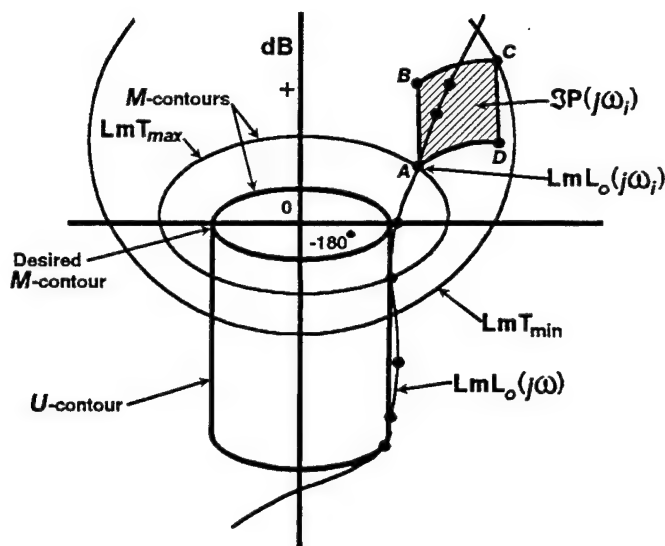


Fig. I.12 Prefilter determination.

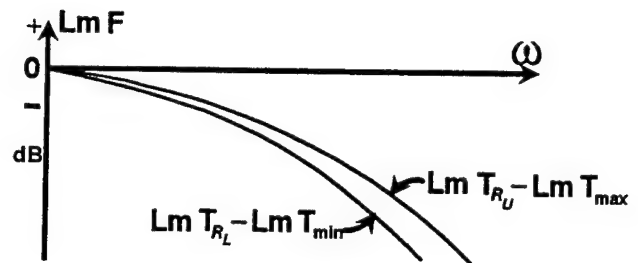


Fig. I.13 Frequency bounds on  $F(s)$ .

### I.3 The MISO Discrete Control System<sup>47</sup>

#### I.3.1 Introduction

The bilinear transformation,  $z$ -domain to the  $w'$ -domain and vice-versa, is utilized in order to accomplish the QFT design for both MISO and MIMO sampled-data (discrete) control system design in the  $w'$ -domain. This transformation enables the use of the MISO QFT analog design technique to be readily used, with minor exceptions, to perform the QFT design for the controller  $G(w')$ . If the  $w'$ -domain simulations satisfy the desired performance specification then by use of the bilinear transformation the  $z$ -domain controller  $G(z)$  is obtained. With this  $z$ -domain controller a discrete-time domain simulation is obtained to verify the goodness of the design. The QFT technique requires the determination of the minimum sampling frequency  $(\omega_s)_{\min}$  bandwidth that is needed for a satisfactory design.<sup>30,47</sup> The larger the plant uncertainty and the narrower the system performance tolerances are, the larger must be the value of  $(\omega_s)_{\min}$ . Although, henceforth, the prime is omitted from  $w'$  whenever the symbol  $w$  is used it is to be interpreted as  $w'$ .

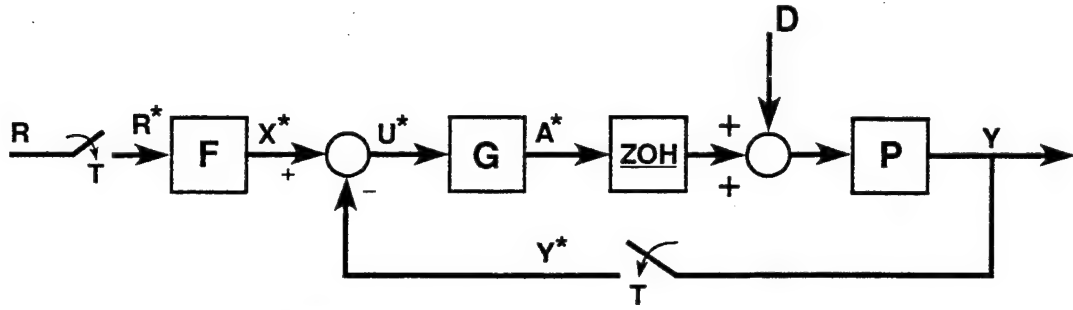


Fig. I.14 A MISO sampled-data control system.

### I.3.2 The MISO Sampled-data Control System

Figure I.14 represents the MISO discrete control, having plant uncertainty, that is to be designed by the QFT technique. The equations that described this system are as follows:

$$P_z(z) = G_{zo}P(z) = (1 - z^{-1})Z\left[\frac{P(s)}{s}\right] = (1 - z^{-1})P_e(z) \quad (I.15)$$

$$L(z) = G_{zo}P(z)G_1(z), \quad P_e \equiv \frac{P(s)}{s}, \quad P_e(z) = Z\left[\frac{P(s)}{s}\right] = Z[P_e] \quad (I.16)$$

For a unit step disturbance:  $D(s) = \frac{1}{s}$

$$P_e(s) = P(s)D(s), \quad P_e(z) = Z[P(s)D(s)] = PD(z) \quad (I.17)$$

$$T_R = \frac{F(z)L(z)}{1+L(z)} \quad T_D = \frac{PD(z)}{1+L(z)} \quad (I.18)$$

$$\begin{aligned} Y(z) &= \left[\frac{L(z)F(z)}{1+L(z)}\right]R(z) + \left[\frac{PD(z)}{1+L(z)}\right]\frac{1}{D(z)} \\ &= Y_R(z) + Y_D(z) = T_R(z)R(z) + Y_D(z) \end{aligned} \quad (I.19)$$

I.3.3 w'-Domain -- The pertinent s-, z-, and w-plane relationships are as follows:

$$\alpha^2 = \left(\frac{\sigma T}{2}\right)^2 < 2, \quad \frac{\omega T}{2} \leq 0.297 \quad (\text{I.20})$$

$$s = \sigma + j\omega, \quad (\text{a}) \quad w = u + jv = \left(\frac{2}{T}\right) \left[\frac{z-1}{z+1}\right] \quad (\text{b}) \quad (\text{I.21})$$

$$z = \frac{Tw + 2}{-Tw + 2} \quad (\text{a}) \quad v = \left(\frac{2}{T}\right) \tan\left(\frac{\omega T}{2}\right) = \left(\frac{\pi}{\omega_s}\right) \tan\left(\frac{\omega \pi}{\omega_s}\right) \quad (\text{b}) \quad (\text{I.22})$$

$$u = \frac{2 \tanh(\sigma T/2)}{T} \quad (\text{c})$$

$$\omega_s = 2\pi/T, \quad z = e^{sT} \angle \omega T = |z| \angle \omega T \quad (\text{I.23})$$

#### I.3.4 Assumptions

The following assumptions are assumed:

- a. Minimum-phase (mp) stable plants
- b. The analogue desired models, Eqs (I.3) and (I.44), yield the desired time response characteristics for the discrete-time system.
- c. The sampling time  $T$  is small enough so that over the BW,  $0 < \omega \leq \omega_h$ , Eq. (I.23) is valid permitting the approximation  $s \approx w$  and in-turn

$$T_R(w) \approx [T_R(s)]_{s=w} \quad (\text{I.24})$$

Both the upper and lower bound  $w$ -domain tracking models are obtained in this manner. The disturbance specification is the same as for the analog case.

#### I.3.5 Nonminimum Phase $L_o(w)$

It is important to note that in the  $w$  domain any practical  $L(w)$  is

nonminimum phase (n.m.p.) containing a zero at  $2/T$  (the sampling zero). This result is due to the fact that any practical  $L(z)$  has an excess of at least one pole over zeros. Thus, the design technique for a stable uncertain plant is modified<sup>30</sup> to incorporate the all-pass filter (apf)

$$A(w) = \frac{w - \frac{2}{T}}{w + \frac{2}{T}} = -A'(w) = - \left[ \frac{\frac{2}{T} - w}{\frac{2}{T} + w} \right] \quad (I.25)$$

as follows: Let the nominal loop transmission be defined as:

$$L_o \equiv -L_{mo}(w)A(w) = L_{mo}(w)A'(w) \quad (I.26)$$

From Eq. (I.26) it is seen that

$$\angle L_{mo}(jv) = \angle L_o(jv) - \angle A'(jv) \quad (I.27)$$

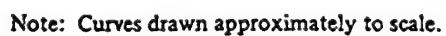
where

$$-\angle A'(jv) = 2 \tan^{-1} \frac{vT}{2} > 0 \quad (I.28)$$

An analysis of Eqs. (I.26) through (I.28) reveals that the bounds  $B_o'(jv_1)$  on  $L_o(jv)$  become the bounds  $B_{mo}(jv_1)$  on  $L_{mo}(jv)$  by shifting, over the desired BW,  $B_o'(jv_1)$  positively (to the right on the NC) by the angle  $\angle A'(jv_1)$ , as shown in Fig. I.15. The U-contour ( $B_h'$ ) must also be shifted to the right by the same amount, at the specified frequencies  $v_1$ , to obtain the shifted U-contour  $B_h(jv_1)$ . The contour  $B_h'$  is shifted to the right until it reaches the vertical line  $\angle L_{1mo}(jv_K) = 0^\circ$ . The value of  $v_K$ , which is function of  $\omega_s$  and the phase margin angle as shown in Fig. I.15,<sup>47</sup> is given by

$$2 \tan^{-1} \left( \frac{v_K T}{2} \right) = 180^\circ - \gamma \quad (I.29)$$

It should be mentioned that loop shaping or synthesizing  $L_o(w)$  can be done directly without the use of an apf.



20

### I.3.6 Plant Templates $\mathcal{SP}(jv_i)$

The plant templates in the  $w$ -domain have the same characteristic as those for the analog case (see Sec. I.2.5) for the frequency range  $0 < \omega_i \leq \omega_s/2$  as shown in Fig. I.16(a). In the frequency range  $\omega_s/2 < \omega_i < \infty$  the  $w$ -domain templates widen once again then eventually approach a vertical line as shown in Fig. I.16(b).

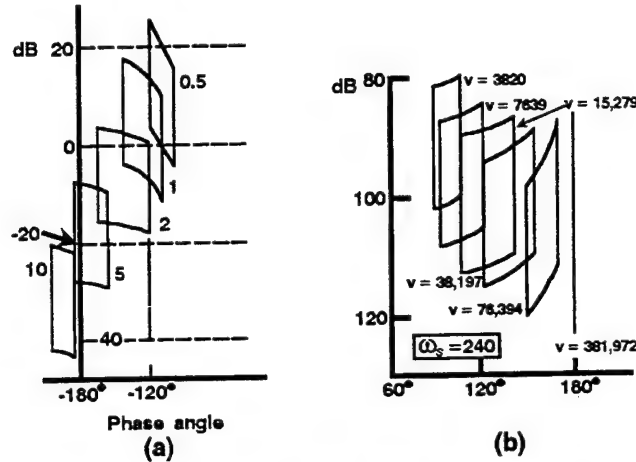


Fig. I.16  $w$ -domain plant templates.

### I.3.7 Synthesizing $L_{mo}(w)$

The frequency spectrum can be divided into four general regions for purpose of synthesizing an  $L_{mo}(w)$  (loop shaping) that will satisfy the desired system performance specifications for the plant having plant parameter uncertainty. These four regions are:

**Region 1:** For the frequency range where Eq. (I.23) is satisfied use the analog templates; i.e.  $\mathcal{SP}(j\omega_i) \approx \mathcal{SP}(jv_i)$ . The  $w$ -domain tracking, disturbance and optimal bounds and the  $U$ -contour are essentially the same as those for the analog system. The templates are used to obtain these bounds on the NC in the same manner as for the analog system.

**Region 2:** For the frequency range  $v_{0.25} < v_i \leq v_h$ , where  $\omega_i \leq 0.25\omega_s$ , use the  $w$ -domain templates. These templates are used to obtain all 3 types of bounds, in the same manner as for the analog

system, in this region and the corresponding  $B'_h(jv_i)$ -contours are also obtained.

Region 3: For the frequency range  $v_h < v_i \leq v_K$ , for the specified value of  $\omega_s$ , only the  $B'_h$ -contours are plotted.

Region 4: For the frequency range  $v_h > v_K$  use the w-domain templates. Since the templates  $\mathcal{S}P_e(jv_i)$  broaden out again for  $v_i > v_K$ , as shown in Fig. I.16, it is necessary to obtain the more stringent (stability) bounds  $B_s$  shown in Fig. I.17. The templates are used only to determine the stability bounds  $B_s$ .

The synthesis (or loop shaping) of  $L_{mo}(w)$  involves the synthesizing the following function:

$$L_{mo}(jv) = P_{eo}(jv) \prod_{k=0}^W [K_k G_k(jv)] \quad (I.30)$$

where the nominal plant  $P_{eo}(w)$  is the plant from the  $J$  plants that has the smallest dB value and the largest (most negative) phase lag characteristic. The final synthesized  $L_{mo}(w)$  function must be one that satisfies the following conditions:

1. In Regions I and II the point on the NC that represents the dB value and phase angle of  $L_{mo}(jv_i)$  must be such that it lies on or above the corresponding  $B_{mo}(jv_i)$  bound (see Fig. I.15).
2. The values of Eq. (I.30) for the frequency range of Region III must lie to the right or just below the corresponding  $B'_h$ -contour (see Fig. I.15).
3. The value of Eq. (I.30) for the frequency range of Region IV must lie below the  $B_s$  contour for negative phase angles on the NC (see condition 4).

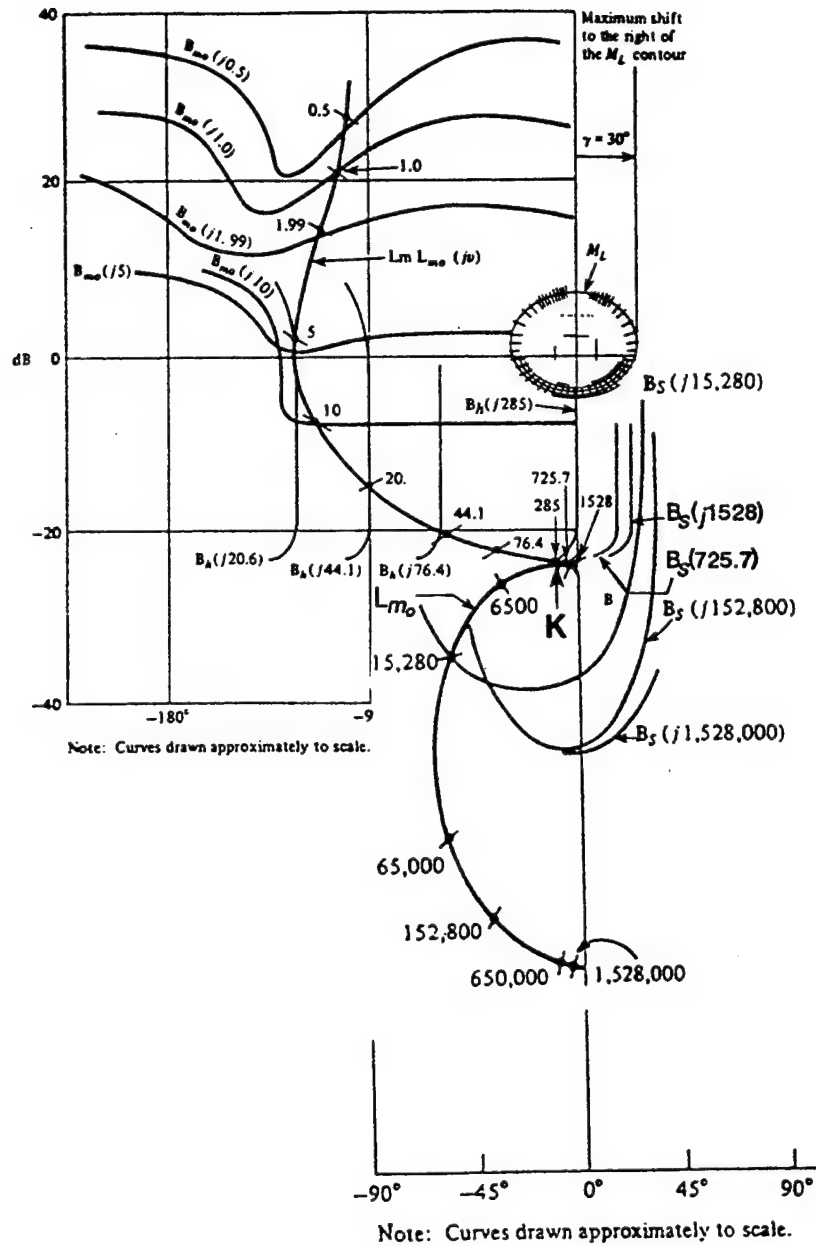


Fig. I.17 A satisfactory design:  $L_{m0}(jv)$  at  $\omega_s = 240$ .



4. In utilizing the bilinear transformation of Eq. (I.21), the  $w$ -domain transfer functions are all equal order over equal order.

5. The Nyquist stability criterion dictates that the  $L_{mo}(jv)$  plot is on the "right side" or the "bottom right side" of the  $B_h(jv_i)$ -contours for the frequency range of  $0 \leq v_i \leq v_K$ . It has been shown that:<sup>36</sup>

(a)  $L_{mo}(jv)$  must reach the right-hand bottom of  $B_h(jv_K)$ , i.e., approximately point K in Fig. I.17, at a value of  $v \leq v_K$ , and

(b)  $\angle L_{mo}(jv_K) < 0^\circ$  in order that there exists a practical  $L_{mo}$  which satisfies the bounds  $B(jv)$  and provides the required stability.

6. For the situation where one or more of the  $J$  LTI plants, that represent the uncertain plant parameter characteristics, represent unstable plants and one of these unstable plants is selected as the nominal plant, then the apf to be used in the QFT design must include all right-hand-plane (rhp) zeros of  $P_{zo}$ . This situation is not discussed. Note: for experienced QFT control system designers  $L_o(v)$  can be synthesized without the use of apf. This approach also is not covered in this chapter. The loop shaping technique of the MIMO QFT CAD package, discussed in Chap. VIII, does not involve the use of an apf.

The synthesized  $L_{mo}(w)$  obtained following the guidelines of this section, is shown in Fig. I.17.

### I.3.8 Prefilter Design

The procedure for synthesizing  $F(w)$  is the same as for the analog case (see Sec. I.2.10) over the frequency range  $0 < v_1 \leq v_h$ . In order to satisfy condition 4 of Sec. I.3.7, a nondominating zero or zeros ("far-left" in the  $w$ -plane) are inserted so that the final synthesized  $F(w)$  is equal order over equal order.

### I.3.9 w-Domain Simulation

The "goodness" of the synthesized  $L_{mo}(w)$  [or  $L_o(w)$ ] and  $F(w)$  is determined by first simulating the QFT w-domain designed control system for all  $J$  plants in the w-domain (an "analog" time domain simulation). See Chap. VIII for MISO QFT CAD packages that expedite this simulation.

### I.3.10 z-Domain

The two tests of the goodness of the w-domain QFT designed system is a discrete-time domain simulation of the system shown in Fig. I.14. To accomplish this simulation, the w-domain transfer functions  $G(w)$  and  $F(w)$  are transformed to the z-domain by use of the bilinear transformation of Eq. (I.21). This transformation is utilized since the degree of the numerator and denominator polynomials of these functions are equal and the controller and prefilter do not contain a zero-order-hold device.

#### I.3.10.1 Comparison of the Controller's w- and z-Domain Bode Plots

Depending on the value of the sampling time  $T$ , warping may be sufficient to alter the loop shaping characteristics of the controller when it is transformed from the w-domain into the z-domain. For the warping effect to be minimal the Bode plots (magnitude and angle) of the w- and z-domain controllers must essentially lie on top of one another within the frequency range  $0 < \omega \leq [(2/3)(\omega_g/2)]$ . If the warping is negligible then a discrete-time simulation can proceed. If not, a smaller value of sampling time needs to be selected.

#### I.3.10.2 Accuracy

The CAD packages that are available to the designer determines the degree of accuracy of the calculations and simulations. The smaller the value of  $T$  the greater the degree of accuracy that is required to be maintained. The accuracy can be enhanced by simulating  $G(z)$  and  $F(z)$  as a set of  $G$ 's and  $F$ 's cascaded transfer functions, respectively; that is

$$G(z) = G_1(z) G_2(z) \dots G_g(z), \quad F(z) = F_1(z) F_2(z) \dots F_f(z) \quad (I.31)$$

### I.3.10.3 Analysis of Characteristic Equation $Q_1(z)$

Depending on the value of  $T$  and the plant parameter uncertainty, the pole-zero configuration in the vicinity of the  $-1 + j0$  point in the  $z$ -plane for one or more of the  $J$  LTI plants can result in an unstable discrete-time response. Thus before proceeding with a discrete-time domain simulation an analysis of the characteristic equation  $Q_1(z)$  for all  $J$  LTI plants must be made. If an unstable system exists an analysis of  $Q_1(z)$  and the corresponding root-locus may reveal that a slight relocation of one or more controller pole in the vicinity of the  $-1 + j0$  point toward the origin may ensure a stable system for all  $J$  plants without essentially effecting the desired loop shaping characteristic of  $G(z)$ .

### I.3.10.4 Simulation and CAD Packages

With the "design checks" of Secs. I.3.10.1 through I.3.10.3 satisfied then a discrete-time simulation is performed to verify that the desired performance specifications have been achieved. In order to enhance the MISO QFT discrete control system design procedure that is presented in this chapter the reader is referred to the CAD flow chart of Chap. VIII.

## I.4 Summary

As stated in the introduction, the purpose of this chapter is to provide the reader, who is familiar with the MISO QFT analog and discrete design techniques,<sup>15,47</sup> an overview of the basic MISO design procedures.

## Chapter II Basics of System Identification

### Nomenclature

ARMAX	-- Auto Regressive Moving Average with eXogeneous inputs
ARX	-- Auto Regressive with eXogeneous inputs
BW	-- Bandwidth
EKF	-- Extended Kalman Filter
LR	-- Linear Regression
LS	-- Least Squares
MV	-- Minimum Variance
RLS	-- Recursive Least Squares
SID	-- System Identification
SNR	-- Signal to Noise Ratio

### II.1 Introduction

Basic problems in System Identification (SID) are elucidated in this chapter and a viable approach to their solution is presented. Determining the controlled "plant's" (the dynamical system's) parameters from its noise corrupted input and output measurements is, what SID is all about. As such, SID stands out in stark contrast to the mathematical modeling based approaches to dynamical system elucidation, so engrained in physics and engineering practice, for SID embraces an empiricism based route to modeling. Therefore SID is a basic scientific tool, for it entails a "black box" approach to modeling, viz., a model of the dynamical sytem is being matched to the input data and the measured output of the sytem.

Linear discrete-time SISO control systems are considered and their transfer function

$$\frac{Y(z)}{U(z)} = \frac{b_1 z^{-1} + b_2 z^{-2} + \dots + b_n z^{-n}}{1 - a_1 z^{-1} - a_2 z^{-2} - \dots - a_n z^{-n}} \quad (\text{II.1})$$

is identified, viz., the  $n+m$  coefficients  $a_1, a_2, \dots, a_n, b_1, \dots, b_m$  are determined. The corruption of the input ( $u$ ) and the output ( $y$ ) by

measurement noise is a major concern and therefore SID entails a statistical approach to modeling. Hence, it should come as no surprise that the methods of statistics have a strong bearing on SID, as expounded in this chapter.

Roughly speaking, SID is the ``dynamic" counterpart of the ``static" Linear Regression (LR) method of statistics, whose broad fields of application encompass the ``softer", i.e., with less structure-endowed, disciplines of economics and the social sciences. Hence, due to its statistical foundations, SID is applicable to a wide variety of economic, scientific, and engineering problems. However, if SID would be a straightforward task, the dependence on mathematical modeling, and indeed, on physics, would be significantly reduced. Unfortunately, though, the SID ``stepping stone" requires that careful attention be given to it.

## II.2 Classical Route to Identification

The classical route to the identification of a (linear) control system's parameters entails the estimation of the state of an augmented and nonlinear dynamical system, and hence, it would appear that system identification falls into the Extended Kalman Filtering (EKF) area<sup>61</sup>. Thus, the system's parameters and the system's state are jointly estimated by the EKF. In Extended Kalman Filtering a linearization concept is employed. However, when the state estimation error is, or becomes, large this linearization-based approach loses its validity and the estimation algorithm fails. In addition, the emphasis in Kalman Filtering is on recursive algorithms, and, at the same time, the complete measurement time history is used. While the recursive approach to estimation is most compatible with using an ever expanding data set, the latter has the delitirious effect of precluding the estimation of time-varying parameters, and, in particular, parameters subject to jumps, as is the case in systems subject to possible failure. Ad-hoc ``forgetting factors", or, the inclusion of parameter drift in the filter dynamics type of fixes could possibly handle slowly varying parameters, but would require a lot of tuning to accommodate parameter

jumps. Moreover, EKF's must be initialized. When no prior information about the system's state and parameters is available and the filter is initialized accordingly, it might take a long time for the erroneous prior information to be "washed out". In conclusion, this identification method suffers from the well known deficiencies of Extended Kalman Filters. Therefore, in the controls community linear regression based approaches for the identification of the parameters of linear control systems, where the linear structure of the dynamics is directly exploited and the system's parameter only (without the system's state) is estimated, are used.

If either the system under consideration is static, as is the case in the linear regression paradigm of statistics, or, if dynamical systems with process noise but with no measurement noise are considered, then Auto Regressive with eXogeneous inputs (ARX) models are obtained. Now, the problem of estimating the parameters of an ARX model leads to a linear regression formulation, whose solution is given by a Least Squares (LS) estimate. Therefore, the identification of the parameters of an ARX model is a relatively simple task. These models are oftentimes discussed in the controls literature. Unfortunately, ARX models are not very interesting in control work, due to the dynamic nature of control systems and the ubiquity of measurement noise.

### II.3 Linear Regression

Linear regression based system identification algorithms applied to the identification of discrete-time dynamical systems with measurement noise yield Auto Regressive Moving Average with eXogeneous inputs (ARMAX) models. Thus, it is important to recognize that notwithstanding the linear structure of the LR, the identification of an ARMAX model is a nonlinear filtering problem. The LR like formulation of the equations that need to be solved in order to identify (determine) the parameter vector, only serves to mask the inherently nonlinear nature of the original SID problem. Thus, in ARMAX models measurement (or sensor) noise is responsible for the introduction of correlation into the "equation error" of the ensuing "LR." Correlation causes the LS based parameter estimates to be "biased", i.e., the parameter estimates are

bad. Hence, when ARMAX models are used it is important to recognize the correlation inherent in the LR's equation error, and it is therefore required to calculate the Minimum Variance (MV) estimate of the parameter, which estimate incorporates the equation error covariance information. In conclusion, the notorious correlation phenomenon encountered in the "Linear" Regression formulation of the problem of identifying ARMAX models is just an alternative manifestation of the difficult nature of the nonlinear filtering problem.

#### II.4 SID Approaches

The elucidation of the basic difficulties of system identification points to the following avenues of approach, which have been explored with a varied degree of success. Roughly speaking, a tradeoff between computational effort and instrumentation hardware has arisen, resulting in the following two approaches:

1. The identification problem of dynamic systems in the presence of sensor noise can be transformed into a static estimation problem, provided that additional variables are being measured. Hence, this approach is viable, provided that additional sensors are used. This affords the use of ARX models for the identification of dynamic systems with sensor noise. Thus, the inclusion of additional sensors reduces the computational effort. This approach is therefore particularly suitable for on - line SID, as required in adaptive and reconfigurable control. This approach is successfully pursued in Refs. 61-63.

2. Treat the ARMAX models associated with dynamic SID. Thus, a rather careful analysis of the attendant stochastic problem is required. Parsimonious measurements are used, however the algorithms developed are iterative and computationally intensive.

In this chapter the second approach is pursued. In Sec. II.5 the mathematics of Linear Regression are discussed. The results of this section are applied to the identification of ARX and ARMAX models in Secs. II.6 and II.7, respectively. When applied to ARMAX models, the

SID algorithms derived in Sec. II.6 for ARX models give poor estimates. Hence, in Sec. II.7 a careful derivation of a SID algorithm for ARMAX models is given, and in Sec. II.8 a mathematically correct (but physically meaningless) interpretation of a dynamic SID problem involving the ARX model of Sec. II.6 is presented. In Sec. II.9, the concepts developed in Secs. II.6 - II.8 are illustrated in the context of a first-order dynamical system, where the measurements are corrupted by noise. In Sec. II.10 the broader aspects of SID are discussed in the light of the insights provided in Secs. II.6 - II.8. The alternative static approach to (dynamic) SID is briefly discussed in Sec. II.11, followed by concluding remarks in Sec. II.12.

## II. 5 Linear Regression (LR)

The simplest estimation problems are static. Static estimation problems are the object of statistics and are referred to as LR problems. Thus, consider the static LR problem where the parameter vector  $\theta \in \mathbb{R}^n$  needs to be estimated by:

$$Z = H\theta + V \quad (\text{II.1})$$

The "measurement vector" is  $Z \in \mathbb{R}^N$ , and the known regressor  $H$  is an  $N \times n$  matrix. The statistics of the "equation error", or measurement noise,  $V \in \mathbb{R}^N$  are specified:  $V$  is a zero-mean Gaussian random vector whose known covariance matrix is:

$$R = E(VV^T) \quad (\text{II.2})$$

$R$  is an  $N \times N$  real, symmetric and positive definite matrix.

The MV parameter estimate is

$$\hat{\theta}_{MV} = (H^T R^{-1} H)^{-1} H^T R^{-1} Z \quad (\text{II.3})$$

and the estimation error covariance is given by



$$E((\theta - \hat{\theta})(\theta - \hat{\theta})^T) = P_{MV}$$

where the nxn real, symmetric and positive definite matrix is given by

$$P_{MV} = (H^T R^{-1} H)^{-1} \quad (II.4)$$

The following is an important special case: the covariance matrix of the equation error is a scaled identity matrix, i.e.,

$$R = r I_N$$

where r is a positive number. In this case, the parameter estimate is particularly simple, viz.,

$$\hat{\theta}_{LS} = (H^T H)^{-1} H^T Z \quad (II.5)$$

and the estimation error covariance is

$$P_{LS} = r (H^T H)^{-1} \quad (II.6)$$

The estimate, Eq. (II.5), is also referred to as the least squares (LS) estimate.

The crucial advantage of the LS parameter estimate of Eq. (II.5) is its independence from the covariance of the equation error, which in this case is solely determined by the measurement noise intensity r. Furthermore, note that in this important special case where the measurement's error covariance matrix is a scaled identity matrix, the LS estimate is in fact the MV estimate.

The SID route to parameter estimation is rooted in the statistical method of LR<sup>7</sup> which is basically a batch-type algorithm. Hence, the SID algorithms developed in the sequel are readily adaptable to a "moving window" type of algorithm, and hence, are most adept at estimating time-varying parameters and parameters subject to jumps. The following is a useful rule of thumb from statistics: It is "good" to have a large number of measurements, viz., the batch size  $N \approx n^2$ . The batch data processing approach to SID is strongly recommended in this chapter.

## II.6 Linear Regression for System Identification 1

An  $n$ 'th order SISO control system is considered. The dynamical system is:

$$y_{k+1} = a_1 y_k + a_2 y_{k-1} + \dots + a_n y_{k-n+1} + b_1 u_k + b_2 u_{k-1} + \dots + b_m u_{k-m+1}, \quad k = 1, 2, \dots$$

(II.7)

The measurement is:

$$z_{k+1} = y_{k+1} + v_{k+1}$$

(II.8)

where the measurement noise  $v_{k+1}$  is a Gaussian random variable with a variance of  $\sigma^2$ . The measurement noise is white, viz.,  $E(v_k v_\ell) = 0$  for all  $k \neq \ell$  (i.e., there is no correlation).

A naive LR approach to SID entails the "substitution" of Eq. (II.8) into Eq. (II.7), whereupon

$$y_{k+1} = a_1 y_k + a_2 y_{k-1} + \dots + a_n y_{k-n+1} + b_1 u_k + b_2 u_{k-1} + \dots + b_m u_{k-m+1}, \quad k = 1, 2, \dots$$

(II.9)

is obtained. Unwittingly, an ARX model has been arrived at. Concatenating  $N$  measurements yields the LR

$$\begin{bmatrix} y_{k+1} \\ y_{k+2} \\ \vdots \\ y_{k+N} \end{bmatrix} = \begin{bmatrix} y_k & y_{k-1} & \dots & y_{k-n+1} & u_k & u_{k-1} & \dots & u_{k-m+1} \\ y_{k+1} & y_k & \dots & y_{k-n+2} & u_{k+1} & u_k & \dots & u_{k-m+2} \\ \vdots & \vdots & & \vdots & \vdots & \vdots & & \vdots \\ y_{k+N-1} & y_{k+N-2} & \dots & y_{k+N-n} & u_{k+N-1} & u_{k+N-2} & \dots & u_{k-m+N-1} \end{bmatrix} \begin{bmatrix} a_1 \\ \vdots \\ a_n \\ b_1 \\ \vdots \\ b_m \end{bmatrix} + \begin{bmatrix} v_{k+1} \\ v_{k+2} \\ \vdots \\ v_{k+N-1} \end{bmatrix}$$

(II.10)

Next, define

$$\mathbf{Z} = \begin{bmatrix} y_{k+1} \\ y_{k+2} \\ \vdots \\ y_{k+N} \end{bmatrix}_{Nx1} \quad (\text{II.11})$$

$$\mathbf{V} = \begin{bmatrix} v_{k+1} \\ v_{k+2} \\ \vdots \\ v_{k+N} \end{bmatrix}_{Nx1} \quad (\text{II.12})$$

and

$$\mathbf{H} = \begin{bmatrix} y_k & y_{k-1} & \cdots & y_{k-n+1} & u_k & u_{k-1} & \cdots & u_{k-m+1} \\ y_{k+1} & y_k & \cdots & y_{k-n+2} & u_{k+1} & u_k & \cdots & u_{k-m+2} \\ \vdots & \vdots & & \vdots & \vdots & \vdots & & \vdots \\ y_{k+N-1} & y_{k+N-2} & \cdots & y_{k+N-n} & u_{k+N-1} & u_{k+N-2} & \cdots & u_{k-m+N} \end{bmatrix}_{Nx(m+n)} \quad (\text{II.13})$$

The parameter vector is

$$\boldsymbol{\theta} = \begin{bmatrix} a_1 \\ \vdots \\ a_n \\ b_1 \\ \vdots \\ b_m \end{bmatrix}_{(m+n) \times 1}$$

Thus, the LR model in Eq. (II.1) is obtained, where the covariance of the "measurement error" is a scaled unity matrix, i.e.,

$$\mathbf{R} = \mathbf{E}(\mathbf{V}\mathbf{V}^T) = \sigma^2 \mathbf{I}_N$$

Hence, the Minimum Variance estimate is the Least Squares estimate given by Eq. (II.5). The estimation error covariance is given by Eq. (II.6).

In the conventional SID literature, a lot of attention is being

given to the recursive (on the number of recorded measurements  $N$ ) form of the above result. One then refers to Recursive Least Squares (RLS) System Identification. The latter is readily derived using the Bayes formula. Thus, given the parameter estimate  $\theta_N$  and the estimation error covariance matrix  $P_N$  which were arrived at after a data record of length  $N$  has been processed, the latest  $N+1$  measurement satisfies the scalar equation

$$y_{k+N+1} = h\theta + v_{k+N+1} \quad (\text{II.14})$$

where the row vector

$$h_{1 \times (m+n)} = (y_{k+N}, y_{k+N-1}, \dots, y_{k+N-n+1}, u_{k+N}, \dots, u_{k-m+N}) \quad (\text{II.15})$$

The  $(N+1)$ 'th measurement is integrated into the estimation algorithm as follows: The  $N+1$  based measurements estimate is

$$\theta_{N+1} = \theta_N + K(y_{k+N+1} - h\theta_N) \quad (\text{II.16})$$

where the Kalman gain is given by

$$K = \frac{1}{hP_N h^T + \sigma^2} P_N h^T \quad (\text{II.17})$$

and the covariance of the updated estimation is

$$P_{N+1} = P_N - \left[ \frac{1}{hP_N h^T + \sigma^2} \right] P_N h^T h P_N \quad (\text{II.18})$$

Note that additional measurements help to improve the parameter estimate, viz.,  $P_{N+1} \leq P_N$ , as expected. At the same time, the parameter estimate supplied by the RLS algorithm at time  $N$  is identical to the parameter estimate arrived at by applying the batch LR algorithm to the very same data record (of length  $N$ ), provided that the recursive algorithm was initialized at some earlier time  $N' < N$  using the estimate and the estimation error covariance supplied by an application of the batch algorithm to an initial data record of length  $N'$ . This result follows from the application of the Matrix Inversion Lemma<sup>11</sup>.

Now, RLS or LS - based SID algorithms are widely used in the controls community to identify the parameters of control systems [specified by Eqs. (II.7) and (II.8)]. At the same time, their estimation performance is more often than not deficient, viz., the parameter estimate is euphemistically referred to as "biased": RLS or LS - based SID "does not work". The root cause for the failure of the RLS or the LS identification algorithms of Eqs. (II.16) through (II.18) or Eqs. (II.5) and (II.6), respectively, is the sloppy "derivation" of the LR in Eq. (II.9). Hence, in the next section, a proper analysis is undertaken.

## II.7 Linear Regression for System Identification 2

In this Section the identification of an ARMAX model is discussed. Hence, a careful stochastic analysis of the parameter estimation process is required. In this respect, the distinction between the true output of the control system at time  $k$ ,  $y_k$ , and the actually recorded measurement  $z_k$  is crucial. Thus,  $y_k$  is an internal variable governed by the dynamics Eq. (II.1) and is not directly accessible to the observer. The observer records the measurements  $z_k$ , which are related to the internal variable  $y_k$  according to the measurement given by Eq. (II.8). It is here assumed that the input variable  $u_k$  is noiseless.

Use the measurement matrix of Eq. (II.8) to backout the internal variable  $y_\ell$ , for  $\ell = k-n+1, \dots, k+N$  [see, e.g., Eq. (II.7)]. Thus

$$\begin{aligned}
 y_{k-n+1} &= z_{k-n+1} - v_{k-n+1} \\
 &\vdots \\
 y_{k+1} &= z_{k+1} - v_{k+1} \\
 y_k &= z_k - v_k \\
 &\vdots \\
 y_{k+N} &= z_{k+N} - v_{k+N}
 \end{aligned}
 \tag{II.19}$$

Next, insert Eq. (II.19) into Eq. (II.7). Furthermore, define the zero mean Gaussian random variable

$$\tilde{v}_l = v_l - a_1 v_{l-1} - a_2 v_{l-2} - \dots - a_n v_{l-n}, \quad \text{where } l = k+1, \dots, k+N \quad (\text{II.20})$$

Hence, the novel LR obtained is:

$$z_{l+1} = a_1 z_l + a_2 z_{l-1} + \dots + a_n z_{l-n+1} + b_1 u_l + b_2 u_{l-1} + \dots + b_m u_{l-m+1} + \tilde{v}_{l+1},$$

$$l = k, \dots, k+N-1$$

(II.21)

The LR, Eq. (II.21), is in appearance similar to the LR of Eq. (II.9). However, the entries of the Z and H matrices now consist of the actual measurements/observables z, and not the unavailable internal variables y:

$$Z = \begin{bmatrix} z_{k+1} \\ z_{k+2} \\ \vdots \\ z_{k+N} \end{bmatrix}_{N \times 1} \quad (\text{VII.22a})$$

$$H = \begin{bmatrix} z_k & z_{k-1} & \dots & \cdot & z_{k-n+1} & u_k & u_{k-1} & \dots & u_{k-m+1} \\ z_{k+1} & z_k & \dots & \cdot & z_{k-n+2} & u_{k+1} & u_k & \dots & u_{k-m+2} \\ \vdots & \vdots & & & \vdots & \vdots & \vdots & & \vdots \\ z_{k+N-1} & z_{k+N-2} & \dots & z_{k+N-n} & u_{k+N-1} & u_{k+N-2} & \cdot & \dots & u_{k-m+N} \end{bmatrix}_{N \times (mxn)}$$

(II.22b)

Moreover, the "equation error" in Eq. (II.21) is the zero-mean Gaussian random variable

$$\tilde{V} = \begin{bmatrix} \tilde{v}_{l+1} \\ \vdots \\ \tilde{v}_{l+N} \end{bmatrix} \quad (\text{II.23})$$

Now, the calculation of the MV estimate of the parameter associated with the LR of Eq. (II.21) requires the evaluation of the covariance of the equation error. Hence, the expectation

$$R = E(\tilde{V}\tilde{V}^T) \quad (\text{II.24})$$

needs to be calculated. The elements of the real symmetric and positive (semi)definite  $R$  matrix are calculated by invoking Eq. (II.20). Thus, the diagonal elements of the matrix  $R$  are all equal, viz.,

$$R_{i,i} = E(\tilde{V}_{k+1}^2) = E((v_{k+i} - a_1 v_{k+i-1} - \dots - a_n v_{k+i-n})^2) = r = \sigma^2 (1 + \sum_{k=1}^n a_k^2)$$

(II.25)

for all  $i = 1, \dots, N$ . The off diagonal elements of the symmetric equation error covariance matrix are

$$R_{i,j} = E(\tilde{V}_{k+1} \tilde{V}_{k+j}) = \sigma^2 (-a_{i-j} + \sum_{k=1}^{n+j-1} a_k a_{i-j+k}) \quad (\text{II.26})$$

for all  $i = 1, \dots, N$ ,  $j = 1, \dots, N$  and  $i > j$ . For example, the 1,2 element of the equation error covariance matrix is

$$\begin{aligned} R_{1,2} = R_{2,1} &= E(\tilde{V}_{k+1} \tilde{V}_{k+2}) = E((v_{k+1} - a_1 v_k - a_2 v_{k-1} - \dots - a_n v_{k-n+1}) (v_{k+2} - a_1 v_{k+1} - \\ &\quad a_2 v_k - \dots - a_n v_{k-n+2})) \\ &= \sigma^2 (-a_1 + a_1 a_2 + a_2 a_3 + \dots + a_{n-1} a_n) \end{aligned}$$

The off diagonal elements of  $R$  no longer vanish. In other words, the equation error random vector  $\tilde{V}$  is not white, e.g.,

$$E(\tilde{V}_1 \tilde{V}_2) \neq 0$$

and there is correlation in  $\tilde{V}$ . Correlation is responsible for the fact that the LS and MV estimates are no longer identical because in Eq. (II.3) the matrix  $R$  is not a scaled identity matrix. Hence the LS formula Eq. (II.5) no longer yields the MV. That's why the widely used and easy to calculate LS estimate of Eq. (II.5) is "biased", viz., is incorrect. The MV estimate of  $\theta$  in Eq. (II.3) should be used instead.

The calculation of the MV estimate requires the knowledge of  $R$ .

Unfortunately,  $R$  is not a priori known and in addition to the expected dependence on the given sensor's measurement error  $\sigma$ ,  $R$  is also determined by the (as yet unknown) coefficients of the system's transfer function denominator. Thus, it is important to realize that [see, e.g., Eqs. (II.25) and (II.26)]:

$$R = \sigma^2 R'(\theta)$$

This calls for an iterative calculation of the MV estimate. Thus, in Eqs. (II.25) and (II.26) the prior estimate  $\hat{\theta}_0$  of the parameter is used to estimate the covariance matrix  $R$ , following which an improved MV estimate of the parameter  $\hat{\theta}_1$  is obtained from Eq. (II.3). Strictly speaking, the prior estimates of the parameters of the system's dynamics only, which are encapsulated in the coefficients  $a_1, \dots, a_n$ , are used. Thus,

$$R = \sigma^2 R' \begin{pmatrix} a_1 \\ a_2 \\ \vdots \\ a_n \end{pmatrix} \quad (\text{II.27})$$

This process is repeated, and the convergence of the obtained parameter estimate sequence  $\hat{\theta}_i$  is gauged.

Numerical experimentation shows that when the above process converges then the so obtained parameter estimate closely approximates the true parameter.

## II.8 Identification of Dynamic Systems with Process Noise Only

In this section the identification of the parameters of a legitimate ARX model is discussed. The dynamics are:



$$y_{k+1} = a_1 y_k + a_2 y_{k-1} + \dots + a_n y_{k-n+1} + b_1 u_k + b_2 u_{k-1} + \dots + b_m u_{k-m+1} + w_k, \quad k = 1, 2, \dots \quad (\text{II.28})$$

The process noise  $w_k$  is a Gaussian random variable with a variance of  $\sigma^2$ . The process noise is white, viz.,  $E(w_k w_l) = 0$  for all  $k \neq l$  (i.e., there is no correlation). The "measurement" equation is however

$$z_{k+1} = y_{k+1} \quad (\text{II.29})$$

i.e., no measurement error is incurred. Equation (II.29) allows to directly replace  $y_{k-n+1}, \dots, y_{k+N}$  in Eq. (II.28) by the respective observables  $z_{k-n+1}, \dots, z_{k+N}$ . Hence, the LR is:

$$\mathbf{Z} = \mathbf{H}\mathbf{\Theta} + \mathbf{W} \quad (\text{II.30})$$

where the vector  $\mathbf{Z}$  and the Regressor matrix  $\mathbf{H}$  are given by Eq. (II.22) in Sec. II.7, or Eqs. (II.11) and (II.13) in Sec. II.6. Indeed, the LR in Eq. (II.30) is very similar to the LR's obtained in Secs. II.6 and II.7. The main difference is in the equation error vector, viz.,

$$\mathbf{W} = \begin{bmatrix} w_k \\ w_{k+1} \\ \vdots \\ w_{k+N-1} \end{bmatrix} \quad (\text{II.31})$$

The statistics of the vector  $\mathbf{W}$  are however identical to the statistics of the vector  $\mathbf{V}$  in Sec. II.6, viz.,

$$E(\mathbf{W}\mathbf{W}^T) = \sigma^2 \mathbf{I}_N \quad (\text{II.32})$$

The point is that now, the LR of Eq. (II.30) renders a legitimate rendition of the dynamical system given by Eqs. (II.28) and (II.29), as opposed to the development in Sec. II.6 where the entries of the measurement vector  $\mathbf{Z}$  and of the regressor matrix  $\mathbf{H}$  entailed a misrepresentation of the physical reality of the situation as modelled by the dynamics of Eqs. (II.7) and (II.8). Hence, a veritable ARX model has

now been obtained and the LS solution given by Eqs. (II.5) and (II.6), which was incorrectly "derived" in Sec. II.6, is indeed valid for the dynamical system of Eqs. (II.28) and (II.29). In conclusion, in ARX models the LS and MV estimates coincide and hence it is easy to identify the parameter  $\theta$ .

### II.8.1 Discussion

Unfortunately, the dynamical system of Eqs. (II.28) and (II.29), while mathematically plausible is, in a SID context, physically meaningless. This is due to the absence of measurement noise in the stochastic system used in Sec. II.8. Now, measurement noise is a physical fact of life whenever an experiment is performed, and certainly so in SID. Therefore, measurement noise should not be ignored in SID work where the empirical approach to modelling is taken. The stochastic model in Sec. II.8 nevertheless represents a mathematically (albeit, not physically) plausible situation where white Gaussian process noise is entering as a disturbance into the dynamical system. Now, process noise does not induce correlation into the equation error, whereas measurement noise does induce correlation into the measurement error. This is why the LS's estimate is unbiased, viz., the LS approach is mathematically correct and SID appears to "work" in digital computer "experiments" involving ARX models where random effects are introduced into the dynamics in the form of process noise only. But, the LS parameter estimate is invariably biased in the case where measurement noise is present, in which case the correlation in the measurement error causes  $R$  not to be a scaled unity matrix, and consequently the LS formula, Eq. (II.5), no longer yields the MV estimate Eq. (II.3). Hence, ARX modelling and the ensuing LS parameter estimation formulae should not be applied to dynamical systems with measurement noise - see, e.g., Eqs. (II.7) and (II.8).

### II.9 Example

The concepts presented in the previous sections are illustrated in the context of the identification of a first-order control system whose dynamics are:

$$y_{k+1} = ay_k + bu_k, \quad k = 1, 2, \dots \quad (\text{II.33})$$

At time  $k+1$  the measurement equation is

$$z_{k+1} = y_{k+1} + v_{k+1} \quad (\text{II.34})$$

The measurement noise  $v_{k+1}$  is a zero mean Gaussian random variable with variance  $\sigma^2$ . The measurement errors  $v_k$  and  $v_l$  are temporally uncorrelated for all  $k \neq l$ .

The data record for time  $k, k+1, \dots, k+N$  is considered and following the analysis in Sec. II.7, the LR is obtained as follows:

$$\begin{aligned} z_{k+1} &= az_k + bu_k + \tilde{v}_{k+1} \\ z_{k+2} &= az_{k+1} + bu_{k+1} + \tilde{v}_{k+2} \\ &\vdots \\ z_{k+N} &= az_{k+N-1} + bu_{k+N-1} + \tilde{v}_{k+N} \end{aligned} \quad (\text{II.35})$$

Let

$$\mathbf{Z} = \begin{bmatrix} z_{k+1} \\ z_{k+2} \\ \vdots \\ z_{k+N} \end{bmatrix}, \quad \mathbf{H} = \begin{bmatrix} z_k & u_k \\ z_{k+1} & u_{k+1} \\ \vdots & \vdots \\ z_{k+N-1} & u_{k+N-1} \end{bmatrix}, \quad \tilde{\mathbf{V}} = \begin{bmatrix} \tilde{v}_{k+1} \\ \tilde{v}_{k+2} \\ \vdots \\ \tilde{v}_{k+N} \end{bmatrix} \quad (\text{II.36})$$

and the parameter vector is

$$\boldsymbol{\Theta} = \begin{bmatrix} a \\ b \end{bmatrix}$$

The covariance matrix of the "equation error" is

$$R = E \left( \begin{bmatrix} \tilde{v}_{k+1} \\ \tilde{v}_{k+2} \\ \vdots \\ \tilde{v}_{k+N} \end{bmatrix} \begin{bmatrix} \tilde{v}_{k+1} & \tilde{v}_{k+2} & \dots & \tilde{v}_{k+N} \end{bmatrix} \right) \quad (\text{II.37})$$

Hence,

$$R = E \left( \begin{bmatrix} v_{k+1} - av_k \\ v_{k+2} - av_{k+1} \\ \vdots \\ v_{k+N} - av_{k+N-1} \end{bmatrix} \begin{bmatrix} v_{k+1} - av_k & v_{k+2} - av_{k+1} & \dots & v_{k+N} - av_{k+N-1} \end{bmatrix} \right)$$

$$= \begin{bmatrix} E((v_{k+1}-av_k)(v_{k+1}-av_k)) & E((v_{k+1}-av_k)(v_{k+2}-av_{k+1})) & \dots & \dots \\ E((v_{k+2}-av_{k+1})(v_{k+1}-av_k)) & E((v_{k+2}-av_{k+1})(v_{k+2}-av_{k+1})) & \dots & \dots \\ \vdots & \vdots & \ddots & \vdots \\ E((v_{k+N}-av_{k+N-1})(v_{k+1}-av_k)) & E((v_{k+N}-av_{k+N-1})(v_{k+2}-av_{k+1})) & \dots & \dots \end{bmatrix}$$

(II.38)

Thus, the equation error covariance is the tridiagonal NxN matrix:

$$R = \sigma^2 \begin{bmatrix} 1+a^2 & -a & 0 & 0 & 0 & 0 & 0 \\ a & 1+a^2 & -a & 0 & 0 & 0 & 0 \\ 0 & -a & 1+a^2 & -a & 0 & 0 & 0 \\ 0 & 0 & 0 & 0 & -a & 1+a^2 & -a \\ 0 & 0 & 0 & 0 & 0 & -a & 1+a^2 \end{bmatrix} \quad (\text{II.39})$$

R is invertible, since for  $a \neq 1$

$$\det [R] = \frac{a^{2(N+1)} - 1}{a^2 - 1}$$

and for  $a \neq 1$

$$\det [R] = N + 1$$

Hence, in order to identify the parameters a and b of the above ARMAX model, and as outlined in Sec. II.7, the following iteration for the estimation of the control system's parameters is obtained:

$$\begin{bmatrix} \tilde{a}_{i+1} \\ \tilde{b}_{i+1} \end{bmatrix} = \left( \begin{bmatrix} z_k & z_{k+1} & \cdots & z_{k+N-1} \\ u_k & u_{k+1} & \cdots & u_{k+N-1} \end{bmatrix} \begin{bmatrix} 1+\tilde{a}_i^2 & -\tilde{a}_i & 0 & 0 & 0 & 0 \\ -\tilde{a}_i & 1+\tilde{a}_i^2 & -\tilde{a}_i & 0 & 0 & 0 \\ 0 & 0 & . & . & . & 0 \\ 0 & 0 & 0 & 0 & -\tilde{a}_i & 1+\tilde{a}_i^2 \end{bmatrix} \right)^{-1} X$$

$$\begin{bmatrix} z_k & u_k \\ z_{k+1} & u_{k+1} \\ \vdots & \vdots \\ z_{k+N-1} & u_{k+N-1} \end{bmatrix}^{-1} \begin{bmatrix} z_k & z_{k+1} & \cdots & z_{k+N-1} \\ u_k & u_{k+1} & \cdots & u_{k+N-1} \end{bmatrix} X$$

$$\begin{bmatrix} 1+\tilde{a}_i^2 & -\tilde{a}_i & 0 & 0 & 0 & 0 \\ -\tilde{a}_i & 1+\tilde{a}_i^2 & -\tilde{a}_i & 0 & 0 & 0 \\ . & . & . & . & . & . \\ 0 & 0 & 0 & 0 & 1+\tilde{a}_i^2 & -\tilde{a}_i \\ 0 & 0 & 0 & 0 & -\tilde{a}_i & 1+\tilde{a}_i^2 \end{bmatrix}^{-1} \begin{bmatrix} z_{k+1} \\ z_{k+2} \\ \vdots \\ z_{k+N} \end{bmatrix}$$

(II.40)

Furthermore, the estimation error's covariance matrix is

$$P = \sigma^2 P' \quad (II.41)$$

where the 2x2 matrix  $P'$  is:

$$\begin{pmatrix} \begin{bmatrix} z_k & z_{k+1} & \dots & z_{k+N-1} \\ u_k & u_{k+1} & \dots & u_{k+N-1} \end{bmatrix} \begin{bmatrix} 1+\tilde{a}^2 & -\tilde{a} & 0 & 0 & 0 & 0 \\ -\tilde{a} & 1+\tilde{a}^2 & -\tilde{a} & 0 & 0 & 0 \\ 0 & -\tilde{a} & 1+\tilde{a}^2 & -\tilde{a} & 0 & 0 \\ 0 & 0 & 0 & 0 & 0 & 0 \\ 0 & 0 & 0 & 0 & -\tilde{a} & 1+\tilde{a}^2 \end{bmatrix}^{-1} \\ \begin{bmatrix} z_k & u_k \\ z_{k+1} & u_{k+1} \\ \vdots & \vdots \\ z_{k+N-1} & u_{k+N-1} \end{bmatrix}^{-1} \end{pmatrix} x$$

(II.42)

For example, if two measurements are taken ( $N = 2$ ), the following explicit parameter estimation formulae for a first-order ARMAX model are obtained:

$$P = \frac{\sigma^2}{(1 + \hat{a}^2 + \hat{a}^4) (u_k z_{k+1} - u_{k+1} z_k)} P'' \quad (\text{II.43})$$

where the elements of the  $2 \times 2$   $P''$  matrix are:

$$\begin{aligned} p_{11}' &= (1 + \hat{a}^2) (u_k^2 + u_{k+1}^2) + 2\hat{a}u_k u_{k+1} \\ p_{12}' &= - (1 + \hat{a}^2) (u_k z_k + u_{k+1} z_{k+1}) - \hat{a}(u_k z_{k+1} + u_{k+1} z_k) \\ p_{21}' &= - (1 + \hat{a}^2) (u_k z_k + u_{k+1} z_{k+1}) - \hat{a}(u_k z_{k+1} + u_{k+1} z_k) \\ p_{22}' &= (1 + \hat{a}^2) (z_k^2 + z_{k+1}^2) + 2\hat{a}z_k z_{k+1} \end{aligned}$$

and the parameter estimates are:

$$\hat{a}_{MV_{i+1}} = \frac{1}{(u_k z_{k+1} - u_{k+1} z_k)^2} [(1 + \hat{a}_i^2 + \hat{a}_i^4) (u_k z_{k+1} - u_{k+1} z_k) (u_k z_{k+2} - u_{k+1} z_{k+1}) + 2\hat{a}_i (1 + \hat{a}_i^2) (u_k z_{k+1} + u_{k+1} z_{k+2}) (u_k z_{k+1} + u_{k+1} z_k)] \quad (\text{II.44a})$$

$$\begin{aligned} \hat{\delta}_{MV_{i+1}} = & \frac{1}{(u_k z_{k+1} - u_{k+1} z_k)^2} [(1 + a^2)(z_k^2 + z_{k+1}^2) + 2az_k z_{k+1}] \times \\ & [(1 + a^2)(u_k z_{k+1} + u_{k+1} z_{k+2}) + a(u_k z_{k+2} + u_{k+1} z_{k+1})] - \\ & [(1 + a^2)(u_k z_k + u_{k+1} z_{k+1}) - a(u_k z_{k+1} + z_k u_{k+1})] \times \\ & [(1 + a^2)(z_k z_{k+1} + z_{k+1} z_{k+2}) + a(z_k z_{k+2} + z_{k+1}^2)] \end{aligned} \quad (\text{II.44b})$$

The estimation errors  $\sigma$ 's are:

$$\begin{aligned} \sigma_a &= \frac{\sigma}{u_k z_{k+1} - u_{k+1} z_k} \sqrt{(1 + \hat{a}^2)(u_k^2 + u_{k+1}^2)} \\ \sigma_b &= \frac{\sigma}{u_k z_{k+1} - u_{k+1} z_k} \sqrt{(1 + \hat{a}^2)(z_k^2 + z_{k+1}^2) + 2\hat{a}z_k z_{k+1}} \end{aligned} \quad (\text{II.45})$$

It is appreciated that the source of difficulty in SID is correlation. The latter is caused by measurement (sensor) noise, not process noise. Hence, it is most instructive to reconsider the identification of this first-order control system in the case where a disturbance, viz., process noise, enters the system and there is no measurement noise. As discussed in Sec. II.8, this yields a legitimate ARX model.

The system dynamics are

$$y_{k+1} = ay_k + bu_k + w_k, \quad k = 1, 2, \dots \quad (\text{II.46})$$

The process noise is a zero mean Gaussian random variable with variance  $\sigma^2$  and the process noise sequence is white, viz.,  $E(w_k w_l) = 0$  for all  $k \neq l$ . The measurement equation is

$$z_{k+1} = y_{k+1} \quad (\text{II.47})$$

Since  $y_k = z_k$  and  $y_{k+1} = z_{k+1}$ , the following holds:

$$z_{k+1} = az_k + bu_k + w_k \quad (\text{II.48})$$

Hence, according to the development in Sec. II.8, the following LR is obtained:

$$\begin{bmatrix} z_{k+1} \\ z_{k+2} \\ \vdots \\ z_{k+N} \end{bmatrix} = \begin{bmatrix} z_k & u_k \\ z_{k+1} & u_{k+1} \\ \vdots & \vdots \\ z_{k+N-1} & u_{k+N-1} \end{bmatrix} \begin{bmatrix} a \\ b \end{bmatrix} + \begin{bmatrix} w_k \\ w_{k+1} \\ \vdots \\ w_{k+N-1} \end{bmatrix}$$

Define

$$\mathbf{Z} = \begin{bmatrix} z_{k+1} \\ z_{k+2} \\ \vdots \\ z_{k+N} \end{bmatrix}, \quad \mathbf{H} = \begin{bmatrix} z_k & u_k \\ z_{k+1} & u_{k+1} \\ \vdots & \vdots \\ z_{k+N-1} & u_{k+N-1} \end{bmatrix}, \quad \mathbf{W} = \begin{bmatrix} w_k \\ w_{k+1} \\ \vdots \\ w_{k+N-1} \end{bmatrix}$$

Now

$$\mathbf{R} = E(\mathbf{W}\mathbf{W}^T) = \sigma^2 \mathbf{I}_N \quad (\text{II.49})$$

viz., the covariance matrix of the equation error is a scaled identity matrix. Hence, the LS estimate is correct, namely the parameter estimate is:

$$\begin{bmatrix} \hat{a} \\ \hat{b} \end{bmatrix} = (\mathbf{H}^T \mathbf{H})^{-1} \mathbf{H}^T \mathbf{Z}$$

$$= \begin{bmatrix} \sum_{i=1}^N z_{k+i-1}^2 & \sum_{i=1}^N z_{k+i-1} u_{k+i-1} \\ \sum_{i=1}^N z_{k+i-1} u_{k+i-1} & \sum_{i=1}^N u_{k+i-1}^2 \end{bmatrix}^{-1} \begin{bmatrix} z_k & z_{k+1} & \cdots & z_{k+N-1} \\ u_k & u_{k+1} & \cdots & u_{k+N-1} \end{bmatrix} \begin{bmatrix} z_{k+1} \\ z_{k+2} \\ \vdots \\ z_{k+N} \end{bmatrix} \quad (\text{II.50})$$

Thus, the explicit formulae for the LS parameter estimates are

$$\hat{a}_{LS} = \frac{\sum_{i=1}^N u_{k+i-1}^2 \sum_{i=1}^N z_{k+i} z_{k+i-1} - \sum_{i=1}^N u_{k+i-1} z_{k+i-1} \sum_{i=1}^N z_{k+i} u_{k+i-1}}{\sum_{i=1}^N u_{k+i-1}^2 \sum_{i=1}^N z_{k+i-1}^2 - (\sum_{i=1}^N u_{k+i-1} z_{k+i-1})^2}$$



$$\hat{b}_{LS} = \frac{\sum_{i=1}^N z_{k+i-1}^2 \sum_{i=1}^N z_{k+i} u_{k+i-1} - \sum_{i=1}^N u_{k+i-1} z_{k+i-1} \sum_{i=1}^N z_{k+i} z_{k+i-1}}{\sum_{i=1}^N u_{k+i-1}^2 \sum_{i=1}^N z_{k+i-1}^2 - (\sum_{i=1}^N u_{k+i-1} z_{k+i-1})^2}$$

(II.51)

No iterations are required.

Moreover, the estimation error covariance is

$$\begin{aligned} P &= \sigma^2 (H^T H)^{-1} \\ &= \sigma^2 \begin{bmatrix} \sum_{i=1}^N z_{k+i-1}^2 & \sum_{i=1}^N z_{k+i-1} u_{k+i-1} \\ \sum_{i=1}^N z_{k+i-1} u_{k+i-1} & \sum_{i=1}^N u_{k+i-1}^2 \end{bmatrix}^{-1} \end{aligned}$$

viz., the  $\sigma$  of the estimation error of the system's a and b parameters is:

$$\begin{aligned} \sigma_a &= \sigma \frac{\sqrt{\sum_{i=1}^N u_{k+i-1}^2}}{\sqrt{\sum_{i=1}^N u_{k+i-1}^2 \sum_{i=1}^N z_{k+i-1}^2 - (\sum_{i=1}^N u_{k+i-1} z_{k+i-1})^2}} \\ \sigma_b &= \sigma \frac{\sqrt{\sum_{i=1}^N z_{k+i-1}^2}}{\sqrt{\sum_{i=1}^N u_{k+i-1}^2 \sum_{i=1}^N z_{k+i-1}^2 - (\sum_{i=1}^N u_{k+i-1} z_{k+i-1})^2}} \end{aligned}$$

(VII.52)

Finally, it is most instructive to compare the direct LS estimate of Eqs. (II.51) and (II.52), and the MV estimate of Eqs. (II.44) and (II.45).

### II.9.1 Identification Experiment

Simulation experiments validate the above insights and derivation. The truth model's parameters are:

$$a = 0.95 \quad \text{and} \quad b = 1$$

and the intensity of the measurement noise is determined by  $\sigma = 0.1$ . The input signal is

$$u_k = \sin(0.1 k), \quad k = 0, 1, \dots, 9$$

and the prior information is

$$\begin{aligned} \hat{a}_0 &= 0.8 \\ \hat{b}_0 &= 1.2 \end{aligned} \quad (\text{II.53})$$

or

$$\begin{aligned} \hat{a}_0 &= 0.5 \\ \hat{b}_0 &= 1.5 \end{aligned} \quad (\text{II.54})$$

The LS estimate is given by Eqs. (II.51) and (II.52), viz.,

$$\begin{aligned} \hat{a} &= 0.9390 \\ \hat{b} &= 1.0257 \end{aligned} \quad (\text{II.55})$$

and the estimation error sigma's are

$$\begin{aligned} \sigma_a &= 0.022 \\ \sigma_b &= 0.065 \end{aligned} \quad (\text{II.56})$$

The MV parameter estimate is iteratively determined according to formulae Eqs. (II.40)-(II.42). The (fast) convergence of the estimates is graphically illustrated in Figs. II.1 and II.2 for the prior information of Eqs. (II.53) and (II.54), respectively. The identification results are summarized in Table II.1.

$\hat{a}_0$	$\hat{b}_0$	$\hat{a}_1$	$\hat{b}_1$	$\hat{a}$	$\hat{b}$
0.8	1.2	0.9425	1.0177	0.9427	1.0173
0.5	1.5	0.9415	1.0200	0.9427	1.0173

Table II.1 Estimation Performance

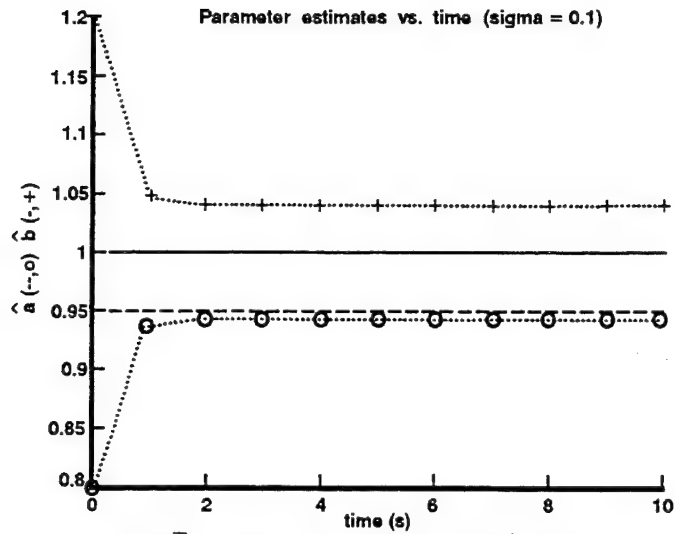


Fig. I.1 Iterated Parameter Estimates ( $\hat{a}_0 = 0.8$ ,  $\hat{b}_0 = 1.2$ )

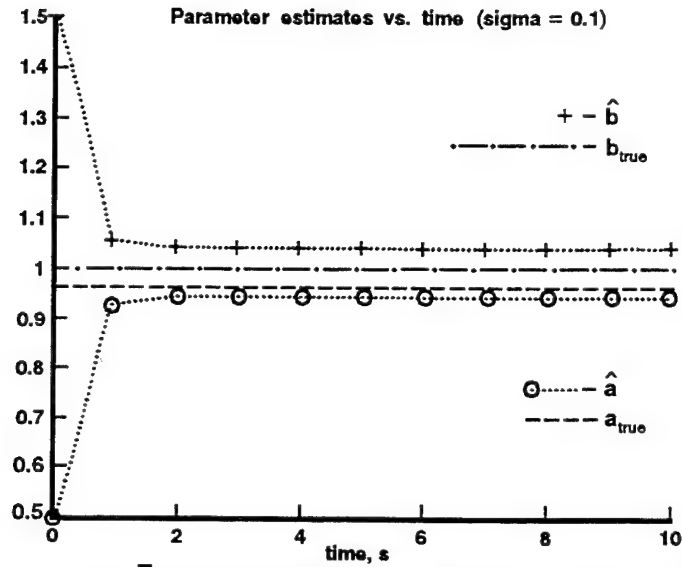


Fig. I.2 Iterated Parameter Estimates ( $\hat{a}_0 = 0.5$ ,  $\hat{b}_0 = 1.5$ )

The estimation error sigma's are

$$\sigma_a = 0.042 \quad \text{and} \quad \sigma_b = 0.108 \quad (\text{II.57})$$

and

$$\sigma_a = 0.05 \quad \text{and} \quad \sigma_b = 0.14 \quad (\text{II.58})$$

for the prior information Eqs. (II.53) and (II.54), respectively.

The experimental results show that

1. The MV estimates are superior to the LS estimates.
2. The calculated confidence level in the MV estimates is lower than in the LS estimates.

Item 2 suggests that the SID scheme based on MV estimation is less prone to the notorious "divergence" of EKF's. Indeed, it is most reasonable to gauge the estimation performance of a SID algorithm using the following metric:

$$\frac{|\hat{a} - a|}{\sigma_a} + \frac{|\hat{b} - b|}{\sigma_b}$$

The conclusion can be made, based upon these two items, that the performance of the SID scheme that is based on MV estimation is superior to the LS based SID, as is to be expected.

## II.10    "Crimes" of System Identification (SID)

Pathological work in SID is performed on two fronts: theory and experimental, as is discussed in this section.

### II.10.1    Theory

In the SID literature there is a strong emphasis on LS estimation, in particular, of the recursive variety. While randomness is included in many investigations, this is done by introducing process noise into the dynamics. Hence, correlation is absent and ARX models are analyzed. Therefore, the LS parameter estimate will be unbiased, i.e., the LS estimate is correct and SID is then easy. Unfortunately, the absence of measurement noise in SID, which inherently is of an empirical and experimental nature, strongly detracts from the physical motivation of this line of work.

It is important to recognize that SID resides in the realm of nonlinear filtering. This is true even for linear dynamical systems with measurement noise. This is in contrast to the state estimation problem in linear systems, which is a linear filtering problem. Now, the situation is further obscured by the use of LR models in SID. This brings about a superficial similarity of the state estimation and SID problems and causes the distinction between the two paradigms to be blurred. Whereas LS estimation is correct in the linear problem of state estimation, the sloppy transposition of the LS method to the nonlinear problem of SID has disastrous consequences. In SID the MV estimation method, augmented by iterations, must be used.

It is even more unfortunate that this "research" can be successfully conducted on digital computers. It is too easy to simulate dynamical systems on digital computers where no measurement error is incurred. Indeed, in the double precision environment of MATLAB and/or MATRIX, the Signal to Noise Ratio (SNR) of numerical noise is very high and is approximately 340 dB. Hence, the digital computer provides a very clean, almost sterilized and unreal environment, where physically infeasible experiments that entail no measurement noise, as described in Sec. II.8, can be conducted - for, after all, the digital computer is a mathematical (or thinking) machine. In contrast, in the analogue world, namely, in physical hardware and in the real world, the best achievable SNR is approximately 60 dB which is a far cry from the clean environment of the digital computer. Hence, these theoretical numerical investigations, which oftentimes are "validated" by digital simulations, have little bearing on engineering applications.

It is unfortunate that a lot of emphasis is being put in the literature on "numerically stable" algorithms for SID. It is maintained that this is tantamount to "barking up the wrong tree". These comments apply to both static and dynamic models. While it is true that the regressor matrix needs to be inverted, it is maintained that relatively unsophisticated numerical matrix inversion algorithms should suffice for the purpose of SID. Namely, there is no need for matrix inversion algorithms that can contend with very high regressor

condition numbers where even the very low level of machine induced numerical noise can cause problems. To see this point, consider the static problem of LR of Eq. (II.1). Attention is called to the result from numerical analysis

$$\frac{||\Delta\theta||}{||\theta||} \leq \kappa \frac{||\Delta Z||}{||Z||} \quad (\text{II.59})$$

which relates the norm of the parameter estimation error to the norm of the equation error (the latter is directly related to the measurement error intensity  $\sigma$  and to the condition number  $\kappa$  of the regressor matrix  $H$ ). The expression given by Eq. (II.59) provides an estimate of the parameter accuracy. Due to the relatively low SNR (approximately 60 dB) and therefore high noise levels encountered in the (real) physical world, the estimation results will become very inaccurate at regressor condition numbers less than a couple of hundreds. Consequently, one need not bother with the inversion of ill conditioned regressor matrices which are difficult to invert because their condition number is in the  $10^{15}$ , where the conditions are ripe for even the very small numerical noise (of approximately  $0.3 \times 10^{-17}$ ) to induce large computation errors.

The emphasis and insistence on recursive, as opposed to batch, SID algorithms is most unfortunate. This is for the following reasons:

1. Recursive estimation requires initialization of the algorithm. If no prior information is available or the prior information is inaccurate, it might contaminate the data driven parameter estimate. Furthermore, it might take a long time for the so caused bad estimates to "wash out of the system".
2. In SID the temporal extent of the data record must be commensurate with the dynamical system's bandwidth in order for the SID experiment to be conducted under conditions of "good excitation", and consequently for the parameter estimate to be reliable. This mandates that the length of the data window in batch SID algorithms must be sufficiently long. While the parameter estimate arrived at the end of a recursive computation using the data in the batch

algorithm's window is identical with the batch SID algorithm supplied estimate, the intermediate parameter estimates generated by a recursive algorithm are obviously based on too short a data record and are therefore unreliable and useless.

### II.10.2 Experimental

As explained in Sec. II.10.1, process noise is benign compared to correlation inducing measurement noise. If no correlation is present the LS estimate is correct. It is therefore deplorable that oftentimes SID algorithms are proposed and then "validated" in a totally noiseless, i.e., in a deterministic environment. Almost every SID algorithm will work in a deterministic environment (in particular, if measurement noise is absent). This "research" is made possible by the sterilized environment of the digital computer with double precision arithmetic. The exercise of these "System Identification" algorithms in an environment where measurement noise has been introduced has a dramatic effect, and the consequences for identification are disastrous.

Furthermore, since in a deterministic environment the only noise present is numerical noise, and the latter is of a very low intensity, the required "identification" interval is very short. This observation has some consequences as far as robust control is concerned. Indeed, the current robust control paradigms are deterministic. Since feedback control is used in robust control, i.e., the system's output is being measured, one could argue that in robust control everything is in place for indirect adaptive control; in other words, all the data is available for a quick and accurate identification of the plant's parameters. Hence, after a very short initial time interval, the plant parameters will be known and the need for robust control which addresses plant uncertainty, is obviated. Obviously, the possible presence of unmodelled input disturbances stands in the way of the proposed approach, even though these could be easily identified in a deterministic (with no measurement noise) environment.

In conclusion, "experiments" with no measurement noise make no

physical sense, neither in SID, nor in robust and/or adaptive control. Not only is the nonlinear nature of SID not fully appreciated, but so is its inverse problem facet. To be concise, under conditions of mediocre excitation, vastly different plants, when subject to the same input, could yield output signals which are very close. In other words, the condition number of the regressor matrix could be relatively large, say a couple of hundreds. Therefore, the following often used "experiment" is flawed and does not help to validate a proposed SID algorithm.

1. Given the input/output pair, invoke the SID algorithm and identify the plant.
2. Apply the input to the so identified plant and calculate (viz., simulate) the output.
3. Verify that the simulated output is indeed close to the output signal used in the identification process.

Based on this "experiment" it is claimed that this is proof that the proposed SID algorithm "works", viz., it is believed that the identified parameters must be close to the true parameters. In reality, this is just a manifestation of an elevated condition number of the linear operator  $H$ , and the identified parameters could be far off the true parameters.

Unfortunately, naively derived (e.g., LS based) SID algorithms don't work. To see this, choose a new input signal and use the identified plant in a simulation in order to obtain a new output signal. Give the new input-output pair to the proposed SID algorithm. In most cases a new plant will be identified which, unfortunately, has little in common with the originally identified plant. Hence, obtaining a small output error is no proof that a SID algorithm works.

The following is a correct validation process for the determination of the effectiveness of a SID algorithm. Thus, as in Sec. II.9.1, the following controlled experiment should be performed:



1. Chose a plant. Thus, the true values of the plant's parameters are known to the experimenter.
2. Chose an input signal and apply it to the known plant. Thus, a simulation is performed in order to obtain the plant's output signal.

Remark: At this stage, also process noise may be injected into the control system.

3. Corrupt the recorded output signal with measurement noise.
4. Give the chosen input signal and the noise corrupted output signal to the SID algorithm and obtain the identified plant's parameters.
5. To assess the performance of the proposed SID algorithm, compare the identified parameters with the original plant parameters used in the simulation.

In light of the above recommended validation procedure for SID, it is sad to see that sometimes the correctness of an identification algorithm is claimed in the literature based on the realization of a small output error and the use of "real" data - where, experimentally obtained data in fact excludes the availability of an underlying dynamical model, and thus absolves the author of the paper from any meaningful evaluation of the proposed SID algorithm's performance.

### II.11 Static Identification

The approach presented in this section differs from the standard formulation of the SID problem in the controls literature, in that the ARMAX model is not used. Instead, and as mentioned in Sec. II.1, a static approach is opted for, which gives rise to an easy to identify ARX model. The algorithmic respite is acquired not without a price, because additional sensors are required.

Strictly speaking, it is postulated that direct measurements of the state vector and its derivatives are available. Obviously, these signals are sampled, but the continuous time dynamical system is not discretized. This measurements - rich scenario is conducive to the elimination of correlation and allows the posing of a static estimation problem - as opposed to the standard ARMAX dynamical model. This then opens the way to directly and rigorously employing the linear LR statistical method, which exclusively applies to static models. The static nature of the LR formulation, in turn, ensures that measurement (or sensor) noise does not "bias" the estimate - as is the case in ARMAX models.

Also in static SID the measurement error covariance matrix  $R$  is not known, for it is  $\theta$  dependent, and the parameter  $\theta$  has yet to be identified. However, a careful stochastic analysis of the static SID method reveals that viz.,  $R$  is a scaled unity matrix, and hence the MV estimate of  $\theta$  can be readily determined using the LS method and is independent of  $\theta$ . Hence, no iterations are required. Moreover, the measurement error's intensity  $\sigma$  can be empirically estimated. Finally, the estimates  $\hat{\theta}$  and  $\sigma$  are used in Eq. (II.4) to obtain the parameter estimation error covariance.

Indeed, the inherently nonlinear SID problem is being transformed into a linear parameter estimation problem. In addition, the vast body of statistical methods and knowledge<sup>7</sup> can be brought to bear on the static SID method. Hence, the following insights are arrived at.

Concerning the number of parameters to be identified, the identification accuracy will increase if the number of parameters to be identified is decreased. Indeed, the net effect of including prior information in the identification algorithm is equivalent to a reduction in the number of parameters subject to identification. In this respect, realize that prior information encompasses the following.

(a) Direct prior information:

(1) Order of system, e.g., in flight mechanics, and for fixed wing aircraft<sup>9</sup>, the order of the "pitch channel" is four.

(2) In flight control work relationships among the parameters from, e.g., flight mechanics are advantageously employed.

(b) Indirect prior information:

Knowledge of the system's bandwidth is instrumental in the selection of the length of the identification interval.

Even at the price of introducing a modelling error, the reduction in the number of parameters to be identified proves beneficial. For example, in flight control<sup>9</sup>, when the small phugoid stability derivatives are equated to zero, an improvement in the short period stability and control derivatives estimates is recorded - provided that the duration of the identification interval is commensurate with the short period (and not the long duration of the phugoid).

Light is shed on the somewhat nebulous notion of "excitation." High amplitude inputs to linear systems enhance the "excitation" level, for the SNR is obviously increased. However, "excitation" has more far reaching consequences in SID than the above mentioned direct scaling effect. Excitation is in part determined by the physical length of the identification time interval and not necessarily by the number of measurements. While it is true that for a predetermined SNR, increasing the number of measurements will reduce the calculated estimation error variance, under poor "excitation" the latter might in fact impair the quality of the identified parameter, and bring about "divergence". Furthermore, the physical length of the identification interval is determined by the bandwidth (BW) of the recorded signals. "Slow" signals require a long identification time interval. Indeed, time scale considerations are important in Dynamical Systems and in System Identification work. Specifically, in the flight control context reference is made to:

BW of short period v.s. phugoid and

BW of  $\alpha$  and  $q$  variables ( $\alpha$  is the angle of attack and  $q$  is the pitch rate) in the respective (normal force)  $Z$  and  $M$  (moment) equations.

In conclusion, the static approach to SID is particularly suitable for on-line work, and has successfully been applied to indirect adaptive and reconfigurable control. In Refs. 62-64 static SID is applied to a flight control problem where the challenge of accommodating time varying plant parameters, and indeed, abrupt changes brought about by a control surface failure, is met. For a general reference on adaptive control see, e.g., Reference 4.

## II.12 Summary

Insights into the most fundamental aspects of SID have been obtained. It is true that in the absence of measurement noise ( $\text{SNR} \rightarrow \infty$ ), the identification of a discrete time system using a digital computer is an easy task. Almost any identification algorithm will work in the absence of measurement noise. In practice, however, measurement noise causes correlation and unaccounted for correlation is responsible for "bias" in the estimated parameters. Hence, the all important correlation problem, which is induced by measurement noise in dynamical systems, needs to be directly addressed. This is the main theme of this chapter. A LR - based MV algorithm with iterations has been developed.

Furthermore, the identification accuracy is determined by the measurements' SNR, and also by the number of parameters to be identified, and by the level of "excitation" of the identification "experiment". These can be summarized as follows:

- Min time to ID =  $f(\text{BW, number of parameters, excitation, SNR})$
- Quality of estimate =  $f(\text{Window length} = N, \text{SNR})$
- Constraints improve estimate and shorten the identification time

## Chapter III Multiple-Input Multiple-Output (MIMO) Plants: Structured Plant Parameter Uncertainty

### III.1 Introduction

The quantitative feedback theory (QFT) synthesis technique for highly structured uncertain linear-time-invariant (LTI) MIMO plants has the following features<sup>32</sup>

1. It is quantitative in nature. The extent of parameter uncertainty is defined a priori and so are the tolerances on the system responses to the cross-coupling interaction  $c_{ij}$  and to external disturbance functions  $(d_e)_{ij}$ .
2. The synthesis problem is converted into a number of single-loop problems, in which structured parameter uncertainty, external disturbance, and performance tolerances are derived from the original MIMO problem. The solutions to these single-loop problems are guaranteed to work for the MIMO plant. It is not necessary to consider the system characteristic equation. Any technique may be used for the single-loop design problems -- state space, frequency response, or even cut and try.
3. The design is tuned to the extent of the uncertainty and the performance tolerances. The design for a MIMO system, as stated previously involves the design of an equivalent set of MISO system feedback loops. The design process for these individual loops is the same as the design of a MISO system described in Chap. I. In general, an  $m \times l$  open-loop MIMO plant can be represented in matrix notation as

$$y(t) = Pu(t) \quad (\text{III.1})$$

where  $y(t)$  =  $m$ -dimensional plant output vector  
 $u(t)$  =  $l$ -dimensional plant input vector  
 $P$  =  $m \times l$  plant transfer function matrix relating  $u(t)$  to  $y(t)$

Consider the MIMO plant of Fig III.1 for which  $P$  is a member of  $\mathcal{P}$  ( $P \in \mathcal{P}$ ), the set of all plant transfer functions relating each input to each output. When a system has variable parameters, which are known or unknown, the transfer function matrix of the plant may be represented by the associated set  $\{p_1, p_2, \dots\}$ . This set of transfer function matrices is contained in  $\mathcal{P}$ . The design method requires that the uncertainty in  $P$  be known or is at least bounded. In any MIMO system with  $m$  inputs there are at most  $m$  outputs which can be independently controlled<sup>18</sup>. Therefore, the same dimensions,  $l = m$ , are used for both the input and output vectors in the design procedure presented here. If the model defines an unequal number of inputs and outputs, the first step is to modify the model so that the dimensions of the input and output are the same. The system is then defined as being of order  $m \times m$ .

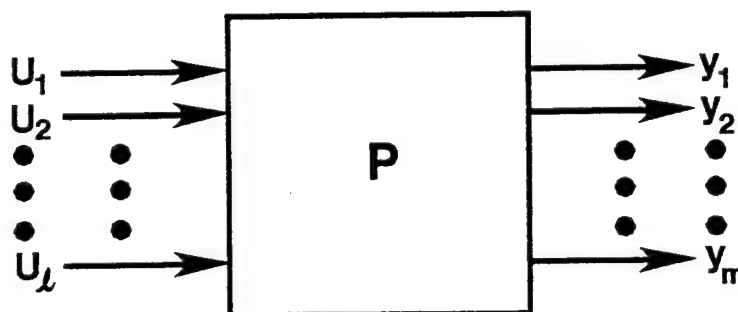


**Fig.III .1 A MIMO plant.**

Horowitz has shown, (see Sec. III.6) by using fixed point theory<sup>21,23</sup> that the MIMO problem for an  $m \times m$  system can be separated into  $m$  equivalent single-loop MISO systems and  $m^2$  prefilter/cross-coupling problems, which are each designed as outlined in Chap. I<sup>17,32</sup>. The cross-coupling is akin to the disturbance  $D$  of Fig. I.5.

### III.2 The MIMO Plant

The  $P$  matrix may be formed from either the system state space matrix representation or from the system linear differential equations. The state space representation for a LTI MIMO system is:

$$\begin{aligned}\dot{\mathbf{x}}(t) &= \mathbf{A}\mathbf{x}(t) + \mathbf{B}u(t) \\ \mathbf{y}(t) &= \mathbf{C}\mathbf{x}(t)\end{aligned}\tag{III.2}$$

where the  $\mathbf{A}$ ,  $\mathbf{B}$  and  $\mathbf{C}$  are constant matrices. The plant transfer function matrix  $\mathbf{P}$  is evaluated as

$$\mathbf{P}(s) = \mathbf{C}[s\mathbf{I} - \mathbf{A}]^{-1}\mathbf{B}\tag{III.3}$$

If the plant model consists of  $m$  coupled linear-time-invariant differential equations, the general plant model for a MIMO system with two inputs and two outputs has the form:

$$\begin{aligned}a(s)y_1(s) + b(s)y_2(s) &= fu_1(s) + gu_2(s) \\ c(s)y_1(s) + d(s)y_2(s) &= hu_1(s) + iu_2(s)\end{aligned}\tag{III.4}$$

where  $a(s)$  through  $d(s)$  are polynomials in  $s$ ,  $f$  through  $i$  are constant coefficients,  $y_1(s)$  and  $y_2(s)$  are the outputs, and  $u_1(s)$  and  $u_2(s)$  are the inputs. In matrix notation the system is represented by:

$$\begin{bmatrix} a(s) & b(s) \\ c(s) & d(s) \end{bmatrix} \mathbf{Y}(s) = \begin{bmatrix} f & g \\ h & i \end{bmatrix} \mathbf{U}(s)\tag{III.5}$$

This is defined as a  $2 \times 2$  system. In the general case with  $m$  inputs and  $m$  outputs, the system is defined as  $m \times m$ . Let the matrix premultiplying the output vector  $\mathbf{Y}(s)$  be  $\mathbf{D}(s)$  and the matrix premultiplying the input vector  $\mathbf{U}(s)$  be  $\mathbf{N}$ . Equation (III.5) may then be written as:

$$\mathbf{D}(s) \mathbf{Y}(s) = \mathbf{N} \mathbf{U}(s)\tag{III.6}$$

The solution of Eq. (III.6) for the output  $\mathbf{Y}(s)$ , where  $\mathbf{D}$  must be nonsingular, yields:

$$\mathbf{Y}(s) = \mathbf{D}^{-1}(s) \mathbf{N} \mathbf{U}(s) = \mathbf{P}(s) \mathbf{U}(s)\tag{III.7}$$

Thus, the  $m \times m$  plant transfer function matrix  $\mathbf{P}(s)$  is:

$$P(s) = D^{-1}(s)N$$

(III.8)

This plant matrix  $P(s) = [p_{ij}(s)]$  is a member of the set  $\mathcal{O} = \{P(s)\}$  of possible plant matrices which are functions of the structured uncertainty in the plant parameters. In practice, only finite set of  $P$  matrices are formed, representing the extreme boundaries of the plant uncertainty under varying conditions. Only LTI systems are considered in this text.

**Example III.1** -- The Kirchoff's Voltage law is applied to the electrical network of Fig. III.2 to yield the following differential equations (the "D" operator notation is used):

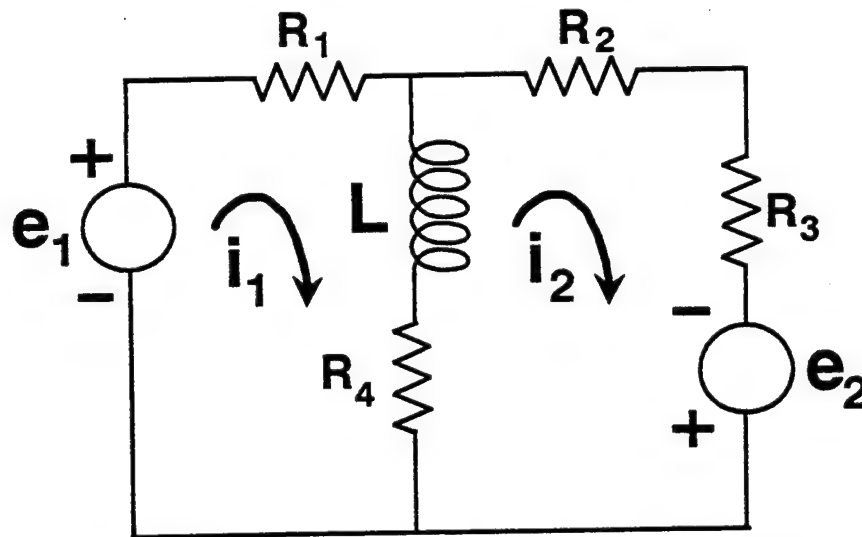


**Fig. III.2** An electrical network

$$e_1(t) = (R_1 + R_4 + LD) i_1(t) - (R_4 + LD) i_2(t) \quad (\text{III.9})$$

$$e_2(t) = -(R_4 + LD) i_1(t) + (R_2 + R_3 + R_4 + LD) i_2(t) \quad (\text{III.10})$$

or

$$(R_1 + R_4 + Ls) I_1(s) - (R_4 + Ls) I_2(s) = E_1(s) \quad (\text{III.11})$$

$$-(R_4 + Ls) I_1(s) + (R_2 + R_3 + R_4 + Ls) I_2(s) = E_2(s) \quad (\text{III.12})$$

Let



$$\mathbf{U} = \begin{bmatrix} u_1 \\ u_2 \end{bmatrix} = \begin{bmatrix} e_1 \\ e_2 \end{bmatrix}$$

$m$  Inputs

and

$$\mathbf{Y} = \begin{bmatrix} y_1 \\ y_2 \end{bmatrix} = \begin{bmatrix} i_1 \\ i_2 \end{bmatrix}$$

$m$  Outputs

Thus, Eqs. (III.11) and (III.12) are of the form:

$$d_{11}(s)Y_1(s) + d_{12}(s)Y_2(s) = n_{11}(s)U_1(s) + n_{12}(s)U_2(s) \quad (\text{III.13})$$

$$d_{21}(s)Y_1(s) + d_{22}(s)Y_2(s) = n_{21}(s)U_1(s) + n_{22}(s)U_2(s) \quad (\text{III.14})$$

where, for this example,  $n_{12} = n_{21} = 0$ . These equations are of the general form:

$$d_{i1}(s)Y_1(s) + \dots + d_{im}(s)Y_m(s) = n_{i1}(s)U_1(s) + \dots + n_{im}(s)U_m(s) \quad (\text{III.15})$$

where  $i = 1, 2, \dots, m$

$$\mathbf{D} = \begin{bmatrix} d_{11} & d_{12} & \dots & d_{1m} \\ d_{21} & d_{22} & \dots & d_{2m} \\ \vdots & \vdots & & \vdots \\ d_{m1} & d_{m2} & \dots & d_{mm} \end{bmatrix} \quad (\text{III.16a}) \quad \mathbf{N} = \begin{bmatrix} n_{11} & n_{12} & \dots & n_{1m} \\ n_{21} & n_{22} & \dots & n_{2m} \\ \vdots & \vdots & & \vdots \\ n_{m1} & n_{m2} & \dots & n_{mm} \end{bmatrix} \quad (\text{III.16b})$$

Thus, Eqs. (III.13) and (III.14) can be expressed as follows:

$$\underset{mxm}{\mathbf{D}} \underset{mx1}{\begin{bmatrix} Y_1 \\ Y_2 \\ \vdots \\ Y_m \end{bmatrix}} = \underset{mxm}{\mathbf{N}} \underset{mx1}{\begin{bmatrix} U_1 \\ U_2 \\ \vdots \\ U_m \end{bmatrix}} \quad (\text{III.17})$$

Which is of the form of Eq. (III.6). For this example, based on Eq. (III.7) and where  $m = 2$ , the expression for  $Y$  is:

$$Y(s) = \begin{bmatrix} p_{11}(s) & p_{12}(s) \\ p_{21}(s) & p_{22}(s) \end{bmatrix} \begin{bmatrix} U_1(s) \\ U_2(s) \end{bmatrix} = \begin{bmatrix} p_{11}(s)U_1(s) + p_{12}(s)U_2(s) \\ p_{21}(s)U_1(s) + p_{22}(s)U_2(s) \end{bmatrix} \quad (\text{III.18})$$

Suppose that  $p_{11}p_{22} = p_{12}p_{21}$ , resulting in

$$|P| = \begin{vmatrix} p_{11} & p_{12} \\ p_{21} & p_{22} \end{vmatrix} = p_{11}p_{22} - p_{12}p_{21} = 0 \quad (\text{III.19})$$

Thus, for this example,  $|P|$  is singular. Equation (III.18) yields:

$$\begin{aligned} Y_2 &= p_{21}U_1 + p_{22}U_2 = p_{21}U_1 + \left( \frac{p_{12}p_{21}}{p_{11}} \right) U_2 \\ &= \frac{p_{21}(p_{11}U_1 + p_{12}U_2)}{p_{11}} = \left( \frac{p_{21}}{p_{11}} \right) Y_1 \end{aligned} \quad (\text{III.20})$$

Equation (III.20) reveals that  $Y_1$  and  $Y_2$  are not independent of each other. Thus, they can not be controlled independently, i.e., an uncontrollable system. Therefore, when  $P$  is singular the system is uncontrollable.

From Eq. (III.18) the signal flow graph (SFG) of Fig. III.3(a) is obtained which represents a plant with structured plant parameter uncertainty with no cross-coupling effects. Figure III.3(b) is the SFG of the compensated MIMO closed-loop control system where the compensator and prefilter matrices are, respectively:

$$G(s) = \begin{bmatrix} g_{11} & g_{12} \\ g_{21} & g_{22} \end{bmatrix} \quad F(s) = \begin{bmatrix} f_{11} & f_{12} \\ f_{21} & f_{22} \end{bmatrix}$$

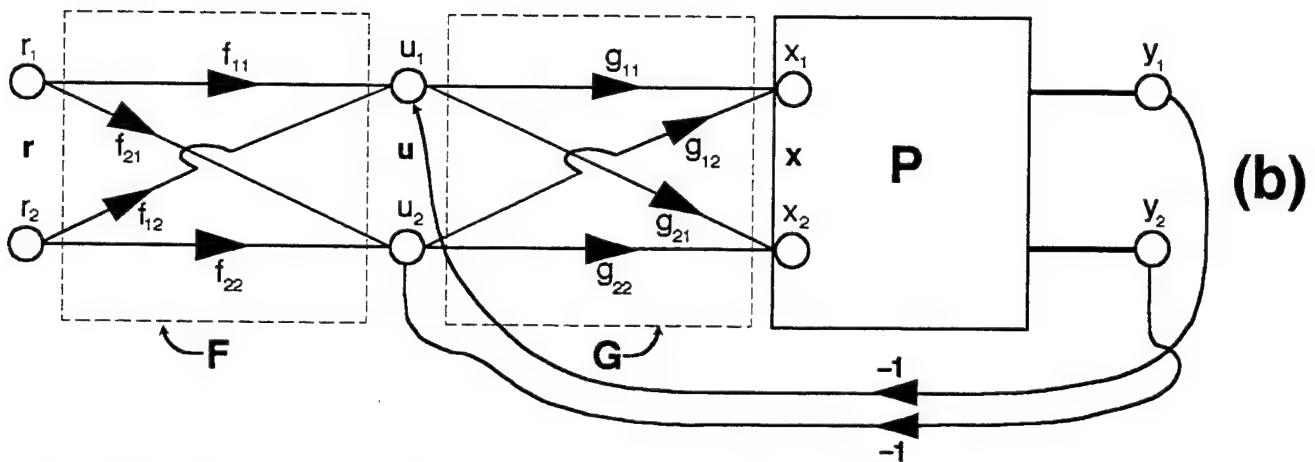
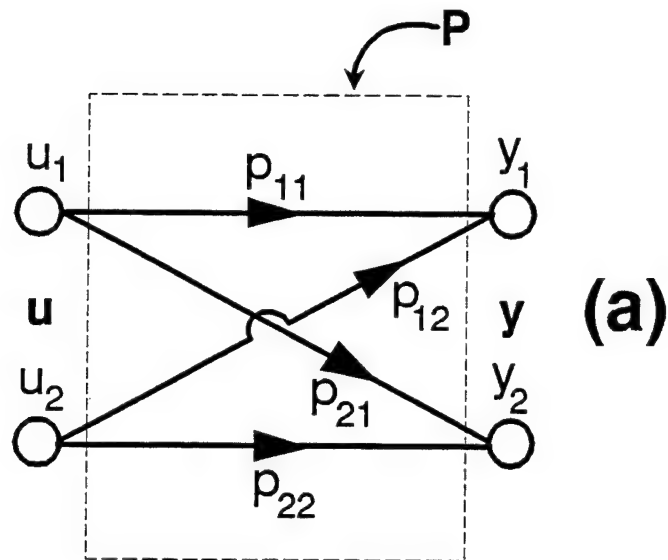


Fig. III.3 The signal flow graph of: (a) Eq. (III.14), and (b) the compensated MIMO control system.

The control ratio matrix  $T$  is:

$$T = \begin{bmatrix} t_{11} & t_{12} \\ t_{21} & t_{22} \end{bmatrix} \quad (\text{III.21})$$

where  $t_{ij} = y_i/r_j$  and the tolerance matrix element is given by  $b_{ij} \geq t_{ij} \geq a_{ij}$ .

### III.3 Introduction to MIMO Compensation

Figure III.3(b) has the  $m \times m$  closed-loop MIMO feedback control structure of Fig. III.4 in which  $F$ ,  $G$ ,  $P$ ,  $T$  are each  $m \times m$  matrices, and  $\mathcal{P} = \{P\}$  is a set of matrices due to plant uncertainty. There are  $m^2$  closed-loop system transfer functions (transmissions)  $t_{ij}(s)$  relating the outputs  $y_i(s)$  to the inputs  $r_j(s)$ , i.e.,  $y_i(s) = t_{ij}(s)r_j(s)$ . In a quantitative problem statement, there are tolerance bounds on each  $t_{ij}(s)$ , giving  $m^2$  sets of acceptable regions  $\tau_{ij}(s)$  which are to be specified in the design, thus  $t_{ij}(s) \in \tau_{ij}(s)$  and  $\mathcal{T}(s) = \{t_{ij}(s)\}$ . The application of QFT to  $2 \times 2$  and  $3 \times 3$  systems has been highly developed and is illustrated in later sections of this chapter.

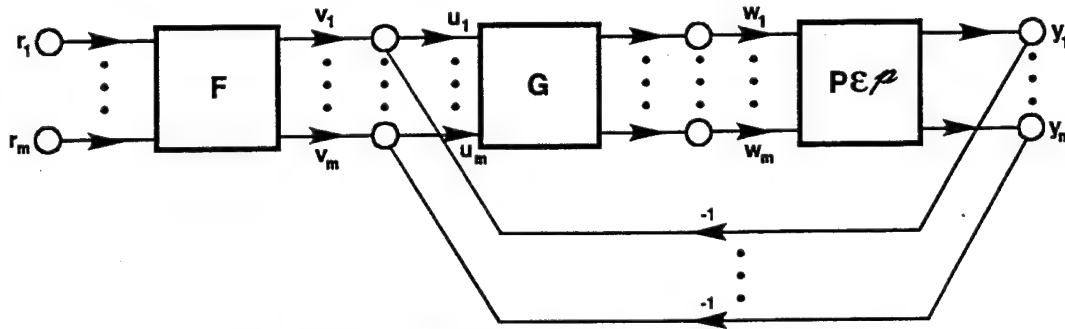


Fig. III.4 MIMO feedback structure.

From Fig. III.4 the following equations can be written:

$$y = Px \quad w = Gu \quad u = v - y \quad v = Fr$$

In these equations  $P(s) = [p_{ij}(s)]$  is the matrix of plant transfer functions,  $G(s)$  is the matrix of compensator transfer functions and is often simplified so that it is diagonal, that is,  $G(s) = \text{diag} \{g_i(s)\}$ , and  $F(s) = \{f_{ij}(s)\}$  is the matrix of prefilter transfer functions which may also be a diagonal matrix. The first two expressions yield:

$$y = PGu$$

which is utilized with the remaining two expressions to obtain

$$y = PG[v - y] = PG[Fr - y]$$

This equation is rearranged to yield:

$$\mathbf{y} = [\mathbf{I} + \mathbf{P}\mathbf{G}]^{-1}\mathbf{P}\mathbf{G}\mathbf{F}\mathbf{r} \quad (\text{III.22})$$

where the system control ratio relating  $\mathbf{r}$  to  $\mathbf{y}$  is:

$$\mathbf{T} = [\mathbf{I} + \mathbf{P}\mathbf{G}]^{-1}\mathbf{P}\mathbf{G}\mathbf{F} \quad (\text{III.23})$$

To appreciate the difficulty of the design problem, note the very complex expression for  $t_{11}$  given by Eq. (III.24), for the case  $m = 3$  with a diagonal  $\mathbf{G}$  matrix. However, the QFT design procedure systematizes and simplifies the manner of achieving a satisfactory system design.

$$\begin{aligned} t_{11} = & ([p_{11}f_{11}g_1 + p_{12}f_{21}g_2 + p_{13}f_{31}g_3] [(1 + p_{22}g_2)(1 + p_{33}g_3 - p_{23}p_{32}g_2g_3] \\ & - [p_{21}f_{11}g_1 + p_{22}f_{21}g_2 + p_{23}f_{31}g_3] [p_{12}g_2(1 + p_{33}g_3) - p_{32}p_{13}g_2g_3] \\ & + [p_{31}f_{11}g_1 + p_{32}f_{21}g_2 + p_{33}f_{31}g_3] [p_{23}p_{12}g_2g_3 - (1 + p_{22}g_2)p_{13}g_3]) / \\ & ( (1 + p_{11}g_1) [(1 + p_{22}g_2)(1 + p_{33}g_3) - p_{23}p_{32}g_2g_3] \\ & - p_{21}g_1[p_{12}g_2(1 + p_{33}g_3) - p_{32}p_{13}g_2g_3] + p_{31}g_1[p_{12}p_{23}g_2g_3 \\ & - p_{13}g_3(1 + p_{22}g_2)] ) \end{aligned}$$

(III.24)

There are  $m^2 = 9$  such  $t_{ij}(s)$  expressions (all have the same denominator), and there may be considerable uncertainty in the nine plant transfer functions  $p_{ij}(s)$ . The design objective is a system which behaves as desired for the entire range of uncertainty. This requires finding nine  $f_{ij}(s)$  and three  $g_i(s)$  such that each  $t_{ij}(s)$  stays within its acceptable region  $\tau_{ij}(s)$  no matter how the  $p_{ij}(s)$  may vary. Clearly, this is a very difficult problem. Even the stability problem alone, ensuring that the characteristic polynomial [the denominator of Eq. (III.24)] has no factors in the RHP for all possible  $p_{ij}(s)$ , is extremely difficult. Most design approaches treat stability for fixed parameter set, neglecting uncertainty, and attempting to cope with the plant uncertainty by trying to design the system to have conservative stability margins. Two highly developed QFT design techniques, Method 1 and Method 2, exist for the design of such systems and are presented in this chapter. In both

approaches the MIMO system is converted into an equivalent set of single-loop systems. Method 1 utilizes the MISO design method of Chap. I. Method 2, "the improved method," is an outgrowth of Method 1 in which the designed components of the previously designed loop that is (are) designed are used in the design of the succeeding loops.

#### III.4 MIMO Compensation

The basic MIMO compensation structure for a two-by-two MIMO system is shown in Fig. III.5. The structure for a three-by-three MIMO system is shown in Fig. III.6. They consist of the uncertain plant matrix  $P$ , the diagonal compensation matrix  $G$ , and the prefilter matrix  $F$ . This chapter considers only a diagonal  $G$  matrix, though a non-diagonal  $G$  matrix allows the designer much more design flexibility.<sup>29</sup> These matrices are defined as follows:

$$G = \begin{bmatrix} g_1 & 0 & \dots & 0 \\ 0 & g_2 & \dots & 0 \\ \vdots & \vdots & \ddots & \vdots \\ 0 & 0 & \dots & g_m \end{bmatrix} \quad F = \begin{bmatrix} f_{11} & f_{12} & \dots & f_{1m} \\ f_{21} & f_{22} & \dots & f_{2m} \\ \vdots & \vdots & \ddots & \vdots \\ f_{m1} & f_{m2} & \dots & f_{mm} \end{bmatrix} \quad P = \begin{bmatrix} P_{11} & P_{12} & \dots & P_{1m} \\ P_{21} & P_{22} & \dots & P_{2m} \\ \vdots & \vdots & \ddots & \vdots \\ P_{m1} & P_{m2} & \dots & P_{mm} \end{bmatrix} \quad (\text{III.25})$$

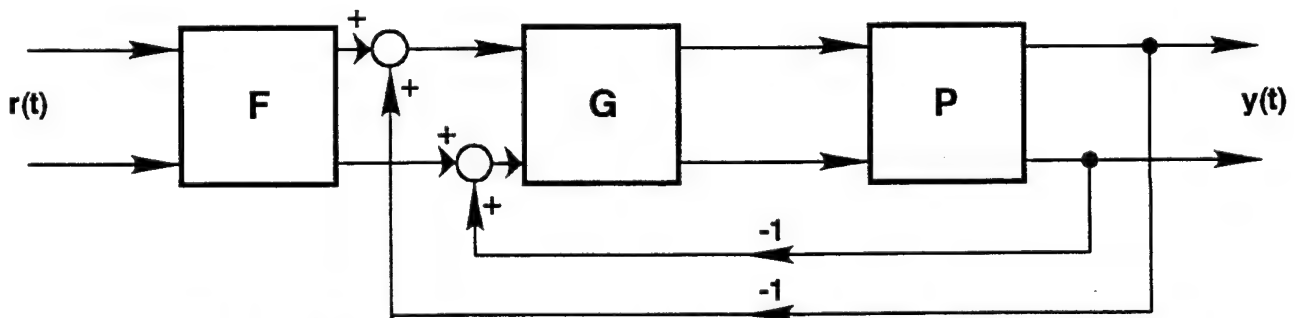


Fig. III.5 MIMO control structure (two-by-two system).

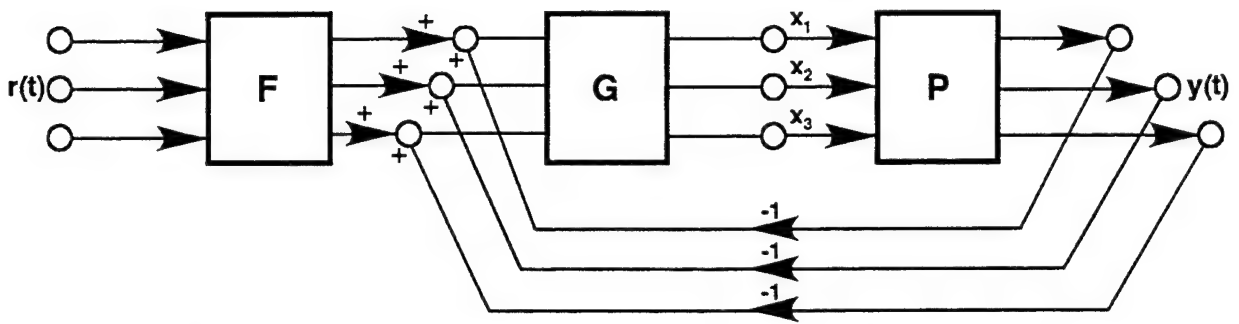


Fig. III.6 MIMO control structure (three-by-three system).

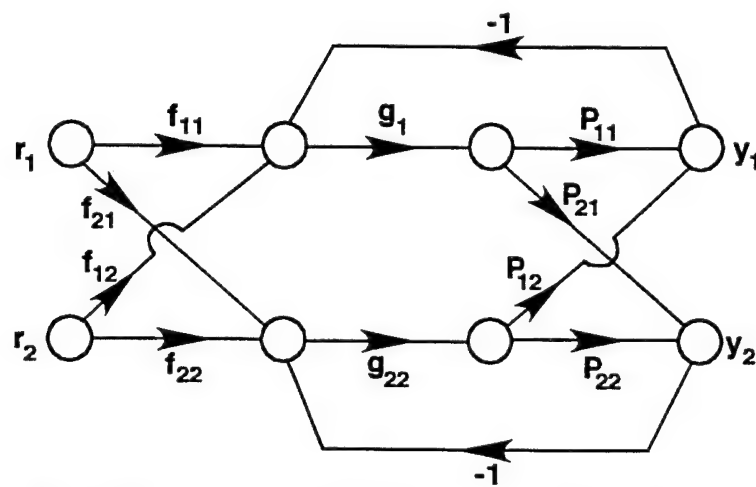


Fig. III.7 Two-by-two MIMO system signal flow graph.

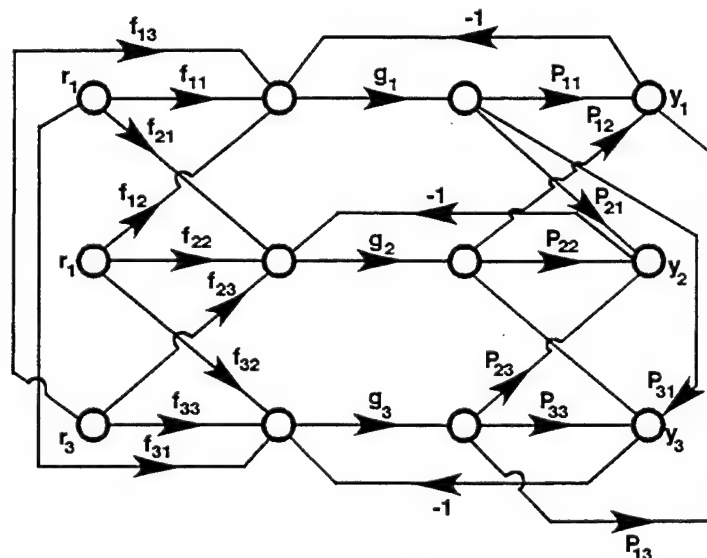


Fig. III.8 Three-by-three MIMO signal flow graph.

The dashes in Eq. (III.25) denote the  $G$ ,  $F$ , and  $P$  matrices for a  $2 \times 2$  system. Substituting these matrices into Eq. (III.23) yields the  $t_{ij}(s)$  control ratios relating the  $i^{\text{th}}$  output to the  $j^{\text{th}}$  input. From these  $t_{ij}(s)$  expressions the SFG of Fig. III.7 is obtained. The SFG of Fig. III.8 for a  $3 \times 3$  system is obtained in a similar manner.

### III.5 Introduction to MISO Equivalents

From Eq. (III.23) obtain

$$T = \frac{(\text{cof}[I + PG])^T PGF}{\det[I + PG]}$$

For a  $3 \times 3$  plant and a diagonal  $G$  matrix, the denominator of this equation becomes:

$$\det[I + PG] = \begin{vmatrix} 1 + p_{11}g_1 & p_{12}g_2 & p_{13}g_3 \\ p_{21}g_1 & 1 + p_{22}g_2 & p_{23}g_3 \\ p_{31}g_1 & p_{32}g_2 & 1 + p_{33}g_3 \end{vmatrix}$$

which is a very "messy" equation for the purpose of analysis and synthesis in achieving a satisfactory design of the control system. In analyzing Eq. (III.23), it is noted that if  $|P(j\omega)G(j\omega)| \gg I$  then  $T \approx F$  and the system becomes insensitive to the parameter variations in  $P$ .

#### III.5.1 Effective MISO Equivalents<sup>32</sup>

The objective of this section is to find a suitable mapping that permits the analysis and synthesis of a MIMO control system by a set of equivalent MISO control systems. This mapping results in  $m^2$  equivalent systems, each with two inputs and one output. One input is designated as a "desired" input and the other as an "unwanted" input (cross-coupling effects and/or external system disturbances). First, Eq. (III.23) is premultiplied by  $[I + PG]$  to obtain

$$[I + PG] T = PGF \quad (\text{III.26})$$



When  $\mathbf{P}$  is nonsingular, then premultiplying both sides of this equation by  $\mathbf{P}^{-1}$  yields

$$[\mathbf{P}^{-1} + \mathbf{G}] \mathbf{T} = \mathbf{G}\mathbf{F} \quad (\text{III.27})$$

Let

$$\mathbf{P}^{-1} = \begin{bmatrix} p_{11}^* & p_{12}^* & \dots & p_{1m}^* \\ p_{21}^* & p_{22}^* & \dots & p_{2m}^* \\ \cdot & \cdot & & \cdot \\ \cdot & \cdot & & \cdot \\ \cdot & \cdot & & \cdot \\ p_{m1}^* & p_{m2}^* & \dots & p_{mm}^* \end{bmatrix} \quad (\text{III.28})$$

The  $m^2$  effective plant transfer functions are formed as

$$q_{ij} = 1/p_{ij}^* = \frac{\det[\mathbf{P}]}{\text{Adj}_{ij}\mathbf{P}} \quad (\text{III.29})$$

The  $\mathbf{Q}$  matrix is then formed as

$$\mathbf{Q} = \begin{bmatrix} q_{11} & q_{12} & \dots & q_{1m} \\ q_{21} & q_{22} & \dots & q_{2m} \\ \cdot & \cdot & & \cdot \\ \cdot & \cdot & & \cdot \\ \cdot & \cdot & & \cdot \\ q_{m1} & q_{m2} & \dots & q_{mm} \end{bmatrix} = \begin{bmatrix} 1/p_{11}^* & 1/p_{12}^* & \dots & 1/p_{1m}^* \\ 1/p_{21}^* & 1/p_{22}^* & \dots & 1/p_{2m}^* \\ \cdot & \cdot & & \cdot \\ \cdot & \cdot & & \cdot \\ \cdot & \cdot & & \cdot \\ 1/p_{m1}^* & 1/p_{m2}^* & \dots & 1/p_{mm}^* \end{bmatrix} \quad (\text{III.30})$$

where

$$\mathbf{P} = [p_{ij}], \quad \mathbf{P}^{-1} = [p_{ij}^*] = [1/q_{ij}], \quad \mathbf{Q} = [q_{ij}] = [1/p_{ij}^*]$$

The matrix  $\mathbf{P}^{-1}$  is partitioned to the form

$$\mathbf{P}^{-1} = [p_{ij}^*] = [1/q_{ij}] = \mathbf{\Lambda} + \mathbf{B} \quad (\text{III.31})$$

where  $\mathbf{\Lambda}$  is the diagonal part and  $\mathbf{B}$  is the balance of  $\mathbf{P}^{-1}$ , thus  $\lambda_{ii} = 1/q_{ii} = p_{ii}^*$ ,  $b_{ii} = 0$ , and  $b_{ij} = 1/q_{ij} = p_{ij}^*$  for  $i \neq j$ . Next, rewrite Eq. (III.27) using Eq. (III.31) and with  $\mathbf{G}$  diagonal. This yields  $[\mathbf{\Lambda} + \mathbf{G}]\mathbf{T} = \mathbf{G}\mathbf{F} - \mathbf{B}\mathbf{T}$  which produces

$$\mathbf{T} = [\Lambda + \mathbf{G}]^{-1}[\mathbf{GF} - \mathbf{BT}] \quad (\text{III.32})$$

This is used to define the desired fixed point mapping where each of the  $m^2$  matrix elements on the right side of Eq. (III.32) can be interpreted as a MISO problem. Proof of the fact that design of the individual MISO feedback loops will yield a satisfactory MIMO design is based on the Schauder fixed point theorem.<sup>21</sup> This theorem is described by defining a mapping on  $\mathfrak{S}$  as follows:

$$\mathbf{Y}(\mathbf{T}_i) \equiv [\Lambda + \mathbf{G}]^{-1}[\mathbf{GF} - \mathbf{BT}_i] \equiv \mathbf{T}_j \quad (\text{III.33})$$

where each  $\mathbf{T}$  is from the acceptable set  $\mathfrak{S}$ . If this mapping has a fixed point, i.e.,  $\mathbf{T}_i, \mathbf{T}_j \in \mathfrak{S}$  such that  $\mathbf{Y}(\mathbf{T}_i) = \mathbf{T}_j$  (see Fig. III.9), then a solution to the robust control problem has been achieved yielding a solution in the acceptable set  $\mathfrak{S}$ . Recalling that

**Enclosure of all acceptable  $\mathbf{T} \in \mathfrak{S}$**

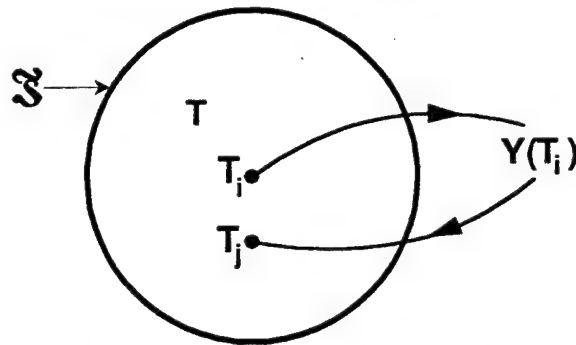


**Fig. III.9 Schauder fixed point mapping.**

$\Lambda$  and  $\mathbf{G}$  in Eq. (III.32) are both diagonal, the 1,1 element on the right side of Eq. (III.33) for the 3x3 case, for a unit impulse input, yields the output

$$y_{11} = \frac{g_{11}}{1 + g_{11}q_{11}} \left[ g_1 f_{11} - \left( \frac{t_{21}}{q_{12}} + \frac{t_{31}}{q_{13}} \right) \right] \quad (\text{III.34})$$

This corresponds precisely to the first structure in Fig. III.10 and is the control ratio that relates the  $i^{\text{th}}$  output to the  $j^{\text{th}}$  input, where  $i = j = 1$  in Eq. (III.34). Similarly each of the nine structures in

Fig. III.10 corresponds to one of the elements of  $Y(T)$  of Eq. (III.32). The general transformation result of  $m^2$  MISO system loops is shown in Fig. III.11. Figure III.10 shows the four effective MISO loops (in the boxed area) resulting from a  $2 \times 2$  system and the nine effective MISO loops resulting from a  $3 \times 3$  system.<sup>32</sup> The control ratio, for unit impulse inputs, for the  $m \times m$  system of Fig. III.11 obtained from Eq. (III.33) have the form

$$y_{ij} = w_{ij}(v_{ij} + c_{ij}) \quad (\text{III.35})$$

where

$$w_{ii} = q_{ii} / (1 + g_i q_{ii}) \quad (\text{III.36})$$

$$v = g_i f_{ij} \quad (\text{III.37})$$

and

$$c_{ij} = - \sum_{k \neq i} \left[ \frac{t_{kj}}{q_{ik}} \right] \quad k = 1, 2, \dots, m \quad (\text{III.38})$$

Equation (III.38) represents the interaction between the loops.

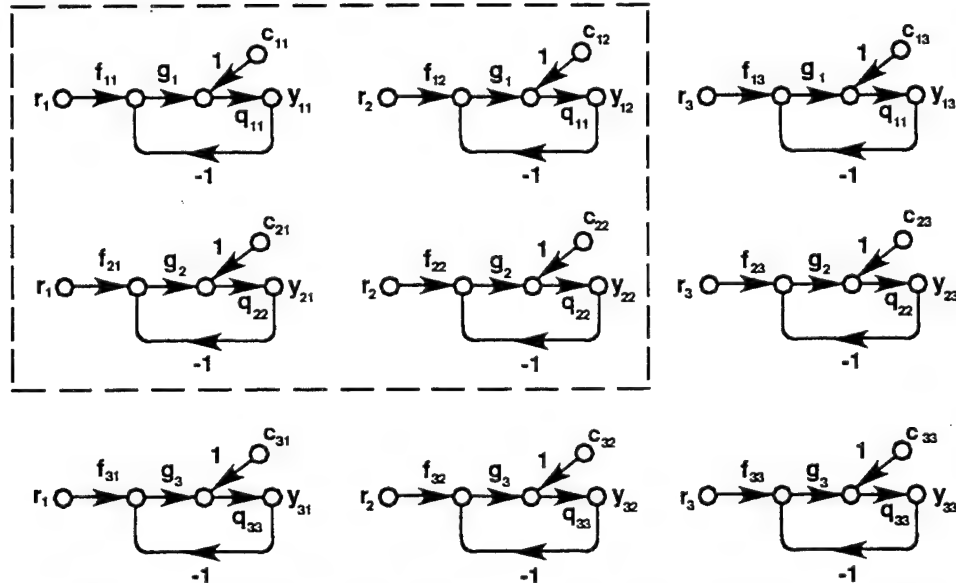


Fig. III.10 Effective MISO loops two-by-two (boxed in loops) and three-by-three (all 9 loops).

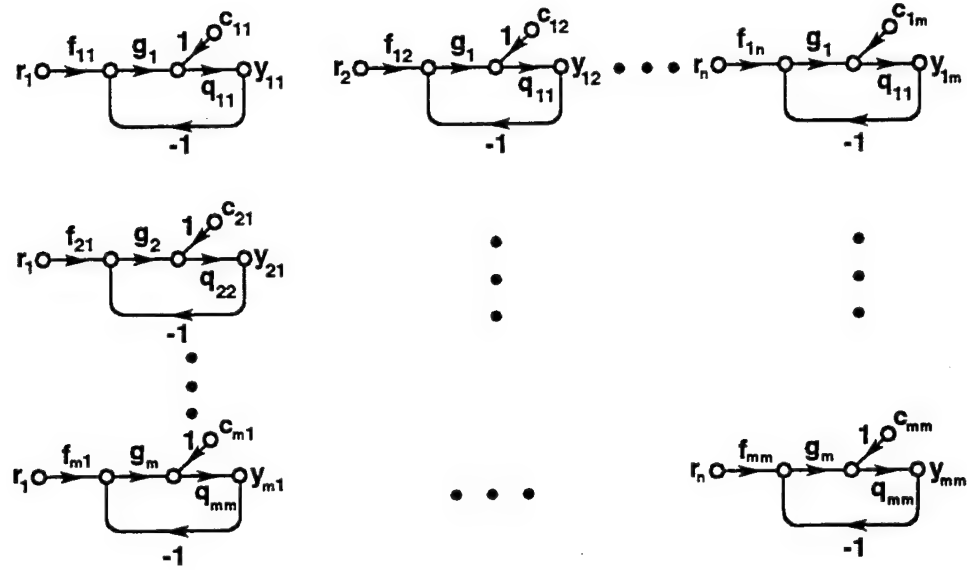


Fig. III.11 Effective MISO loops (in general).

Thus, Eq. (III.35) represents the control ratio of the  $i^{\text{th}}$  MISO loop where the transfer function  $w_{ii}v_{ij}$  relates the  $i^{\text{th}}$  output to  $i^{\text{th}}$  "desired" input  $r_i$  and the transfer function  $w_{ii}c_{ij}$  relates the  $i^{\text{th}}$  output to the  $j^{\text{th}}$  "cross-coupling effect" input  $c_{ij}$ . The transfer function of Eq. (III.35) can thus be expressed, with  $r_i(s) = 1$  (a unit impulse function), as

$$y_{ij} = (y_{ij})_{r_j} + (y_{ij})_{c_{ij}} = y_{r_j} + y_{c_{ij}} \quad (\text{III.39a})$$

or

$$t_{ij} = t_{r_{ij}} + t_{c_{ij}} \quad (\text{III.39b})$$

where

$$t_{r_j} = y_{r_j} = w_{ii}v_{ij} \quad (\text{III.40a})$$

$$t_{c_{ij}} = y_{c_{ij}} = w_{ii}c_{ij} \quad (\text{III.40b})$$

and where now the upper bound, in the low frequency range is expressed

as

$$b_{ij} = b'_{ij} + \tau_{c_{ij}} \quad (\text{III.40c})$$

Thus

$$\tau_{c_{ij}} = b_{ij} - b'_{ij} \quad (\text{III.40d})$$

represents the maximum portion of  $b_{ij}$  allocated towards cross-coupling effect rejection and  $b'_{ij}$  represents the upper bound for the tracking portion of  $t_{ij}$ . For any particular loop there is a cross-coupling effect input which is function of all the other loop outputs. The object of the design is to have each loop track its desired input while minimizing the outputs due to the cross-coupling effects.

In each of the nine structures of Fig. III.10 it is necessary that the control ratio  $y_{ij}(s)$ , with  $r(s) = 1$ , must be a member of the acceptable set  $t_{ij} \in \mathfrak{T}_{ij}(s)$  (see Fig. III.9). All the  $g_i(s)$ ,  $f_{ij}(s)$  must be chosen to ensure that this condition is satisfied, thus constituting nine MISO design problems. If all of these MISO problems are solved, there exists a fixed point, and then  $y_{ij}(s)$  on the left side of Eq. (III.33) may be replaced by a  $t_{ij}$  and all the elements of  $T$  on the right side by  $t_{kj}$ . This means that there exist nine  $t_k$  and  $t_{kj}$ , each in its okay set, which is a solution to Fig. III.4. If each element is 1:1, then this solution must be unique. A more formal and detailed treatment is given in Reference 21. Note that if the plant has transmission zeros in the right-half-plane (r.h.p.) it only indicates that  $q_{ij}$  may be n.m.p. or the  $\det P$  may have zeros in the r.h.p.

### III.6 Effective MISO Loops of the MIMO System

There are two design methods for designing MIMO systems. In the first method each MISO loop in Figs. III.10 and III.11 is treated as an individual MISO design problem, which is solved using the procedures explained in Chap. I and References 15 and 47. The  $f_{ij}(s)$  and  $g_i(s)$  are

the compensator elements of the  $F(s)$  and  $G(s)$  matrices described previously.

The cross-coupling effect  $c_{ij}(s)$  expressed by Eq. (III.38) represents the interaction between the loops, i.e.,

$$c_{ij} = - \sum_{k \neq i} \left[ \frac{b_{kj}}{q_{ik}} \right], \quad k = 1, 2, \dots, m \quad (\text{III.41})$$

where the numerator  $b_{kj}$  is the upper response bound, ( $T_{R_d}$  or  $T_D$  in Fig. I.6.), for the respective input/output relationship. These are obtained from the design specifications.<sup>32</sup> The first subscript  $k$  refers to the output variable, and the second subscript  $j$  refers to the input variable. Therefore,  $b_{kj}$  is a function of the response requirements on the output  $y_k$  due to the input  $r_j$ . The lower bound  $a_{kj}$  needs defining only when there is a command input.

### III.6.1 Example: The 2x2 plant

For this example a diagonal  $G$  matrix is utilized. Using a diagonal matrix results in restricting the design freedom available to achieve the desired performance specifications. This is offset by simplifying the design process. The elements of a diagonal  $G$  are denoted with a single subscript, i.e.,  $g_i$ . The  $P$  and  $P^{-1}$  matrices are, respectively:

$$P = \begin{bmatrix} p_{11} & p_{12} \\ p_{21} & p_{22} \end{bmatrix} \quad (\text{III.42})$$

$$P^{-1} = \frac{1}{\Delta} \begin{bmatrix} p_{22} & -p_{12} \\ -p_{21} & p_{11} \end{bmatrix} \quad (\text{III.43})$$

where  $\Delta = p_{11}p_{22} - p_{12}p_{21}$ . From Eq. (III.29):

$$P^{-1} = \begin{bmatrix} \frac{1}{q_{11}} & \frac{1}{q_{12}} \\ \frac{1}{q_{21}} & \frac{1}{q_{22}} \end{bmatrix} \quad (\text{III.44})$$

where

$$\begin{aligned} q_{11} &= \frac{\Delta}{p_{22}}, & q_{12} &= \frac{-\Delta}{p_{12}}, \\ q_{21} &= \frac{-\Delta}{p_{21}}, & q_{22} &= \frac{\Delta}{p_{11}} \end{aligned} \quad (\text{III.45})$$

Substituting Eq. (III.44) into Eq. (III.27) yields:

$$\begin{bmatrix} \frac{1}{q_{11}} + g_1 & \frac{1}{q_{12}} \\ \frac{1}{q_{21}} & \frac{1}{q_{22}} + g_2 \end{bmatrix} \begin{bmatrix} t_{11} & t_{12} \\ t_{21} & t_{22} \end{bmatrix} = \begin{bmatrix} g_1 f_{11} & g_1 f_{12} \\ g_2 f_{21} & g_2 f_{22} \end{bmatrix} \quad (\text{III.46})$$

The responses due to input 1, obtained from Eq. (III.46), are:

$$\begin{aligned} \left( \frac{1}{q_{11}} + g_1 \right) t_{11} + \frac{t_{21}}{q_{12}} &= g_1 f_{11} \\ \frac{t_{11}}{q_{21}} + \left( \frac{1}{q_{22}} + g_2 \right) t_{21} &= g_2 f_{21} \end{aligned} \quad (\text{III.47})$$

The responses due input 2, obtained from Eq. (III.46), are:

$$\begin{aligned} \left( \frac{1}{q_{11}} + g_1 \right) t_{12} + \frac{t_{22}}{q_{12}} &= g_1 f_{12} \\ \frac{t_{12}}{q_{21}} + \left( \frac{1}{q_{22}} + g_2 \right) t_{22} &= g_2 f_{22} \end{aligned} \quad (\text{III.48})$$

These equations are rearranged to a format that readily permits the synthesis of the  $g_i$ 's and the  $f_{ij}$ 's that will result in the MIMO control system achieving the desired system performance specifications. Equations (III.47) and (III.48) are manipulated to achieve the following format:

$$\begin{aligned}
 \text{For input } r_1: t_{11} &= \frac{g_1 f_{11} - \frac{t_{21}}{q_{12}}}{\frac{1}{q_{11}} + g_1} & t_{21} &= \frac{g_2 f_{21} - \frac{t_{11}}{q_{21}}}{\frac{1}{q_{22}} + g_2} \\
 \text{For input } r_2: t_{12} &= \frac{g_1 f_{12} - \frac{t_{22}}{q_{12}}}{\frac{1}{q_{11}} + g_1} & t_{22} &= \frac{g_2 f_{22} - \frac{t_{12}}{q_{21}}}{\frac{1}{q_{22}} + g_2}
 \end{aligned} \tag{III.49}$$

Multiplying the  $t_{11}$  and  $t_{12}$  equations by  $q_{11}$  and the  $t_{21}$  and  $t_{22}$  equations by  $q_{22}$  in Eq. (III.49), respectively, yields the equations shown in Fig. III.12. Associated with each equation in this figure is its corresponding SFG.

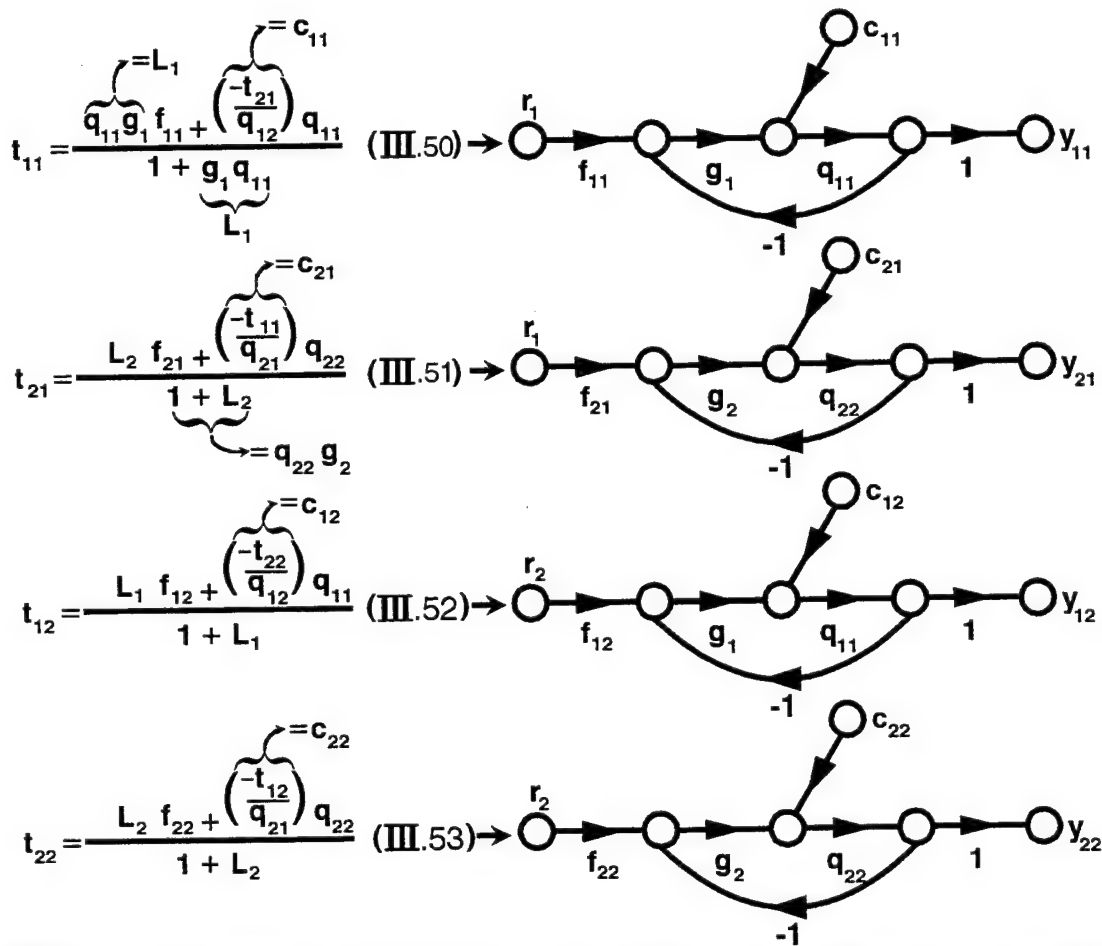


Fig. III.12 2x2 MISO structures and their respective  $t_{ij}$  equations.



Equations (III.50) through (III.53) are of the format of Eqs. (III.35) through (III.40). Note:

1. Can automatically obtain  $t_{22}$  and  $t_{21}$  from the expressions for  $t_{11}$  and  $t_{12}$  by interchanging  $1 \rightarrow 2$  and  $2 \rightarrow 1$  in the equations for  $t_{11}$  and  $t_{12}$ .
2. The  $c_{ij}$  term in these equations represent the cross-coupling effect from the other loops. These terms are functions of the other  $t_{kj}$ 's and the structured parameter uncertainty of the plant.
3. Theoretically, by making  $|L_i(j\omega)|$  "large enough," so that  $c_{ij} \approx 0$  a "decoupled system" is achieved.

In a similar fashion, the  $t_{ij}$  expressions and their corresponding SFG may be obtained for any  $m \times m$  control system.

### III.6.2 Performance Bounds

Based upon unit impulse inputs, from Eq. (III.39) obtain:

$$t_{ij} = t_{r_{ij}} + t_{c_{ij}} \quad (\text{III.54})$$

Let

$\phi_{ij}$  be the actual value of  $t_{ij}$   
 $\tau_{r_{ij}}$  be the actual value of  $t_{r_{ij}}$   
 $\tau_{c_{ij}}$  be the actual value of  $t_{c_{ij}}$

A  $2 \times 2$  control system is used to illustrate the concept of performance bounds. The "actual value" expression corresponding to the  $t_{11}$  expression of Eq. (III.50) is

$$\phi_{11} = \tau_{r_{11}} + \tau_{c_{11}}$$

where the  $\tau_r$  term represents the transmission due to input  $r_1$  and the  $\tau_c$  term represents the transmission due to the cross-coupling effects. For LTI system, the linear superposition theorem is utilized in

the development of the performance bounds.

For all  $P \in \mathcal{P}$  and  $t_{21} \in \tau_{21}$ , and  $c_{11} = -t_{21}/q_{12}$ , the output  $\phi_{11}$  must satisfy the performance specifications on  $t_{11}$ . Thus, it is necessary to apriori specify the closed-loop transfer functions  $t_{ij}$ . Consider the specifications on  $b_{11}$  and  $a_{11}$  on  $t_{11}$ , as illustrated in Fig. III.13 [see Eqs. (III.40c) and (III.40d)] for m.p. system. Only magnitudes need be considered for m.p. system since the magnitude determines the phase.

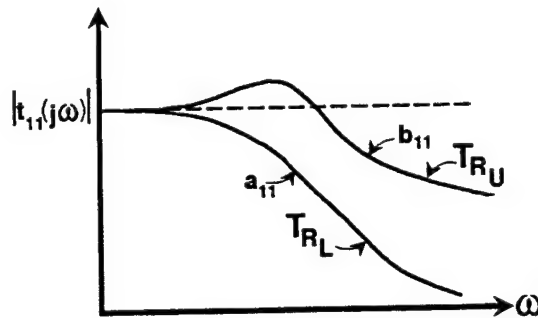


Fig. III.13 Upper and lower tracking bounds.

Thus, in terms of the actual values:

$$\begin{array}{ccc} a_{11} \leq |\phi_{11}(j\omega)| \leq b_{11}(j\omega) \\ \leq |\tau_{x_{11}} + \tau_{c_{11}}| \leq \\ \uparrow \leq \qquad \qquad \qquad \leq \uparrow \\ \text{lower bound} \qquad \qquad \qquad \text{upper bound} \end{array} \quad (\text{III.55})$$

Since the relative phases of the  $\tau$ 's are not known and not required for m.p. systems, then to ensure the achievement of the desired performance specifications Eq. (III.55) is expressed as follows:

$$a_{11}(j\omega) \leq ||\tau_{x_{11}}| - |\tau_{c_{11}}|| \quad \text{-- the smallest bound} \quad (\text{III.56})$$

and

$$|\tau_{x_{11}}| + |\tau_{c_{11}}| \leq b_{11}(j\omega) \quad \text{-- the largest bound} \quad (\text{III.57})$$

This represents an overdesign since it is more restrictive. A pictorial representation of Eqs. (III.56) and (III.57), for  $\omega = \omega_i$ , is shown in

Fig. III.14. Note that the  $\tau$ 's in this figure and the remaining discussion in this section represent only magnitudes. From this figure the following expression is obtained:

$$\Delta\tau = \Delta\tau_{r_{11}} + 2\tau_{c_{11}} = b_{11} - a_{11} \quad (\text{III.58})$$

In the "low frequency range" the bandwidth (BW) of concern,  $0 < \omega < \omega_h$ ,  $\Delta\tau$  is split up based upon the desired performance specifications. As is discussed later, for the high frequency range only an upper bound is of concern thus there is no need to be concerned with a "split." In Fig. III.14, for illustrative purposes only,  $\tau_{c_{11}} = 0.02$  and  $\Delta\tau_{r_{11}} = 0.2$  at  $\omega = \omega_i$ .

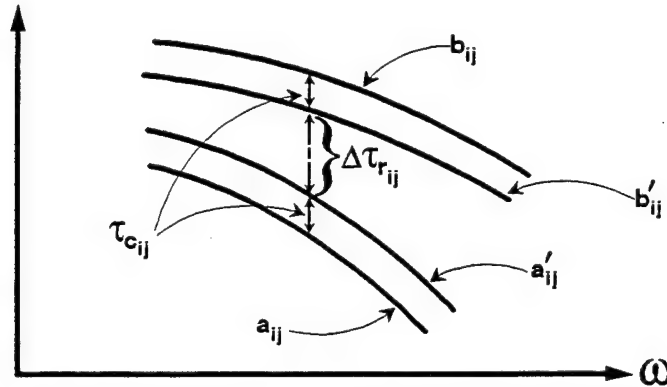


Fig. III.14 Allocation for tracking and cross-coupling specifications for  $t_{ij}$  responses.

**Example III.2** -- Consider the bound determinations  $B_R$ ,  $B_c$ , and  $B_o$  on  $L_1 = g_1 q_{11}$ , for a 2x2 system. Thus,  $b_{r_{11}}$ , based upon

$$a'_{ij} = (\tau_{r_{11}})_L \leq |t_{r_{11}}| \leq (\tau_{r_{11}})_U = b'_{ij} \quad (\text{III.59})$$

and Fig. III.14, for  $t_{11}$  can be determined in the same manner as for a MISO system (see Chap. I). Referring to Fig. III.12 and to Eq. (III.50), the bound on the cross-coupling effect, is determined as follows:

$$|t_{c_{11}}| = \left| \frac{c_{11}g_{11}}{1 + L_1} \right| \leq \tau_{c_{ij}} = \tau_{c_{11}} = 0.05 \quad (\text{III.60})$$

where for the cross-coupling effect the upper bound for  $t_{c_{11}}$  is given by

$$|t_{c_{ij}}| = |t_{c_{11}}| \leq b_{c_{ij}} = b_{c_{11}} \quad \text{where } i = j = 1$$

Substituting the expression for  $c_{11}$  into Eq. (III.60) and then manipulating this equation the following constraint on  $L_1(j\omega_i)$  is obtained:

$$|1 + L_1| \geq \frac{|c_{11}g_{11}|}{\tau_{c_{11}} = 0.05} = 20 \left| \frac{t_{21}g_{11}}{g_{12}} \right| = 20 \left| \frac{b_{21}g_{11}}{g_{12}} \right| \quad (\text{III.61})$$

where the upper bound  $b_{21}$  is inserted for  $t_{21}$ . It is necessary to manipulate this equation in a manner that permits the utilization of the Nichols Chart (NC). This is accomplished by making the substitution of  $L = 1/\ell$  into this equation. Thus,

$$\left| 1 + \frac{1}{\ell_1} \right| = \left| \frac{1 + \ell_1}{\ell_1} \right| \geq 20 \left| \frac{b_{21}g_{11}}{g_{12}} \right| \quad (\text{III.62})$$

Inverting this equation yields:

$$\left| \frac{\ell_1}{1 + \ell_1} \right| \leq \frac{1}{20} \left| \frac{g_{12}}{b_{21}g_{11}} \right| \quad (\text{III.63})$$

which is of the mathematical format that allows the use of the NC for the graphical determination of the cross-coupling bound  $b_{c_{11}}$ .<sup>15</sup> Equations (III.61) and (III.62) and Eq. (III.63) are, respectively, of the following mathematical format:

$$\begin{aligned} |A| &\geq |B| & (a) \\ |C| &\leq |D| & (b) \end{aligned} \quad (\text{III.64})$$

In determining this bound, it is necessary to insert the actual

plant parameters into these equations. That is, for each of the  $J$  plant models,  $P_i$  ( $i = 1, 2, \dots, J$ ), insert the corresponding plant parameters into these equations and determine the magnitudes  $A_i$ ,  $B_i$ ,  $C_i$ , and  $D_i$ . The following magnitudes, for each value of  $\omega_i$ , are used from these  $J$  sets of values to determine the cross-coupling bound:

$$\begin{aligned} |A_i|_{\min} &\geq |B_i|_{\max} \\ |C_i|_{\max} &\leq |D_i|_{\min} \end{aligned} \quad (\text{III.65})$$

"High bounds" on the NC require h.g., thus, in order to minimize the required compensator gain, the optimum choice of the

$$\Delta\tau_{r_{11}}, \tau_{c_{11}} \quad (\text{III.66})$$

specifications are the ones that result in achieving essentially the same tracking and cross-coupling bounds, i.e.,

$$b_{c_{11}} \approx b_{r_{11}} \quad (\text{III.67})$$

A recommended method for determining an appropriate set of constraints (specifications) on Eq. (III.66) is to initially do a design based on the following assumption:

$$\Delta\tau_{r_{11}} = b'_{11} - a'_{11}$$

With this design, determine how big  $\tau_{c_{11}}$  is and then, by trial and error if a CAD package is not available, adjust  $\tau_{c_{11}}$  until the condition

$$\Delta\tau_{r_{11}} \approx 2\tau_{c_{11}}$$

is satisfied. The MIMO/QFT CAD discussed in Chap. VIII automates this procedure. This procedure is illustrated in Fig. III.15. Depending on the starting quantities, by decreasing (increasing) one quantity and increasing (decreasing) the other quantity expedites achieving the condition of Eq. (III.67). By the procedure just described, the optimal bound  $b_{o_{11}}$  is given by Eq. (III.67).

In a similar manner determine the other bounds required for the other  $L_i$ 's, using QFT design Method 1. This may require trial and error; i.e., in loop shaping  $L_1$ , based on Eqs. (III.40) and (III.52), it is necessary to obtain the bounds for  $L_o$ , which satisfy the specifications for both  $t_{11}$  and  $t_{12}$ . Once these specifications are satisfied then proceed to do the looping shaping to determine  $L_{o_1}$ .<sup>32</sup>

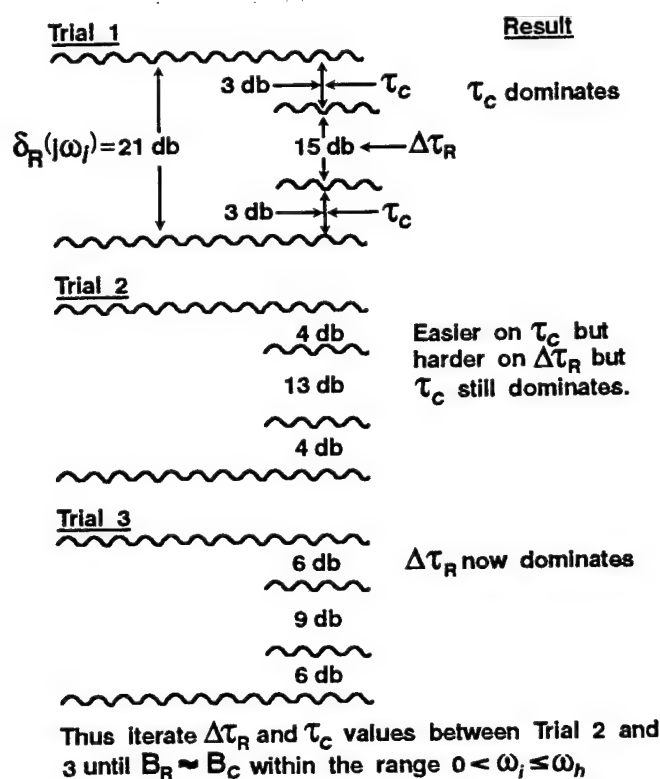


Fig. III.15 Procedure pictorial representation to achieve  $B_R \approx B_C$

### III.6.3 QFT Design Method 2

The QFT design Method 2, for many problems, may yield a better control system design. This method is an improvement over Method 1 in that it utilizes the resulting designed  $g_i$ 's and  $f_{ij}$ 's of the first MISO equivalent loop that is designed in the design of the succeeding loops, etc. This feature of Method 2 reduces the overdesign in the early part

of the design process. Method 2 may involve a trade-off in the design parameters. The final MISO equivalent loop to be designed uses the exact transfer functions of the previously designed  $g_i$ 's and  $f_{ij}$ 's thus this loop has the least amount of overdesign.<sup>32</sup>

The order in which the MISO loops are designed is important. Any order may be chosen but some orders may produce less overdesign (lower bandwidth) than others. The general rule in the choice of the design order of the loops is that the most constrained loop is chosen as the starting loop. That is, choose the "starting" loop  $i$  for which it is most important to minimize the BW requirements. Some of the factors involved in determining the BW requirements are:

1. Sensor noise
2. Loop  $i$  has severe bending mode problems that other loops do not have.
3. The "high frequency gain" (h.f.g.) uncertainty of  $q_{ii}$  may be very much greater than for the other loop. The h.f.g. uncertainty may effect the size of the templates.

Professor Horowitz provides the following insight:

(1) Analyze the various  $q_{ii}$  templates over a reasonable range of frequencies: almost vertical at low and high (for the analog case) frequencies. For the discrete case, up to the frequency range in which the templates first narrow, before widening again for  $\omega_i > \omega_s/2$  ( $\omega_s$  sampling frequency), rather than the final frequency range ( $\omega_i > \omega_s/2$ ) in which the templates approach a vertical line.<sup>47</sup>

(2) If the feedback requirements per loop are roughly the same, which indicates the  $t_{ii}$  specifications are about the same, and the  $t_{ij}$ ,  $i \neq j$ , also roughly similar for the different loops, then the loop with the smallest  $q_{ii}$  templates should be the "starting loop." That is, the loop with the smallest amount of feedback should be

chosen as the starting loop. The reason for this choice is that there is a tendency towards BW propagation as the design proceeds from the first loop to the final loop that is designed. Thus, the second loop to be designed should be the one having the second smallest feedback requirement. Also, see the discussion on page 196.

All of these factors emerge from the transparency of QFT which helps to reduce the trial and error that is involved in achieving a satisfactory design. If, in choosing the loop with the most severe BW limitation causes a design problem in the succeeding designed loops, then try a different starting loop selection. This is based on the knowledge, that in general, the B.W. of the succeeding designed loops are higher than the BW of the previously designed loops. Further insight into satisfying the BW requirement is given in Chap. VII.

If Method 2 can not satisfy the BW requirements for all loops then Method 1 must be used, assuming the diagonal dominance condition (see Sec. III.7) is satisfied. If Method 1 can not be used then it is necessary to reevaluate the performance specifications, etc.

#### III.6.4 Summary

For the cross-coupling effect rejections problem, the responses must be less than some bound, that is:

$$(y_{ij})_{c_{ij}} \leq \tau_{c_{ij}} = b_{c_{ij}}$$

Thus the loop equations become

$$\tau_{ij} \geq (y_{ij})_{c_{ij}} = \frac{c_{ij}|g_{11}|}{|1 + g_1 g_{11}|} \quad (\text{III.68})$$

where  $g_1 g_{11} = L_1$ . Equation (III.68) is manipulated to yield:

$$|1 + L_1| \geq \frac{c_{ij}|g_{11}|}{\tau_{ij}} \quad (\text{III.69})$$

Substituting Eq. (III.41) into Eq. (III.69) yields:



$$|1 + L_1| \geq \left| -\sum_{k \neq i} \frac{b_{kj}}{g_{ik}} \right| \frac{|g_{11}|}{\tau_{ij}} \quad (\text{III.70})$$

For example, in 3x3 system for the first loop,  $L_1$ , where  $i = 1$ ,  $j = 2$ , and in the first term  $k = 2$  and in the second term  $k = 3$ , Eq. (III.70) becomes:

$$|1 + L_1| \geq \frac{\left| \frac{b_{22}}{g_{12}} + \frac{b_{32}}{g_{13}} \right| |g_{11}|}{\tau_{c_{12}}} \quad (\text{III.71})$$

Remember to use only the magnitude in the cross-coupling calculations. This assumes the worst case.

### III.7 Constraints on the Plant Matrix<sup>21</sup>

In order to use the QFT technique the following critical condition must be satisfied.

Condition 1:  $P$  must be nonsingular for any combination of possible plant parameters, thus  $P^{-1}$  exists.

In the high frequency range  $y_{r_i}(j\omega)$  approaches zero as  $\omega \rightarrow \infty$ . Therefore, Eq. (III.39) can be approximated by

$$t_{ij} \approx y_{c_{ij}} \quad (\text{III.72})$$

Thus from Eqs. (III.35), (III.36) and (III.41), with impulse input functions, Eq. (III.72) can be expressed as

$$y_{c_{ij}} = \frac{c_{ij}g_{11}}{1 + g_i g_{11}} \quad (\text{III.73})$$

Consider first the 2x2 plant, i.e.,  $m = 2$ . Specifying that  $|y_{c_{ii}}| \leq b_{ii}$  (the given upper bound in the high frequency range), Eqs. (III.41) and (III.73) yield, for  $i = j = 1$ :

$$b_{11} \geq \left| \frac{-b_{21}}{q_{12}} \right| \left| \frac{q_{11}}{1 + L_1} \right| \quad (\text{III.74})$$

For  $i = 2, j = 1$ , where it is specified that  $(Y_c)_{21} \leq b_{21}$  (the given cross-coupling upper bound)\*, Eqs. (III.41) and (III.75) yield:

$$b_{21} \geq \left| \frac{-b_{11}}{q_{21}} \right| \left| \frac{q_{22}}{1 + L_2} \right| \quad (\text{III.75})$$

Equations (III.74) and (III.75) are rearranged to

$$|1 + L_1| \geq \frac{b_{21}}{b_{11}} \left| \frac{q_{11}}{q_{12}} \right| \quad (\text{III.76})$$

$$|1 + L_2| \geq \frac{b_{11}}{b_{21}} \left| \frac{q_{22}}{q_{21}} \right| \quad (\text{III.77})$$

Multiplying Eqs. (III.76) by Eq. (III.77), where  $L_1 = L_2 \approx 0$  in the high frequency range, results in

$$1 \geq \left| \frac{q_{11}q_{22}}{q_{12}q_{21}} \right| \quad (\text{III.78})$$

Since

$$P = \begin{bmatrix} p_{11} & p_{12} \\ p_{21} & p_{22} \end{bmatrix}, \quad P^{-1} = [p_{ij}^*] = \frac{1}{\Delta} \begin{bmatrix} p_{11} & -p_{12} \\ -p_{21} & p_{11} \end{bmatrix}, \quad Q = [q_{ij}] = \begin{bmatrix} q_{11} & q_{12} \\ q_{21} & q_{22} \end{bmatrix}$$

and

$$q_{ij} = \frac{1}{p_{ij}^*}$$

then

---

\*Henceforth, the cross-coupling bound notation  $b_{e_{ij}}$  is simplified to  $b_{ij}$  for  $i \neq j$ .

$$\begin{aligned}
q_{11} &= \frac{1}{p_{11}^*} = \frac{\Delta}{p_{22}} & q_{12} &= \frac{1}{p_{12}^*} = \frac{-\Delta}{p_{12}} \\
q_{21} &= \frac{1}{p_{21}^*} = \frac{-\Delta}{p_{21}} & q_{22} &= \frac{1}{p_{22}^*} = \frac{\Delta}{p_{11}}
\end{aligned}
\tag{III.79}$$

Substituting Eqs. (III.79) into Eq. (III.78) yields Condition 2.

Condition 2 (2x2 plant): As  $\omega \rightarrow \infty$

$$\begin{aligned}
|p_{11}p_{22}| &> |p_{12}p_{21}| & (a) \\
&\text{or} & \\
|p_{11}p_{22}| - |p_{12}p_{21}| &> 0 & (b)
\end{aligned}
\tag{III.80}$$

Since  $p_{11}$  and  $p_{22}$  are elements of the principal diagonal of  $\mathbf{P}$ , then Eq (III.80) is the diagonal dominance condition for the 2x2 plant. Equation (III.80(a)) must also be satisfied for all frequencies. This condition is obtained considering only the left column of the MISO loops for the 2x2 plant of Fig III.10. This condition may also be obtained by using the right column of the MISO loops in Fig III.10 since the loop transmissions  $L_1$  and  $L_2$  are again involved in the derivation. If Eq. (III.80) is not satisfied then refer to Item 3 on page 127.

Next consider the 3x3 plant, i.e.,  $m = 3$ . For  $i = j = 1$  (the left column of Fig. III.10), where  $L_1 = L_2 = L_3 \approx 0$  as  $\omega \rightarrow \infty$  and where it is specified that

$$|y_{c_{11}}| \leq b_{11}, \quad |y_{c_{21}}| \leq b_{21}, \quad |y_{c_{31}}| \leq b_{31}$$

Eqs. (III.41) and (III.73) yield, for  $i = 1, 2, 3$  respectively,

$$1 \geq \left| \frac{a_{11}}{b_{11}} \right| \left[ \left| \frac{b_{21}}{a_{12}} \right| + \left| \frac{b_{31}}{a_{13}} \right| \right] \quad (\text{III.81})$$

$$1 \geq \left| \frac{a_{22}}{b_{21}} \right| \left[ \left| \frac{b_{11}}{a_{21}} \right| + \left| \frac{b_{31}}{a_{23}} \right| \right] \quad (\text{III.82})$$

$$1 \geq \left| \frac{a_{33}}{b_{31}} \right| \left[ \left| \frac{b_{11}}{a_{31}} \right| + \left| \frac{b_{21}}{a_{32}} \right| \right] \quad (\text{III.83})$$

Letting

$$\lambda_1 = \frac{b_{21}}{b_{11}} \quad \lambda_2 = \frac{b_{31}}{b_{11}} \quad (\text{III.84})$$

Equations (III.81) through (III.83) become, respectively,

$$1 \geq |a_{11}| \left[ \left| \frac{\lambda_1}{a_{12}} \right| + \left| \frac{\lambda_2}{a_{13}} \right| \right] \quad (\text{III.85})$$

$$\lambda_1 \geq |a_{22}| \left[ \left| \frac{1}{a_{21}} \right| + \left| \frac{\lambda_2}{a_{23}} \right| \right] \quad (\text{III.86})$$

$$\lambda_2 \geq |a_{33}| \left[ \left| \frac{1}{a_{31}} \right| + \left| \frac{\lambda_1}{a_{32}} \right| \right] \quad (\text{III.87})$$

From Eqs. (III.86) and (III.87) and using

$$\gamma_{ij} = \left[ \frac{a_{1i} a_{1j}}{a_{1j} a_{1i}} \right]_{\substack{i=2 \\ j=3}} = \frac{a_{22} a_{33}}{a_{23} a_{32}} \quad (\text{III.88})$$

the following expressions for  $\lambda_1$  and  $\lambda_2$  are obtained

$$\lambda_1 \geq \frac{\left| \frac{a_{22}}{a_{21}} \right| + \left| \frac{a_{22} a_{33}}{a_{23} a_{31}} \right|}{|1 - \gamma_{23}|} \quad (\text{III.89})$$

$$\lambda_2 \geq \frac{\left| \frac{q_{33}}{q_{31}} \right| + \left| \frac{q_{22}q_{33}}{q_{21}q_{32}} \right|}{|1 - \gamma_{23}|} \quad (\text{III.90})$$

Substitute Eqs. (III.89) and (III.90) into Eq. (III.85) to obtain

$$\left| \frac{q_{11}}{q_{12}} \right| \left[ \left| \frac{q_{22}}{q_{21}} \right| + \left| \frac{q_{22}q_{33}}{q_{23}q_{31}} \right| \right] + \left| \frac{q_{11}}{q_{13}} \right| \left[ \left| \frac{q_{33}}{q_{31}} \right| + \left| \frac{q_{33}q_{22}}{q_{21}q_{32}} \right| \right] \leq |1 - \gamma_{23}| \quad (\text{III.91})$$

Substituting  $q_{ij} = 1/p_{ij}^*$  into Eq. (III.91) yields:

$$\left| \frac{p_{12}^*}{p_{11}^*} \right| \left[ \left| \frac{p_{21}^*}{p_{22}^*} \right| + \left| \frac{p_{23}^*p_{31}^*}{p_{22}^*p_{33}^*} \right| \right] + \left| \frac{p_{13}^*}{p_{11}^*} \right| \left[ \left| \frac{p_{31}^*}{p_{33}^*} \right| + \left| \frac{p_{21}^*p_{32}^*}{p_{22}^*p_{33}^*} \right| \right] \leq \left| 1 - \frac{p_{23}^*p_{32}^*}{p_{22}^*p_{33}^*} \right| \quad (\text{III.92})$$

Multiplying Eq. (III.92) by

$$p_{11}^*p_{22}^*p_{33}^* = p_{123}^*$$

yields Condition 3.

Condition 3 (3x3 plant; applies only for QFT design Method 1)

As  $\omega \rightarrow \infty$

$$|p_{123}^*| \geq |p_{12}^*| \left[ |p_{21}^*p_{33}^*| + |p_{23}^*p_{31}^*| \right] + |p_{13}^*| \left[ |p_{22}^*p_{31}^*| + |p_{21}^*p_{32}^*| \right] + |p_{11}^*p_{23}^*p_{32}^*| \quad (\text{III.93})$$

See Reference 21 for higher order plants. This condition is necessary

only if Eq. (III.8) is used to generate the plant.

Condition 1 ensures controllability of the plant since the inverse of  $P$  produces the effective transfer functions used in the design. If the  $P$  matrix, resulting from the original ordering of the elements of the input and output vectors does not satisfy Condition 2, then a reordering of the input and output vectors may result in satisfying these conditions.

### III.8 Basically Non-Interacting (BNIC) Loops

A basically non-interacting (BNIC) loop<sup>32</sup> is one in which the output  $y_k(s)$  due to the input  $r_j(s)$  is ideally zero. Plant uncertainty and loop interaction (cross-coupling) makes the ideal response unachievable. Thus, the system performance specifications describe a range of acceptable responses for the commanded output and a maximum tolerable response for the uncommanded outputs. The uncommanded outputs are treated as cross-coupling effects (akin to disturbances).

For an LTI plant, having no parameter uncertainty, it is possible to essentially achieve zero cross-coupling effects. That is, the output  $y_k \approx 0$  due to  $c_{ij}$ . This desired result can be achieved by postmultiplying  $P$  by a matrix  $W$  to yield:

$$P_n = PW = [p_{ii_n}] \quad \text{where } p_{ij_n} = 0 \text{ for } i \neq j$$

resulting in a diagonal  $P_n$  matrix for  $P$  representing the nominal plant case in the set  $\mathcal{O}$ . With plant uncertainty the off-diagonal terms of  $P_n$  will not be zero but "very small" in comparison to  $P$ , for the non-nominal plant cases in  $\mathcal{O}$ . In some design problems it may be necessary or desired to determine a  $P_n$  upon which the QFT design is accomplished. Doing this minimizes the effort required to achieve the desired BW and minimizes the cross-coupling effects. Since  $|t_{ij}(j\omega)| \leq b_{ij}(j\omega)$ ,  $i \neq j$ , for all  $\omega$ , it is clearly best to let

$f_{ij} = 0$ , for  $i \neq j$ . Thus,

$$t_{ij} = t_{c_{ij}} = \frac{C_{ij}Q_{ii}}{1 + L_{ii}} \text{ for all } i \neq j$$

This was done on an AFTI-16 design by Professor I. Horowitz as shown in Fig. III.16. In general, an upper bound  $b_{ij}$ ,  $i \neq j$ , is specified in order to achieve the performance specification:

$$|\tau_{c_{ij}}| \leq b_{ij} \text{ for all } P \in \mathcal{P}$$

A system designed to this specification is called BNIC.

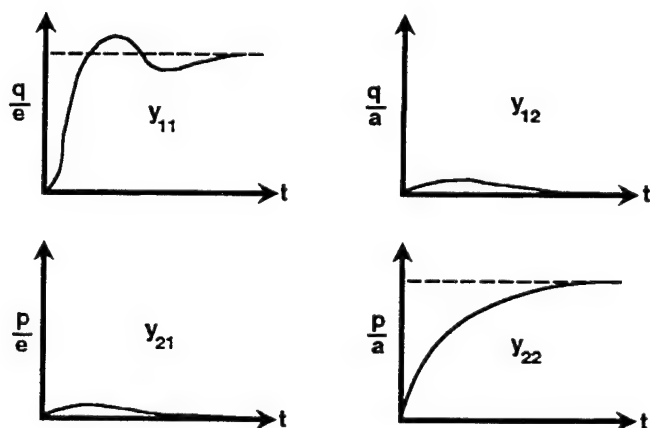


Fig. III.16 Output time response sketches for a  $2 \times 2$  plant: a – aileron deflection, q – pitch rate, e – elevator deflection, and p – roll rate.

### III.9 Summary

This chapter describes the multiple-input multiple-output closed-loop system and the plant matrix. Guidelines for finding the  $P$  matrix, which relates the input vector to the output vector, are given.

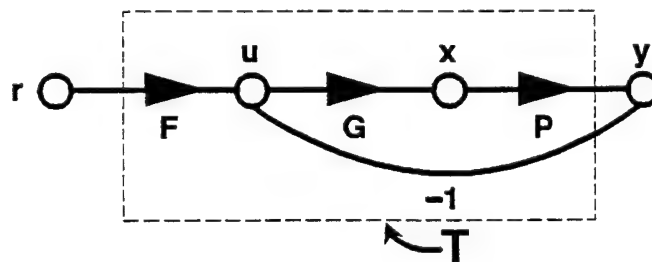
The method of representing a MIMO system by an equivalent set of MISO systems is presented using  $P^{-1}$ . Two design approaches, which are discussed in detail in Chaps. IV and V, respectively, are available in which the equivalent MISO loops are designed according to the MISO design method outlined in Chap. 18<sup>15</sup> and Chap. 16<sup>47</sup>. Since the  $g_i$ 's are the same for all  $m$  MISO systems in each row of FIG. III.11, the compensator must be "good enough" (large enough gain over the desired BW) to handle the "feedback needs" of the worst of the  $m$  systems for each value of  $\omega_i$  within the BW. If it is possible to find the  $f_{ij}$ 's and the  $g_i$ 's which satisfy the performance specifications for the  $m^2$  systems then it is guaranteed that these prefilters and compensators, when used as elements in the MIMO systems of Fig. III.7 or III.8, satisfy the design specifications of the original MIMO system. Thus, the  $m \times m$  MIMO has been converted into  $m$  design problems.

### III.10 Problems

**PIII.1** The plant matrix and the desired control ratio matrix for a  $2 \times 2$  system are:

$$P = \begin{bmatrix} \frac{1}{s+1} & \frac{0.2}{(s+1)(s+2)} \\ \frac{0.5}{s+1} & \frac{0.5s}{(s+1)(s+2)} \end{bmatrix} \quad T = \begin{bmatrix} \frac{2}{s+2} & 0 \\ 0 & \frac{2}{s+2} \end{bmatrix}$$

The one degree of freedom is shown in the figure where  $I$  is the identity matrix and  $I = F$



(a) Determine  $P^{-1}$ .



(b) Determine  $\mathbf{G}$  that results in achieving the desired  $\mathbf{T}$ .

(c) Suppose the actual compensator transfer function is:

$$\mathbf{G} = \begin{bmatrix} \frac{(0.5 + \epsilon_1)s}{s + 2} & g_{12} \\ \frac{-(0.5 + \epsilon_2)}{s - 0.2} & g_{22} \end{bmatrix} \quad \text{where } \epsilon_1 > 0, \epsilon_2 > 0$$

Determine  $t_{11}(s)$  and  $t_{21}(s)$ . Do these control ratios yield stable responses? Hint: Analyze  $\mathbf{T} = [\mathbf{I} + \mathbf{P} \mathbf{G}]^{-1} \mathbf{P} \mathbf{G}$ , especially  $\mathbf{P} \mathbf{G}$ .

(d) For this part assume  $t_{11}(s) = t_{22}(s) = (s - 2)/[(s + 2)(\tau s + 1)]$  and  $t_{12}(s) = t_{21}(s) = 0$  where  $\tau > 0$ . Determine  $\mathbf{G}(s)$  and compare it with  $\mathbf{G}$  of part (b).

**PIII.2.** In 2x2 MIMO system, the system poles due to feedback, are the zeros of  $\Delta = \det[\mathbf{I} + \mathbf{P} \mathbf{G}]$ . Assume that  $\mathbf{G}$  is a diagonal matrix. Prove that the zeros of interest are those of

$$\Delta' = (1 + g_1 q_{11})(1 + g_2 q_{22}) - \frac{q_{11} q_{22}}{q_{12} q_{21}}$$

Hint: show that  $(\Delta/p_{11}) = (\Delta'/q_{11})$ .

**PIII.3.** Let Fig. III.1 represent a 2x2 MIMO plant where the plant is described by:

$$\begin{aligned} \ddot{y}_1 + A\dot{y}_1 + By_1 + Cy_2 &= E_1\dot{u}_1 + E_2u_1 + E_3u_2 \\ J\dot{y}_2 + K\dot{y}_1 + Hy_1 &= Qu_2 \end{aligned}$$

(a) Determine  $\mathbf{P}$ .

(b) Determine  $\mathbf{P}^{-1}$  directly from  $\mathbf{P}$ . Suppose  $\mathbf{P}$  has the form where  $\Delta = n_{11}n_{22} - n_{12}n_{21}$ . By dividing  $d$  into  $\Delta$  you should obtain the quotient  $E_1Qs + E_2Q$  and no remainder. This

$$P = \frac{\begin{bmatrix} n_{11} & n_{12} \\ n_{21} & n_{22} \end{bmatrix}}{d} \quad \text{thus} \quad P^{-1} = \frac{\begin{bmatrix} n_{22} & -n_{12} \\ -n_{21} & n_{11} \end{bmatrix}}{\Delta} d$$

reveals that for most practical MIMO plants of the above form if  $P^{-1}$  is derived from  $P$  then the common poles of the elements of  $P$  should not appear as common zeros of the elements of  $P^{-1}$ .

(c) Utilizing Eq. (III.6) prove that the remainder is zero.

Hint:  $P = M^{-1}N$  and  $U = P^{-1}y$ .

## Chapter IV Design Method - The Single-loop (MISO) Equivalents<sup>17</sup>

### IV.1 Introduction

Let  $\tau_{ij}(s)$  be the set of acceptable transfer functions  $t_{ij}(s) = y_i(s)/r_j(s)$  [output  $y_i(s)$  in response to the command input  $r_j(s)$  in Fig. III.4]. Let the plant inverse matrix  $P^{-1} = [1/q_{ij}]$ , so the plant set  $P^{-1}$  generates sets of  $q_{ij} = \{q_{ij}\}$ . Replace the  $m \times m$  MIMO problem by  $m$  single loops and  $m^2$  prefilters (see Fig. III.10 for  $m = 3$ ). In Fig. III.10,  $P^{-1} = [1/q_{ij}]$ , and the uncertainty in  $P$  generates sets  $Q = \{q_{ij}\}$ . The cross-coupling effect

$$c_{11} = -\left(\frac{t_{21}}{q_{12}} + \frac{t_{31}}{q_{13}}\right) \quad t_{k1} \in \tau_{k1} \quad (\text{IV.1})$$

in Fig. III.10 is any member of a set  $c_{11}$  generated by the  $t_{k1}$  in  $\tau_{k1}$  and the  $q_{1k}$  in  $q_{1k}$ ,  $k = 2, 3$ .

In general in Fig. III.10,

$$c_{ij} = \{c_{ij}\}, \quad c_{ij} = -\sum_{k \neq i} \left( \frac{t_{kj}}{q_{ik}} \right), \quad t_{kj} \in \tau_{kj} \quad (\text{IV.2})$$

for the set of acceptable  $t_{kj}$  transfer functions. For the top row of MISO loops in Fig. III.10, the MISO design problem is to find  $L_1 = g_1 q_{11}$  and  $f_{11}$  such that the output is a member of the set  $\tau_{11}$  for all  $q_{11}$  in  $q_{11}$  and for all  $c_{11}$  in  $c_{11}$ . Similarly, for the middle MISO loop in the top row of Fig. III.10 find  $L_1 = g_1 q_{11}$  and  $f_{12}$  so that its output is in  $\tau_{12}$  for all  $q_{11}$  in  $q_{11}$  and all  $c_{12}$  in  $c_{12}$ , etc. Note that  $L_1$  is the same for all the MISO structures in the first row of Fig. III.10, etc. In each of these three structures, the uncertainty problem (due to the sets  $q_{1i}$ ,  $c_{1i}$ ) gives bounds on the level of feedback  $L_1$  needs, and so the toughest of these

bounds must be satisfied by  $L_1$ . That is, for each row there will exist, assuming a diagonal prefilter matrix  $F$ , three cross-coupling bounds and one tracking bound; thus, the toughest portions of these four bounds are combined to form the optimal bound to be used in loop shaping  $L_1$ .

If the designer designs these MISO systems to satisfy their above stated specifications, then it is guaranteed that these same  $f_{ij}$ ,  $g_i$  satisfy the MIMO uncertainty problem. It is not necessary to consider the highly complex system characteristic equation [denominator of Eq. (III.24)] with its uncertain  $p_{ij}$  plant parameters. System stability (and much more than that) for all  $P$  in  $\mathcal{P}$  is automatically guaranteed. It is easier to present the important ideas by means of a design example.

#### IV.2 Design Example

The power of the technique is illustrated by presenting the results of Reference 32, done as a Master's thesis by a typical graduate student who like nearly all control graduates, has had no courses dealing with uncertainty. The plant and uncertainties are

$$p_{ij} = \frac{sA_{ij} + B_{ij}}{s^2 + Es + F}$$

$A_{11} \in [2, 4]$	$A_{12} \in [-0.5, 1.1]$	$A_{22} \in [5, 101]$
$A_{31} \in [-0.8, -1.8]$	all other $A_{ij} = 0$	
$B_{11} \in [-0.15, 1]$	$B_{12} \in [-1, -2]$	
$B_{13} \in [1, 4]$		
$B_{21} \in [1, 2]$	$B_{22} \in [5, 10]$	$B_{23} \in [-1, 4]$
$B_{31} \in [-1, -2]$	$B_{32} \in [15, 25]$	
$B_{33} \in [10, 20]$		
$E \in [-0.2, 2]$	$F \in [0.5, 2]$	

(IV.3)

Note that  $p_{12}$  is always nonminimum phase (n.m.p.) and  $p_{11}$  is also n.m.p. for part of the structured parameter uncertainty range. Also, the plant is unstable for part of the parameter range. At small  $\omega$  there is no

diagonal dominance in any row, nor in columns 1,2. Hence, Rosenbrock's technique<sup>68</sup> cannot be used even if there was no parameter uncertainty.

Since the MISO plants in Fig. III.10 are  $q_{11} = [\det \mathbf{P}]/[\text{Adj}_{ii} \mathbf{P}]$ , it follows that if  $\det \mathbf{P}(s)$  has right-half-plane (RHP) zeros, the equivalent single-loop transmissions are n.m.p. (see Sec. V.10). The technique can still be used, but success can be guaranteed only if the performance tolerances are compatible with the n.m.p. character, just as in the single-loop system (see App. A.2).<sup>37,47</sup> For this design example,  $\det \mathbf{P}(s)$  has all its zeros in the interior of the left-half-plane (LHP), so this problem does not arise.

#### IV.2.1 Performance Tolerances

Performance tolerances are on the magnitudes of the elements of the 3x3 closed loop system transmission matrix  $\mathbf{T} = [t_{ij}(s)]$ , in the frequency domain  $|t_{ij}(j\omega)|$  which suffices when they are minimum-phase (m.p.). In fact, as previously noted<sup>20</sup>, time-domain specifications on the system output and on as many of its derivatives as desired, may then be achieved by means of bounds on  $|t_{ij}(j\omega)|$ . They are shown in Fig. IV.1(a) for  $|t_{ii}(j\omega)|$ ,  $i = 1,2,3$ , and in Fig. IV.1(b) for  $|t_{12}|$ ,  $|t_{32}|$ . The four remaining specifications are  $|t_{ij}(j\omega)| \leq 0.1$  for all  $\omega$ . The first five are called interacting and the latter four basically non-interacting (BNIC), because ideally zero  $t_{13}$ ,  $t_{21}$ ,  $t_{23}$ ,  $t_{31}$  are desired for all  $\omega$ . But this is impossible because of parameter uncertainty, so upper bounds must be assigned. The matter of m.p. or n.m.p. character of the BNIC elements is of no concern;  $t_{12}$ ,  $t_{32}$  are deliberately chosen interacting in order to obtain a design problem with considerable variety. The functions which satisfy the assigned tolerances on  $t_{ij}$  constitute a set  $\tau_{ij}$ .

#### IV.2.2 Sensitivity Analysis

An important aspect in the design of a control system is the insensitivity of the system outputs to items such as: sensor noise, parameter uncertainty, cross-coupling effects, and external system disturbances. The effect of these items on system performance can be

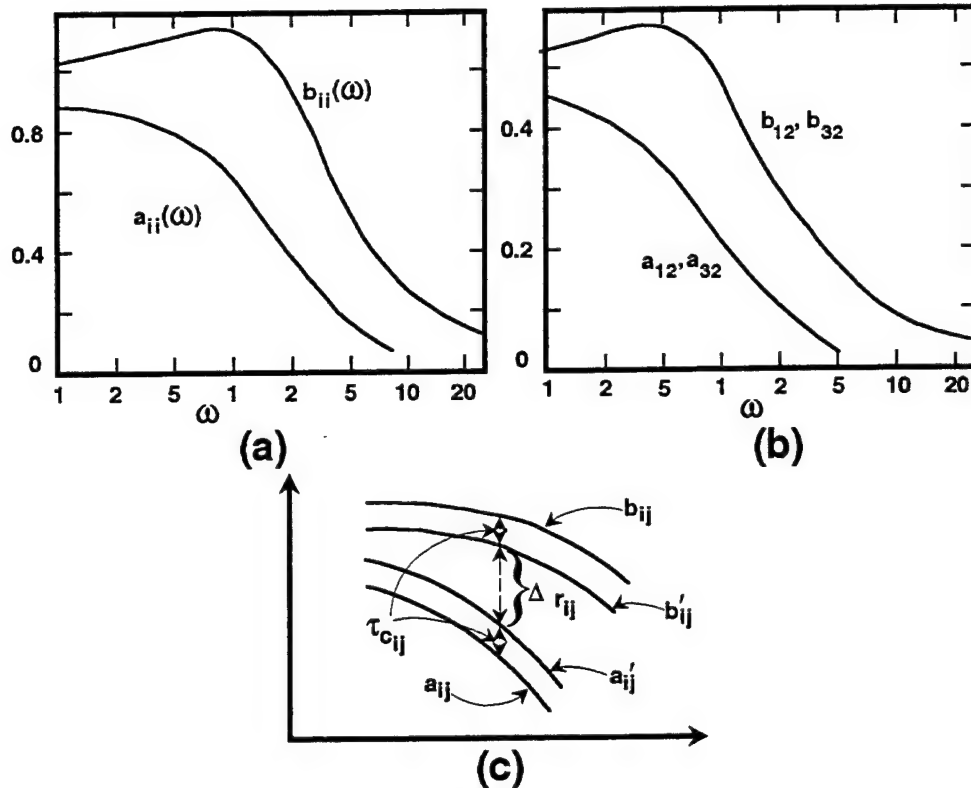


Fig. IV.1 Tolerances (a) on  $|t_{ii}(j\omega)|$ , (b) on  $|t_{12}|$ ,  $|t_{32}(j\omega)|$ , and (c) allocation.

expressed in terms of the sensitivity function<sup>15</sup>

$$S_{\delta}^T = \frac{\delta}{T} \left[ \frac{\partial T}{\partial \delta} \right] \quad (\text{IV.4})$$

where  $\delta$  represents the variable parameter in  $T$ . Figure IV.2 is used for the purpose of analyzing the sensitivity of a system to three of these items.

Using the linear superposition theorem, where

$$Y = Y_R + Y_c + Y_N$$

and  $L = GP$ , the following transfer functions and sensitivity functions are obtained, respectively:

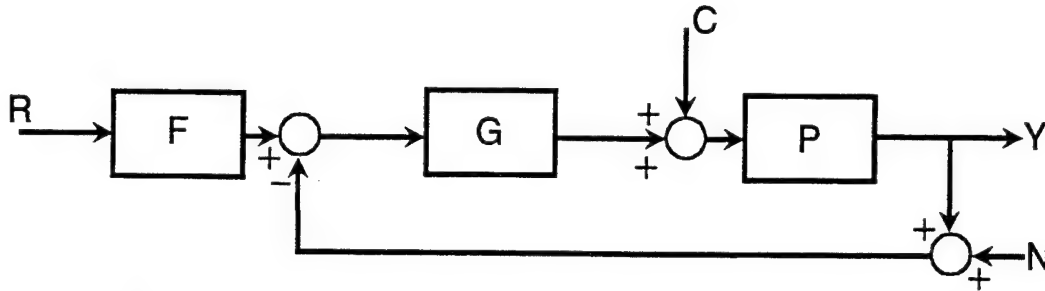


Fig. IV.2 An example of system sensitivity analysis

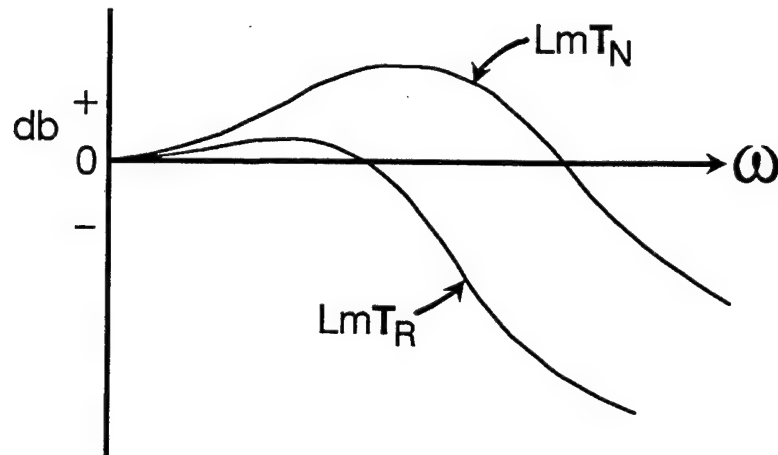


Fig. IV.3 Frequency response characteristics for system of Fig. IV.2

$$\begin{aligned} T_R = \frac{Y_R}{R} &= \frac{FL}{1+L} \quad (a) & T_N = \frac{Y_N}{N} &= \frac{-L}{1+L} \quad (b) \\ T_C = \frac{Y_C}{C} &= \frac{P}{1+L} \quad (c) \end{aligned} \quad (IV.5)$$

$$\begin{aligned} S_P^{T_R} &= \frac{FG}{1+L} \quad (a), & S_P^{T_N} &= \frac{-G}{1+L} \quad (b) \\ S_P^{T_C} &= \frac{1}{1+L} \quad (c) \end{aligned} \quad (IV.6)$$

Since sensitivity is a function of frequency, it is necessary to achieve a slope for  $Lm L_o(j\omega)$  that minimizes the effect on the system due to sensor noise. This is the most important case, since the "minimum BW" of Eq. (IV.5(b)) tends to be greater than the BW of Eq. (IV.5(a)), as illustrated in Fig. IV.3. Based on the magnitude characteristic of

$L_o$  for low and high frequency ranges, then:

For the low frequency range, from Eq. (IV.6(b)) --

$$S_P^{T_N} \approx \left| \frac{-1}{P(j\omega)} \right| \quad (\text{IV.7})$$

For the high frequency range, from Eq. (IV.6(b)) --

$$S_P^{T_N} \approx |-G(j\omega)| = \left| \frac{-L(j\omega)}{P(j\omega)} \right| \quad (\text{IV.8})$$

The BW characteristics, with respect to sensitivity, are illustrated in Fig. IV.4. As seen from this figure, the low frequency sensitivity given by Eq. (IV.7) is satisfactory but the high frequency sensitivity given by Eq. (IV.8) is unsatisfactory since it can present a serious noise rejection problem.

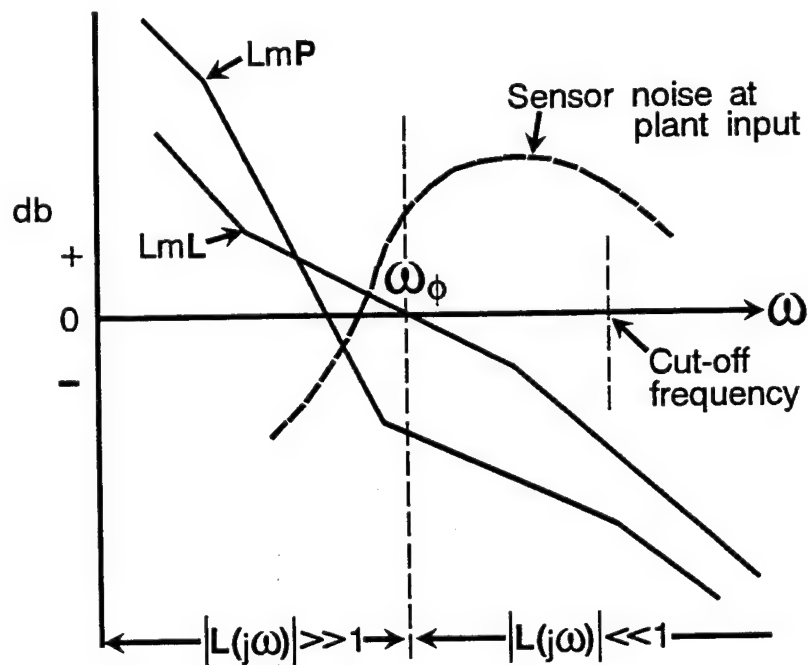


Fig. IV.4 Bandwidth characteristics of Fig. IV.2



Based upon the analysis of Fig. IV.4, it is necessary to try to make the phase margin frequency  $\omega_\phi$  (the loop transmission BW), small enough in order to minimize the sensor noise effect on the system's output. For most practical systems  $n \geq w + 2$  and

$$\int_0^\infty \log[S_P^\pi] d\omega = 0 \quad (\text{IV.9})$$

For

$$\begin{aligned} |S_P^\pi| < 1 &\rightarrow \log[S_P^\pi] < 0 & (a) \\ |S_P^\pi| > 1 &\rightarrow \log[S_P^\pi] > 0 & (b) \end{aligned} \quad (\text{IV.10})$$

Thus, the designer must try to locate the condition of Eq. (IV.10(b)) in the "high frequency" (h.f.) range where the system performance is not of concern, i.e., the noise effect on the output is negligible.

The analysis for external disturbance effect (see Chap. VI) on the system output is identical to that for cross-coupling effects. For either case, low sensitivity is conducive to their rejection.

#### IV.2.3 Simplification of the Single-loop Structures

For the second row of Fig. III.10  $y_{ij}(s)$  has the two components due to  $r_j(s) = 1$  and to  $c_{ij}(s)$ . Their respective outputs are:

$$y_{ri} = \frac{f_{ij}L_i}{1 + L_i} \quad (a) \quad y_{cij} = \frac{c_{ij}q_{ii}}{1 + L_i} \quad (b) \quad (\text{IV.11})$$

$$\text{where } L_i = g_i q_{ii} \quad (c)$$

At a fixed  $P \in \mathcal{P}$  (and hence  $m^2 q_{ij}$ )  $|Y_{c_{ij}}|_{\max}$  occurs at

$$|c_{ij}|_{\max} = \left| \sum_{k \neq i} \frac{t_{kj}}{q_{ik}} \right|_{\max}$$

The relative phases of the  $t_{kj}/q_{ik}$  are not known so the extreme magnitude of

$$|c_{ij}|_{\max} = \left| \sum_{k \neq i} \frac{t_{kj}}{q_{ik}} \right|_{\max} = \left| \sum_{k \neq i} \frac{b_{kj}}{q_{ik}} \right|_{\max} \quad (\text{IV.12})$$

resulting from among the J plants must be used in the design. That is, where  $b_{ii}$  and  $b_{ki}$  represent the upper bounds of the control ratio  $t_{ii}$  and  $t_{ki}$ , respectively, in Fig. IV.1(a) and (b), respectively. Also shown in this figure are the corresponding lower bounds  $a_{ii}$  and  $a_{ki}$ , respectively.

There are two kinds of performance tolerances, i.e., tolerances on  $t_{ii}$  and on  $t_{ij}$  for  $i \neq j$  (BNIC). For the BNIC ( $k, i = 1,3; 2,1; 2,3; \text{etc.}$ ) it is necessary that

$$\begin{aligned} |y_{xi} + y_{c_{ij}}| &= |\tau_{ij}(j\omega) + \tau_{c_{ij}}(j\omega)|_{\max} \leq |\tau_{ij}|_{\max} + \\ &|\tau_{c_{ij}}|_{\max} = |\tau_{c_{ij}}|_{\max} \leq b_{ij}(j\omega) \end{aligned} \quad (\text{IV.13})$$

because the relative phase of the two terms is not known, so it is clearly best to force  $\tau_{ij} = 0$  by setting  $f_{ij} = 0$  ( $i \neq j$ ) in Eq. (IV.11) for (1,3; 2,1; 2,3; 3,1). Let some fixed  $P$  be chosen as the nominal plant matrix  $P_o = [p_{ij}]$ , generating a nominal  $P_o^{-1} = [1/q_{ij}]$  and the nominal loop transmissions  $L_{io} = g_i q_{iio}$ , so  $L_i = L_{io} q_{ii}/q_{iio}$ . In this example, the nominal plant parameters of Eq. (IV.3) are chosen as:

$$\begin{array}{lll} A_{11} = 2 & B_{11} = 0.1 & A_{12} = 1.1 \\ B_{12} = -1 & B_{13} = 4 & B_{21} = 2 \\ A_{22} = 5 & B_{22} = 5 & B_{23} = 4 \\ A_{31} = 1.8 & B_{31} = 1 & B_{32} = 20 \\ B_{33} = 10 & E = 2 & F = 2 \end{array} \quad (\text{IV.14})$$

Using Eqs. (IV.11(b)) and (IV.12) the condition given by Eq. (IV.13) can now be written (for the BNIC  $t_{ij}$ ) to yield the following design specification:

specification:

$$\left| \frac{1}{1 + L_{io} \frac{q_{ii}}{q_{iio}}} \right| \leq \frac{b_{ij}}{c_{ij} q_{ii}} = \frac{b_{ij}}{\sum_{k \neq i} \left| \frac{q_{ii}}{q_{ik}} \right| b_{ki}} \quad (\text{IV.15})$$

Specification type described by Eq. (IV.15) is denoted as a D-type, specifically  $D_{ij}$ .

The specifications on the interacting  $t_{ij}$  terms (all  $t_{ii}$  and  $t_{12}, t_{32}$ ) are, using Eq. (IV.11),

$$a_{ij}(\omega) \leq |\tau_{ij}(j\omega) + \tau_{c_{ik}}(j\omega)| \leq b_{ij}(\omega)$$

with  $a_{ij}, b_{ij}$  being the designated bounds shown in Fig. IV.1. Suppose that due to the uncertainty in  $q_{ii}$ ,  $|\tau_{ij}|$  of Eq. (IV.11) is in the interval  $[a'_{ij}, b'_{ij}]$  [see Fig. IV.1(c)]. Since the relative phases of  $\tau_{ij}, \tau_{c_{ij}}$  are not a priori known, it is necessary that:

$$|b'_{ij} + \tau_{c_{ij}}| \leq b_{ij}, \quad |a'_{ij} - \tau_{c_{ij}}| \geq a_{ij} \quad (\text{IV.16})$$

From Eq. (IV.11) the above may be summarized by Eq. (IV.16) and

$$\Delta \left| \frac{L_i}{1 + L_i} \right| \leq \frac{b'_{ij}}{a'_{ij}} \quad (a) \quad \left| \frac{1}{1 + L_i} \right| \leq \left| \frac{\tau_{c_{ij}}}{c_{ij} q_{ii}} \right|_{\max} = \frac{\tau_{c_{ij}}}{\sum_{k \neq i} \left| \frac{q_{ii}}{q_{ik}} \right|_{\max} b_{ki}} \quad (b) \quad (\text{IV.17})$$

Equation (IV.17(a)) is denoted as  $A_{ij}$ , Eq. (IV.17(b)) as  $B_{ij}$ . Note that Eq. (IV.17(b)) is almost the same as  $D_{ij}$  of Eq. (IV.15) except that  $\tau_{c_{ij}}$  is not known and must be suitably chosen together with  $a'_{ij}, b'_{ij}$  subject to Eq. (IV.16). The results of this section are summarized in Table IV.1.

### IV.3 High Frequency Range Analysis

The analysis in the h.f. range, for the case of  $i = j$ , can be

based upon the fact that the filter  $f_{ii}$  when designed to yield the desired response has the value  $|f_{ii}(j\omega)| \approx 0$ . Thus,  $t_r$  in Eq. (III.27) can be neglected. For a 2x2 system, consider the bounds shown in Fig. IV.5, for  $i = j = 1$ . Based upon the knowledge of the control system to be designed, the designer selects the value of  $\omega_{h.f.}$  above which the cross-coupling effects have no effect on system performance. Thus, as shown in Fig. IV.5, the lower bound  $a_{11}$  is "dropped" to zero and only the upper bound  $b_{11}$  is used -- eliminating the need to determine  $b'_{11}$ . Thus, from Eq. (III.76):

$$|1 + L_1| \geq \frac{b_{21}}{b_{11}} \left| \frac{q_{11}}{q_{12}} \right| = \lambda \left| \frac{q_{11}}{q_{12}} \right| \quad \text{where } \lambda = \frac{b_{21}}{b_{11}} \quad (\text{IV.18})$$

In a similar manner, for  $L_2$ , from Eq. (III.77), obtain:

$$|1 + L_2| \geq \frac{b_{11}}{b_{21}} \left| \frac{q_{22}}{q_{21}} \right| = \frac{1}{\lambda} \left| \frac{q_{22}}{q_{21}} \right| \quad (\text{IV.19})$$

Remember that these equations apply in the h.f. range where the lower bounds are neglected.

Note: (1)  $t_{21}$  still needs to be specified even when  $f_{21} = 0$ ; (2) the  $\lambda$  ratio can be anything; and based upon the location of "noisy sensors" might require a trade-off in the phase margin frequency specification for each loop.

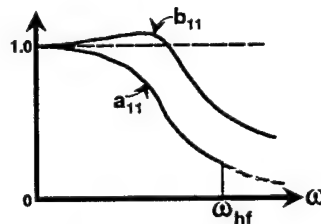


Fig. IV.5 High-frequency (h.f.) cut-off for  $a_{11}$ .

Multiplying Eq. (IV.18) by Eq. (IV.19) yields:

$$|1 + L_1| |1 + L_2| \geq \left| \frac{q_{11}q_{22}}{q_{12}q_{21}} \right| = \left| \frac{p_{12}p_{21}}{p_{11}p_{22}} \right| \quad (\text{IV.20})$$

For the 2x2 plant, the diagonal dominance condition, for  $\omega \rightarrow \infty$  (say  $\omega > \omega_h$ ) is given by:

$$\left| \frac{p_{12}p_{21}}{p_{11}p_{22}} \right| < 1 \quad (\text{IV.21})$$

which must be true over the entire range of  $P \in \mathcal{P}$ . Let

$$\gamma_{12} = \frac{p_{12}p_{21}}{p_{11}p_{22}} \quad (\text{IV.22})$$

Remember that

$$P = \begin{bmatrix} p_{11} & p_{12} \\ p_{21} & p_{22} \end{bmatrix} \rightarrow P^{-1} = \frac{1}{\det P} \begin{bmatrix} p_{22} & -p_{12} \\ -p_{21} & p_{11} \end{bmatrix}$$

and

$$\begin{aligned} q_{11} &= \frac{\det P}{p_{22}} = \frac{p_{11}p_{22} - p_{12}p_{21}}{p_{22}} = p_{11}(1 - \gamma) \quad (a) \\ q_{22} &= \frac{\det P}{p_{11}} = p_{22}(1 - \gamma) \quad (b) \end{aligned} \quad (\text{IV.23})$$

Thus, it is the zeros of the q's which determine if the system is m.p. not the zeros of the p's.

#### IV.4 Stability Analysis

A 2x2 plant is used to discuss the stability analysis for a MIMO system. The Nyquist stability criterion<sup>15</sup> should be applied in the polar plot domain, especially for n.m.p. q's. By substituting the equation

Table IV.1 Constraints on the equivalent single-loop structures

$\Lambda_{11}, \Lambda_{12}$	$B_{11}$	$B_{12}$	$D_{13}$
$\Delta \left  \frac{L_1}{1+L_1} \right  \leq \frac{b'_{11} b'_{12}}{a'_{11} a'_{12}}$	$\frac{1}{1+L_1} \leq \frac{b_{21} \left  \frac{q_{11}}{q_{12}} \right  + b_{31} \left  \frac{q_{11}}{q_{13}} \right }{b_{21} \left  \frac{q_{11}}{q_{12}} \right  + b_{31} \left  \frac{q_{11}}{q_{13}} \right }$	$\frac{b_{12}}{d_{12}}$	$b_{13}$
$D_{21}$	$A_{22}$	$B_{22}$	$D_{23}$
$\frac{1}{1+L_2} \leq \frac{b_{11} \left  \frac{q_{22}}{q_{21}} \right  + b_{31} \left  \frac{q_{22}}{q_{23}} \right }{b_{11} \left  \frac{q_{22}}{q_{21}} \right  + b_{31} \left  \frac{q_{22}}{q_{23}} \right }$	$\Delta \left  \frac{L_2}{1+L_2} \right  \leq \frac{b_{22}}{a_{22}}$	$\frac{1}{1+L_2} \leq \frac{b_{12} \left  \frac{q_{22}}{q_{21}} \right  + b_{32} \left  \frac{q_{22}}{q_{23}} \right }{b_{12} \left  \frac{q_{22}}{q_{21}} \right  + b_{32} \left  \frac{q_{22}}{q_{23}} \right }$	$b_{23}$
$D_{31}$	$B_{32}$	$A_{32}, A_{33}$	$B_{33}$
$\frac{1}{1+L_3} \leq \frac{b_{11} \left  \frac{q_{33}}{q_{31}} \right  + b_{21} \left  \frac{q_{33}}{q_{32}} \right }{b_{11} \left  \frac{q_{33}}{q_{31}} \right  + b_{21} \left  \frac{q_{33}}{q_{32}} \right }$	$\frac{b_{32}}{d_{32}}$	$\Delta \left  \frac{L_3}{1+L_3} \right  \leq \frac{b_{32} b_{33}}{a_{32} a_{33}}$	$\frac{1}{1+L_3} \leq \frac{b_{13} \left  \frac{q_{33}}{q_{31}} \right  + b_{23} \left  \frac{q_{33}}{q_{32}} \right }{b_{13} \left  \frac{q_{33}}{q_{31}} \right  + b_{23} \left  \frac{q_{33}}{q_{32}} \right }$

for  $t_{21}$  into the equation for  $t_{11}$  in Eq. (III.50), with  $f_{ij} = 0$  for  $i \neq j$ , yields:

$$t_{11} = \frac{f_{11}L_1(1 + L_2)}{(1 + L_1)(1 + L_2) - \gamma_{12}} \quad (\text{IV.24})$$

Thus, the denominator of Eq. (IV.24) yields the characteristic equation:

$$(1 + L_1)(1 + L_2) - \gamma_{12} = 0 \quad (\text{IV.25})$$

At "low" frequencies  $|L_1|$  and  $|L_2|$  are both  $\gg |\gamma_{12}|$  and at h.f.  $|L_1| = |L_2| \approx 0 \rightarrow 1 - \gamma_{12} = 0$ .

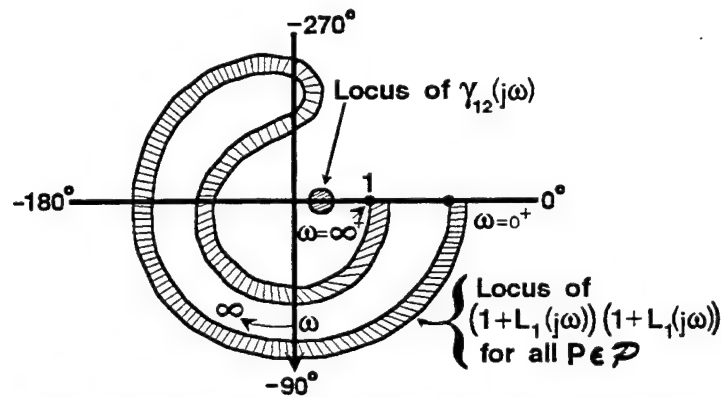


Fig. IV.6 Polar plots of Eq. (IV.25)

Figure IV.6 shows the polar plot of  $(1 + L_1)(1 + L_2)$  for all  $P \in \mathcal{P}$  (shaded area) and the locus of critical points represented by  $\gamma_{12}$ . For a LTI plant, with no parameter uncertainty, whose characteristic equation is  $G(s)H(s) + 1 = 0$  the "locus of critical points" is the  $-1 + j0$  point. Thus, for this  $2 \times 2$  plant the polar plot in Fig. IV.6 can not encircle the  $\gamma_{12}$  locus for  $P \in \mathcal{P}$  or  $(1 + L_1)(1 + L_2) - \gamma_{12}$  can not encircle the origin. Since the diagonal dominance condition must be satisfied, i.e., as  $\omega \rightarrow \infty$   $|p_{11}p_{22}| \gg |p_{12}p_{21}|$  then the magnitude  $|\gamma_{12}|$  better be  $< 1$  or the  $\gamma_{12}$  locus will be encircled resulting in an unstable system.

#### IV.5 Equilibrium and Trade-Offs

There are interactions between the rows of Fig. III.10 via the

specifications  $b_{ij}$ . Consider the following two examples.

**Example IV.1 -- Trade-off Example #1**

The SFG for a 2x2 plant is shown in Fig. IV.7. For this example assume  $|t_{ij}|_{\max} \equiv b_{ij}$  and let the  $\phi$ 's represent the actual values of the outputs (see Sec. III.6.2).

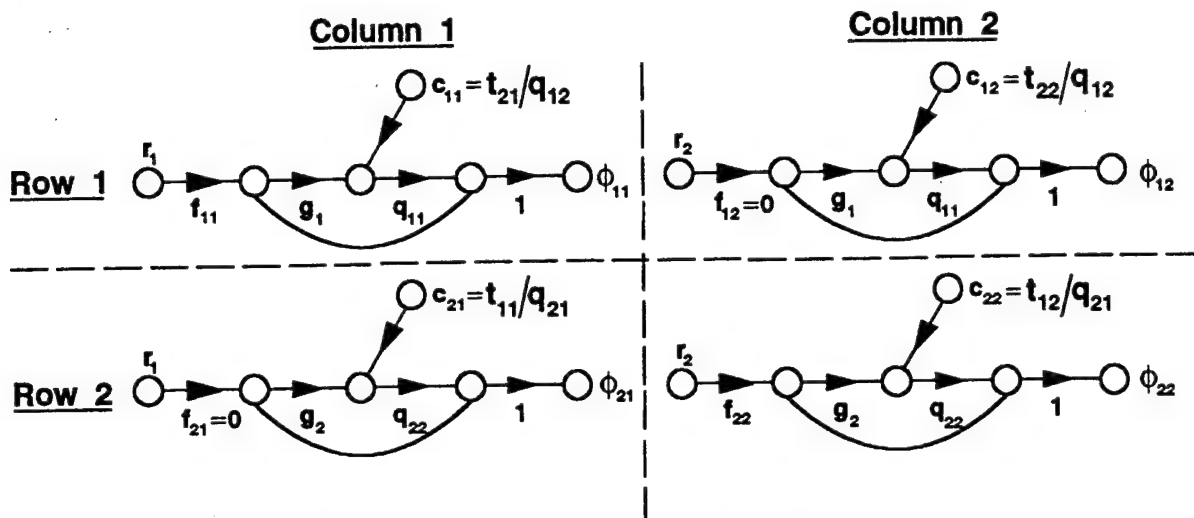


**Fig. IV.7 Equilibrium and trade-offs for a 2x2 plant.**

(a) Consider -- Suppose, for a fixed value of  $\omega_i$ :

---  $\phi_{12}$  "dominates" in the first row of Fig. IV.7, i.e. dominates  $L_1$  and

---  $\phi_{21}$  "dominates" in the second row, i.e., dominates  $L_2$

--- then if the value of the specification  $b_{22}$  is lowered it helps  $\phi_{12}$  which decreases the demand on  $L_1$ .

(b) Assume the terms that dominate in each row are in different columns. Thus, it is possible to ease the design by being concerned with one or more  $b_{ij}$ 's. For example:



<u>Column 1</u>	<u>Column 2</u>	
$c_{11} = \frac{-b_{21}}{q_{12}}$	$c_{12} = \frac{-b_{22}}{q_{12}}$	<u>Row 1</u>
$c_{21} = \frac{-b_{11}}{q_{21}}$	$c_{22} = \frac{-b_{12}}{q_{21}}$	<u>Row 2</u>

If the 1,1 and 2,2 terms dominate then it is possible to ease the design by decreasing  $b_{21}$  and  $b_{12}$ .

#### Example IV.2 -- Trade-off Example #2

For Row 1, Column 1, from the SFG of Fig. III.10 for a 3x3 plant:

$$c_{11} = -\left(\frac{b_{21}}{q_{12}} + \frac{b_{31}}{q_{13}}\right), \quad c_{21} = -\left(\frac{b_{11}}{q_{21}} + \frac{b_{31}}{q_{23}}\right), \quad c_{31} = -\left(\frac{b_{11}}{q_{31}} + \frac{b_{21}}{q_{32}}\right)$$

The same process, as done in Example IV.1, is used here in doing a "trade-off" on the specifications for one or more  $b_{ij}$  in order to hopefully achieve the desired dominance through the analysis of:

$$|1 + L_i| \geq \frac{|q_{11}|}{b_{11}} \left[ \frac{b_{21}}{|q_{12}|} + \frac{b_{31}}{|q_{13}|} \right], \geq \frac{|q_{22}|}{b_{21}} \left[ \frac{b_{11}}{|q_{21}|} + \frac{b_{31}}{|q_{23}|} \right], \geq \frac{|q_{33}|}{b_{31}} \left[ \frac{b_{11}}{|q_{31}|} + \frac{b_{21}}{|q_{32}|} \right]$$

For example, suppose  $b_{21}$  is decreased from 0.1 to  $\delta$ . (Decrease of  $b_{21}$  is permissible because the BNIC  $|t_{21}| \leq b_{21}$  is required.) This decreases  $|c_{11}|$  and  $|c_{31}|$  in Fig. III.10, which eases the burden on  $L_1$  and  $L_3$  for satisfying  $y_{11} \in \tau_{11}$  and  $y_{31} \in \tau_{31}$ , assuming that  $y_{11}$  and  $y_{31}$  dominate  $L_1$  and  $L_3$ , respectively. But it makes it harder on  $L_2$ , because now  $|y_{21}| \leq \delta$  instead of 0.1. This does not matter if  $y_{22}$  dominates  $L_2$ . If so,  $b_{21}$  can be decreased until say  $y_{21}$  imposes the same burden on  $L_2$  as does  $y_{22}$ , denoted by  $y_{21} \sim y_{22}$ . Any further decrease of  $b_{21}$  involves 'trade-off', i.e., sacrifice of  $L_2$  for the sake of  $L_1$  and/or  $L_3$ . However, it is conceivable that before  $y_{21} \sim y_{22}$  occurs, either  $y_{12}$  (or  $y_{13}$ )  $\sim y_{11}$ , or  $y_{32}$  (or  $y_{33}$ )  $\sim y_{31}$ . There are a bewildering multitude of possibilities and options.

As illustrated by these examples, it may be possible to modify one

or more  $b_{ij}$  until the dominant terms lie in the same column. To accomplish this may require a "trade-off" in one or more of the system's performance specifications. There are a bewildering multitude of possibilities and options. Is there a simple rule for determining when 'free' easing of burdens is no longer possible, and only 'trade-off' is available? This question is partly answered by the following definition and theorem.

### Definition

Equilibrium exists when it is impossible to reduce the burden on any  $L_i$ , without increasing it on some other  $L_j$ .

### Theorem

A necessary and sufficient condition for equilibrium is when all the  $L_i$  are dominated by the members of the same column, i.e.  $y_{ij}$ ,  $i = 1, 2, \dots, m$  dominate the  $L_i$ , with  $j$  any fixed column. This does not preclude  $y_{ij}, \sim y_{ik} \sim \dots$  for one or more  $i, k$ . See Reference 32 for proof.

Clearly, a number of equilibria can exist, as any column may be chosen. This variety offers the designer very useful design freedom. He may wish to economize on some  $L_x$ , according to the circumstances - for example, if the sensor on  $y_x$  is noisier than the others, or  $q_{xx}$  has elastic modes in a rather low  $\omega$  range, so it is important to reduce  $|L_x(j\omega)|$  rapidly compared with  $\omega$ . It is also emphasized that all the above discussion is at a fixed  $\omega_i$  value. It may be desirable and it is certainly possible to have different columns dominating at different  $\omega_i$  values, and the design technique offers this kind of flexibility. The potential profit to be gained by exploiting column dominance is greater at high frequency because the  $\delta_R$  tolerances are greater in this range of  $\omega$ , i.e.,  $\delta_R = b_{ii} - a_{ii}$  is greater than in the "low frequency" range.

The above analysis led to the low and medium frequency bounds on  $L_{i0}$  shown in Fig. IV.8.

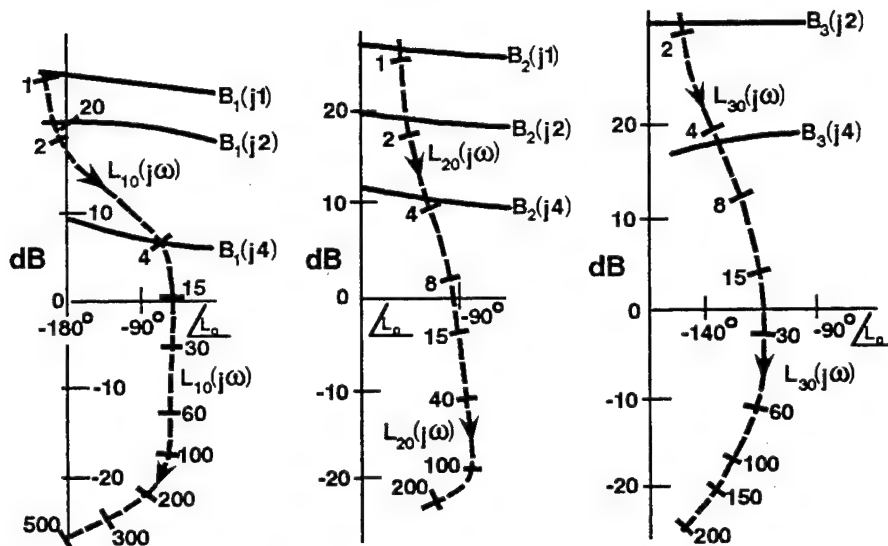


Fig. IV.8 Bounds in Nichols Chart on  $L_{i0}(j\omega)$ ,  $i = 1, 2, 3$ , and  $L_i$  designed.

### Trade-off

After equilibrium has been reached, it is still possible and may be desirable to do 'trade-off' -- that is, sacrifice one or more  $L_{i0}$  for others, e.g., in the situations noted above. Thus, say column 1 dominates all  $L_i$  but it is highly desirable to reduce  $L_1$ . In Fig. III.10 one or both of  $b_{21}, b_{31}$  may be reduced thereby decreasing  $|c_{11}|$  but making the specifications harder on  $y_{21}, y_{31}$ . Assuming that  $y_{11} \approx y_{12}$  then it is also necessary to reduce one or both of  $b_{22}, b_{32}$ . At low  $\omega$  values, the amount of such improvement is quite limited, because  $b_{ij} > a_{ij}$  (in the interacting  $y_{ij}$ ), and the difference between  $b_{ij}$  and  $a_{ij}$  is small at low  $\omega$  (see Figs. IV.5 (a) and (b)). Also, as  $b_{ij} \rightarrow a_{ij}$ , the sacrifice of  $L_i \rightarrow \infty$ , for the sake of very small improvement of some other  $L$ . In serious situations, the designer can then consider modifying the  $(a_{ij}, b_{ij})$  tolerances. This is another of the valuable insights offered by the design technique. The trade-off situation is radically different in the high frequency range.

#### IV.5.1 Trade-off In High Frequency Range

At large  $\omega$ , the  $a_{ij}(\omega)$  of the interacting  $t_{ij}$  of Figs. IV.1(a) and (b) become so small that they can be made zero. Hence, the  $A_{ij}$  in Table IV.1 can be ignored and each  $\tau_{c_{ij}} = b_{ij}$ , so all the constraints in the table are now of the D type, i.e., replace the  $B_{ij}$  by  $D_{ij}$ . There is now no limit on the permissible reduction of the  $b_{ij}$  and the problems of 'equilibrium' and 'trade-off' become so simplified, as to permit analytical derivation of the bounds  $B_i(j\omega)$  on  $L_{i0}(j\omega)$ . First the claim that the  $b_{ij}$  are optimally chosen so that  $D_{1i} \sim D_{1j}$ , ... ,  $D_{mi} \sim D_{mj}$ , for all  $i, j$  is easily proven. Suppose, (with no loss of generality), that  $D_{11}$  dominates  $L_1$ . Reduce  $b_{12}$  (recall it has replaced  $\tau_{c_{12}}$ ) until  $D_{12} \sim D_{11}$ . This certainly doesn't hurt  $L_1$  and helps  $D_{12}$ ,  $i \neq 1$ . Hence, if any  $D_{12}$  dominates  $L_i$  this reduction of  $b_{12}$  helps  $L_i$ . If not, a single  $D_{12}$  does so, then there is at least no harm in this reduction of  $b_{12}$ . Similarly, reduce  $b_{13}$ , until  $D_{13} \sim D_{12} \sim D_{11}$ . Using exactly the same argument, one can deduce that  $D_{23} \sim D_{22} \sim D_{21}$ , etc., for each row.

The above result applies even if the  $|q_{11}/q_{12}|_{\max}$  are different in the elements of row 1, etc. However, if they are the same, as they are in this case then let  $v_{ij} \triangleq |q_{ii}/q_{ij}|_{\max}$  which appear in row  $i$  of Table IV.1

The above give

$$\frac{b_{11}}{v_{12}b_{21} + v_{13}b_{31}} = \frac{b_{12}}{v_{12}b_{22} + v_{13}b_{32}} = \frac{b_{13}}{v_{12}b_{23} + v_{13}b_{33}} \triangleq \lambda_1 \quad (\text{IV.27})$$

$$\frac{b_{k1}}{\sum_{i \neq k} v_{ki}b_{i2}} = \frac{b_{k2}}{\sum_{i \neq k} v_{ki}b_{i2}} = \dots \triangleq \lambda_k \quad (\text{IV.28})$$

Consider the  $m$  equations

$$\frac{b_{k1}}{\sum_{i \neq k} v_{ki}b_{i1}} = \lambda_k \quad \text{for } k = 1, 2, \dots, m \quad (\text{IV.29})$$

which constitute a linear homogeneous set in the  $m$   $b_{ki}$ . For a solution to exist the determinant of the coefficient matrix must be zero. This matrix, denoted by  $\phi$  has  $v_{ij}$  for its off-diagonal and  $\lambda_i$  as its diagonal elements. Exactly the same matrix results by taking any  $\alpha$  value in the set of  $m$  equations

$$\frac{b_{kk}}{\sum v_{ki} b_{ia}} = \lambda_k, \quad k = 1, 2, \dots, m \quad (\text{IV.30})$$

The choice of the  $\lambda_k$  is up to the designer but he or she can choose only  $m - 1$  of them. The condition  $\det \phi = 0$ , determines the last  $\lambda$  value. In this way, the designer can deliberately sacrifice some loops in order to help others.

For any fixed  $j$ , the above set of  $m$  equations in  $b_{kj}$  ( $k = 1, \dots, m$ ) is homogeneous, so the ratios  $b_{kj}/b_{lj}$   $k = 2, \dots, m$  are determined by the choice of the  $\lambda_k$ . Even if the  $b_{kj}/b_{lj}$  emerge very large, one can always make the  $b_{lj}$  small enough so that the  $b_{kj}$  satisfy the tolerances. Hence, it is not necessary to solve the equations for the  $b_{kj}/b_{lj}$ . Of course, this is true only because all  $a_{kj} = 0$ . If the above approach is used at lower  $\omega$ , where some or all  $a_{kj} \neq 0$ , the  $b_{kj}/b_{lj}$  should be calculated, in order to be certain that the tolerances are not violated.

### Example IV.3 -- Trade-off Example #3

Equations (III.38) - (III.41) for the 2x2 plant, where  $f_{ij} = 0$  ( $i \neq j$ ), in the high frequency range simplify to:

<u>Column 1</u>	<u>Column 2</u>	
<u>Row 1</u> $t_{11} \approx \frac{c_{11}q_{11}}{1 + L_1} \leq b_{11}$	$t_{12} \approx \frac{c_{12}q_{11}}{1 + L_1} \leq b_{12}$	(a) (b) (IV.31)
<u>Row 2</u> $t_{21} \approx \frac{c_{21}q_{22}}{1 + L_2} \leq b_{21}$	$t_{22} \approx \frac{c_{22}q_{22}}{1 + L_2} \leq b_{22}$	(c) (d)

Substitute into these equations the expressions for  $c_{ij}$ 's from

Example IV.1 to obtain the following set of equations:

$$\begin{array}{cc}
 \text{Column 1} & \text{Column 2} \\
 \text{Row 1} & \frac{-b_{21}q_{11}/q_{12}}{1 + L_1} \leq b_{11} \quad (a) \quad \frac{b_{22}q_{11}/q_{12}}{1 + L_1} \leq b_{12} \quad (b) \\
 \text{Row 2} & \frac{-b_{11}q_{22}/q_{21}}{1 + L_2} \leq b_{21} \quad (c) \quad \frac{-b_{12}q_{22}/q_{21}}{1 + L_2} \leq b_{22} \quad (d)
 \end{array} \quad (\text{IV.32})$$

The equations in Eq. (IV.32) are rearranged, in order to perform a frequency domain analysis, as follows:

$$\begin{array}{cc}
 \text{Column 1} & \text{Column 2} \\
 \text{Row 1} & |1 + L_1| \geq \left| \frac{q_{11}}{q_{12}} \right| \left| \frac{-b_{21}}{b_{11}} \right| \quad (a) \quad |1 + L_1| \geq \left| \frac{q_{11}}{q_{12}} \right| \left| \frac{-b_{22}}{b_{12}} \right| \quad (b) \\
 \text{Row 2} & |1 + L_2| \geq \left| \frac{q_{22}}{q_{21}} \right| \left| \frac{-b_{11}}{b_{21}} \right| \quad (c) \quad |1 + L_2| \geq \left| \frac{q_{22}}{q_{21}} \right| \left| \frac{-b_{12}}{b_{22}} \right| \quad (d)
 \end{array} \quad (\text{IV.33})$$

Suppose that

$$|\lambda_1| = \left| \frac{b_{21}}{b_{11}} \right| > \left| \frac{b_{22}}{b_{12}} \right| = |\lambda_2| \quad (\text{IV.34})$$

and

$$|1/\lambda_1| = \left| \frac{b_{11}}{b_{21}} \right| < \left| \frac{b_{12}}{b_{22}} \right| = |1/\lambda_2| \quad (\text{IV.35})$$

then the 1,1 term [Eq. (IV.33(a))] dominates over the 1,2 term [Eq. (IV.33(b))] and the 2,2 term [Eq. (IV.33(d))] term dominates over the 2,1 term [Eq. (IV.33(c))]. Thus a diagonal dominance exists. The objective is to balance the dominance across all columns. For example, in this case,  $b_{22}$  is increased until both terms match, i.e.,

$$\lambda_1 = -b_{21}/b_{11} = -b_{22}/b_{12} = \lambda_2 = \lambda$$

then

$$|1 + L_1| \geq \left| \frac{q_{11}}{q_{12}} \right| \lambda$$

for the 1,1 and 1,2 terms of Eq. (IV.33) and

$$|1 + L_2| \geq \left| \frac{q_{22}}{q_{21}} \right| \frac{1}{\lambda}$$

for the 2,1 and 2,2 terms of Eq. (IV.33). Thus the dominance is now "balanced" across all columns for this 2x2 plant.

Note that in the high frequency range the problems of equilibrium and trade-off become simplified. This simplification permits an analytical derivation of the bounds  $B_i(j\omega)$  on  $L_{i0}(j\omega)$ .

#### IV.5.2 Some Universal Design Features

For a 3x3 system the bounds  $B_i(j\omega)$  on  $L_{30}(j\omega)$  tend to be significantly larger (more stringent) than those on  $L_{10}$ ,  $L_{20}$  in the low and middle  $\omega$  range, where the trade-off opportunities are limited because the interacting  $a_{ij} \neq 0$ . In the higher  $\omega$  range, when Eqs. (IV.27) and (IV.28) apply, there is much greater scope for such trade-off. This was utilized to help  $L_3$  in the higher  $\omega$  range by setting  $\lambda_1 = \lambda_2 = \lambda$ , and solving  $\det \Phi = 0$  for  $\lambda_3$ . As the  $v_{ij}$  are functions of  $\omega$ ,  $\det \Phi = 0$  gives a relation between the  $\lambda_i$  which is also a function of  $\omega$ . The result is shown in Fig. IV.9 for  $\omega > 100$ , for which the  $v_{ij}(j\omega)$  are fairly constant with  $\omega$ . Given  $|1 + L_i|^{-1} \leq \lambda_i$ , and  $L_i = L_{i0}q_{ii}/q_{iio}$ , one can find the bounds on  $L_{i0}$ , which of course depend on the set  $Q = \{q_{ii}\}$ . The results are shown in Fig. IV.10, where: Fig. IV.10(a) corresponds to  $\lambda_1 = \lambda_2 = 1$ ,  $\lambda_3 = 2.3$  dB; Fig. IV.10(b) corresponds to  $\lambda_1 = \lambda_2 = 0.7$ ,  $\lambda_3 = 2.7$  dB; and Fig. IV.10(c) corresponds to  $\lambda_1 = \lambda_2 = 0.5$ ,  $\lambda_3 = 3$  dB. The  $q_{ii}(j\omega)$  are almost constant with  $\omega$  for  $\omega_i > 100$ , so these bounds apply for all  $\omega_i > 100$ . As expected, the larger  $\lambda$  becomes, the easier it is on  $L_{10}L_{20}$  and the harder it is on  $L_{30}$ . The big difference in the bounds in Fig. IV.10 is due to the small  $\lambda$  compared with the large  $\lambda_3$  that were deliberately used. For this reason the actual  $L_{30}(j\omega)$  was able to reach its final asymptotic slope at  $\omega \sim 250$  (see Fig. IV.11) compared with  $\sim 450$ , 230 for

$L_{10}, L_{20}$  even though  $|L_{30}|$  is much more than  $|L_{10}|, |L_{20}|$  at low and medium  $\omega$ . The  $L_{i0}$  chosen to satisfy the bounds are shown in Fig. IV.11. Design simulation results were highly satisfactory and are shown in Fig. IV.12 for extreme plant parameter combinations.

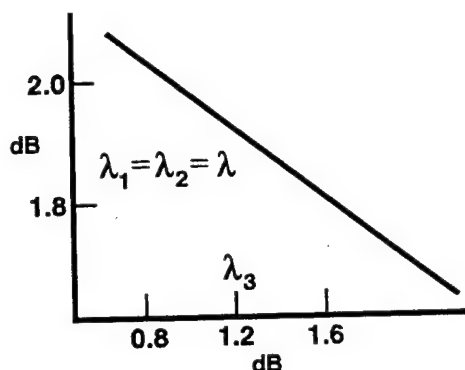


Fig. IV.9 Optimum relation between  $\lambda_1 = \lambda_2$  and  $\lambda_3$  for  $\omega > 100$ .

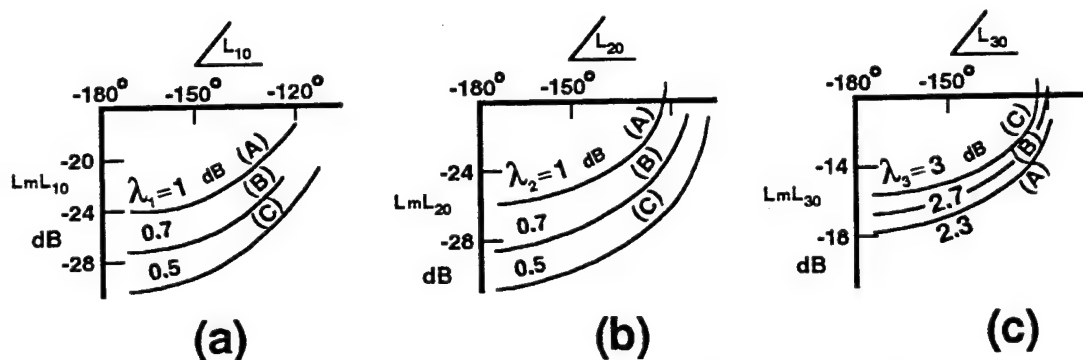


Fig. IV.10 The resulting bounds on  $L_{i0}$  for various  $\lambda$  values for  $\omega > 100$ .

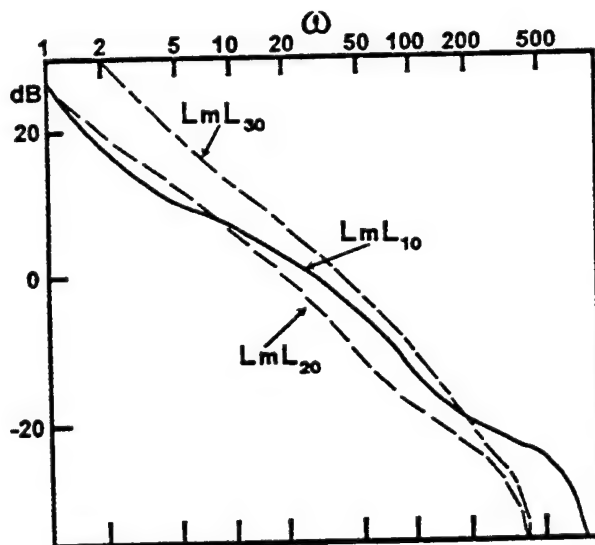


Fig. IV.11 Bode plots of  $L_{i0}(j\omega)$



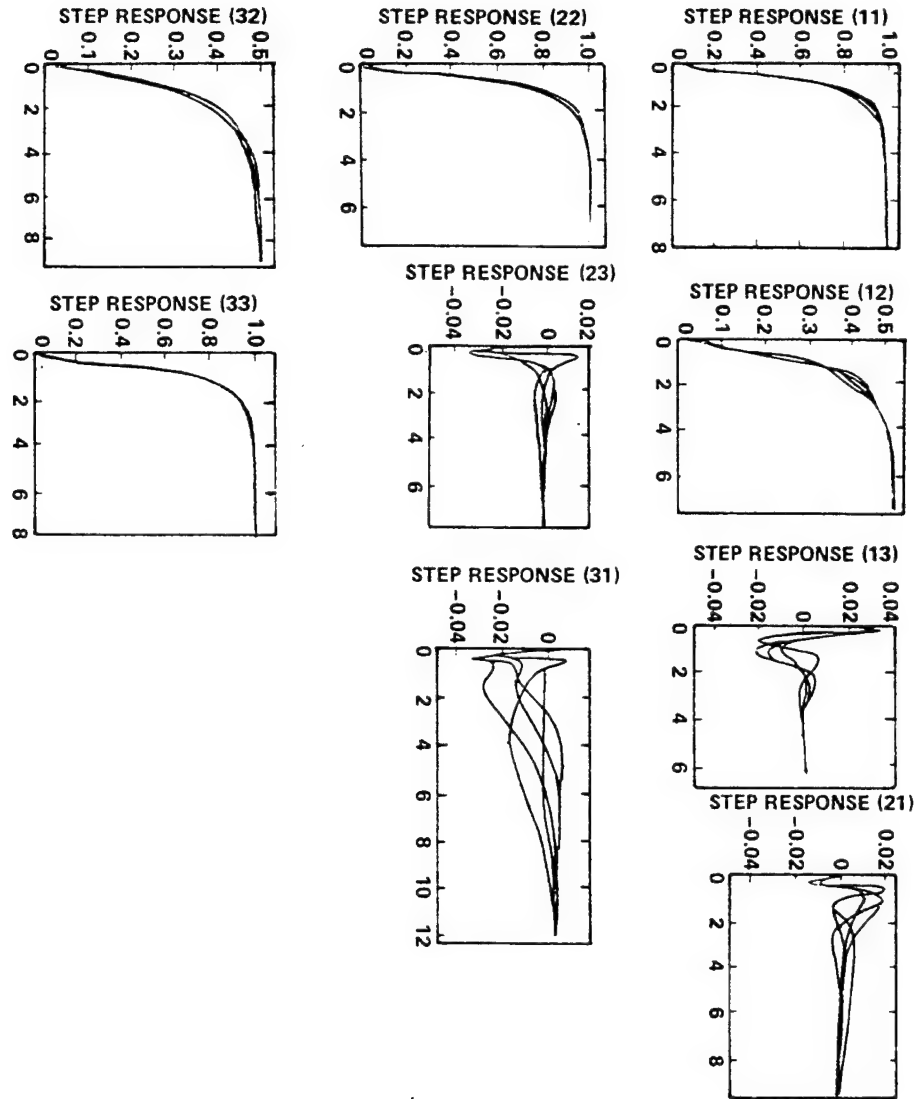


Fig. IV.12 Simulation results for representative step responses.

#### IV.5.3 Examples -- Bounds Determination

##### Example IV.4 -- 2x2 Plant

Consider the 1,1 MISO equivalent of Fig. III.10, with  $r_1 \neq 0$  and  $r_2 = 0$ . Thus:

$$t_{11} = t_{r_{11}} + t_{c_{11}} \quad \text{where}$$

$$t_{r_{11}} = \frac{L_1 f_{11}}{1 + L_1}, \quad t_{c_{11}} = \frac{q_{11} c_{11}}{1 + L_1}, \quad c_{11} = \frac{-t_{21}}{q_{12}}$$

The 1,1 cross-coupling expression for the bound determination

becomes:

$$t_{c_{11}} = \left| \frac{q_{11}c_{11}}{1 + L_1} \right| \leq \tau_{c_{11}} \quad (\text{IV.36})$$

This expression is rearranged to the following format:

$$|1 + L_1| \geq \left| \frac{q_{11}c_{11}}{\tau_{c_{11}}} \right| = \left| \frac{q_{11}}{q_{12}} \right| \frac{b_{21}}{\tau_{c_{11}}} \quad (\text{IV.37})$$

where  $|\tau_{21}| = b_{21}$ .

Next, consider the 2,1 MISO equivalent of Fig. III.10, with  $f_{21} = 0$ . For this example, since

$$t_{21} \approx t_{c_{21}}$$

then the upper bound for  $t_{c_{21}}$  is  $b_{21}$ , i.e.,

$$\tau_{c_{21}} = b_{21} \geq \left| \frac{c_{21}q_{22}}{1 + L_2} \right|$$

This expression is rearranged to the following format:

$$|1 + L_2| \geq \frac{b_{11}}{b_{21}} \left| \frac{q_{22}}{q_{21}} \right| \quad (\text{IV.38})$$

where the maximum magnitude  $b_{11}$ , from Fig. IV.1(c) is used for  $t_{11}$ .

Equations (IV.37) and (IV.38) are inverted, respectively, to yield the following equations:

$$\begin{aligned} \left| \frac{1}{1 + L_1} \right| &\leq \left| \frac{q_{12}}{q_{11}} \right| \frac{\tau_{c_{11}}}{b_{21}} \leq M_{m_1} \quad (a) \\ \left| \frac{1}{1 + L_2} \right| &\leq \left| \frac{q_{21}}{q_{22}} \right| \frac{b_{21}}{b_{11}} \leq M_{m_2} \quad (b) \end{aligned} \quad (\text{IV.40})$$

By letting  $\ell_1 = 1/L_1$  and  $\ell_2 = 1/L_2$ , these equations become

$$\left| \frac{\ell_1}{1 + \ell_1} \right| \leq M_{m_1} \quad (a) \quad \left| \frac{\ell_2}{1 + \ell_2} \right| \leq M_{m_2} \quad (b) \quad (\text{IV.41})$$

which are now of the mathematical format required in order to use the N.C. Note that:

$$\angle \ell = -\angle L \quad (\text{IV.42})$$

Thus, based on Eqs. (IV.41) and (IV.42), the rotated or inverse NC must be used in conjunction with the templates to determine the cross-coupling effect bounds  $B_{c1}(j\omega_i)$  and  $B_{c2}(j\omega)$  for  $\ell_1$  and  $\ell_2$ , respectively.<sup>15</sup> These bounds are transposed to the regular NC to become bounds for  $L_1$  and  $L_2$ , respectively.

#### Example IV.5 -- Boundary Determination for Example IV.4

Consider for Eqs. (IV.40(b)) and (IV.41(b)) that:

$$Lm \left( \frac{b_{21}}{b_{11}} \right) = -40 \text{ dB} \quad Lm \left( \frac{q_{21}}{q_{22}} \right) = Lm q_{21} - Lm q_{22} \quad Lm q_{21} = 4 \text{ dB}$$

Thus

$$\begin{aligned} Lm \left[ \frac{1}{1 + L_2} \right] &= Lm \left[ \frac{\ell_2}{1 + \ell_2} \right] \leq -40 \text{ dB} + 4 \text{ dB} - Lm q_{22} \\ &= -36 \text{ dB} - Lm q_{22} \leq Lm M_{m_2} \end{aligned} \quad (\text{IV.43})$$

For this example,  $B_{c2}$  is determined in the high frequency range where the templates are essentially a straight line. Assume for this example that  $q_{21}$  is independent of  $q_{22}$  (not true in flight control). The graphical technique for determining this boundary is illustrated in Fig. IV.13 as follows:

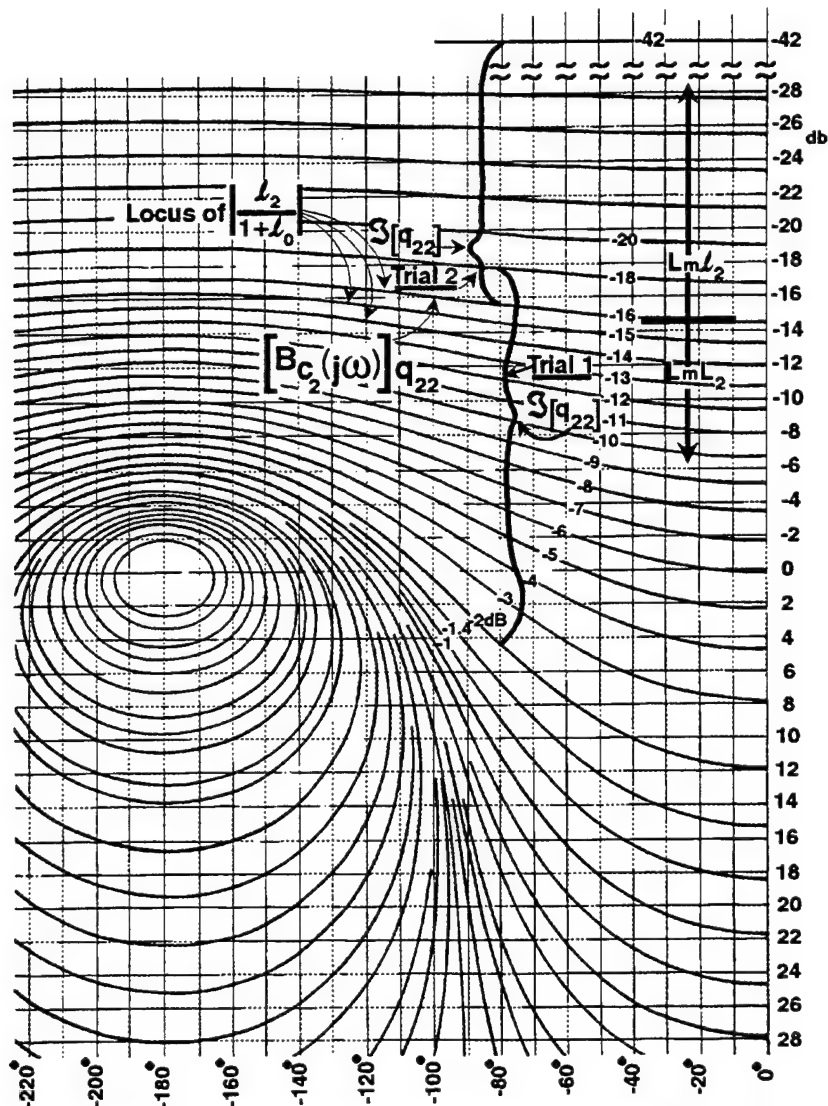


Fig. IV.13 Cross-coupling bound determination for  $L_m L_2$  on the inverse Nichols Chart.

Trial 1: From Eq. (IV.43)

First trial  
value for  $q_{22}$

↓

$$L_m q_{22h} = -36 \text{ dB} - (-18 \text{ dB}) = -18 \text{ dB} \neq L_m q_{22h} = +6 \text{ dB}$$

$$L_m q_{22l} = -36 \text{ dB} - (-2 \text{ dB}) = -34 \text{ dB} \neq L_m q_{22l} = -20 \text{ dB}$$

↓

Trial 2:

↓

$$L_m q_{22h} = -36 \text{ dB} - (-42 \text{ dB}) = -6 \text{ dB} = L_m q_{22h} = +6 \text{ dB}$$

$$L_m q_{22l} = -36 \text{ dB} - (-16 \text{ dB}) = -20 \text{ dB} = L_m q_{22l} = -20 \text{ dB}$$

Actual value  
of  $q_{22}$

↓

↓

↓

In Trial 2 the trial and actual values agree resulting in obtaining a point on  $B_{c_2}$ . In a similar manner other points for this boundary can be obtained. This procedure is automated in the MIMO QFT CAD package of Chap VIII.

Usually the dominating case(s) on a grid line are quickly found. Thus, the optimal  $L_{20}$  must lie on or below the boundary

$$-B_{c_2}(j\omega_i) \text{ vs } \angle \ell_2$$

on the inverted NC where the values

$$-B_{c_2}(j\omega_i) \text{ vs } \angle \ell_2$$

for various values of  $-\angle \ell_2 = \angle L_2$ , are plotted on the regular NC to obtain the boundary

$$[B_{c_2}(j\omega_i)]_{q_{22} \text{ REG}}$$

then  $L_{20}$  must lie on above this boundary.

For Prob. IV.1, in trying to satisfy the requirements for both  $L_1$  and  $L_2$ , Eqs. (IV.37) and (IV.38), respectively, assume that the specifications are met for  $L_1$  and not for  $L_2$ . Thus, for this situation by reducing  $b_{11}$  allows a reduction in  $b_{21}$  proportionally to maintain the requirement of Eq. (IV.37) and in turn satisfy Eq. (IV.38) for a satisfactory  $L_2$  since for this example it is stipulated that the  $q$ 's are independent. When the  $q$ 's are not independent then it is necessary to obtain the templates

$$\mathfrak{S}\left(\frac{q_{12}(j\omega_i)}{q_{11}(j\omega_i)}\right) \quad \mathfrak{S}\left(\frac{q_{21}(j\omega_i)}{q_{22}(j\omega_i)}\right)$$

in order to determine the bounds.

**Example IV.6 -- Cross-coupling Boundary Determination for a 3x3 Plant**

Consider the 3x3 MIMO control system of Fig. III.10. From Eq. (IV.14) obtain

$$\begin{bmatrix} \frac{1}{Q_{11}} + g_1 & \frac{1}{Q_{12}} & \frac{1}{Q_{13}} \\ \frac{1}{Q_{21}} & \frac{1}{Q_{22}} + g_2 & \frac{1}{Q_{23}} \\ \frac{1}{Q_{31}} & \frac{1}{Q_{32}} & \frac{1}{Q_{33}} + g_3 \end{bmatrix} \begin{bmatrix} t_{11} & t_{12} & t_{13} \\ t_{21} & t_{22} & t_{23} \\ t_{31} & t_{32} & t_{33} \end{bmatrix} = \begin{bmatrix} f_{11}g_1 & f_{12}g_1 & f_{13}g_1 \\ f_{21}g_2 & f_{22}g_2 & f_{23}g_2 \\ f_{31}g_3 & f_{32}g_3 & f_{33}g_3 \end{bmatrix}$$

(IV.44)

The first row of Eq. (IV.44) yields:

$$t_{11} = \frac{f_{11}L_1}{1 + L_1} + \frac{-Q_{11}\left[\frac{t_{21}}{Q_{12}} + \frac{t_{31}}{Q_{13}}\right]}{1 + L_1} = t_{r_1} + \frac{Q_{11}C_{11}}{1 + L_1} = t_{r_1} + t_{c_{11}}$$

(IV.45)

In a similar manner the expressions for the 1,2 and 1,3 expressions for row one of Fig. III.10 are obtained.

Given that  $|t_{ij}|_{\max} \equiv b_{ij}$  and assume, for  $|t_{11}|_{\max} = b_{11}$ , that  $\phi_{11}$  (the actual control ratio) is satisfied. Thus, for this situation it might be difficult to satisfy  $\phi_{22}$ ,  $\phi_{33}$ , etc. If this is the case, then the designer needs to do a "trade-off" in trying to achieve the best performance possible. Performing the design in the high frequency range simplifies the task as discussed in Example IV.5. The equations for the determination of the cross-coupling bounds are:

For the first row of Fig. III.10:

$$|1 + L_1| \geq \frac{|a_{11}|}{b_{11}} \left[ \frac{b_{21}}{|a_{12}|} + \frac{b_{31}}{|a_{13}|} \right], \geq \frac{|a_{11}|}{b_{12}} \left[ \frac{b_{22}}{|a_{12}|} + \frac{b_{32}}{|a_{13}|} \right], \geq \frac{|a_{11}|}{b_{13}} \left[ \frac{b_{23}}{|a_{12}|} + \frac{b_{33}}{|a_{13}|} \right]$$

(a)
(b)
(c)

(IV.46)

For the second row:

$$|1 + L_2| \geq \frac{|a_{22}|}{b_{21}} \left[ \frac{b_{11}}{|a_{21}|} + \frac{b_{31}}{|a_{23}|} \right], \geq \frac{|a_{22}|}{b_{22}} \left[ \frac{b_{12}}{|a_{21}|} + \frac{b_{32}}{|a_{23}|} \right], \geq \frac{|a_{22}|}{b_{23}} [ \quad ]$$

(a)
(b)
(c)

(IV.47)

For the third row:

$$|1 + L_3| \geq \frac{|a_{33}|}{b_{31}} \left[ \frac{b_{11}}{|a_{31}|} + \frac{b_{21}}{|a_{32}|} \right], \geq ( \quad ), \geq ( \quad )$$

(a)
b)
(c)

(IV.48)

Consider the interactions between the rows of Fig. III.10 via the  $b_{ij}$  specifications. For example, suppose  $b_{21}$  is decreased from 0.1 to a  $\delta$  value. The decrease is okay because for BNIC  $|t_{21}| \leq b_{21}$  is required. This decrease in turn decreases  $|c_{11}|$  and  $|c_{31}|$  which eases the burden on  $L_1$  and  $L_3$  for satisfying  $y_{11} \in \mathfrak{S}_{11}$  and  $y_{31} \in \mathfrak{S}_{31}$ . This is based upon the fact that  $y_{11}$  and  $y_{31}$  dominate  $L_1$  and  $L_3$ , respectively. Thus, the design for  $L_2$  is more difficult because  $|y_{21}| \leq \delta$  instead of 0.1. This may not matter if  $y_{22}$  dominates  $L_2$ . If so,  $b_{21}$  can be decreased until, for example,  $y_{21}$  imposes the same burden on  $L_2$  as does  $y_{22}$  ( $y_{21} \sim y_{22}$ ). Any further decrease in  $b_{21}$  may involve a "trade-off." i.e., requiring a sacrifice on the specifications on  $L_2$  for the sake of  $L_1$  and/or  $L_3$ . However, it is conceivable that before  $y_{21} \sim y_{22}$  occurs, either  $y_{12}$  (or  $y_{13}$ )  $\sim y_{11}$  or  $y_{32}$  (or  $y_{33}$ )  $\sim y_{31}$ . There are other trade-offs that may be possible to investigate.

In summary, for the h.f. range, the main factors to keep in mind in trying to achieve column dominance are:

1. Adjust the  $b_{ij}$ 's until one column dominates.

2. Once Item 1 is accomplished, try to make the nondominant elements in each row equal the dominant ones by reducing the  $b_{ij}$ 's in each denominator. This will make all three columns equal and allows one to use any column as the constraining column. This reduces the 3x3 matrix of constraints to a single constraint on each loop, i.e.,

$$|1 + L_1| \geq A, \quad |1 + L_2| \geq B, \quad |1 + L_3| \geq C$$

3. From Sec. III.7, with respect to Condition 2 (e.g. a 2x2 plant) if

$$\left| \frac{P_{12}P_{21}}{P_{11}P_{22}} \right| < 1$$

is not true then renumber the output terminals. For example:

$$\phi_1 \rightarrow \phi'_2 \quad \phi_2 \rightarrow \phi'_1$$

Thus, for the original 2x2 plant:

$$\Phi = \begin{bmatrix} \phi_1 \\ \phi_2 \end{bmatrix} = [P_{ij}] \begin{bmatrix} u_1 \\ u_2 \end{bmatrix} = \begin{bmatrix} P_{11}u_1 + P_{12}u_2 \\ P_{21}u_1 + P_{22}u_2 \end{bmatrix}$$

For the renumbered system:

$$\Phi = \begin{bmatrix} \phi'_1 \\ \phi'_2 \end{bmatrix} = \begin{bmatrix} P_{21}u_1 + P_{22}u_2 \\ P_{11}u_1 + P_{12}u_2 \end{bmatrix} = \begin{bmatrix} P'_{21} & P'_{22} \\ P'_{11} & P'_{12} \end{bmatrix} \begin{bmatrix} u_1 \\ u_2 \end{bmatrix}$$

which results in Condition 2 being satisfied, i.e.,



$$\left| \frac{p'_{22}p'_{11}}{p'_{12}p'_{21}} \right| > 1$$

4. Items 1 - 3 apply to an mxm plant as well.

#### IV.6 Summary

The reader is urged, in performing a QFT design, to constantly refer to Chap. VII. This chapter discusses the case of plants having r.h.p. zeros and/or poles. It should be noted that if each  $p_{ij}$  of  $P$  does not have the same value of excess of poles over zeros then as  $\omega \rightarrow \infty$  the templates may not be straight lines.

#### IV.7 Problems

IV.1 In a 2x2 MIMO system  $r_1 \neq 0$  and  $r_2 = 0$ , thus only  $t_{11}$  and  $t_{21}$  are involved in the design. The specifications on  $t_{11}$  are:

$\omega$	0.1	0.2	0.5	1	2	5	10
$b_{11}$	1.02	1.07	1.09	0.97	0.65	0.25	0.05
$a_{11}$	0.95	0.92	0.80	0.55	0.20	0	0

The specification on  $t_{21}$  is that  $b_{21} = 0.01$  for all values of  $\omega$  and the specification on each  $L_i$  satisfies

$$Lm \left| \frac{L_i}{1 + L_i} \right| \leq 2.3 \text{ dB}$$

The plant is described as follows:

$$q_{11} = k_{11}, \quad q_{12} = k_{12}, \quad q_{21} = k_{21}, \quad q_{22} = k_{22}$$

$$0.2 \leq k_{11} \leq 1, \quad 0.5 \leq k_{12} \leq 2, \quad 2 \leq k_{21} \leq 5, \quad 0.1 \leq k_{22} \leq 0.5$$

Note: the  $q$ 's are assumed as real numbers (gain uncertainty only) thus  $\gamma_{\max} = [(1)(0.5)]/[(0.5)(2)] = 0.5$ . Choose the following nominal values:

$$q_{11_0} = 0.2 \quad q_{22_0} = 0.1$$

(a) Find the bounds on  $L_{1_0}$  at  $\omega = 0, 1, 0.2, 0.5, 1$  and  $2$ .

(b) Use

$$\left| \frac{1}{1 + L_2} \right| \leq \left( \frac{b_{21}}{b_{11}} \right) \left( \frac{q_{21}}{q_{22}} \right)$$

to find the bounds on  $L_{2_0}$  for the same values of  $\omega$  as in part (a).

Hint: use the "inverse NC" for this purpose, i.e., let  $\ell_2 = 1/L_2$  to obtain the form  $\ell_2/(1 + \ell_2)$ .

**IV.2** Given  $T = [I + PG]^{-1}PGF$  whose poles are given by

$$(1 + p_{11}g_1)(1 + p_{22}g_2) - p_{12}g_2p_{21}g_1$$

Prove that instead, one can consider the zeros of

$$(1 + q_{11}g_1)(1 + q_{22}g_2) - \frac{q_{11}q_{22}}{q_{12}q_{21}}$$

for determining the stability of the system.

**IV.3** Given a 2x2 plant whose Q matrix is

$$Q = \frac{1}{s} \begin{bmatrix} k_{11} & k_{12} \\ k_{21} & k_{22} \end{bmatrix} \quad \text{where}$$

$$1 \leq k_{11} \leq 2, \quad 0.5 \leq k_{12} \leq 2, \quad 5 \leq k_{21} \leq 10, \quad 0.5 \leq k_{22} \leq 1$$

$$|q_{11}q_{22}| < |q_{12}q_{21}| \quad \text{as } s \rightarrow \infty, \quad r_1(t) = 0$$

The specifications based upon input  $r_2(t)$  are:

$$|t_{12}| < 0.1 \quad \text{for all } \omega$$

and for  $\text{Lm } t_{22}(j\omega)$

$\omega$	0	0.5	1	2	5	10	20
$\text{Lm } b(j\omega)$	0	1	1	0	-4	-10	-20
$\text{Lm } a(j\omega)$	0	-2	-4	-8	-20	$-\infty$	$-\infty$

Additional specifications on  $L_1$  and  $L_2$ , respectively, are

$$\text{Lm } \left| \frac{L_1}{1 + L_1} \right| \leq 3 \text{ dB} \quad \text{Lm } \left| \frac{L_2}{1 + L_2} \right| \leq 3 \text{ dB}$$

(a) Design  $L_1(s)$  and  $L_2(s)$  by designing  $L_1(s)$  first and letting  $f_{12} = 0$ .

(b) Redesign  $L_2(s)$  where  $0.5 \leq k_{22} \leq 1.2$  and  $L_1(s)$  of part (a) is not affected by the change in  $k_{22}$ .

## Chapter V MIMO System Design Method Two-Modified Single-Loop Equivalents<sup>17,22,79</sup>

### V.1 Introduction

The design technique of Chap. IV inherently involves some over-design, as seen from Eq. (IV.1), in which  $t_{21}$ ,  $t_{31}$  can be any members of their acceptable sets  $\tau_{21}$ ,  $\tau_{31}$  and  $q_{12}$ ,  $q_{13}$  any members of their uncertainty sets. As noted in Sec. IV.2, it is therefore necessary to use the worst case values which leads to overdesign. Actually, in the real world, there is a correlation between the  $t_{21}$ ,  $t_{31}$  and the  $q_{11}$ ,  $q_{13}$ , etc, that is, it is possible that  $q_{12}$  is large when  $t_{21}$  is large, etc. Such correlation can only help make  $c_{11}$  smaller. Thus, for Method One, it is not possible to use this correlation, and so one must take the largest  $t_{21}$ , the smallest  $q_{12}$ , etc. This is the price paid for converting the MIMO problem into the much simpler MISO problems, and avoiding having to work with the horrendous denominator in Eq. (III.24).

Another disadvantage of Method One is that there emerges a certain inequality (see Sec. III.7, the diagonal dominance condition) which must be satisfied by the plant elements: for  $m = 2$ , as  $\omega \rightarrow \infty$  it is:

$$|p_{11}(j\omega)p_{22}(j\omega)| > |p_{12}(j\omega)p_{21}(j\omega)| \text{ for all } p \in \mathcal{P} \quad (V.1)$$

or vice versa. (Rosenbrock's<sup>68</sup> dominance condition is tougher. It requires this inequality to be satisfied over the entire frequency range, not just as  $s \rightarrow \infty$ . His method can therefore not be used for the 3x3 example of Chap. IV). The equivalent of Eq. (V.1) for  $m = 3$ , as  $\omega \rightarrow \infty$ , is

$$|p_{123}^*| = |p_{11}^*p_{22}^*p_{33}^*| > |p_{11}^*p_{23}^*p_{32}^*| + |p_{12}^*p_{21}^*p_{33}^*| + |p_{12}^*p_{23}^*p_{31}^*| + |p_{13}^*p_{22}^*p_{31}^*| + |p_{13}^*p_{21}^*p_{32}^*| \quad (V.2)$$

It turned out that Eq. (V.2) was not satisfied by the FY-16CV 3x3

lateral system for any  $p \in \mathcal{O}$ . Thus, it was necessary to seek a modification of the technique that succeeds in avoiding the condition of Eq. (V.2), and involves less over design than Method One. This modification lead to the development of Method Two<sup>22</sup>. The necessary constraints for Method Two are discussed in Sec. V.6 and in Appendix A.

In summary, Method One is used when the diagonal dominance condition can be satisfied and when the BW constraints can not be satisfied by Method Two (this BW constraint is discussed in a latter section). Method Two is used when the diagonal dominance condition can not be satisfied and/or where overdesign needs to be minimized. The MIMO QFT CAD package (Chap. VIII) has implemented both design methods.

## V.2 Design Equations For The 2x2 System

In Method Two the same design equations as before are used for  $t_{11}$ ,  $t_{12}$  or alternatively  $t_{21}$ ,  $t_{22}$  (as in Fig III.10 for  $m = 2$ ). Thus, for Fig. V.1 and for an impulse input, Eqs. (III.35) through (III.38) yield:

$$\begin{aligned} t_{1j} = y_{1j} &= \frac{f_{1j}L_1 + c_{1j}q_{11}}{1 + L_1} \quad (a) & L_i &= g_i q_{ii} \quad (b) \\ c_{1j} &= \frac{-t_{2j}}{q_{12}} \quad (c) & t_{2j} &\in \tau_{2j} \quad (d) & P^{-1} &= [p_{ji}^*] = [1/q_{ji}] \quad (e) \end{aligned} \quad (V.3)$$

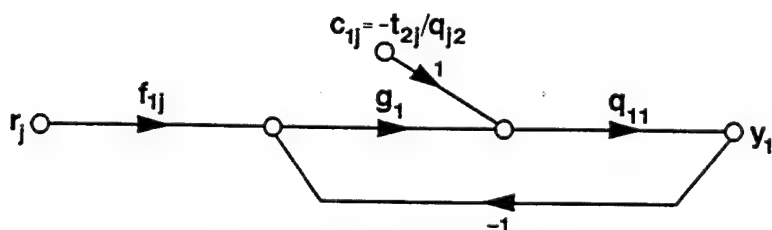


Fig. V.1 MISO structure for  $t_{1j}$   
( $j=1, 2$ ), Eq. (V.3)

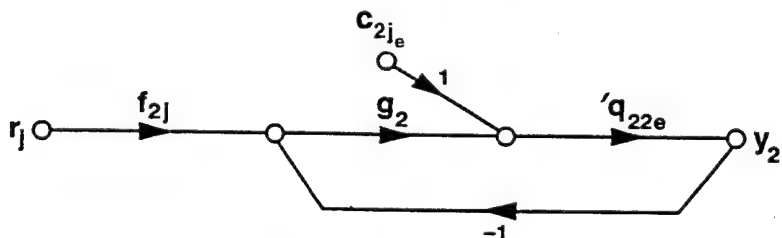


Fig. V.2 MISO structure for  $t_{2j}$   
( $j=1, 2$ ), Eq. (V.4)

The objective is to choose  $f_{11}(s)$ ,  $f_{12}(s)$ ,  $g_1(s)$  such that the  $y_{1j}(s)$  has no right-half-plane (RHP) poles, and satisfy the tolerances on  $|t_{ij}(j\omega)|$ ,  $\forall P \in \mathcal{P}$  and  $\forall t_{2j} \in \tau_{2j}$  appearing in  $c_{1j}$ . These are precisely the MISO design problems of Sec. III.6 through III.8.

When  $t_{1j}$  is substituted for  $y_{1j}$  in Eq. (V.3), the resulting equations are exact. Hence, if indeed  $y_{1j} \in \tau_{1j}$  for all  $t_{2j}$  (of  $c_{1j}$ )  $\in \tau_{2j}$ ,  $P \in \mathcal{P}$ , then the design objectives for  $t_{1j}$  have been achieved by the  $f_{11}$ ,  $f_{12}$ ,  $g_1$  but only if actually  $t_{2j} \in \tau_{2j}$ .

The final step, in the 2x2 system, is to choose  $f_{21}$ ,  $f_{22}$ ,  $g_2$  to ensure that the  $t_{2v}(s)$  have no RHP poles and that  $t_{2v} \in \tau_{2v}$   $P \in \mathcal{P}$ . In Secs III.6 and III.7 the design equations are again Eq. (V.3) with 2 replacing 1 and the  $c_{2v}$  containing  $t_{1v}$ . Instead, here, there are used equations independent of the  $t_{1v}$ , by simply finding  $t_{2j}$  from  $T = (I + PG)^{-1}PGF$ :

$$\begin{aligned} t_{2j} &= \frac{f_{2j}L_{2e} + c_{2j}}{1 + L_{2e}} \quad (a) & L_{2e} &= g_2 Q_{22e} = \frac{g_2 Q_{22}(1 + L_1)}{1 - \gamma_{12} + L_1} \quad (b) \\ \gamma_{ji} &= \frac{p_{ij}p_{ji}}{p_{ii}p_{jj}} \quad (c) & c_{2j} &= \frac{g_1 f_{1j} p_{21}(1 - \gamma_{12})}{1 - \gamma_{12} + L_1} \quad (d) \quad (V.4) \\ P &= [p_{ji}] \quad (e) \end{aligned}$$

with the MISO structures of Fig. V.2. This design is done after the design of Eq. (IV.17(a)) has been completed by means of Eqs. (V.3(a-d)), so that  $L_1$ ,  $f_{11}$ , and  $f_{12}$  are known (Use  $L_1$  not  $L_{10}$  -- see Appendix A). It is then necessary to find  $g_2$ ,  $f_{21}$ , and  $f_{22}$  so that in Fig. V.2 the outputs  $y_{21}$  and  $y_{22}$  are stable and satisfy the tolerances on  $|y_{21}|$  and  $|t_{22}|$ , respectively. These are single-loop problem similar to Fig. V.1, except that only the uncertainty  $P \in \mathcal{P}$  need be considered, as the  $c_{2j}$  in Eqs. (V.4(a-e)) are not functions of the elements of  $\tau_{ij}$ , which they are in Eqs. (V.3(a-d)). At each step, design execution is that of a MISO single-loop system -- which is what makes this design procedure so tractable.

The theoretical justification of the above design procedure is as follows:

1. The design specifications are satisfied for  $t_{2v}$  of Fig. V.2, by the proper choice of the  $f_{2v}$  and  $g_2$  for the given  $f_{1v}$  and  $g_1$ .
2. Thus, the design is satisfactory for  $t_{21}$  and  $t_{22}$  because Eqs. (V.4(a-b)) are exactly the expressions for  $t_{21}$  and  $t_{22}$ , (even if the specifications for  $t_{12}$  and  $t_{11}$  are not satisfied).
3. Now Fig. V.1 has been designed [via Eqs. (V.3(a-d))] so that  $y_{11}$  and  $y_{12}$  are stable and satisfy the specifications on  $t_{11}$  and  $t_{12}$   $\forall P \in \mathcal{P}$ , if the  $t_{2j}$  appearing in  $c_{1j}$  are in  $\tau_{2j}$  (which they are).
4. The equations for  $y_{11}$  and  $y_{12}$  correspond precisely to those for  $t_{11}$  and  $t_{12}$ , respectively.

Thus, no fixed point theory is needed to rigorously justify this design procedure, although the idea and approach are motivated by the fixed point method in Method One. There, the design equations for  $t_{21}$  and  $t_{22}$  are of the same form as Eqs. (V.3(a-d)), with the  $c_{2j}$  functions of  $t_{1j}$ , so fixed point theory is required to justify Method One.

### V.3 Design Guidelines

The following items are intended to provide the reader with a heuristic insight to the design process.

1. Designation of the order of loop shaping -- The order in which the loops are to be designated and designed, i.e.,  $L_1$ ,  $L_2$ , etc, in order to achieve arbitrarily small (a.s.) sensitivity<sup>22</sup>, is based upon the following:

- (a) Choose the loop that satisfies

$$q_{ii} = \frac{\det P}{(\text{Adj} P)_{ii}} \quad \text{be m.p.} \quad (\text{V.5})$$

as Loop 1  $\rightarrow q_{ii} = q_{11}$ . Note: for non-square plants the use of a weighting matrix  $W = \{w_{ij}\}$  is required in order to achieve an effective square plant matrix  $P_e = PW$  since a square plant is required for a QFT design (see Sec. V.10). If Eq. (V.5) is not satisfied, see Constraint 1 in Sec. V.8.1, then an adjustment of the "weighting" factors  $w_{ij}$  may result in satisfying this requirement. Even if this requirement is not achievable a satisfactory design may still be possible depending upon the application (see Appendix B).

(b) When applying Method Two, if  $q_{11}$  is m.p. then  $q_{22e}$ , etc. will all be m.p.

(c) When applying Method Two, in general, if more than one loop can be m.p. choose the loop that has the toughest or most stringent specifications as Loop 1.

2. Template width -- If  $\exists \omega_h \in$  for all  $\omega > \omega_h$  so that the width of  $\Im q_{11}(j\omega)$  does not exceed  $180^\circ - \gamma$ , where  $\gamma$  is the desired phase margin angle  $\gamma$ , then it is possible to achieve a.s. tolerances. If this condition is not satisfied then it is impossible to achieve a.s. tolerances for  $\omega > \omega_h$ . This prevents a.s. sensitivity if

$$q_{ii} = \frac{k \prod (s + z_v)}{\prod (s + p_u)} \quad (\text{V.6})$$

with gain  $k$  (a  $\pm$  uncertainty value) is independent of the signs of  $z_v$  and/or  $p_u$ . Must exclude numerator or denominator factors of the form  $(1 + Ts)$  where  $T$  has a  $\pm$  uncertainty value and is



independent of other parameters. See Constraint 2 in Sec. V.8.1.

3. For the 2x2 plant if

(a)  $\gamma$  is "small" then  $q_{22e} \approx q_{22}$ .

(b)  $\gamma_{ji}$  is "large, i.e.,  $|\gamma_{ji}| \approx 1$  then  $q_{22e}$  can be unstable. This may be okay but may lead to a wide BW for  $L_2$ .

4. If there are transmission zeros in the RHP it only indicates that  $q_{ij}$  may be n.m.p. or the  $\det P$  may have zeros in the RHP.

#### V.4 Reduced Overdesign<sup>17</sup>

Figures V.1 and V.2 are the same as Fig. III.10 (for 2x2 system)<sup>21</sup> in which  $t_{21}$  and  $t_{22}$  appear in the cross-coupling  $c_{11}$  and  $c_{12}$ , respectively. There is inherent overdesign in Fig. V.1 because in reality there is a correlation between the  $t_{21}$  and  $t_{22}$  and the  $q_{ij}$  of  $P^{-1}$ . This correlation is not being exploited. The uncertainties in  $t_{21} \in \tau_{21}$  and  $t_{22} \in \tau_{22}$  are assumed independent of  $P \in \mathcal{P}$  in Figs. V.1 and V.2. But such overdesign does not exist in Fig. V.2 because  $c_{21}$  and  $c_{22}$  are not functions of the elements of any  $\tau_{ij}$ . In Fig. III.10, for the second row of the 2x2 system, the design for  $t_{21}$  and  $t_{22}$ , by Method One involved overdesign precisely as in the first row of this figure and in Fig. V.1. The above procedure can, of course be reversed with  $y_{21}$  and  $y_{22}$  using Eq. (V.3) with 1 replaced by 2 and with  $t_{11}$  and  $t_{12}$  using Eqs. (V.4) by exchanging numbers 1,2.

#### V.5 3x3 Design Equations

Let  $y_{ij}$ ,  $j = 1,2,3$ , be the same as in Secs. III.6 and III.7, that is:

$$y_{1j} = \frac{f_{1j}L_1 + c_{1j}q_{11}}{1 + L_1}, \quad L_1 = g_1q_{11}, \quad c_{1j} = -\sum t_{kj}/q_{1k} \quad (V.7)$$

giving MISO problems.  $L_1$  and the three  $f_{1j}$  are chosen so that  $y_{1j}$  are stable and satisfy the tolerances on  $t_{1j}$  for all  $t_{kj} \in \tau_{kj}$  appearing in  $c_{1j}$  in Eq. (V.5(c)) and for all  $P \in \mathcal{P}$ . The equations for  $y_{2j}$  are obtained from the second row of Fig. III.11 in which  $t_{1j}$  and  $t_{3j}$  appear, but the  $t_{1j}$  are replaced by the  $y_{1j}$  of Eq. (V.7), giving for  $j = 1, 2, 3$

$$y_{2j} = \frac{f_{2j}L_{2e} + c_{2j}}{1 + L_{2e}} \quad (a), \quad L_{2e} = \frac{g_2q_{22}}{1 - \frac{y_{12}}{1 + L_1}} \quad (b),$$

$$p_{21}^e = \frac{L_1 p_{21}^*}{1 + L_1} \quad (c), \quad L_{2e} = g_2 q_{22e} \quad (d),$$

$$c_{2j} = \frac{L_{2e}}{g_2} \left( t_{3j} \left[ \frac{p_{21}^* p_{13}^*}{p_{11}^* (1 + L_1)} - p_{23}^* \right] - f_{1j} p_{21}^* \right) \quad (e), \quad (V.8)$$

$$P^{-1} = [p_{ij}^*] \quad (f)$$

again resulting in MISO problems.  $L_1$  and the  $f_{1j}$  are known from the designs of Eqs. (V.7). In Eqs. (V.8) the  $f_{2j}$  and  $L_{2e}$  are chosen so that  $y_{2j}$  are stable for all  $t_{3j} \in \tau_{3j}$  appearing in  $c_{2j}$  and, of course, for all  $P \in \mathcal{P}$ . Although the forms for  $c_{2j}$  and  $L_{2e}$  in Eqs. (V.8) are different from those in Eqs. (V.7), they are otherwise identical in form, so the design techniques for both are basically the same, as detailed in Reference 22.

Finally, MISO design equations for  $t_{3j}$  are obtained by finding  $t_{3j}$  from  $T = [I + PG]^{-1}PGF$ , or from the third row of Fig. III.10 for  $i = 3$  and eliminating  $t_{1i}$  and  $t_{2i}$  by means of Eqs. (V.7) and (V.8). Thus, the resulting equations are:

$$\begin{aligned}
t_{3j} &= \frac{f_{3j}L_{3e} + c_{3j}}{1 + L_{3e}} \quad (a), \quad L_{3e} = \frac{L_3\zeta}{\zeta - \Lambda} \quad (b), \quad L_3 = g_3q_{33} \quad (c), \\
\zeta &= (1 + L_1)(1 + L_{2e}) - \gamma_{12} \quad (d) \\
\Lambda &= \gamma_{23}(1 + L_1) + \gamma_{13}(1 + L_{2e}) - (\gamma_{12}\mu_2 + \gamma_{13}\mu_3) \quad (e) \\
\mu_2 &= \frac{p_{23}^*p_{31}^*}{p_{21}^*p_{33}^*} \quad (f), \quad \mu_3 = \frac{p_{32}^*p_{21}^*}{p_{31}^*p_{22}^*} \quad (g), \\
c_{3j} &= \frac{f_{1j}L_1q_{33}\eta_1 + f_{2j}L_2q_{33}\eta_2}{\zeta - \Lambda} \quad (h), \\
\eta_1 &= q_{22}p_{21}^*p_{32}^* - p_{31}^*(1 + L_{2e}) \quad (i), \\
\eta_2 &= q_{11}p_{12}^*p_{31}^* - p_{32}^*(1 + L_1) \quad (j)
\end{aligned} \tag{V.9}$$

Note: See Eq. (III.88) for the expressions for the  $\gamma_{ij}$  terms of Eq. (V.9).

Since  $L_1$ ,  $L_2$ ,  $f_{1j}$ , and  $f_{2j}$  are known, the only unknowns in the Eq. (V.9) are the  $f_{3j}$  and  $g_3$ . These equations constitute single-loop uncertainty problems, for which the technique of Chap. I<sup>15,47</sup> applies, i.e. they are chosen so that the  $t_{3j}$  are stable and satisfy the tolerances  $\tau_{3j}$ . Note, again, that at each step, design execution is that of MISO single-loop systems.

The justification of the above design approach is the same as for the 2x2 case. Suppose the nine  $f_{ij}$  and three  $g_i$  in Eqs. (V.9(a-j)) are such that the  $t_{3j}$  are stable and their tolerances are satisfied, which is so by definition here. Now the design based on Eqs. (V.8(a-e)) guarantees that the  $t_{2j}$  tolerances are satisfied, providing the  $t_{3j}$  appearing in  $c_{2j}$  are  $\in \tau_{3j}$  - which is the case here. Hence, the  $t_{2j}$  tolerances are also satisfied. Finally, the design based on Eqs. (V.7(a-c)) guarantees that the  $t_{1j}$  tolerances are satisfied, providing that the  $t_{2j}$  and  $t_{3j}$ , appearing in  $c_{1j}$  are  $\in \tau_{2j}$  and  $\tau_{3j}$ , respectively, which have been established. In the above, there is some overdesign in Eqs. (V.7(a-c)) because the  $t_{ij} \in \tau_{kj}$ , ( $k = 2,3$ ), ( $j = 1,2,3$ ) appear as cross-coupling effects uncorrelated to the plant uncertainty. In Eqs. (V.8(a-f)) there is less overdesign because only the  $t_{3j}$  so appear, while there is no such overdesign in Eqs. (V.9(a-j)). Of course, the order can be

changed and equations of the form of Eqs. (V.7(a-c)) are used for the second or third channel, etc.

#### V.6 Example V.1 -- 3x3 System Design Equations

Consider the design of a 3x3 control system for which  $r_1(t) \neq 0$  and  $r_2(t) = r_3(t) = 0$  (thus,  $f_2 = f_3 = 0$ ). This example entails four parts: part (1) -- the set-up of the pertinent equations, and parts (2)-(4) -- the design approach. It is assumed that the loop to be designed first is row 1 of Fig. III.10.

Part (1) The pertinent equations are (refer to Figs. III.10 and III.12):

Row 1

$$t_{11} = \frac{f_{11}L_1 - Q_{11}\left(\frac{t_{21}}{Q_{12}} + \frac{t_{31}}{Q_{13}}\right)}{1 + L_1} \quad (a), \quad t_{12} = \frac{C_{12}Q_{11}}{1 + L_1} \quad (b),$$

$$t_{13} = \frac{C_{13}Q_{11}}{1 + L_1} \quad (c)$$

(V.10)

Row 2

$$t_{21} = \frac{f_{21}L_2 - Q_{22}\left(\frac{t_{11}}{Q_{21}} + \frac{t_{31}}{Q_{23}}\right)}{1 + L_2} \quad (a), \quad t_{22} = \frac{C_{22}Q_{22}}{1 + L_2} \quad (b), \quad (V.11)$$

$$t_{23} = \frac{C_{23}Q_{22}}{1 + L_2} \quad (c)$$

Row 3

$$t_{31} = \frac{f_{31}L_3 - Q_{33}\left(\frac{t_{21}}{Q_{32}} + \frac{t_{11}}{Q_{31}}\right)}{1 + L_3} \quad (a), \quad t_{32} = \frac{C_{32}Q_{33}}{1 + L_3} \quad (b), \quad (V.12)$$

$$t_{33} = \frac{C_{33}Q_{33}}{1 + L_3} \quad (c)$$

Part (2) Utilizing Method One, the  $b_{ij}$ 's are substituted into Eq. (V.10) in order to yield the  $f_{11}$  and  $g_1$  that satisfy the design specifications. In general, it is necessary that  $L_1$  and  $f_{1j}$  be designed so that the  $y_{1j}$ 's are stable and satisfy the specifications on  $t_{1j}$  for all  $t_{kj} \in \tau_{kj}$  in  $c_{ij}$  and for all  $P \in \mathcal{P}$ .

Part (3) Substitute  $t_{11}$  obtained in Part (2) into Eqs. (V.11) and (V.12). Apply Method Two to design  $f_{21}$  and  $g_2$  [see Eq. (V.8)]. In general, design  $f_{2j}$  and  $L_{2c}$  so that the  $y_{2j}$ 's are stable for all  $t_{3j} \in \tau_{3j}$  in  $c_{2j}$  and for all  $P \in \mathcal{P}$ .

Part (4) Substitute  $t_{11}$  and  $t_{21}$  obtained in Parts (2) and (3) into Eq. (V.12). Apply Method Two to design  $f_{31}$  and  $g_3$  [see Eq. (V.9)]. Thus, it is now possible to obtain  $t_{31}$ , that hopefully meets the specifications, in terms of only the parameters, that is, the  $b_{ij}$ 's are not involved in the design of  $f_{31}$  and  $g_3$ . This is the concept of Method Two which results in Eq. (V.12) having only two unknowns:  $f_{31}$  and  $g_3$ .

Note that one may initially start the design with a diagonal prefilter  $F$  matrix in order to simplify the design process. If the design specifications can not be achieved with a diagonal prefilter then it will be necessary to utilize a non-diagonal prefilter matrix.

#### V.7 mxm System, $m > 3$

The procedure for generating the design equations for  $mxm$  MIMO systems with  $m > 3$ , should be clear from the preceding sections. One uses for any channel (say the first) design equations in which all the  $t_{ij}$  ( $i \neq 1$ ) appear as cross-coupling effects. Denote these as Eqs. A. These equations can be derived or obtained from Reference 21, Eqs. (4a,b) with  $u = 1$ . For the next chosen channel (say the second), the design starts with Eqs. (4a,b) of Reference 21, with  $u = 2$ , in which all the  $t_{1j}$  and  $t_{2j}$  are eliminated by means of Eqs. A. Denote the resulting design equations as Eqs. B. For the next chosen channel (say the third), start again with Eqs. (4a,b) of Reference 14, with  $u = 3$ , but

eliminate all the  $t_{1j}$  and  $t_{2j}$  by means of Eqs. A and B. The process continues until the end, and the theoretical justification is the same as given previously for  $m = 2, 3$ .

Mixtures of the first and second techniques may also be used. For example, for the  $3 \times 3$  system, Eqs. (V.7) type equations are used for the first two rows of Fig. III.10 for both channels 1, 2 and Eqs. (V.9(a-j)) for channel 3. The theoretical justification is now as follows: the design for channel 3 is correct by definition then the fixed point theory, precisely as in Reference 21, is used to justify the designs for channels (1,2). This method was used for the  $3 \times 3$  FY16-CCV lateral design modes<sup>44</sup>.

The two sets of design equations for  $t_{1j}$  and  $t_{2j}$  are taken as the mappings on the acceptable sets  $\tau_{ij}$  and the third set of mappings is simply  $t_{3j} \in \tau_{3j}$ . The nine  $f_{ij}$  and the three  $g_i$  have been chosen so that these mappings map  $\tau_{ij}$  into themselves, etc., so a fixed point exists, etc., as in (Reference 21). For larger  $m$ , it is clear that a larger variety of mixtures is possible, giving the designer useful flexibility. However, the designer must understand MISO design theory used in the design execution, which reveals the cost of feedback and the available tradeoffs among the loops, in order to be able to exploit this flexibility to its fullest extent.

There are additional important advantages in Method Two since the diagonal dominance conditions given by Eqs (V.1) and (V.2) are no longer necessary. Instead the principal condition to be satisfied [to achieve "arbitrarily small (a.s.) sensitivity"] is that  $\det P$  has no RHP zeros. The reader is referred to Reference 22 for details.

## V.8 Conditions for Existence of a Solution

This section considers the conditions required for the applicability of the QFT design technique. Also, it considers the inherent, irreducible conditions applicable for LTI compensations in general, and

compares the two sets of conditions. This is done for a.s. sensitivity which is defined as the BW achievement of a.s. sensitivity of the  $t_{ij}$  over arbitrarily large (a.l.) BW. Such a.s. sensitivity also achieves attenuation over a.l. BW of external disturbances acting on the plant. This problem has also been studied in an abstract setting by Zames and Bensoussan<sup>80</sup>.

In Fig. V.1, it is required that  $y_{11} \in \tau_{11}$  and  $y_{12} \in \tau_{12}$  for all  $P \in \mathcal{O}$ ,  $t_{21} \in \tau_{21}$  and  $t_{22} \in \tau_{22}$ . In the general  $m$  case, the cross-coupling component in, for example,  $y_{11}$  is:

$$y_{c_{11}} = \frac{c_{1j}q_{11}}{1 + g_1q_{11}} = - \sum_{k \neq 1} \left[ t_{k1} \left( \frac{(\text{Adj } P)_{1k} / (\text{Adj } P)_{11}}{1 + g_1 \frac{\det P}{(\text{Adj } P)_{11}}} \right) \right] \quad (\text{V.13})$$

RHP poles of  $(\text{Adj } P)_{1k}$  are normally cancelled by similar poles in  $\det P$ , since  $(\text{Adj } P)_{1k}$  is a term in the expansion of  $\det P$ . RHP zeros of  $(\text{Adj } P)_{11}$  are, of course, normally cancelled by similar ones in the denominator. There may be exceptional cases when in  $\det P$ , for example, a RHP pole of  $(\text{Adj } P)_{1k}$  is cancelled by an identical zero of  $p_{ik}^*$  and does not appear in the other terms of  $\det P$ . Such cases are excluded.

#### **V.8.1 Conditions For "a.s. Sensitivity" In Single-Loop Design**

In Eqs. (V.3), it is seen that a.s. tolerances over a.l. BW (i.e. "a.s. sensitivity") for  $t_{11}$ ,  $t_{12}$  are achievable if  $L_1 = g_1q_{11}$  can be made a.l. over a.l. BW. Indeed this is at least theoretically possible, if  $q_{11}$  satisfies certain constraints. These have been detailed in Appendix 1 of Reference 21 so are only qualitatively described here by means of Fig. V.3.

Figure V.3 is the extended logarithmic complex plane (NC). Since  $P$  ranges over  $\mathcal{O}$ , the set  $\{L_1 = g_1(j\omega)q_{11}(j\omega)\}$  is not a single complex number (at any fixed  $\omega$ ) in the NC but a region, denoted as  $\mathcal{S}_p[L(j\omega)]$ , the template of  $L_1$ , which is the same as  $\mathcal{S}_p[q_{11}(j\omega)]$  but translated vertically

by  $20\log[g_1(j\omega)]$  dB and horizontally by  $\angle g_1(j\omega)$  degrees, because  $L_1 = g_1 q_{11}$ . In a design with significant plant uncertainty  $\mathcal{S}_p[L_1(j\omega)]$  must lie relatively high up, above the zero dB line as shown in Fig. V.3 for  $\omega_1$ . This is so over the important  $\omega$  range of  $t_{11}$  and  $t_{12}$  (their bandwidths generally), in order to achieve the desired sensitivity reduction. Such large values for  $\mathcal{S}_p[L_1(j\omega)]$  can be maintained theoretically for any finite  $\omega$  range, if  $q_{11}$  is m.p. For those  $\omega$  for which  $\mathcal{S}_p[L_1(j\omega)]$  is so located, the uncertainty in the magnitude and phase of  $q_{11}(j\omega)$  (i.e., the area of  $\mathcal{S}_p[q_{11}(j\omega)]$ , can be a.l. [Note, however, that in order to maintain  $\mathcal{S}_p[L_1(j\omega)]$  above the zero dB line, any zeros of  $q_{11}(j\omega)$  on the  $j\omega$  axis must be known and finite in number in order for  $g_1(s)$  to be assigned poles there. (Obviously, transcendental compensation can be used for special countable cases.) If the range of such  $j\omega$  axis zeros is uncertain, then the specifications

$$a_{ij}(j\omega) \leq |t_{ij}(j\omega)| \leq b_{ij}(j\omega), \quad \forall \rho \in \rho \quad (V.14)$$

$$\tau_{ij} = t_{ij}(j\omega) = \text{set of acceptable } t_{ij}(j\omega) \quad (V.15)$$

must be modified to permit such zeros of  $t_{ij}$ .

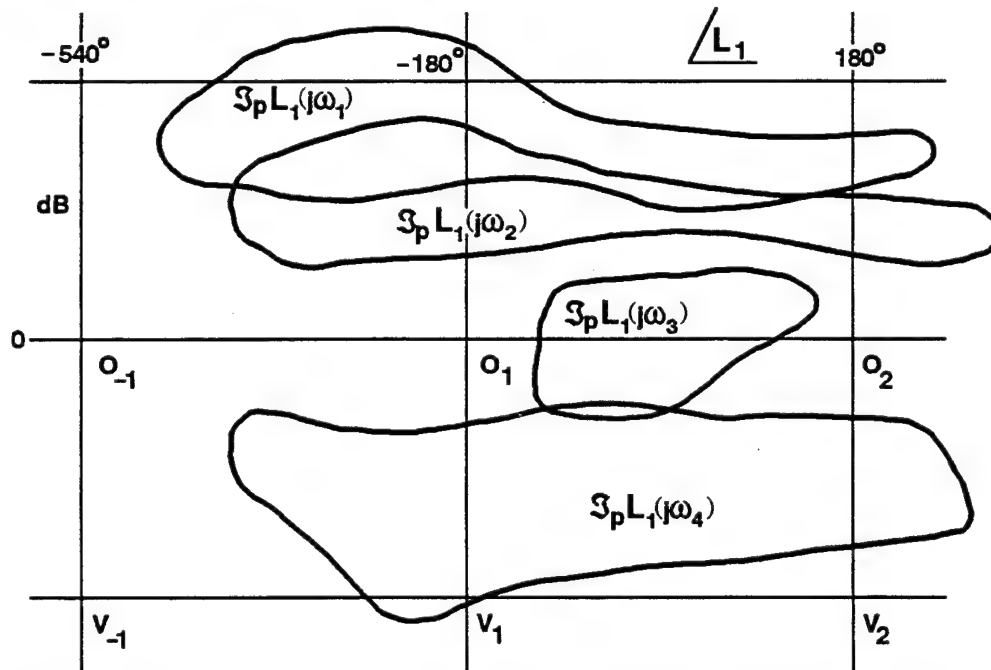


Fig. V.3 Templates of  $L_1(j\omega)$  on logarithmic complex plane (Nichols Chart).



Sooner or later  $L_1(j\omega)$  must decrease and  $\rightarrow 0$  as  $\omega \rightarrow \infty$ . Stability over the range of  $\mathcal{P}$  requires that  $\mathfrak{S}_p[L_1(j\omega)]$  move downward in between the vertical lines  $V_1$  and  $V_2$  without the points ...  $0_1 0_1 0_2$ , ... lying in any of the  $\mathfrak{S}_p[L_1(j\omega)]$ . This appears to allow  $(360^\circ - 2\gamma)$  degrees phase width for  $\mathfrak{S}_p[q_{11}(j\omega)]$ , with phase margin angle  $\gamma$ . However,  $\angle L_1(j\omega)$  must be negative, on the average, in order for  $|L_1(j\omega)|$  to decrease. So in practice only  $(180^\circ - \gamma)$  phase width is tolerable in this range. As  $\omega$  increases and the  $\mathfrak{S}_p[L_1(j\omega)]$  descend lower on the chart below the zero dB line, clearly their width may increase again, but it is essential that the points ...  $0_1, 0_2$ , ... never be a part of any  $\mathfrak{S}_p[L_1(j\omega)]$ . Unstable  $q_{11}$  are included in the above discussion and don't require separate treatment. It follows from the above that the manageable uncertainties depend on the assigned  $t_{ij}$  tolerances, but two important constraints (also see Sec. V.3), for  $m \leq 3$ , are stated here for the case of "a.s. sensitivity":

#### Constraint 1

$$q_{11} = \det \mathbf{P} / (\text{Adj. } \mathbf{P})_{11} \text{ must be m.p.}$$

If this constraint is not satisfied, for Method Two, the theoretically attainable benefits of feedback are limited. They may nevertheless suffice for the specific system being designed (see References 30, 37, and 42).

#### Constraint 2

Suppose  $\exists \omega_h, \epsilon$  for all  $\omega > \omega_h$ , the width of  $\mathfrak{S}_p[q_{11}(j\omega)]$  exceeds  $(180^\circ - \gamma)$ ,  $\gamma$  being a desired phase margin angle, then it is impossible to achieve a.s. tolerances for  $\omega > \omega_h$ . This prevents "a.s. sensitivity" if

$$q_{ii} = \frac{k \prod (s + z_v)}{\prod (s + p_u)}$$

with the  $k$  uncertainty including a sign change which is independent

of the signs of the  $z_v$  and  $p_u$ . Also excluded is a factor  $(1 + \tau s)$  in the numerator or denominator of  $q_{ii}$ , with the uncertainty in  $\tau$  including a sign change which is independent of other parameters.

A good way to apply this constraint, for Method Two, is to obtain:

$$\lim_{\omega \rightarrow \infty} \left[ \frac{\det P}{\det P_o} \right]$$

where  $P_o$  represents the nominal plant matrix. This ratio must not change sign over the range of uncertainty, i.e.,  $P \in \mathcal{O}$ . This automatically takes care of all loops. If this condition is not satisfied then it is impossible, by the usual LTI design techniques, to achieve significant sensitivity reduction.

#### V.8.2 Applications of Sec. V.8.1 to Design Method Two

Constraints 1 and 2 therefore apply to the  $q_{ii} = \det P / (\text{Adj } P)_{ii}$  of the first channel  $i$ , used in the design technique of Secs. V.2 and V.5. So from Constraint 1,  $q_{ii}$  must be m.p.  $\forall P \in \mathcal{O}$  (RHP poles are tolerable), for "a.s. sensitivity" design. Suppose  $P = [p_{ij}]$  has each  $p_{ij} \rightarrow k_{ij}/s^\lambda$  as  $s \rightarrow \infty$ . For  $m = 2$ :

$$q_{ii} = \frac{p_{11}p_{22} - p_{12}p_{21}}{p_{jj}} \rightarrow \frac{k_{11}k_{22} - k_{12}k_{21}}{k_{jj}s^\lambda} \quad (\text{V.16})$$

Let  $K = [k_{ij}]$ , so Constraint 2 states that there may be no change in the sign of  $\det K/k_{jj}$  as  $P$  ranges over  $\mathcal{O}$ . In this chapter it is assumed that all  $k_{ij} > 0$  for all  $P \in \mathcal{O}$ , so Constraint 2 gives  $k_{11}k_{22} > k_{12}k_{21} \forall P \in \mathcal{O}$ , or vice versa. To remove the ambiguity it is also assumed that the plant terminals are numbered so that for at least one  $P \in \mathcal{O}$ ,  $k_{11}k_{22} > k_{12}k_{21}$ , so Constraint 2 yields

$$k_{11}k_{22} > k_{12}k_{21} \quad \forall P \in \mathcal{O} \quad (\text{V.17})$$

This is a diagonal dominance condition as  $s \rightarrow \infty$  which applies only to the first channel being designed when applying Method Two. Zames and

Bensoussan<sup>80</sup> have defined a diagonal condition as  $s \rightarrow \infty$ , in more abstract form.

The above applies to the first channel, say no. 1, for which Eqs. (V.3) are used. Equations (V.4) are used for the second channel. The m.p. condition of Constraint 1 therefore applies to  $q_{22}(1 + L_1)$ , most of which is not new because m.p.  $(1 + L_1)$  and  $\det P$  are already required. As for Constraint 2, there are two extremes. "A.s. sensitivity" can be achieved by  $L_1 BW \gg$  that of  $L_2$  [denoted by  $BW(L_1) \gg BW(L_2)$ ], and then Eq. (V.4(b)) implies Constraint 2 applies to  $q_{22}$ . It can also be achieved by the opposite strong inequality, and then Constraint 2 applies to  $p_{22}$ . For the condition assumed with Eqs. (V.16) and (V.17), with no sign changes in the  $k_{ij}$ , the results are the same. It may also be so in the general case but this would require consideration of simultaneous sign changes among the  $k_{ij}$ , which is not done here.

For  $m = 3$  the application of the constraints to the first channel makes it applicable to  $q_{11}$ . Application to the second, Eqs. (V.8), gives the same results as for the  $m = 2$  case, because  $L_{2c}$  has the same form in both cases [compare to Eqs. (V.4(b)) and (V.8(b))]. If "a.s. sensitivity" is achieved (as it may be) by  $BW(L_1) \gg BW(L_2) \gg BW(L_3)$ , the result is that the constraints of Sec. V.8.1 apply to  $q_{11}$ ,  $q_{22}$ ,  $q_{33}$ . If the opposite is done, in the notation of Eq. (V.9), they apply to  $q_{11}$ ,  $q_{22}/(1 - \gamma_{12})$ , and

$$\frac{q_{33}(1 - \gamma_{12})}{1 - (\gamma_{12} + \gamma_{23} + \gamma_{13}) + (\gamma_{12}\mu_2 + \gamma_{13}\mu_3)}$$

It has not been ascertained whether these two sets of constraints are identical. However, Sec. V.8.3 shows that the constraints of Sec. V.8.1 must always apply to each  $q_{ii}$ ,  $i = 1$  to  $m$ . Constraints for  $m > 3$  may be similarly developed.

When BW is a specification it is important that one template for each loop be obtained at their respective loop BW specification.

### V.8.3 Inherent Constraints

It is important to determine whether the constraints in Sec. V.8.2 are due to the specific design technique or are inherent in the problem itself. For this purpose examine Eq. (V.4(a)) for  $t_{22}$ . How can "a.s. sensitivity" of  $t_{22}$  be achieved despite large uncertainty in  $P$ ? Clearly by large  $L_{2c}$ , the usual feedback method. Large  $L_{2c}$  is achieved by large  $g_2q_{22}$  because large  $L_1$  (needed likewise for small  $t_{11}$  sensitivity) gives  $L_{2c} = g_2q_{22}$ . The latter also attenuates  $c_{22}$ , which may not be small because of  $g_1$  in its numerator. This same principle applies to all  $t_{ij}$ , and is basically the same as that derived from examination of Eq. (V.3), i.e., there is need for a.l.  $L_2$  and  $L_1$  over a.l. BW in order to achieve "a.s. sensitivity". But do the constraints of Sec. V.8.1 apply to  $q_{22}$  and  $q_{11}$ ?

This is indeed so, and proven by Eq. (V.3(a)) and its analog for  $t_{2j}$  (by interchanging 1,2), by simply asking whether a stable  $t_{11}$  is possible if  $1 + L_1$  has RHP zeros? For if not, and since a.l.  $L_1$  over an a.l. BW is needed, it follows that  $L_1$  (and  $L_2$ ) must satisfy the constraints. Suppose  $(1 + L_1)$  has RHP zeros. These are RHP poles of  $t_{11}$ , unless in Eq. (V.3(a)), for  $i = 1$ , the numerator of  $t_{11}$  has these same zeros. Suppose it has them, and there is a small change in  $f_{21}$ . Since  $F$  is outside the feedback loops, system stability is unaffected. The zeros of  $1 + g_1q_{11}$  in Eq. (V.3(a)) are thereby unaffected, so neither should the zeros of the numerator of Eq. (V.3(a)), for  $i = 1$ . The term  $f_{11}g_1q_{11}$  is unaffected, but  $t_{21}$  is affected [see Eqs. (V.4) with  $i = 1$ ]. Hence, the hypothesis  $(1 + L_1)$  has RHP zeros is untenable, so the constraints apply to  $q_{11}$  and  $q_{22}$ .

Comparing these results with Sec. V.8.2, the conclusion is that "a.s. sensitivity" may be achieved by design Method Two, with plant constraints which are inherent and irreducible, i.e., not more severe than inherently necessary. This is achieved by letting  $BW(L_1) \gg BW(L_2) \gg BW(L_3)$ , wherein Constraints 1 and 2 are the only constraints applicable to  $q_{11}$ ,  $q_{22}$ ,  $q_{33}$ , which have been shown to be inherent. This is associated with the following design order: first  $L_1$  [Eqs. (V.7)], second  $L_2$  [Eqs. (V.8)], third  $L_3$  [Eqs. (V.9)]. The design procedure is facili-

tated by such inequalities, because then in Eq. (V.8(b)),  $L_{2c} \rightarrow L_2 = g_2 q_{22}$  over its important design range, and  $L_{3c} \rightarrow L_3 = g_3 q_{33}$ . If other factors are equal ( $\mathfrak{F}_p[q_{ii}]$ ) tolerances on  $t_{ij}$ ,  $i = 1, 2, 3$  for each  $i$ , there is a natural tendency for this order of the inequalities because of the inherent greater overdesign of  $L_1$ , lesser of  $L_2$ , and least of  $L_3$  (recall Sec. V.4 and the last paragraph in Sec. V.5).

However, the above is rather of theoretical, academic interest, because it applies only for "a.s. sensitivity", defined at the beginning of Sec. V.8. Thus, it applies if one is given a plant with specific uncertainty range and is challenged to achieve a.s. performance tolerances over a.l. bandwidths. However, given a MIMO plant set  $\mathcal{P}$  and sets of tolerances  $\tau_{ij}$  ( $i, j = m$ ), it is conceivable that the latter are not achievable by Method Two, but are inherently achievable. The reason (e.g., for  $m = 2$ ) is that in Eqs. (III.35) through (III.38), the demand on  $L_1$  to achieve the desired sensitivity reduction, may be greater than is inherently needed, because of the overdesign, discussed in Sec. V.4, and is therefore unachievable, because of the nature of  $\mathcal{P}$  (e.g., it has some n.m.p. elements). Thus, a specific problem may be incompatible with the constraints only due to this overdesign. There may exist as yet undiscovered better methods with reduced demand on  $L_1$ , which renders them compatible with the constraints. From Sec. V.4, it is clear that the best method is achieved with Eqs. (V.3) by maximum use of the correlation which exists between the  $\mathcal{P}$  uncertainty and the  $t_{2j} \in \tau_{2j}$  in Eqs. (V.3). A suggestion for this purpose has been given in Reference 21. One subdivides the plant set into subsets  $\mathcal{P}_j$  which are correlated with the subsets  $\tau_{ju}$  of  $\tau_{ij}$ . Equations (V.3), similarly Eqs. (V.7) and (V.8), are now applied to these pairs  $\mathcal{P}_u, \tau_{ju}$  separately for each  $u$ . This approach, to the knowledge of the authors, has not as yet been attempted in any numerical problem.

It is worth noting that the constraints of the diagonal dominance type as  $s \rightarrow \infty$ , appear in the design technique of Reference 21. However, they are always present there, even if "a.s. sensitivity" is not attempted. In design Method Two the constraints are in effect only for "a.s. sensitivity." Hence, it is possible that a specific synthesis

problem with given  $\tau_{ij}$ ,  $\mathcal{O}$  sets may not be solvable by Method One, but is solvable by Method Two. This is the case in Reference 21.

### V.9 Nondiagonal G

The constraints on  $P$  in Sec. V.8 are deduced on the assumption that  $G$  is diagonal. Are these constraints eased if a nondiagonal  $G$  is used? To answer this question, let  $H$  be a fixed LTI pre-compensator matrix inserted ahead of the plant and let  $V = PH$  be the new effective plant in the set  $v = \{PH, P \in \mathcal{O}\}$ . The design techniques with diagonal  $G$ , are now applied to set  $v$  instead of set  $\mathcal{O}$ . If  $H$  is helpful in overcoming some constraint, then it is necessary that the constraint violated by  $\mathcal{O}$ , is not violated by  $v$ . The constraint  $\det P$  is m.p.  $VP \in \mathcal{O}$  is not eased at all, because  $\det V = (\det P)(\det H)$ , and obviously cancellation of RHP zeros of  $\det P$  by  $\det H$  cannot be done for many reasons. The other important constraint involving diagonal dominance as  $s \rightarrow \infty$ , is also not eased, because it applies to the sign of  $\det V$  not changing, as  $s \rightarrow \infty$ . Thus, the constraints on  $\mathcal{O}$  for "a.s. sensitivity" are not eased by a non-diagonal  $G$ .

However,  $H$  may be very helpful in reducing the amount of feedback needed to achieve specified tolerance sets given by Eqs. (V.14) and (V.15), for a given plant set  $\mathcal{O}$ , so that a design unachievable by diagonal  $G$  (say, because of n.m.p.  $P$  or sensor noise problems) may be achievable via  $H$ . For example in Eq. (V.4(a)),  $L_{2c}$  must handle the uncertainties due to  $L_{2c}$  itself and attenuate the effective cross-coupling set  $\{c_{2j}\}$ . For basically noninteracting tolerances on  $t_{kj}$  ( $k \neq i$ ),  $f_{ij}$  is made zero, so only the latter need exist. It may be possible to considerably reduce  $|c_{2j}|_{\max}$  by means of  $H$ , by making  $V = PH$  quasi-diagonal, even though  $P$  has large non-diagonal components.

Off diagonal plant elements appear in all the design Eqs. (III.39) through (III.41), Eq. (V.4), and Eqs. (V.7) through (V.9) in the 'cross-coupling' components, so their reduction via  $H$  is desirable. How is this systematically done in the case of significant  $P$  uncertainty? For  $m = 2$ , let the normalized  $H$  have 1 for its diagonal elements and  $h_{12} = \mu$ ,

$h_{21} = v$ . Then  $v_{12} = \mu p_{11} + p_{12}$  and  $v_{21} = p_{21} + v p_{22}$ . The objective is to minimize over  $\mathcal{O}$   $\max |v_{12}|, |v_{21}|$  at each  $\omega$ . Sketches of the sets

$$\left( \frac{p_{12}(j\omega)}{p_{11}(j\omega)} \right), \left( \frac{p_{22}(j\omega)}{p_{21}(j\omega)} \right)$$

in the complex plane, are clearly very helpful in choosing  $\mu(j\omega)$ ,  $v(j\omega)$ . However, one should check the effect on the resulting sets of  $v_{11} = p_{11} + v p_{12}$ ,  $v_{22} = \mu p_{21} + p_{22}$ , because of the obligations on the loop transmissions due to their uncertainties. The final choice depends on the relative importance of the two terms in the numerators of  $y_{1j}, y_{2j}$  in Eqs. (V.3) and (V.4). (See Reference 21, Secs. 3.2, 4 for discussion relevant to this topic).

If the elements of  $P$  have a RHP pole in common, i.e.,  $P = P_1/(s - p)$ , then one should not try to diagonalize  $P$  by means of  $PH = \Lambda$  diagonal, because in practice  $H = P_1^{-1}\Lambda$  with  $P_1^{-1} \neq P^{-1}$  exactly, giving  $PH = PP_1^{-1}\Lambda$  with RHP dipoles. Instead, one tries to diagonalize  $P_1$  by means of  $P_1H = \Lambda$ , giving  $H = P_1^{-1}\Lambda$ , and  $PH$  and  $P_1P_1^{-1}\Lambda/(s - p)$ .

#### V.10 Achievability of a m.p. Effective Plant $\det P$

For some control systems (e.g., flight control) there are often available more control inputs ( $\ell$ ) than outputs ( $m$ ). The inputs and outputs of an aircraft may be selected in such a manner as to yield the  $m \times m$  aircraft plant matrix  $P(s)$ . If the constraint  $\det P(s)$  be m.p. is not satisfied then it may be possible to achieve a m.p.  $\det P_e(s)$  for an effective  $m \times m$  plant  $P_e(s)$  by augmenting the basic  $m \times \ell$  plant  $P_b$  by a  $\ell \times m$  gain matrix  $W = [w_{ij}]$  or a frequency sensitivity matrix  $W = [w_{ij}(j\omega)]$  as shown in Fig. V.4. The expression for the output  $y(s)$  may be obtained by two different approaches:

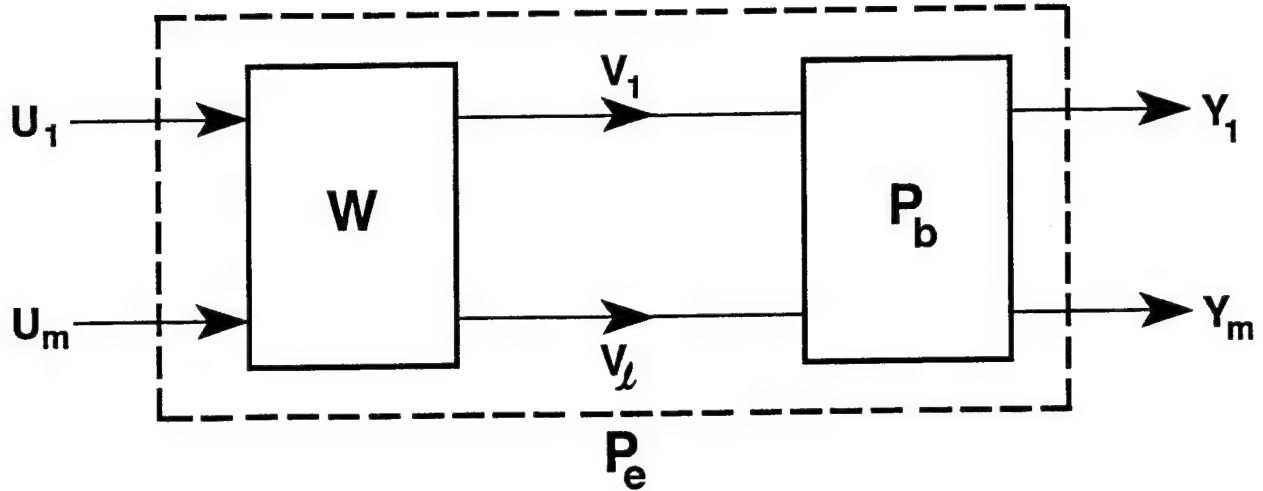


**Fig. V.4 An mxm Effective Plant  $P_e(s)$**

Case A From the differential equations describing the system of Fig. V.4 obtain

$$D(s)y(s) = N(s)u(s) \quad (\text{V.18})$$

where  $D(s)$  and  $N(s)$  are mxm matrices of polynomials and the output  $y(s)$  and input  $u(s)$  are mx1 vectors. Equation (V.18) is manipulated to yield

$$y(s) = D^{-1}(s)N(s)u(s) = P_e u(s) \quad (\text{V.19})$$

where the effective plant matrix is given by

$$P_e(s) = D^{-1}(s)N(s) \quad (\text{V.20})$$

Thus from Eq. (V.20) the following expressions are obtained:

$$D(s)P_e(s) = N(s) \quad (\text{V.21})$$

$$\det D(s) \det P_e(s) = \det N(s) \quad (\text{V.22})$$

$$\det P_e(s) = \frac{n_e(s)}{d_e(s)} \quad (\text{V.23})$$



where  $n_c(s) = \det N(s)$ ,  $d_c(s) = \det D(s)$ , and  $n_c(s)$  and  $d_c(s)$  are polynomials. Thus,  $n_c(s)$  must not have any RHP zeros in order for Eq. (V.23) to be m.p. and satisfy the constraint that  $\det P_c(s)$  be m.p.

Case B From the block diagram of Fig. V.4, where  $v(s)$  is a  $\ell \times 1$  vector and  $W$  is only a gain matrix the following expressions are obtained:

$$y(s) = P_b v(s) \quad (V.24)$$

$$v(s) = W u(s) \quad (V.25)$$

$$y(s) = P_b(s) W(s) u(s) \quad (V.26)$$

From Eqs. (V.19) and (V.26) it is seen that the effective plant matrix can also be expressed by

$$P_e(s) = P_b(s) W \quad (V.27)$$

where  $P_b(s) = [p_{ij}(s)]$ ,  $p_{ij}(s) = n_{ij}(s)/d(s)$ ,  $W = [w_{ij}]$ ,  $n_{ij}(s)$  and  $d(s)$  are polynomials,  $m \leq \ell$ , and  $w_{ij}$  is a gain to be determined in order to try to achieve a m.p.  $\det P_e(s)$ . Note that although in this section all the  $p_{ij}(s)$  are considered to have a common denominator, i.e.,  $d(s) = d_{ij}(s)$ , in general the  $p_{ij}$  elements of  $P_b(s)$  can have different denominators

By use of the Binet-Cauchy formula<sup>46</sup> Eq. (V.27) may be expressed as follows:

$$\det P_e(s) = \det [P_b(s) W] = \sum_i [p_i(s) w_i] \quad (V.28)$$

where  $p_i(s)$  and  $w_i$  are the determinants of appropriate  $m \times m$  submatrices of  $P_b(s)$  and  $W(s)$ , respectively. A sufficient condition for  $\det [P_b(s) W]$  to be m.p. is that at least one  $p_i(s)$  be m.p. A short proof of this fact is as follows: let  $p_i(s)$  be the determinant of the  $m \times m$  submatrix of  $P_b(s)$

formed by the columns indexed by  $i_1, \dots, i_m$ . Assume that this  $p_i(s)$  is m.p. Choose  $W$  so that the  $m \times m$  submatrix formed by the rows indexed by  $i_1, \dots, i_m$ , is the identity matrix while all remaining rows are zero. Then, clearly  $\det [P_b(s)W] = p_i(s)$ . The number of terms in the summation of Eq. (V.28) is given by

$$\alpha_z = \frac{\ell!}{(\ell - m)!m!} \quad (V.29)$$

Let the submatrices of  $P_b$  and  $W$ , of Eq. (V.28), be represented, respectively, by  $P_{bw}$  where  $w = 1, 2, \dots, \alpha_z$ . The  $\det P_b(s)$  obtained from Eq. (V.28) is

$$\begin{aligned} \det P_b(s) = & \det P_{b_1} \det W_{b_1} + \det P_{b_2} \det W_{b_2} + \dots \\ & + \det P_{b_v} \det W_{b_v} + \dots + \det P_{b_{\alpha_z}} \det W_{b_{\alpha_z}} \end{aligned} \quad (V.30)$$

where

$$P_{b_v} = \left[ \frac{n_{ij}(s)}{d(s)} \right] \quad (V.31)$$

and

$$W_{b_v} = [w_{ij_v}] \quad (V.32)$$

Thus each term in Eq. (V.30) can be expressed as

$$\det P_{b_v} \det W_{b_v} = \frac{1}{d^m(s)} \det |n_{ij}(s)| \det |w_{ij_v}| \quad (V.33)$$

which permits Eq. (V.30) to be written as follows:

$$\begin{aligned}
\det \mathbf{P}_e(s) &= \frac{1}{d^m(s)} \sum (\det |n_{ij}(s)_1| \det |w_{ij_1}| \\
&\quad + \det |n_{ij}(s)_2| \det |w_{ij_2}| + \dots \\
&\quad + \det |n_{ij}(s)_{\alpha_z}| \det |w_{ij_{\alpha_z}}|) = \frac{n'_e(s)}{d^m(s)}
\end{aligned} \tag{V.34}$$

where  $n'_e(s)$  is a polynomial. Since Eq. (V.23) and (V.34) represent the same open-loop system of Fig. V.4 then

$$\frac{n_e(s)}{d_e(s)} = \frac{n'_e(s)}{d^m(s)} \tag{V.35}$$

which results in  $d_e(s) = d(s)$  and

$$n_e(s) = \frac{n'_e(s)}{d^{m-1}(s)} \tag{V.36}$$

Based upon Eqs. (V.34) through (V.36)  $d^{m-1}(s)$  must be a factor of  $n_{ij}(s)_w$ .

The following development illustrates that a sufficient condition for the existence of a m.p.  $\det \mathbf{P}_e(s)$  is that at least one  $\det \mathbf{P}_b(s)$  must be m.p. Assume

$$\det |n_{ij}(s)_1| \det |w_{ij_1}| = \det |n_{ij}(s)_1| k_1 \tag{V.37}$$

in Eq. (V.34) is m.p. where  $k_1 = \det |w_{ij_1}|$  is a scalar. Factor out  $d^{m-1}(s)$  from every term in Eq. (V.36) and let

$$k_1 \frac{\det |n_{ij}(s)_1|}{d^{m-1}(s)} = k_1 N_1(s) \tag{V.38}$$

Also, let the summation of the remaining terms, after factoring out

$d^{m-1}(s)$  from each term, be expressed as

$$k_2 N_2(s) = \frac{1}{d^{m-1}(s)} [ \det |n_{ij}(s)|_2 \det |w_{ij_2}| + \dots + \det |n_{ij}(s)_{\alpha_x}| \det |w_{ij_{\alpha_x}}| ] \quad (\text{V.39})$$

where  $k_2$  is a scalar. Note:  $k_1$ ,  $k_2$ , and  $N_2(s)$  are now functions of  $w_{ij}$  which are to be selected in order to try to achieve a m.p.  $P_c(s)$ . Based upon Eqs. (V.38) and (V.39), Eq. (V.29) can be expressed as follows:

$$\det P_c(s) = \frac{1}{d(s)} [ k_1 N_1(s) + k_2 N_2(s) ] \quad (\text{V.40})$$

In order for  $\det P_c(s)$  to be m.p. then the zeros of

$$k_1 N_1(s) + k_2 N_2(s) = 0 \quad (\text{V.41})$$

must all be in the LHP. Equation (V.41) is manipulated to the mathematical format of

$$\left( \frac{k_1}{k_2} \right) \left[ \frac{N_1(s)}{N_2(s)} \right] = -1 \quad (\text{V.42})$$

which permits a root-locus analysis of Eq.(V.40). Since the zeros of Eq. (V.42) are in the LHP then the weighting factors  $w_{ij}$  are selected in hopes that all roots of Eq. (V.41) lie in the LHP for all  $P_b \in P$ . This assumes that throughout the region of plant parameter uncertainty, the initially chosen m.p. submatrix in Eq. (V.34) is m.p. for all  $P_b \in P$  and be expressed by Eq. (V.38). To enhance the achievability of m.p.  $\det P_c(s)$  the following guidelines may be used:

1. Determine the number  $\alpha$ , submatrices of  $P_{bw}$  of Eq. (V.34) that are m.p.

2. Select one of the m.p. submatrices to be identified as Eq. (V.38).

3. The values of  $w_{ij}$  of  $W_{bw}$  associated with

(a) The remaining  $\alpha_y - 1$  m.p.  $P_{bw}$  be altered in such a manner as to increase the values of their corresponding  $\det W_{bw}$ .

(b) The  $\alpha_z - \alpha_y$  non m.p.  $P_{bw}$  be altered in such a manner as to decrease the value of their corresponding  $\det W_{bw}$ .

By changing the values of the gains  $w_{ij}$  in the manner described will result in the  $\alpha_y - 1$  m.p. terms of Eq. (V.39) to dominate in the resulting expression for  $N_2(s)$ . This dominance of the  $\alpha_y - 1$  terms in  $N_2(s)$  may result in  $N_2(s)$  being m.p. Also, it may enhance the achieveability of a m.p.  $P_c(s)$  by the analysis of Eq. (V.42).

Once the  $n_{ij}(s)$  and  $w_{ij}$  are specified, in order to simplify the root-locus computational effort, it is necessary to factor out  $d(s)$  from the numerator polynomials of Eqs. (V.38) and (V.39). Depending upon the CAD package that is utilized in determining  $d(s)$  and the numerator polynomials of these equations, a perfect factoring may not exist.

Now consider the most general case, i.e.,

$$\det P_{b_v} = \det \left| \frac{n_{ij}(s)_w}{d_{ij}(s)_w} \right| \frac{n_w(s)}{d_w(s)} \quad (V.43)$$

and

$$\det W_{b_v} = \det \left| \frac{w_{ij}(s)_w}{h_{ij}(s)_w} \right| = \frac{w_w(s)}{h_w(s)} \quad (V.44)$$

where the  $d_{ij}(s)$  and  $h_{ij}(s)$  are not all the same and where  $n_w(s)$ ,  $d_w(s)$ ,  $w_w(s)$  and  $h_w(s)$  are scalar polynomials. Hence

$$\det \mathbf{P}_e(s) = \sum_{\alpha_z} \left[ \frac{n_w(s) w_w(s)}{d_w(s) h_w(s)} \right] \quad (\text{V.45})$$

For each value of  $w$ ,  $n_w(s)/d_w(s)$  has a range of uncertainty which may be correlated with that of the remaining  $\alpha_z - 1$  submatrices of  $\mathbf{P}(s)$ . Thus for the general case some or all of the  $n_w(s)/d_w(s)$  may have RHP zeros and/or poles. The problems now becomes one of trying to choose fixed  $w_w(s)$  and  $h_w(s)$  polynomials so that the  $\det \mathbf{P}_e(s)$  has no RHP zeros over the entire range, or failing that to have them as relatively "far-off"; as possible. This problem has been studied by several researchers and the resulting techniques may be used for this purpose<sup>27,114</sup>.

Thus, the Binet-Cauchy formula permits the determination if an m.p. effective plant  $\det \mathbf{P}_e(s)$  is achievable over the region of plant uncertainty.

### V.11 Summary

This chapter has presented synthesis techniques for highly uncertain mxm MIMO LTI feedback systems with output feedback, with the following features:

- (a) There is detailed control over the  $m^2$  individual system transfer functions.
- (b) The MIMO uncertainty problem is rigorously converted into a number of MISO uncertainty problems. Solutions of the latter are guaranteed to be satisfactory for the former. Relatively simple MISO single loop feedback techniques can be used to solve the MISO problems.
- (e) For "arbitrary small sensitivity" over arbitrary large bandwidth (BW), the technique in Secs. V.2 through V.5, give constraints on the plant which are inherent and irreducible, i.e. every LTI compensation technique has these constraints.

- (d) Part of the constraints (at infinite  $s$ ) in (c) were always present in the previously developed MISO equivalent technique<sup>21</sup>, i.e., even if "a.s. sensitivity" was not required. They are present in the new techniques only for a.s. sensitivity. Also, fixed point theory is not required for justification of the new technique.
- (e) The overdesign inherent in the fixed point techniques<sup>21</sup>, has been reduced but some overdesign is still present.
- (f) These techniques are applicable to the design of a reconfigurable aircraft with surface failures<sup>26</sup>.

The reader is urged, in performing a QFT design, to constantly refer to Chap. VII and to Appendix A.

## Chapter VI MIMO System With External Disturbance Inputs<sup>77</sup>

### VI.1 Introduction

Previous chapters have dealt with MIMO tracking control systems with no external disturbances being applied to the plant. This chapter considers the analysis and design of a MIMO external disturbance rejection control system. The literature has not thoroughly treated this disturbance rejection problem. The material in this chapter is extracted from an AFIT Master's thesis<sup>77</sup> dealing with the air-to-air aerial refueling flight control problem. Although this chapter addresses the specific aerial refueling problem, the design procedures can be applied to other MIMO external disturbance problems.

#### VI.1.1 Aerial Refueling Background

The United States Air Force (USAF) maintains a fleet of large cargo/transport aircraft. Refueling these aircraft during flight provides unlimited range of operation for this fleet of aircraft. However, long flights and multiple air-to-air refuelings can seriously strain and fatigue the pilot, decreasing flight safety, and extending recovery time between missions. Hence, automatic control of the receiving aircraft during aerial refueling operations is most beneficial.

Cargo/transport aircraft are generally large and have high moments of inertia. Piloting a large, high inertia aircraft during air-to-air refueling requires intense concentration. The pilot must maintain a very precise position relative to the tanker. He/she maintains position visually, applying the appropriate control inputs when changes in position occur. The pilot must compensate for changes in aircraft dynamics due to taking on fuel, specifically, movements in center-of-gravity and changes in the moments of inertia  $I_{xx}$  and  $I_{yy}$ . Besides dynamic changes, the pilot must contend with maintaining position in the presence of wind gusts. Since these aircraft can take on large amounts of fuel, up to 250,000 pounds, air-to-air refueling can take up to 30



minutes. Compound this over long flights and multiple refuelings, and "the pilot's fatigue level increases and can reach an unsafe level. This could endanger the flight crew, and possibly impact USAF's capability to perform its mission.

One way to ease the pilot workload is to implement an automatic flight control system (AFCS) for air-to-air refueling. The AFCS needs to be able to maintain a precise position of the receiving aircraft (receiver) relative to the tanker in the presence of such disturbances as wind gusts, and in the changes of mass and moments of inertia. This AFCS is designed to precisely regulate position relative to the tanker by applying the control synthesis techniques of Quantitative Feedback Theory (QFT). For the regulation problem, a MIMO QFT design method is developed to address the rejection of the disturbances entering the system at the output.

#### VI.1.2 Problem Statment

During air-to-air refueling, the receiver aircraft will change position relative to the tanker. The pilot must pay close attention and take corrective action to maintain position. Excessive changes in position will disconnect the refueling boom from the receiver. An AFCS must be designed to regulate the receiver's position, thus reducing the pilot workload and fatigue factor. By using MIMO QFT, an AFCS is designed that operates throughout the range of the changing aircraft dynamics and rejects disturbances including those at the output.<sup>9</sup>

#### VI.1.3 Assumptions

The following assumptions are made:

- Only the desired outputs are of interest for final performance.
- Position of the receiver aircraft relative to the tanker during air-to-air refueling can be accurately measured.

- The CAD packages used, MIMO/QFT, EASY5x, MATRIXx and Mathematica are adequate for the design process.

The first assumption is required in applying MIMO QFT. The second assumption is required because no sensors are currently in place to measure the position of the receiver relative to the tanker. The third assumption is concerned with the limits of CAD packages and their numerical robustness.

#### **VI.1.4 Research Objectives**

The research objectives of this chapter are: (1) to utilize the aircraft models, developed in Reference 77, for the QFT design process using a published document<sup>75</sup> containing C-135 cargo aircraft stability derivatives tables and plots; (2) to present a design for multi-channel control laws using MIMO QFT for several flight conditions with special emphasis on aircraft center-of-gravity and weight changes; (3) to simulate the design for linear and nonlinear performance on MATRIXx, and nonlinear performance on EASY5x; (4) to evaluate the new control law; and (5) to validate the MIMO QFT design with disturbances at the output.

#### **VI.1.5 Scope**

This chapter applies the MIMO QFT technique to the design of an AFCS regulator for the automatic maintenance of the three-dimensional separation ( $x$ ,  $y$ , and  $z$ ) of a receiver aircraft relative to a tanker. The AFCS controls the receiver and is independent of the tanker in as much as the tanker is used as the point of reference. MIMO QFT design techniques are developed for disturbances at the system output. The MIMO/QFT CAD package (see Chapter VIII) is utilized to achieve this design. The AFCS is designed to reject disturbances at the  $x$ ,  $y$ , and  $z$  outputs in order to keep the receiver aircraft in a volume specified as the area of boom operation<sup>75</sup>. Models are developed for disturbances due to wind gusts and received fuel. The MIMO QFT plant is the bare-aircraft model augmented by a typical Mach-hold, altitude-hold, wing-leveler autopilot. QFT compensators control the reference signal of the

autopilot to maintain "formation" during air-to-air refueling. The control system is simulated for linear performance in MATRIXx. A full six-degree-of-freedom nonlinear simulation is performed in EASY5x.

#### VI.1.6 Methodology

The design approach requires six steps:

- Generate linear time-invariant (LTI) state-space models of the aircraft for different weights and center of gravity.
- Implement a Mach-hold, altitude-hold, wing leveler autopilot that operates for all aircraft models.
- Model the disturbance due to wind gusts and refueling.
- Design the AFCS using QFT.
- Simulate the design on MATRIXx and EASY5x to validate the AFCS design.

#### VI.1.7 Overview of Chapter

Section VI.2 discusses how the external disturbances are incorporated into the 6 DOF aircraft equations. The MIMO QFT mathematical expressions are reformulated based upon these modified aircraft equations. The air-to-air refueling AFCS concept is discussed in Sec. VI.3. The AFCS design process is shown in Sec. VI.4 followed by Sec. VI.5 which presents the linear and nonlinear simulations.

#### VI.2 Air-to-Air Refueling FCS Design Concept

The aircraft (A/C) modeled in this chapter is the cargo variant of the C-135 class aircraft (C-135B). This A/C is chosen because of the availability of the aerodynamic data<sup>75</sup>. This chapter describes the modeling of the C-135B. A Mach-hold, altitude hold, and wing-leveler autopilot is included in the C-135B model<sup>9</sup>. Wind gusts and fuel transfer disturbance models are developed in this

chapter, as well as the AFCS concept.

### **VI.2.1 C-135B Modeling**

EASY5x is used to develop the state-space six-degrees-of-freedom bare (uncontrolled) A/C model. EASY5x is a computer aided design (CAD) tool written by Boeing Computer Services used to model, simulate, and analyze dynamic systems. The user need only provide A/C stability derivatives, flight conditions, and desired input/outputs. Sixteen bare A/C plants are developed to account for the uncertainty of the C-135B during air-to-air refueling. The 16 models are based on two different coefficients of lift,  $C_L = 0.2, 0.6$ , for eight different A/C weights. The Mach 0.69 at 28,500 feet flight condition is considered. These discrete values are selected based on the availability of data, normal refueling speed and altitude, and represent weights ranging from empty/low fuel to loaded/full fuel A/C. Typically, during air-to-air refueling, the C-135B will have a  $C_L$  between 0.27 and 0.45<sup>75</sup>. Therefore, the 16 plant models envelop the structured uncertainty of the C-135B during air-to-air refueling.

The six-degrees-of-freedom state-space models, generated by EASY5x, are loaded into MATRIX<sub>x</sub>. MATRIX<sub>x</sub> is used to design the autopilot using root-locus design techniques. The autopilot is designed to control all 16 plant cases. The bare aircraft and autopilot are shown in Fig. VI.1. An autopilot is used for two reasons: (1) autopilots reduce the high frequency cutoff of the aircraft, and (2) all aircraft have autopilots. Lowering the cutoff frequency of the aircraft reduces high frequency parameter uncertainty which in turn reduces the size of the QFT templates. Since autopilots are available, using it in the QFT design eliminates duplication of a control system to provide input to the bare aircraft, reducing cost and overhead. The inputs to the autopilot are thrust, elevator, aileron, and rudder commands. The outputs are z-position (altitude), x-position, and y-position in a local inertial reference frame where x is positive out the nose of the aircraft, y out the right wing, and altitude is positive up. The three outputs frame of reference is translated from the aircraft center of gravity (cg) to the approximate location of the air-to-air refueling receptacle on the top of the aircraft.

The Mach hold command input is used to control the x position, altitude hold controls altitude, and the rudder command is used to control the y position. Mach and altitude are self evident, rudder is chosen over aileron because the rudder does not roll the aircraft. By using the rudder for the QFT

controller, good performance is obtained while leaving the aileron controller to handle wing leveling.

### VI.2.2 Disturbance Modeling

Disturbance models are generated by developing augmented state-space models of the aircraft in the presence of wind gusts and fuel transfer inputs. The development in Chapter 3 of Reference 77, based upon external disturbance inputs represented by the vector  $\mathbf{d}$ , considers three disturbance components: pitch plane wind induced disturbance  $\Gamma_{pitch}$ , lateral channel wind induced disturbance  $\Gamma_{lat}$ , and refueling disturbance  $\Gamma_{rf}$ . Total disturbance modeled is

$$\Gamma \mathbf{d} = \Gamma_{pitch} \mathbf{d}_{pitch} + \Gamma_{lat} \mathbf{d}_{lat} + \Gamma_{rf} \mathbf{d}_{rf} \quad (\text{VI.1})$$

where  $\Gamma_{pitch}$  and  $\Gamma_{rf}$  augment the state-space equation containing the states that identify pitch plane flight behavior. In the same manner,  $\Gamma_{lat}$  augments the lateral channel states. The state-space equation now takes on the form

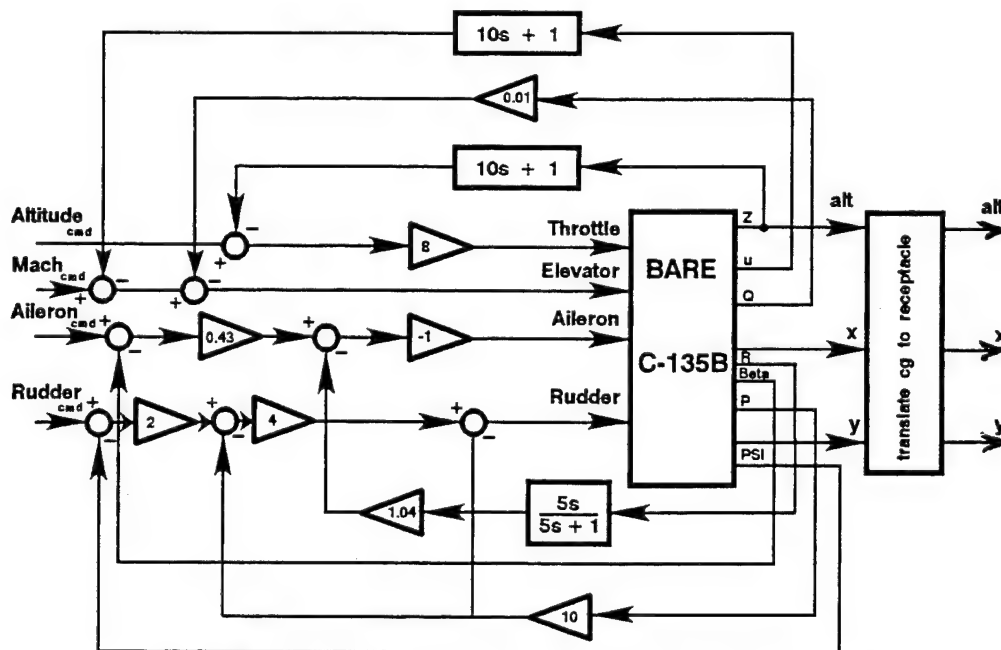


Fig. VI.1 C-135B bare aircraft with autopilot.

$$\begin{aligned}\dot{\mathbf{x}} &= \mathbf{Ax} + \mathbf{Bu} + \mathbf{\Gamma d} \\ \mathbf{y} &= \mathbf{Cx}\end{aligned}\tag{VI.2}$$

Note, as the disturbances are applied to the bare aircraft, they enter into the inner most loop, around which the autopilots, and later, the QFT loops are closed.

### VI.3 Plant and Disturbance Matrices

Based on zero initial conditions, then from Eq. (VI.2)

$$\mathbf{s}\mathbf{x} = \mathbf{Ax} + \mathbf{Bu} + \mathbf{\Gamma d}\tag{VI.3}$$

$$\mathbf{x} = [\mathbf{sI} - \mathbf{A}]^{-1}\mathbf{Bu} + [\mathbf{sI} - \mathbf{A}]^{-1}\mathbf{\Gamma d}\tag{VI.4}$$

$$\begin{aligned}\mathbf{y} = \mathbf{Cx} &= \mathbf{C}[\mathbf{sI} - \mathbf{A}]^{-1}\mathbf{Bu} + \mathbf{C}[\mathbf{sI} - \mathbf{A}]^{-1}\mathbf{\Gamma d} \\ &= \mathbf{P(s)}\mathbf{u} + \mathbf{P_d(s)}\mathbf{d}\end{aligned}\tag{VI.5}$$

where

$$\begin{aligned}\mathbf{P(s)} &= \mathbf{C}[\mathbf{sI} - \mathbf{A}]^{-1}\mathbf{B} \\ \mathbf{P_d(s)} &= \mathbf{C}[\mathbf{sI} - \mathbf{A}]^{-1}\mathbf{\Gamma} = \{\mathbf{p_{d_i}}\}\end{aligned}\tag{VI.6}$$

and where the plant model  $\mathbf{P_F}$  is partitioned into the two matrices  $\mathbf{P(s)}$  and  $\mathbf{P_d(s)}$ ,  $\mathbf{P(s)} = \mathbf{P_e(s)}$  for a square plant matrix  $\mathbf{P(s)}$ , and the matrix  $\mathbf{P_d(s)}$  models the transmission from the external disturbance inputs to the output of  $\mathbf{P_F}$ . If  $\mathbf{P(s)}$  is not a square matrix then a weighting matrix  $\mathbf{W(s)}$  must be used to yield  $\mathbf{P_e(s)} = \mathbf{P(s)W}$ . Equation (VI.5) is represented in Fig. VI.2. Thus the QFT formulation of Sec. VI. 5 is applicable for this problem.

### VI.4 Control Problem Approach

The tanker's position is assumed fixed and hence the receiver aircraft's position is measured from this frame of reference. In this approach the control problem can be viewed as a formation flying

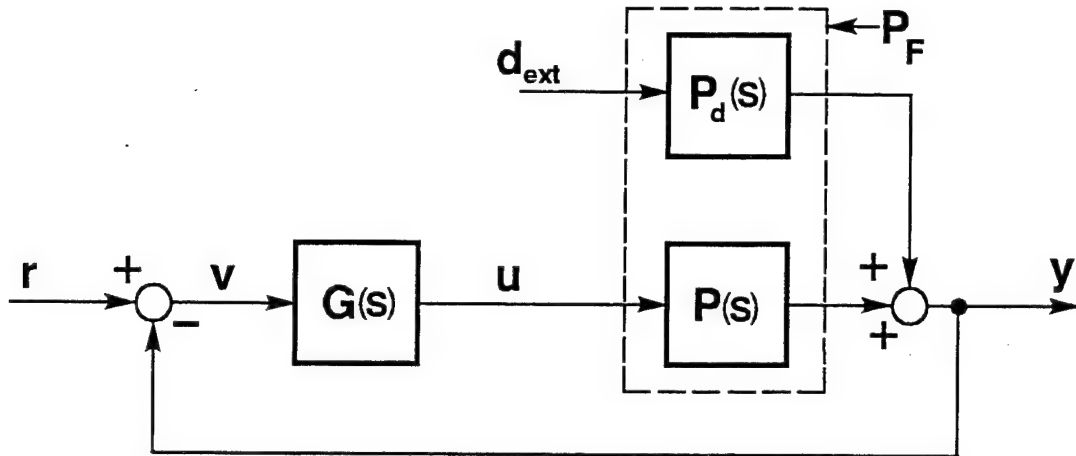
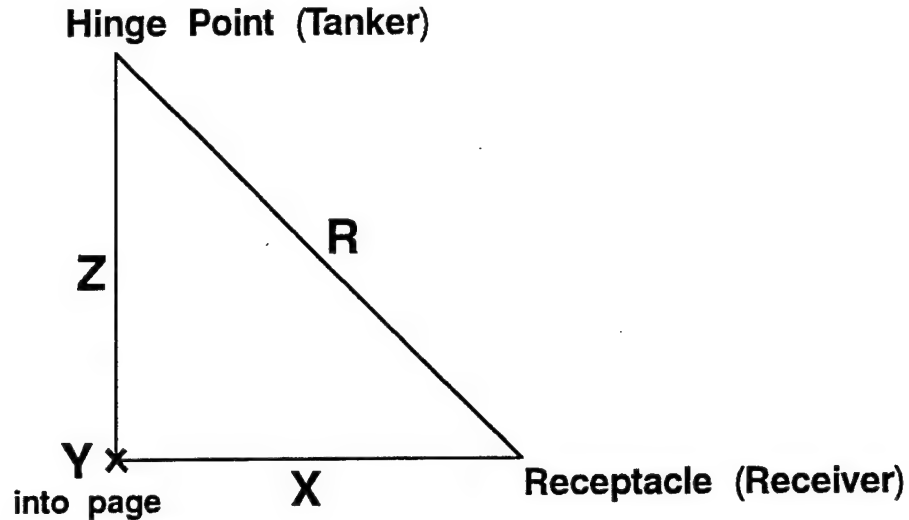


Fig. VI.2 QFT controller with output external disturbance.

problem. The receiver maintains the total obligation of regulating its position. The tanker is free to change course, altitude, and velocity while the receiver compensates for these changes and maintains relative position. Equations are developed that identify perturbations from the set position. These perturbations are viewed as disturbances by the receiver. The perturbations are caused by wind gusts and disturbances due to refueling. Other, unmodeled, disturbances may include the tanker changing course. The control problem's goal is to minimize the perturbations to be within a specified volume of space where the refueling boom can operate. Normal boom operating position and length defines this volume.

The KC-135 tanker refueling boom has the following operational constraints: (1) nominal boom operation position is 30 degrees down from horizontal, (2) the boom can move as much as four degrees up and down from normal position and continue delivering fuel, (3) it can move as much as ten degrees up and down from normal position and maintain its connection to the receiver, but cannot deliver fuel, (4) horizontal movement is limited to 10 degrees left and right while maintaining fuel flow, (5) the disconnect limit horizontally is 15 degrees left and right, (6) nominal boom length is 477.5 inches (39.8 ft), (7) it can expand or constrict 13.5 inches and maintain refueling, (8) it can expand or constrict as much as 73.5 inches and maintain contact but not refueling<sup>75</sup>. These dimensions provide a maximum perturbation from nominal boom position of approximately 2.85 feet up or down, 7 feet left or right, in order to maintain fuel flow. In order to maintain connection, the maximum perturbation can be 7.5 feet up or down, and 11.5 feet left or right.



**Fig. VI.3 Control problem geometry.**

Using the tanker as the point of reference, the relationship in Fig. VI.3 can be used to develop the equations required to define the regulation control problem.  $R$  is the nominal boom length measured from the boom hinge point on the tanker.  $Z$  is the vertical distance between the boom hinge point and receiver aircraft's refueling receptacle.  $X$  is the horizontal distance between these same points.  $Y$  measures the distance between the center line of the boom hinge point and receiver receptacle.

The following equations are derived

$$R^2 = X^2 + Y^2 + Z^2 \quad (\text{VI.7})$$

where

$$\begin{aligned} R &= \bar{R} + r \\ X &= \bar{X} + x \\ Y &= \bar{Y} + y \\ Z &= \bar{Z} + z \end{aligned} \quad (\text{VI.8})$$

which are the sums of the nominal positions (overbar terms) and perturbations (lower case terms). Substituting Eq. (VI.8) into Eq. (VI.7) and squaring the terms, yields

$$\bar{R}^2 + 2r\bar{R} + r^2 = \bar{X}^2 + 2x\bar{X} + x^2 + \bar{Y}^2 + 2y\bar{Y} + y^2 + \bar{Z}^2 + 2z\bar{Z} + z^2 \quad (\text{VI.9})$$



Since  $r, x, y, z \ll \bar{R}, \bar{X}, \bar{Y}, \bar{Z}$  respectively, Eq. (VI.9) is approximated as

$$\bar{R}^2 + 2r\bar{R} = \bar{X}^2 + 2x\bar{X} + \bar{Y}^2 + 2y\bar{Y} + \bar{Z}^2 + 2z\bar{Z} \quad (\text{VI.10})$$

Taking the derivative with respect to time where the overbar terms are constant yields

$$\bar{R} \frac{dr}{dt} = \bar{X} \frac{dx}{dt} + \bar{Y} \frac{dy}{dt} + \bar{Z} \frac{dz}{dt} \quad (\text{VI.11})$$

Integrating, rearranging, and setting  $r = 0$  yields:

$$r = \frac{\bar{X}}{\bar{R}}x + \frac{\bar{Y}}{\bar{R}}y + \frac{\bar{Z}}{\bar{R}}z = 0 \quad (\text{VI.12})$$

defining

$$\begin{aligned} x &= x_T - x_R \\ y &= y_T - y_R \\ z &= z_T - z_R \end{aligned} \quad \begin{array}{l} \text{T - Tanker} \\ \text{R - Receiver} \end{array} \quad (\text{VI.13})$$

Thus,  $r = 0$  if and only if,  $x = y = z = 0$ . Therefore, the control problem is to design the compensator  $G$  of Fig. VI.4 that will satisfy Eqs. (VI.12) and (VI.13).

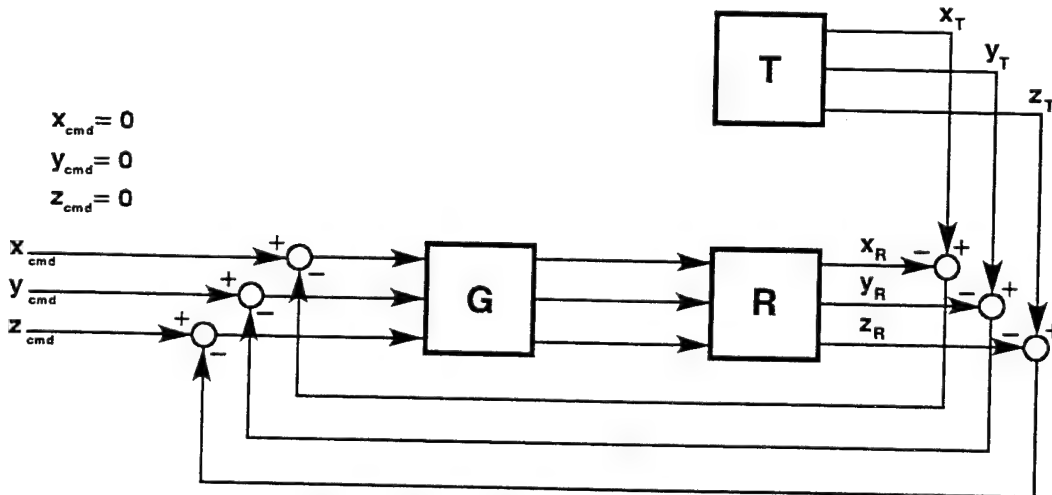


Fig. VI.4 Control problem.

## VI.5 MIMO QFT with External Output Disturbance

Output disturbance rejection is the primary design criterion in this chapter. Previous discussions of MIMO QFT did not consider external disturbance in the calculation of disturbance rejection bounds. Therefore, equations including the external disturbance are developed in this chapter. The following development quantifies external uncertain disturbances. Figure VI.2 represents an  $m \times m$  MIMO closed-loop system in which  $F(s)$ ,  $G(s)$ ,  $P(s)$ , and  $P_d(s)$  are  $m \times m$  matrices.  $\mathcal{P}(s) = \{P(s)\}$  and  $\mathcal{P}_d(s) = \{P_d(s)\}$  are sets of matrices due to plant and disturbance uncertainties respectively. The objective is to find a suitable mapping that permits the analysis and synthesis of a MIMO control system by a set of equivalent MISO control systems.

From Fig. VI.2, the following equations are written

$$\mathbf{y} = \mathbf{P}(s)\mathbf{u} + \mathbf{P}_d(s)\mathbf{d}_{\text{ext}} \quad \mathbf{u} = \mathbf{G}(s)\mathbf{v} \quad \mathbf{v} = \mathbf{r} - \mathbf{y} \quad (\text{VI.14})$$

For the regulator case with zero tracking input

$$\mathbf{r} = [0, 0, 0]^T \quad (\text{VI.15})$$

From Eqs. (VI.14) and (VI.15,) where henceforth the  $(s)$  is dropped in the continuing development,

$$\mathbf{v} = -\mathbf{y} \quad \mathbf{u} = -\mathbf{G}\mathbf{y} \quad (\text{VI.16})$$

which yields

$$\mathbf{y} = -\mathbf{P}\mathbf{G}\mathbf{y} + \mathbf{P}_d\mathbf{d}_{\text{ext}} \quad (\text{VI.17})$$

Equation (VI.17) is rearranged to yield:

$$\mathbf{y} = [\mathbf{I} + \mathbf{PG}]^{-1} \mathbf{P}_d \mathbf{d}_{\text{ext}} \quad (\text{VI.18})$$

Based upon unit impulse disturbance inputs for  $\mathbf{d}_{\text{ext}}$ , the system control ratio relating  $\mathbf{d}_{\text{ext}}$  to  $\mathbf{y}$  is

$$\mathbf{T}_d = [\mathbf{I} + \mathbf{PG}]^{-1} \mathbf{P}_d \quad (\text{VI.19})$$

Premultiply Eq. (VI.19) by  $[\mathbf{I} + \mathbf{PG}]$  yields

$$[\mathbf{I} + \mathbf{PG}] \mathbf{T}_d = \mathbf{P}_d \quad (\text{VI.20})$$

Premultiplying both sides of Eq. (VI.20) by  $\mathbf{P}^{-1}$  results in

$$[\mathbf{P}^{-1} + \mathbf{G}] \mathbf{T}_d = \mathbf{P}^{-1} \mathbf{P}_d \quad (\text{VI.21})$$

Let

$$\mathbf{P}^{-1} = \begin{bmatrix} p_{11}^* & p_{12}^* & \cdots & p_{1m}^* \\ p_{21}^* & p_{22}^* & \cdots & p_{2m}^* \\ \vdots & \vdots & & \vdots \\ p_{m1}^* & p_{m2}^* & \cdots & p_{mm}^* \end{bmatrix} \quad (\text{VI.22})$$

The  $m^2$  effective plant transfer functions are formed as

$$q_{ij} \equiv \frac{1}{p_{ij}^*} = \frac{\det \mathbf{P}}{\text{adj } \mathbf{P}_{ij}} \quad (\text{VI.23})$$

the  $\mathbf{Q}$  matrix is then formed as

$$\mathbf{Q} = \begin{bmatrix} q_{11} & q_{12} & \dots & q_{1m} \\ q_{21} & q_{22} & \dots & q_{2m} \\ \vdots & \vdots & & \vdots \\ q_{m1} & q_{m2} & \dots & q_{mn} \end{bmatrix} = \begin{bmatrix} 1/p_{11}^* & 1/p_{12}^* & \dots & 1/p_{1m}^* \\ 1/p_{21}^* & 1/p_{22}^* & \dots & 1/p_{2m}^* \\ \vdots & \vdots & & \vdots \\ 1/p_{m1}^* & 1/p_{m2}^* & \dots & 1/p_{mn}^* \end{bmatrix} \quad (\text{VI.24})$$

where  $\mathbf{P} = [p_{ij}]$ ,  $\mathbf{P}^{-1} = [p_{ij}^*] = [1/q_{ij}]$ , and  $\mathbf{Q} = [q_{ij}] = [1/p_{ij}^*]$ . Partition the  $\mathbf{P}^{-1}$  matrix as follows:

$$\mathbf{P}^{-1} = [p_{ij}^*] = [1/q_{ij}] = \mathbf{A} + \mathbf{B} \quad (\text{VI.25})$$

where  $\mathbf{A}$  is the diagonal part of  $\mathbf{P}^{-1}$  and  $\mathbf{B}$  is the balance of  $\mathbf{P}^{-1}$ . Thus  $\lambda_{ii} = 1/q_{ii} = p_{ii}^*$ ,  $b_{ii} = 0$ , and  $b_{ij} = 1/q_{ij} = p_{ij}^*$  for  $i \neq j$ . Substituting Eq. (VI.25) into Eq. (VI.21) with  $\mathbf{G}$  diagonal, results in

$$[\mathbf{A} + \mathbf{B} + \mathbf{G}] \mathbf{T}_d = [\mathbf{A} + \mathbf{B}] \mathbf{P}_d \quad (\text{VI.26})$$

Rearranging Eq. (VI.26) produces

$$\mathbf{T}_d = [\mathbf{A} + \mathbf{G}]^{-1} [\mathbf{A} \mathbf{P}_d + \mathbf{B} \mathbf{P}_d - \mathbf{B} \mathbf{T}_d] = \{\mathbf{t}_{d_i}\} \quad (\text{VI.27})$$

This equation defines the desired fixed point mapping, where each of the  $m^2$  matrix elements on the right side of Eq. (VI.27) are interpreted as MISO problems. Proof of the fact that the design of each MISO system yields a satisfactory MIMO design is based on the Schauder fixed point theorem<sup>21</sup>.

The theorem defines a mapping  $\mathbf{Y}(\mathbf{T}_d)$

$$\mathbf{Y}(\mathbf{T}_d) = [\mathbf{A} + \mathbf{G}]^{-1} [\mathbf{A} \mathbf{P}_d + \mathbf{B} \mathbf{P}_d - \mathbf{B} \mathbf{T}_d] \quad (\text{VI.28})$$

where each member of  $\mathbf{T}_d$  is from the acceptable set  $\mathfrak{F}_d$ . If this mapping has a fixed point, i.e.,

$\mathbf{T}_d \in \mathfrak{F}_d$ , then this  $\mathbf{T}_d$  is a solution of Eq. (VI.27).

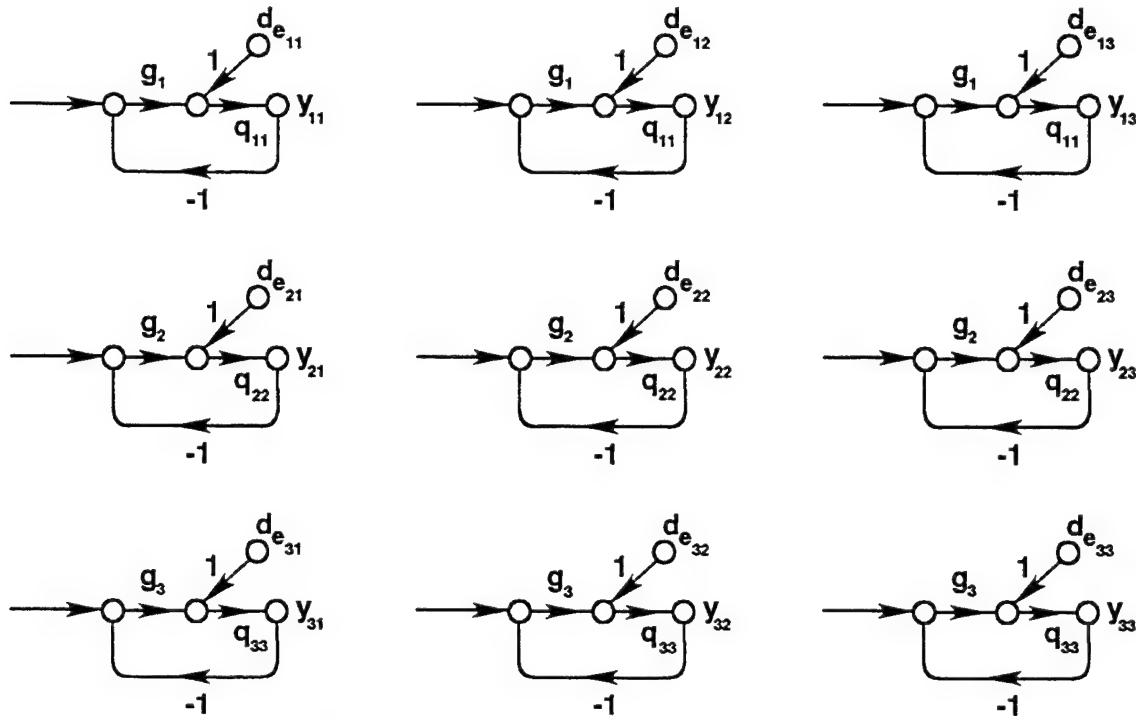


**Fig. VI.5 3x3 MISO Equivalent Loops for External Output Disturbance ( $r = 0$ ).**

Figure VI.5 shows the effective MISO loops resulting from a 3x3 system. Since  $\Lambda$  and  $G$  in Eq. (VI.27) are diagonal, the (1,1) element on the right side of Eq. (VI.28) for the 3x3 case, for a unit impulse input, provides the output

$$Y_{d_{11}} = \frac{q_{11}}{1 + g_1 q_{11}} \left[ \frac{p_{d_{11}}}{q_{11}} + \frac{p_{d_{21}}}{q_{12}} + \frac{p_{d_{31}}}{q_{13}} - \left[ \frac{t_{c_{21}}}{q_{12}} + \frac{t_{c_{31}}}{q_{13}} \right] \right] \quad (VI.29)$$

Equation (VI.29) corresponds precisely to the first structure in Fig. VI.5. Similarly, each of the nine structures in this figure corresponds to one of the elements of  $Y(T_d)$  of Eq. (VI.28). The control ratios for the external disturbance inputs  $d_{ex_i}$  and the corresponding outputs  $y_i$  for each feedback loop of Eq. (VI.28) have the form

$$Y_{ii} = w_{ii} (d_{e_i}) \quad (\text{VI.30})$$

where  $w_{ii} = q_{ii}/(1 + g_i q_{ii})$  and

$$d_{e_i} = (d_{ext})_{ij} - c_{ij}$$

$$= \sum_{k=1}^x \frac{p_{d_{kj}}}{q_{ik}} - \sum_{k \neq i}^m \frac{t_{c_{kj}}}{q_{ik}} \quad \begin{array}{l} x = \text{number of disturbance inputs} \\ m = \text{dimension of square MIMO system} \end{array}$$

(VI.31)

Thus, Eq. (VI.31), the interaction term, not only contains the cross-coupling interaction but also the external disturbances, i.e.:

$$(d_{ext})_{ij} = \sum_{k=1}^x \frac{p_{d_{kj}}}{q_{ik}}$$

$$c_{ij} = \sum_{k \neq i}^m \frac{t_{c_{kj}}}{q_{ik}}$$

(VI.32)

where  $(d_{ext})_{ij}$  represents the external disturbance effects and  $c_{ij}$  represents the cross-coupling effects.

Additional equations, quantifying both the external disturbance  $(d_{ext})_{ij}$  and the internal cross-coupling effects  $c_{ij}$ , are derived to utilize the improved method QFT design technique. These equations are used to define the disturbance bounds for subsequent loops based on the completed design of a single loop. For this development, the equations for the case of a 2x2 MIMO system are presented.

From Eq. (VI.30) and for the 1-2 loop case, which is the output of loop 1 due to disturbance input 2, including the cross-coupling terms from loop 2, yields, for unit impulse inputs, the following control ratio:

$$t_{d_{12}} = y_{12} = w_{11} (d_{e_{12}}) = \frac{q_{11}}{1 + L_1} \left[ \frac{p_{d_{12}}}{q_{11}} + \frac{p_{d_{22}}}{q_{12}} - \frac{t_{d_{22}}}{q_{12}} \right] \quad (\text{VI.33})$$

Substituting in for  $t_{d_{22}}$

$$t_{d_{12}} = \frac{q_{11}}{1 + L_1} \left[ \frac{p_{d_{12}}}{q_{11}} + \frac{p_{d_{22}}}{q_{12}} - \frac{q_{22}d_{e_{22}}}{(1 + L_2)q_{12}} \right] \quad (\text{VI.34})$$

$$t_{d_{12}} = \frac{q_{11}}{1 + L_1} \left[ \frac{p_{d_{12}}(1 + L_2)q_{12} + p_{d_{22}}(1 + L_2)q_{11} - q_{22}q_{11}d_{e_{22}}}{(1 + L_2)q_{11}q_{12}} \right] \quad (\text{VI.35})$$

$$t_{d_{12}} = \frac{(1 + L_2)(p_{d_{12}}q_{12} + p_{d_{22}}q_{11}) - q_{22}q_{11} \left[ \frac{p_{d_{12}}}{q_{21}} + \frac{p_{d_{22}}}{q_{22}} - \frac{t_{d_{22}}}{q_{21}} \right]}{(1 + L_1)(1 + L_2)q_{12}} \quad (\text{VI.36})$$

rearranging, and substituting in for  $d_{e_{22}}$  yields

$$t_{d_{12}} = \frac{(1 + L_2)(p_{d_{12}}q_{12} + p_{d_{22}}q_{11}) - \frac{q_{22}q_{11}p_{d_{12}}}{q_{21}} - q_{11}p_{d_{22}} + \frac{q_{22}q_{11}t_{d_{22}}}{q_{21}}}{(1 + L_1)(1 + L_2)q_{12}} \quad (\text{VI.37})$$

$$t_{d_{12}} = \frac{(1 + L_2)(p_{d_{12}}q_{12} + p_{d_{22}}q_{11})q_{21} - q_{22}q_{11}p_{d_{12}} - q_{11}q_{21}p_{d_{22}} + q_{22}q_{11}t_{d_{22}}}{(1 + L_1)(1 + L_2)q_{12}q_{21}} \quad (\text{VI.38})$$

where  $\gamma_{12} = q_{11}q_{22}/q_{21}q_{12}$ . Solving for  $t_{d_2}$  yields

$$t_{d_2}((1 + L_1)(1 + L_2)) = \frac{(1 + L_2)(p_{d_2}q_{12} + p_{d_2}q_{11})}{q_{12}} - \frac{q_{11}p_{d_2}}{q_{12}} - \gamma_{12}p_{d_2} + \gamma_{12}t_{d_2} \quad (\text{VI.39})$$

$$t_{d_2}((1 + L_1)(1 + L_2) - \gamma_{12}) = (1 + L_2)\frac{q_{11}}{q_{12}}p_{d_2} + (1 + L_2)p_{d_2} - \frac{q_{11}}{q_{12}}p_{d_2} - \gamma_{12}p_{d_2} \quad (\text{VI.40})$$

$$t_{d_2} = \frac{L_2\frac{q_{11}}{q_{12}}p_{d_2} + (1 + L_2 - \gamma_{12})p_{d_2}}{L_1(1 + L_2) + 1 + L_2 - \gamma_{12}} \quad (\text{VI.41})$$

Equation (VI.41) is rearranged as follows:

$$t_{d_2} = \frac{\frac{L_2\frac{q_{11}}{q_{12}}p_{d_2}}{1 + L_2 - \gamma_{12}} + p_{d_2}}{1 + \frac{L_1(1 + L_2)}{1 + L_2 - \gamma_{12}}} \quad (\text{VI.42})$$

From Eq. (VI.42) the effective plant is defined as:

$$q_{11_e} \equiv \frac{q_{11}(1 + L_2)}{1 + L_2 - \gamma_{12}} \quad (\text{VI.43})$$

Substituting Eq. (VI.43) into Eq. (VI.42), yields:

$$t_{d_2} = \frac{\frac{L_2p_{d_2}q_{11_e}}{q_{12}(1 + L_2)} + p_{d_2}}{1 + g_1q_{11_e}} \quad (\text{VI.44})$$

Thus, in general, for the 2x2 case, the improved method control ratio of the  $j^{\text{th}}$  interaction input to the  $i^{\text{th}}$  system output is



$$t_{d_v} = \frac{\frac{L_k p_{d_v} q_{ii}}{q_{ik}(1 + L_k)} + p_{d_v}}{1 + g_i q_{ii}} \quad \text{where } i = 1, 2 \text{ and } k \neq i \quad (\text{VI.45})$$

The interaction bounds (the optimal bounds for a pure regulator control system), representing the cross-coupling and the external disturbance effects, are calculated at a given frequency to satisfy

$$(B_{D_v})_{ij} \geq |t_{d_v}| = \left| \frac{\frac{L_k p_{d_v} q_{ii}}{q_{ik}(1 + L_k)} + p_{d_v}}{1 + g_i q_{ii}} \right| \quad \text{where } i = 1, 2 \text{ and } k \neq i \quad (\text{VI.46})$$

or

$$|1 + g_i q_{ii}| \geq \frac{1}{(B_{D_v})_{ij}} \left| \frac{L_k p_{d_v} q_{ii}}{q_{ik}(1 + L_k)} + p_{d_v} \right| \quad \text{where } i = 1, 2 \text{ and } k \neq i \quad (\text{VI.47})$$

The improved QFT method uses these equations to reduce the overdesign inherent in the original design process. The order in which loops are designed is important. Any order can be used, but some orders produce less overdesign (less bandwidth) than others. The last loop designed has the least amount of overdesign, therefore the most constrained loop is done first by the original method. Then the design is continued through the remaining loop by the second method. The first loop is then redesigned using the improved method.

At this point it is important to point out that when the interaction term specification is considered, the designer must decide how much is to be allocated for the cross-coupling effects and how much for the external disturbance effects. In other words, the designer can "tune" the external disturbance rejection specification depending on the nature of the interaction term for a particular loop. For example, if one loop is only affected by external disturbance, the interaction term specification would consider external disturbance effects only. But if the loop interaction term is a mix of cross-coupling and external disturbance, the designer must then "tune" the interaction term specification accordingly. Since each loop may not exhibit the same interaction characteristics, interaction term specification

tuning provides flexibility in the QFT design process .

## **VI.6 AFCS Design**

This section applies the QFT design technique to a real-world problem. The intent of this chapter is to present to the reader a design problem, with as much details as space permits, from the onset of the specification of the control problem to the verification of the design results by means of a linear and nonlinear simulations.

### **VI.6.1 Introduction**

The details for the QFT AFCS design are now presented. First the disturbance rejection specification is identified. Next, design of the loop transmissions for all three channels is described. Previous chapters provide the detailed step-by-step guide for the QFT design process.

### **VI.6.2 Disturbance Rejection Specification**

The primary goal in designing the AFCS system is to regulate the position of the aircraft receiving fuel relative to the tanker. As discussed in Sec. VI.5, any deviation from the nominal set position is considered a disturbance. Hence a disturbance rejection specification is determined based on modeled disturbance inputs and the basic QFT design pretense of unit impulse inputs. Since the most severe disturbance is due to wind, the disturbance specification is "tuned" to the wind input of 10 ft/sec. A maximum deviation from the nominal set position of 2 feet in any direction is specified which will confine the receiving aircraft to a volume that permits continued fuel delivery. Therefore the following disturbance specification is derived. Given an impulse input of magnitude 10 feet/sec, the system response will deviate no more than 2 ft. Additionally, the system will attenuate to half the maximum deviation in less than 1 second. Equation (VI.48) identifies the transfer function for the disturbance rejection specification, and Fig. VI.6 shows the disturbance rejection model response to an 10 ft/sec impulse input.

$$\text{Disturbance rejection model} = \frac{400s}{(s + 1)(s + 5)^3} \quad (\text{VI.48})$$

An analysis of the Lm plot of the disturbance rejection specification which is superimposed over the Lm  $P(s)$  MISO loop plots (see Fig. VI.7) reveals<sup>77</sup> that MISO loops  $\{2,1\}$ ,  $\{3,1\}$ ,  $\{3,2\}$ ,  $\{1,3\}$ , and  $\{2,3\}$  are below the disturbance specification before compensation is applied.

### VI.6.3 Loop Shaping

The order of loop shaping is determined by the amount of cross coupling each MISO loop exerts on each other. Since channel 2 couples strongly into channel 1 it is designed first. The improved method is applied to utilize the known  $g_2$  to recalculate the disturbance bounds for channel 1. Channel 1 is then designed. Channel 3 is designed last since it is completely decoupled and thus a 1x1 SISO system.

The bandpass of the plants are relatively low, a benefit of the autopilot. In shaping the loops the overall system bandpass is designed to remain approximately equal to the plant bandpass. This requirement may require tradeoffs on meeting certain higher frequency bounds.

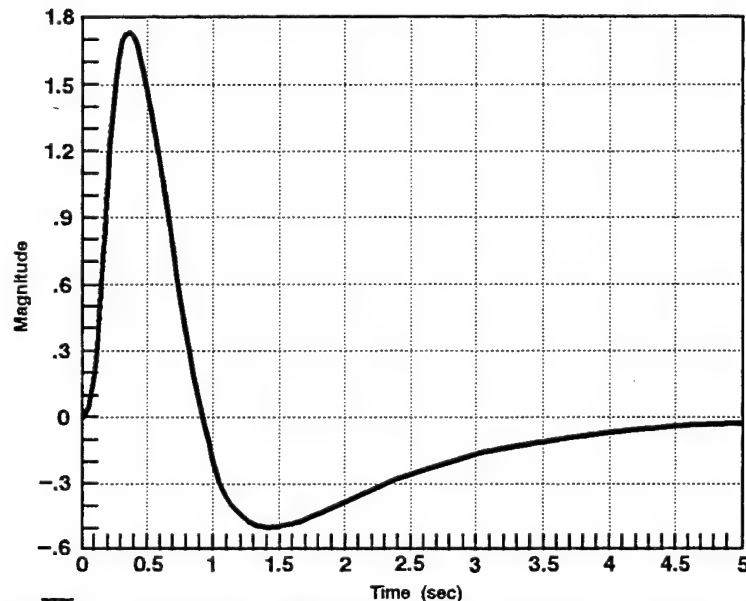


Fig. VI.6 Disturbance rejection model response to 10/sec impulse.

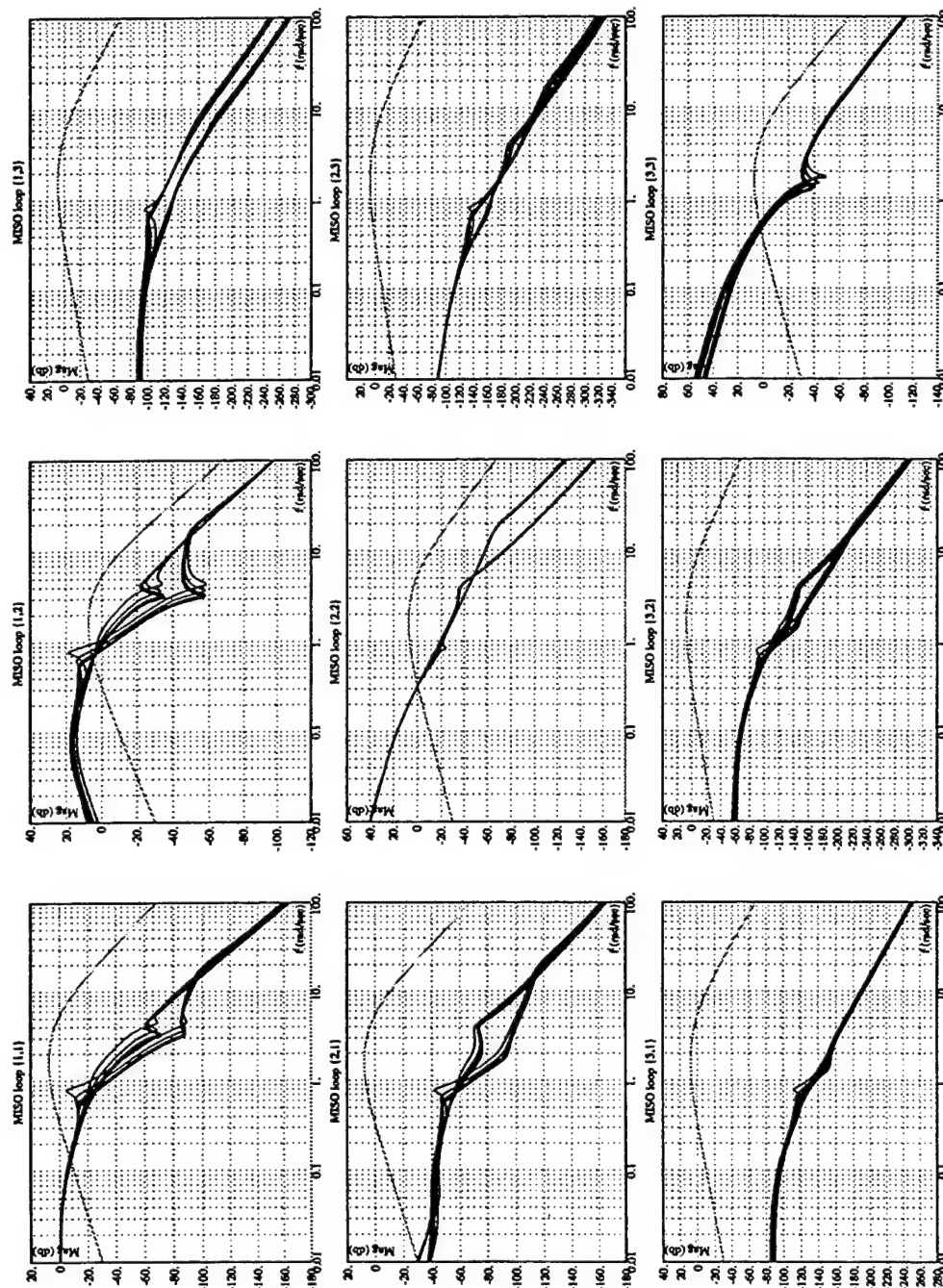


Fig. VI.7 P(s) Log magnitude plot.

#### VI.6.4 Channel 2 Loop Design

For channel 2 plant case 2 is chosen to be the nominal loop. Plant 2 is chosen because through initial design attempts it proved to be the most difficult to shape around the stability contour. A successful shaping of plant case 2 guarantees stability for all plant cases. Templates, stability and disturbance boundaries are calculated and composite bounds are formed in the MIMO QFT CAD

disturbance boundaries are calculated and composite bounds are formed in the MIMO QFT CAD Package. The channel 2 plants are 360 degrees out of phase between the plants derived from the aircraft plant with  $C_L = 0.2$  and  $C_L = 0.6$ . This is evident from the 360 degree wide templates and the stretching of the bounds over 360 degrees. The phase difference does not present a problem as the MIMO CAD Package is able to accommodate this scenario. Compensator  $g_2$  poles and zeros are added to shape the loop. Channel 2 is relatively easy to shape and proved to have the lowest order compensator,  $g_2$ .

As shown in Fig. VI.8, the channel 2 loop easily satisfies all QFT loop shaping requirements for composite bound and stability contours, guaranteeing a stable design satisfying the disturbance rejection specification. Fig. VI.9 shows the loop shapes on the NC for all 16 plants. From this figure the 360 degree phase difference in some plants is evident. Though there is a phase difference, each plant correctly goes around the stability contour indicating a stable design for all plant cases. The following compensator is designed for this channel:

$$g_2 = \frac{(s + 0.25)(s + 0.75)(s + 1.2)(s + 1.3)}{s(s + 0.98 \pm j1)(s + 10)(s + 20)(s + 120)}$$

(VI.49)

#### **VI.6.5 Channel 1 Loop Design**

After  $g_2$  is designed the improved method (Method 2) is applied using the equations derived in Sec. VI.5. Utilizing the known structure of  $g_2$  a more accurate calculation of the cross-coupled disturbance from the compensated channel 2 to the uncompensated channel 1 is achieved. The disturbance and hence the composite bounds are generated, based upon Eq. (VI.43). These have smaller magnitude compared to those obtained by Method 1, thus overdesign is reduced.

For the same reason as in channel 2, the nominal loop for channel 1 is given by plant case 2. Again, as in channel 2 the templates show a 360 degree phase difference between the two plant cases of  $C_L = 0.2$  and  $0.6$ . But unlike channel 2 there is a magnitude uncertainty evident in the channel 1 templates, see Appendix E in Reference 77. The magnitude uncertainty arises due to the strong

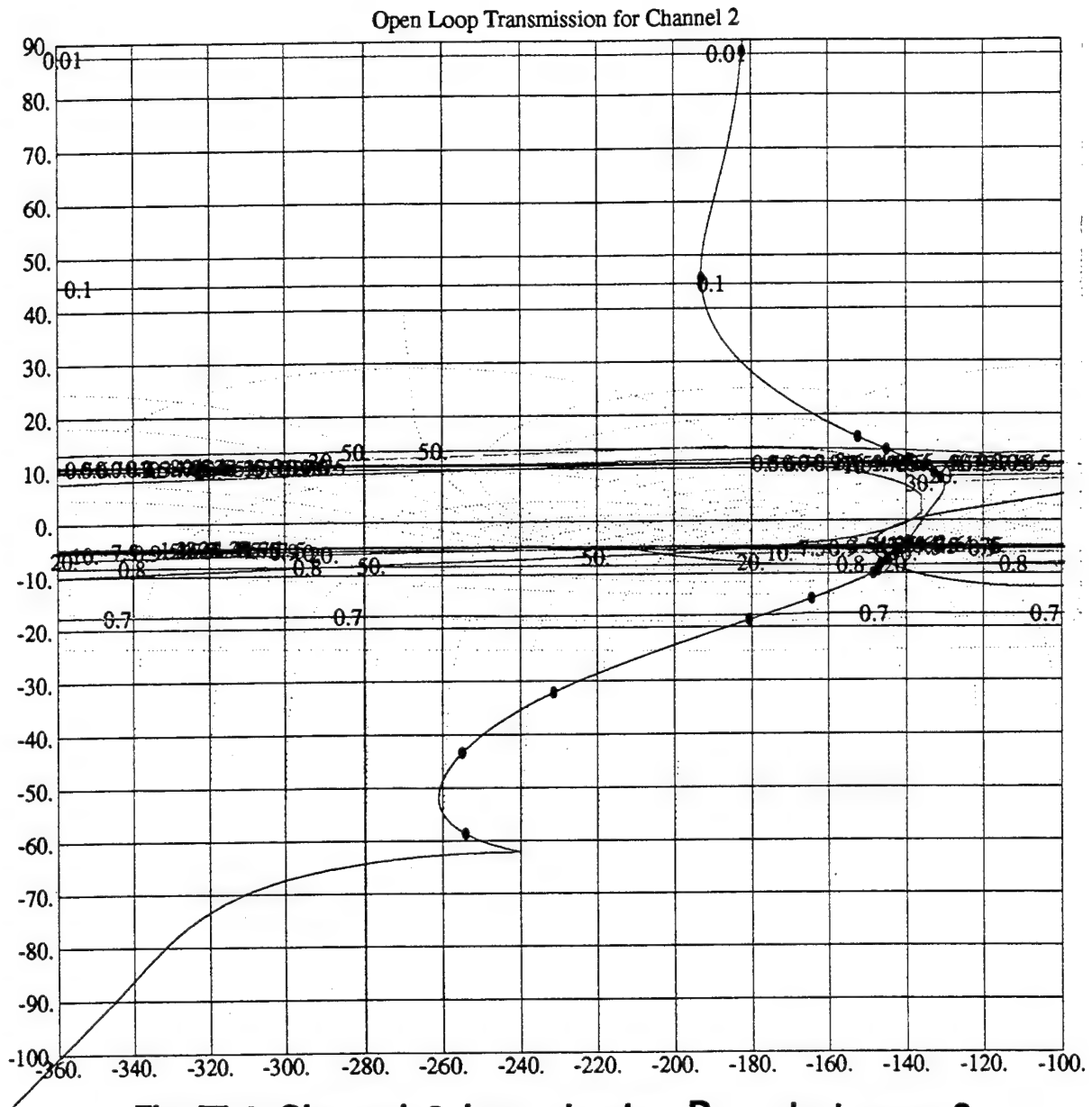


**Fig. VI.8 Channel 2 loop shaping  $P_o$  = plant case 2.**

coupling from channel 2 into channel 1, and also from the difference in the effect of wind disturbance between the 2 classes of aircraft plants based on  $C_L$ . The plants of  $C_L = 0.6$  have a larger wind induced disturbance as shown in Appendix D of Reference 77. Therefore these plants have not only more external disturbance, but also larger cross coupling disturbance.

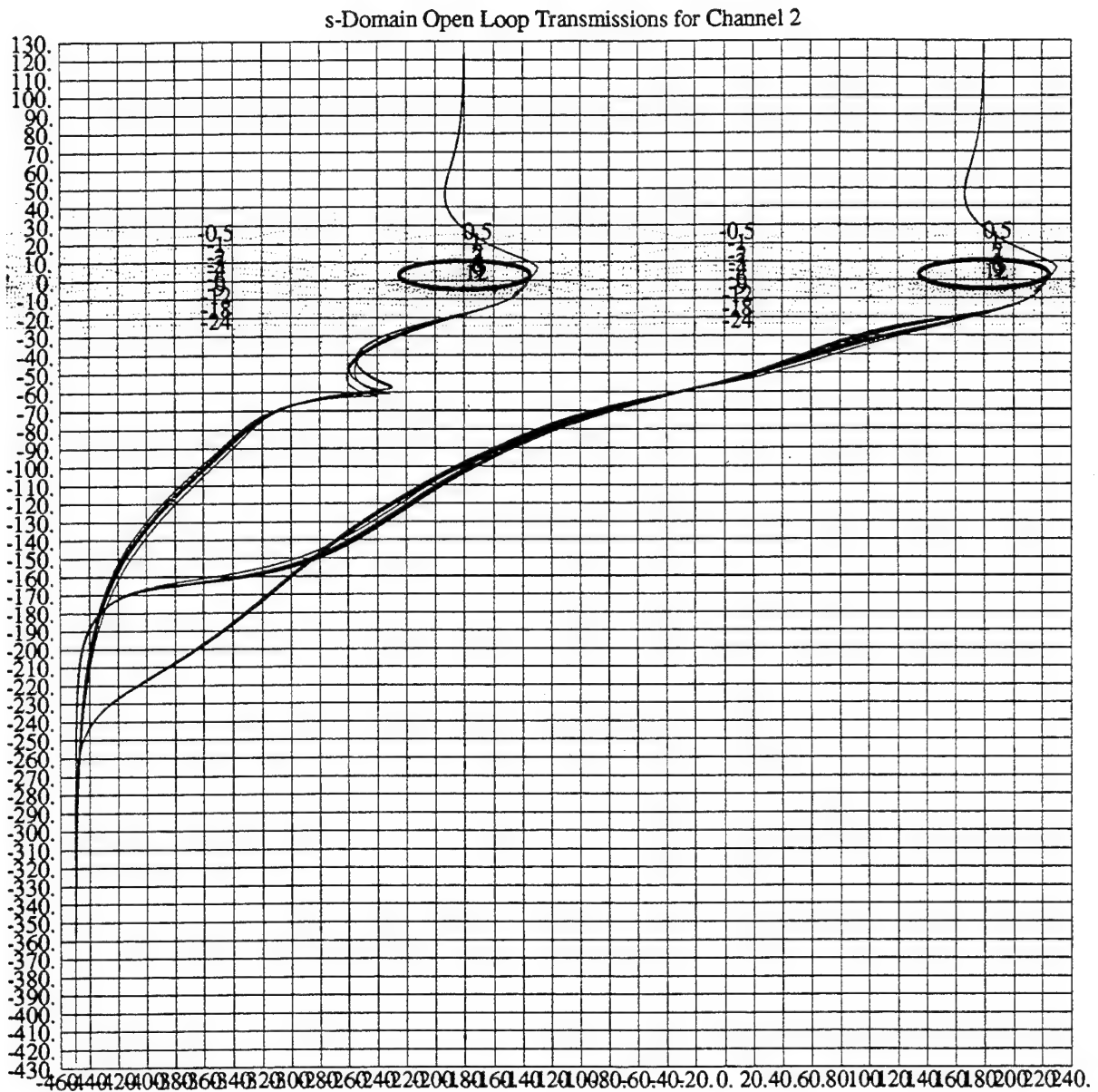


**Fig. VI.9 Channel 2 Nichols plot all plant cases.**

The loop shaping is more difficult for channel 1. The loop tends to curl at certain frequencies as shown in Fig. VI.10. The curling causes a large change in phase with little or no change in magnitude. This type of behavior makes it difficult to shape a loop that is stable, satisfies the composite bound criteria, and maintains a low system bandpass. The loop for channel 1 is shaped with a compromise

on the bandpass. A lag-lead compensator is used to "stretch" the low frequency curl. Additional lag-lead compensators are tried to further "stretch" the curl but caused the loop to increase in magnitude as the frequency increased. A loop shape is finally achieved that satisfies the lower frequency bounds, stability, and slightly increases the system bandpass. The channel 1 compensator,  $g_1$ , has a higher order than the channel 2 compensator. This is an indicator of the difficulties in achieving a loop shape that satisfies design criteria.

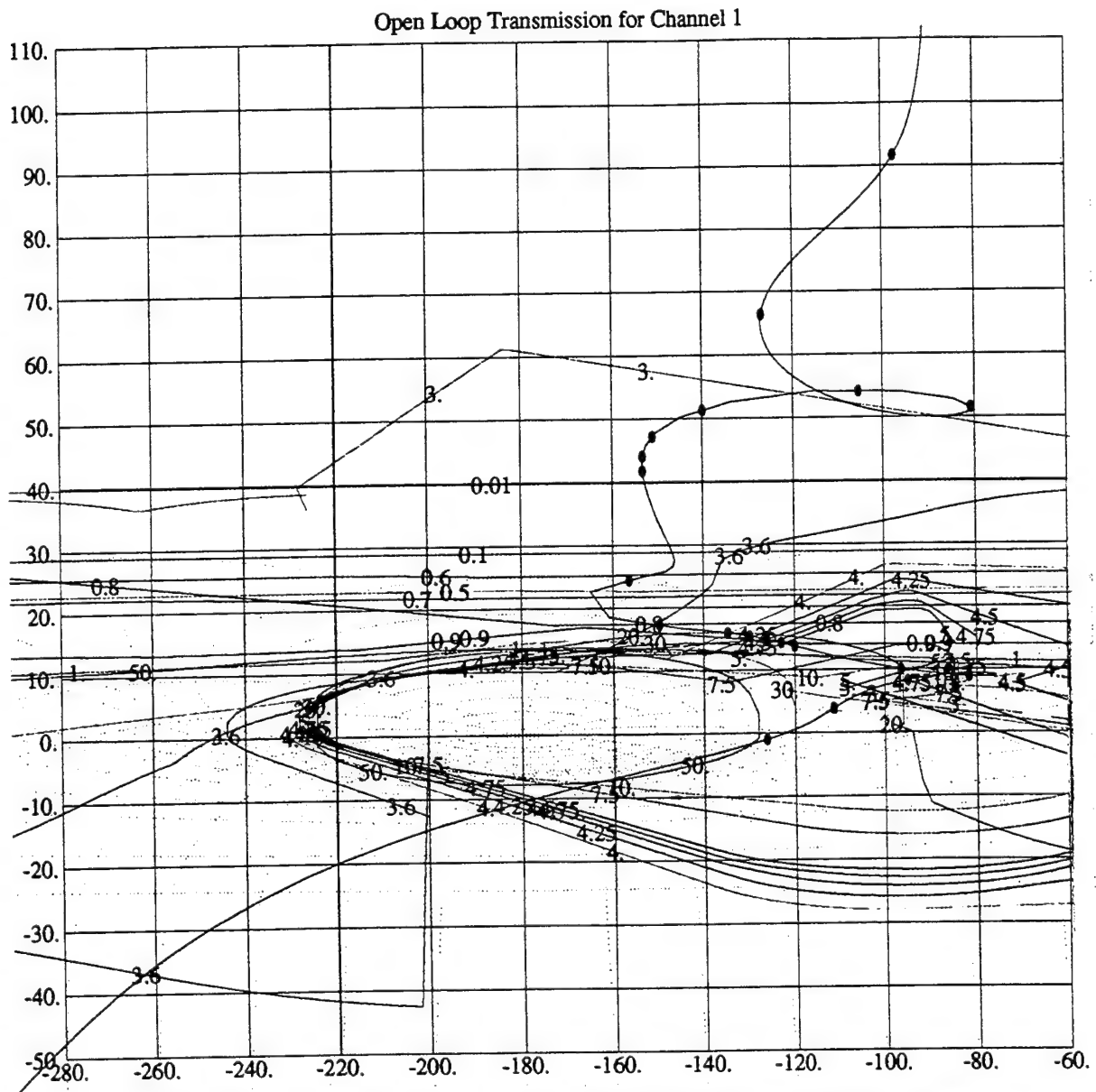


Fig. VI.10 Channel 1 loop shaping  $P_o$  = plant case 2.



The Nichols plot of all 16 plants in Fig. VI.11 shows the uncertainty in the low frequency range of the plants. Though there is large phase and magnitude differences between the plants the QFT method is able to achieve a design that satisfies stability and disturbance rejection for all plant cases. The following compensator is designed for channel 1:

$$g_1 = \frac{(s + 0.3)(s + 0.25 \pm j0.433)(s + 3)(s + 9)(s + 1.14 \pm j3.747)(s + 20)}{s(s + 2)(s + 0.32 \pm j3.184)(s + 90)(s + 135 \pm j65.38)(s + 1100)}$$

(VI.50)

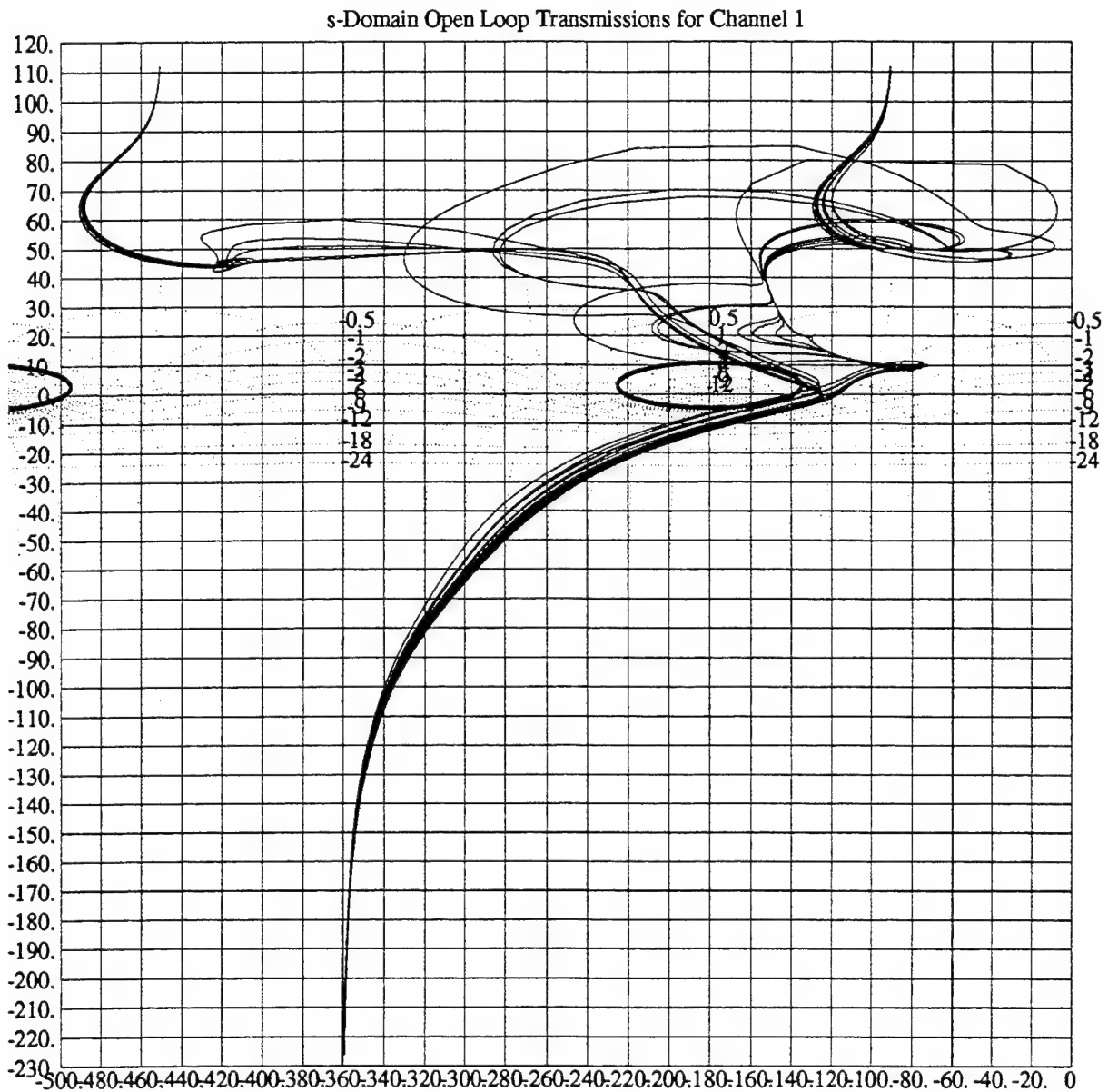


Fig. VI.11 Channel 1 Nichols plot all plant cases.

### VI.6.6 Channel 3 Loop Design

Channel 3 exhibits none of the channel 1 or channel 2 characteristics. The channel 3 templates have relatively small phase and magnitude uncertainty. There is no coupling from channels 1 or 2 into channel 3. The external disturbances have similar effects on channel 3 for all plant cases.

The lack of cross coupling disturbance and relatively certain external disturbance is evident in Fig. VI.12 where the bounds collapse around the stability contour. The channel 3 loop has a tendency to curl up as the frequency increases. The main difficulty is to add compensation to shape the loop around the bounds and stability contour at +180 degrees and then add further compensation to keep the loop from penetrating the stability region at -180 degrees. To achieve stability the very low frequency bounds are penetrated. This tradeoff is considered acceptable since channel 3, y position has the largest margin of disturbance allowed, 7.5 feet, as detailed in Sec. VI.4.

The Nichols plot of Fig. VI.13 shows a very tight grouping of all plant cases. Again, further evidence of relatively small uncertainty in channel 3. Notice the large change in phase with no decrease in magnitude. This is deemed acceptable since it occurs below the zero dB line at frequencies below the cutoff. The transfer function for the channel 3 compensator is:

$$g_3 = \frac{(s + 0.05)(s + 0.1)(s + 0.2)(s + 0.6)(s + 1.5 \pm j2.6)(s + 5)(s + 37.5)}{s(s + 0.00025)(s + 0.6 \pm j1.91)(s + 10)(s + 35 \pm j35.707)(s + 37.5)}$$

(VI.51)

### VI.6.7 Closed Loop Lm Plots

The overall equivalent MISO system closed loop Lm plots are shown in Fig. VI.14. From these plots you can easily see that disturbance rejection specification is met for all MISO loops except for as noted in the low frequency portion of the MISO loop {3,3}. The closed loop MISO plots of Fig. VI.14 are an excellent indicator of success in meeting the design specification.

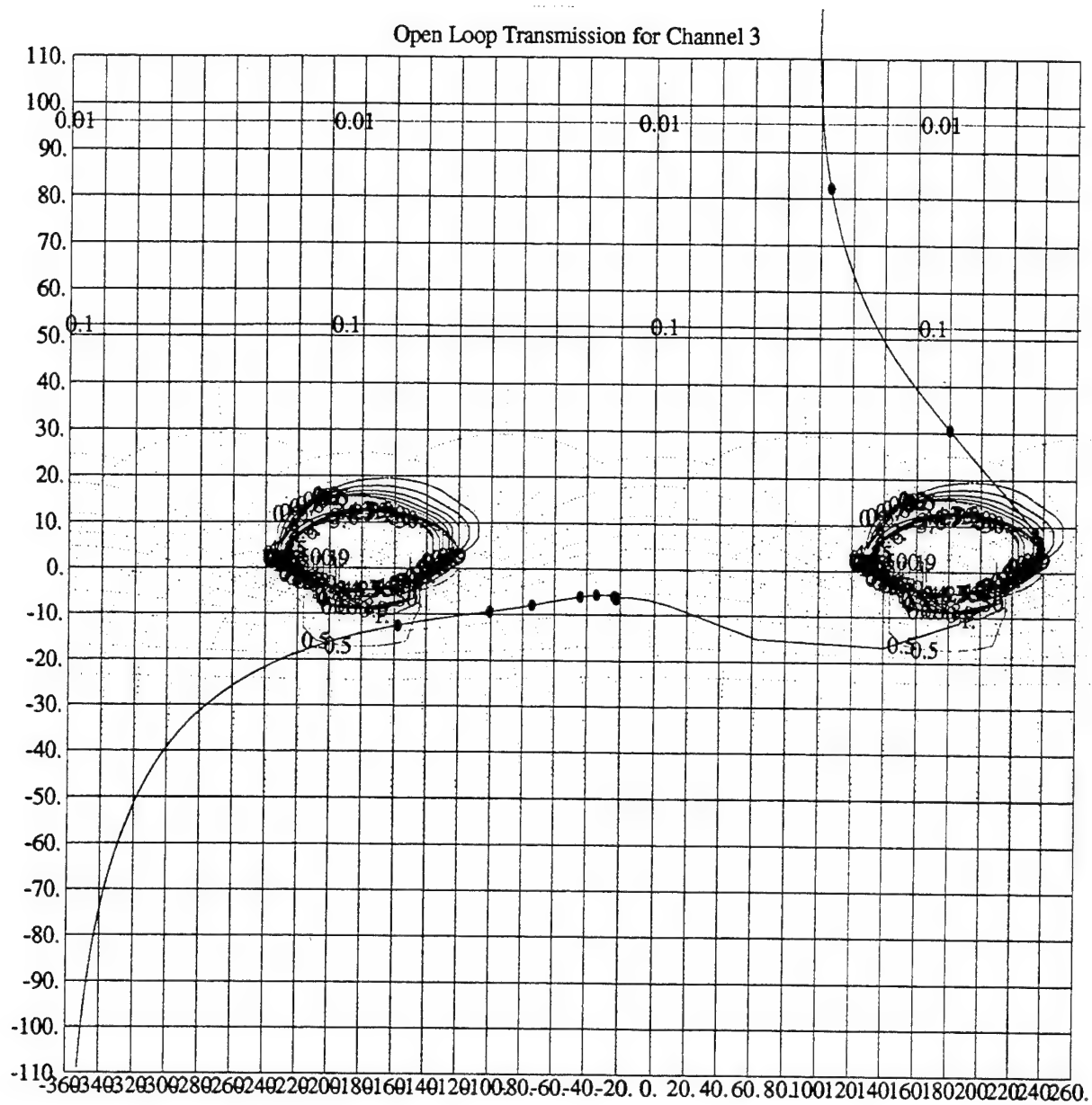


**Fig. VI.12 Channel 3 loop shaping  $P_o$  = plant case 2.**

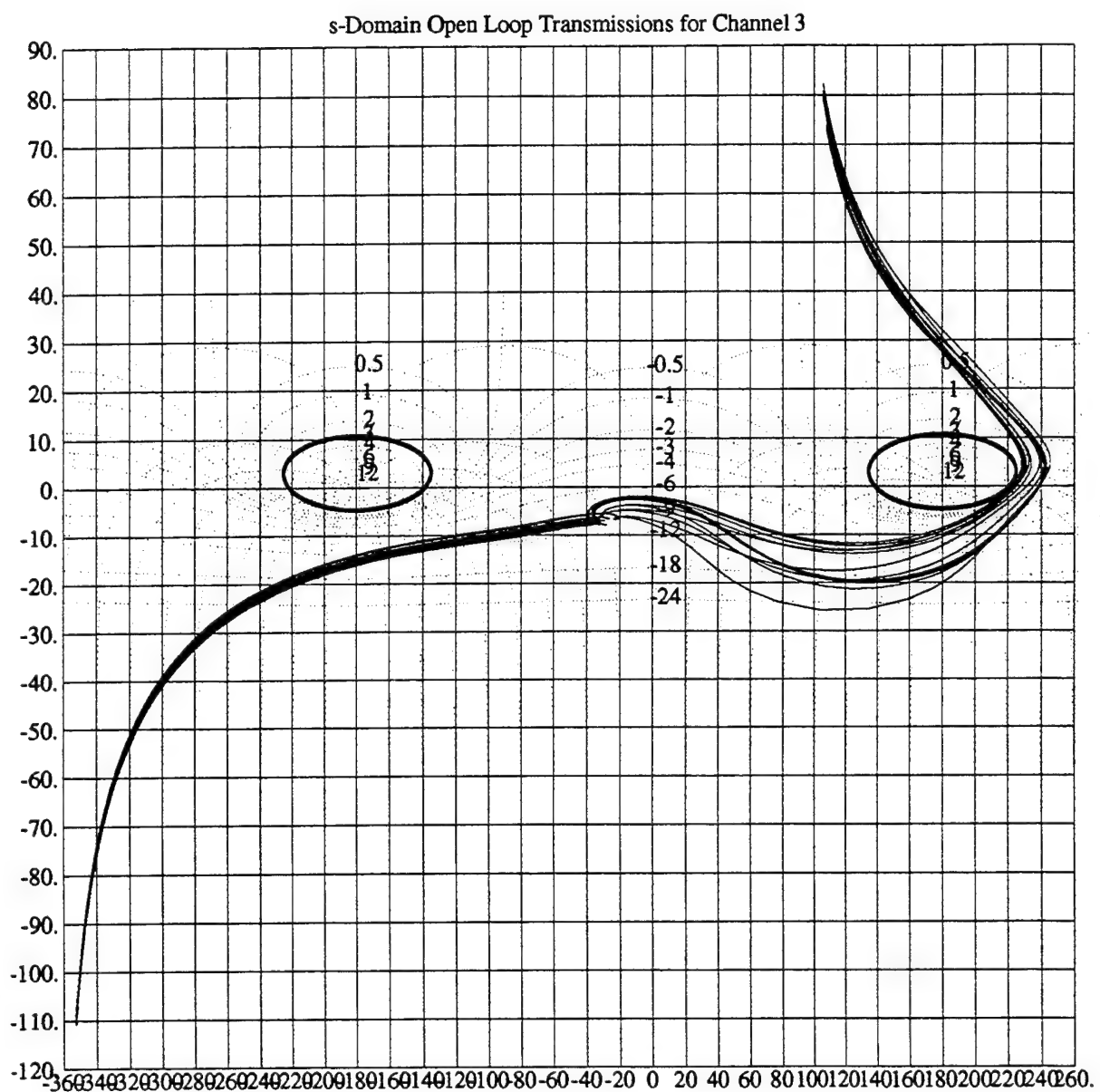


**Fig. VI.13 Channel 3 Nichols plot all plant cases.**

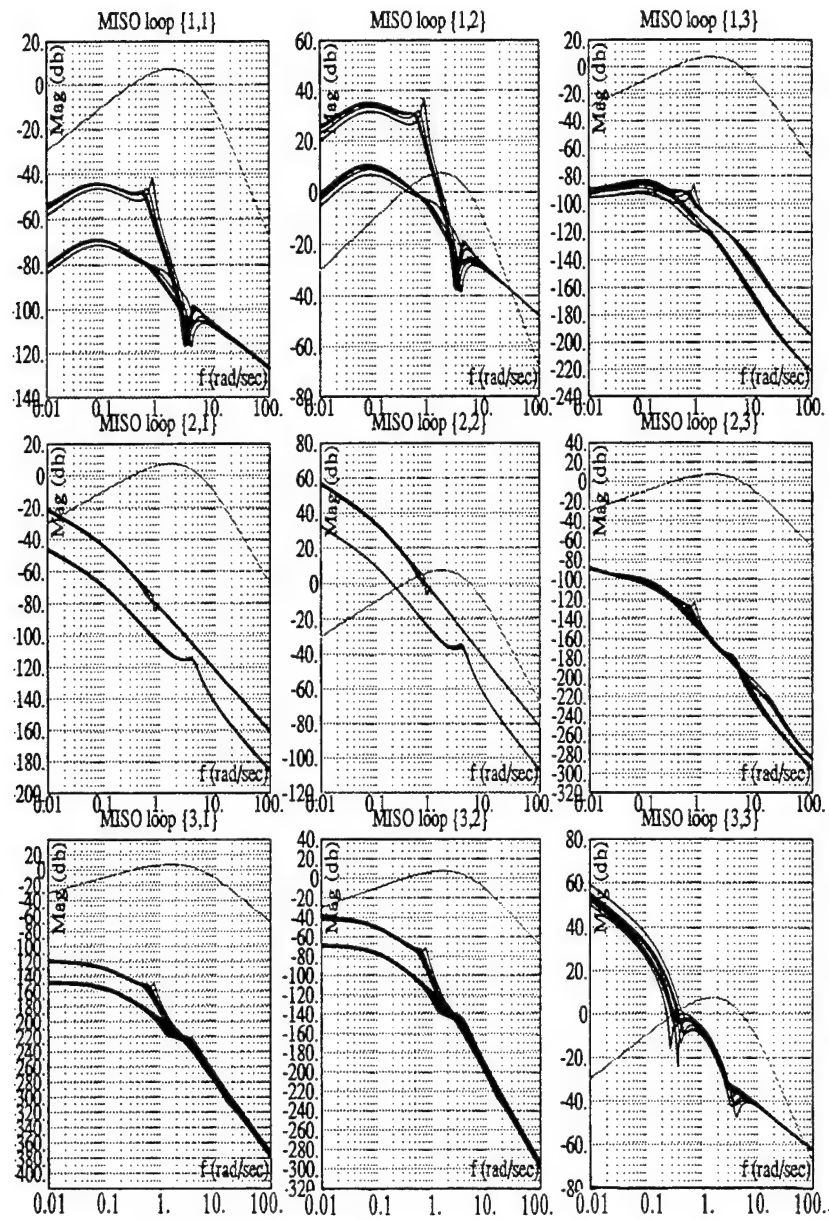


Fig. VI.14 MISO equivalent system  $L_m$  plots.

## VI.7 Air-to-Air Refueling Simulations

In this section the compensators designed in the previous sections are installed in the AFCS and simulations are run to analyze their performance. Linear simulations are run for all plant cases in MATRIX<sub>x</sub>. Nonlinear simulations are for two plant cases, one for each  $C_L = 0.2$  and  $0.6$ , are performed in EASY5x.

### VI.7.1 Linear Simulations

Linear simulation are performed in MATRIX<sub>x</sub> with the modeled external disturbances forcing the system to deflect from the set point. The simulations are executed in the presence of all external disturbances simultaneously. The results of the linear separation for channel 1 (Z separation) demonstrate excellent results with very little perturbation from the set point. Figure VI.15 presents the channel 1 response. The plots demonstrate two distinct responses corresponding to the aircraft lift coefficient  $C_L$ . The aircraft with  $C_L = 0.2$  show a maximum perturbation of approximately 0.0025 feet. Also the response dampens faster for the aircraft modeled with  $C_L = 0.2$ . The aircraft with  $C_L = 0.6$  deflected to a maximum value of approximately 0.008 feet with slower dampening.

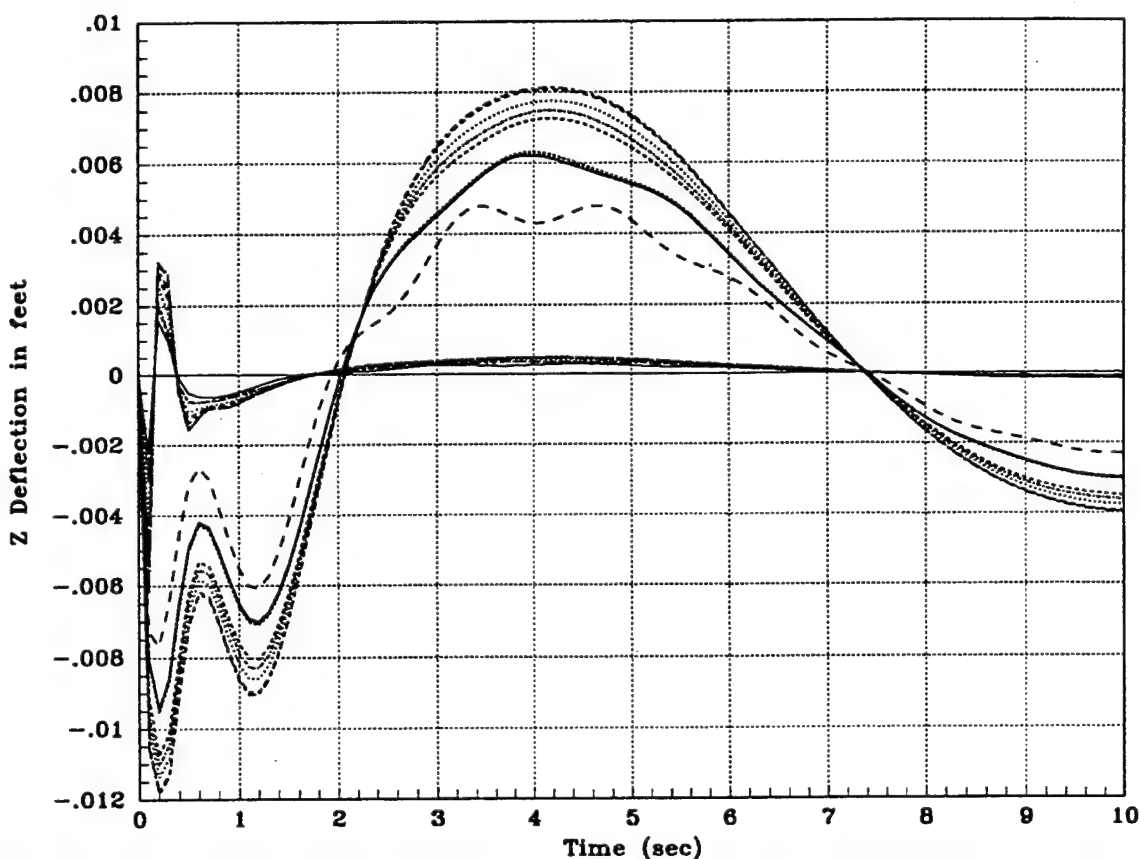


Fig. VI.15 Linear simulation - Z separation deflections all plant cases.

The channel 2 (X separation) linear simulation demonstrates similar characteristics for response based on  $C_L$ . Again, excellent rejection of external disturbance is achieved as shown in Fig. VI.16.  $C_L = 0.2$  aircraft have a maximum deflection of approximately 0.025 feet, while  $C_L = 0.6$  aircraft deflect approximately 0.425 feet from the set point. Recall that the aircraft with  $C_L = 0.6$  have a larger uncompensated perturbation due to external wind disturbance.

Channel 3 (Y separation) has the largest perturbation from the set point in the linear simulation, see Fig. VI.17. The maximum perturbation in channel 3 is approximately 1.9 feet. Though considerably larger than channels 1 and 2, the channel 3 perturbation remains within the design specification.

### VI.7.2 Nonlinear Simulations

The nonlinear simulation are performed in EASY5x. EASY5x has a Dryden wind gust model preprogrammed in the CAD package. The Dryden wind gust model is used in the nonlinear simulations

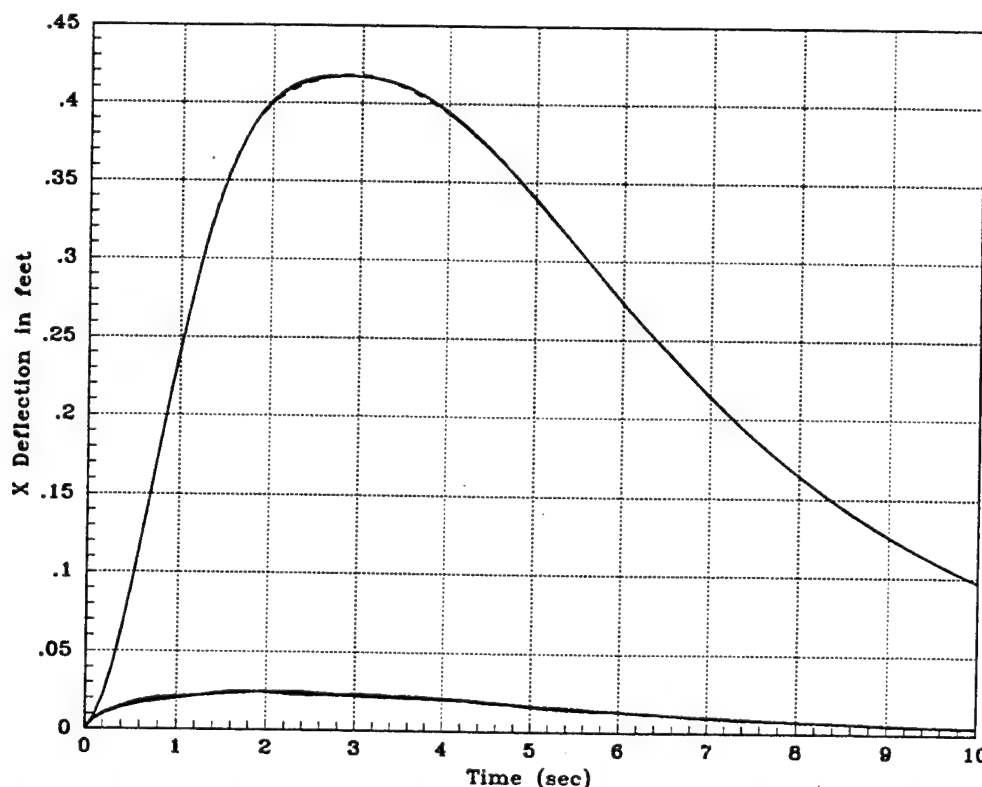
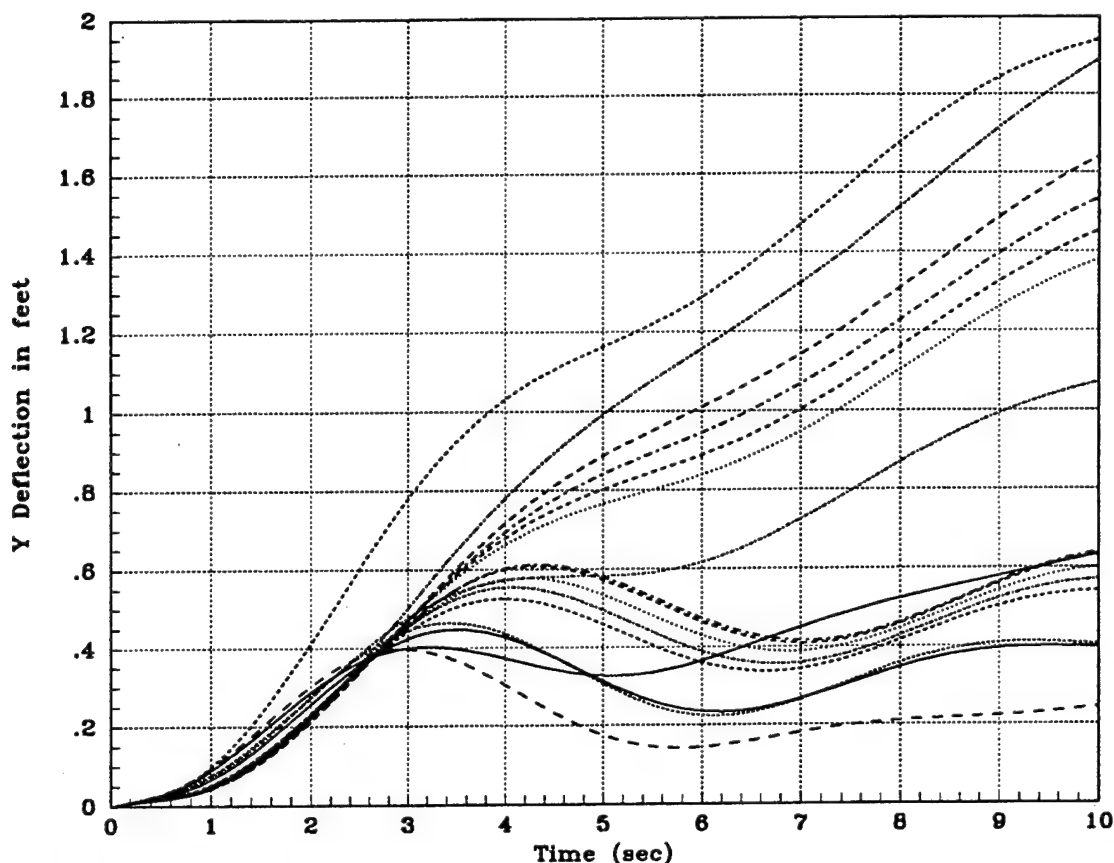


Fig. VI.16 Linear simulation - X position deflection all plant cases.



**Fig. VI.17 Linear simulation - Y position deflection all plant cases.**

versus the disturbance model developed in Secs. VI.2.2 and VI.4. Two nonlinear simulations are run. One representing an aircraft with  $C_L = 0.2$  and the second for  $C_L = 0.6$ . The nonlinear simulations require considerable time to setup and perform, therefore, time limitation prevented performing a nonlinear simulating for each plant case.

The nonlinear simulations demonstrate the same excellent results that are achieved in the linear simulation. The nonlinear results are consistent with the linear results, namely very small perturbations for channels 1 and 2, with a larger deflection in channel 3, are recorder as shown in Figs. VI.18 and VI.20. As in the linear simulations, the nonlinear simulations are within the design specifications.

Also presented in the nonlinear simulation plots, Figs. VI.19 and VI.21, are the control surface and thrust response of the autopilot. The aileron, rudder, and elevator responses are well within the physical capability of these devices. On the other hand the thrust requirements are probably beyond



thrust response of the autopilot. The aileron, rudder, and elevator responses are well within the physical capability of these devices. On the other hand the thrust requirements are probably beyond engine response capability. The engine response is most likely due to the autopilot design. The autopilot is a "text book" design and is not very sophisticated. A QFT design using the actual C-135B autopilot can probably achieve similar results without extreme engine response requirements.

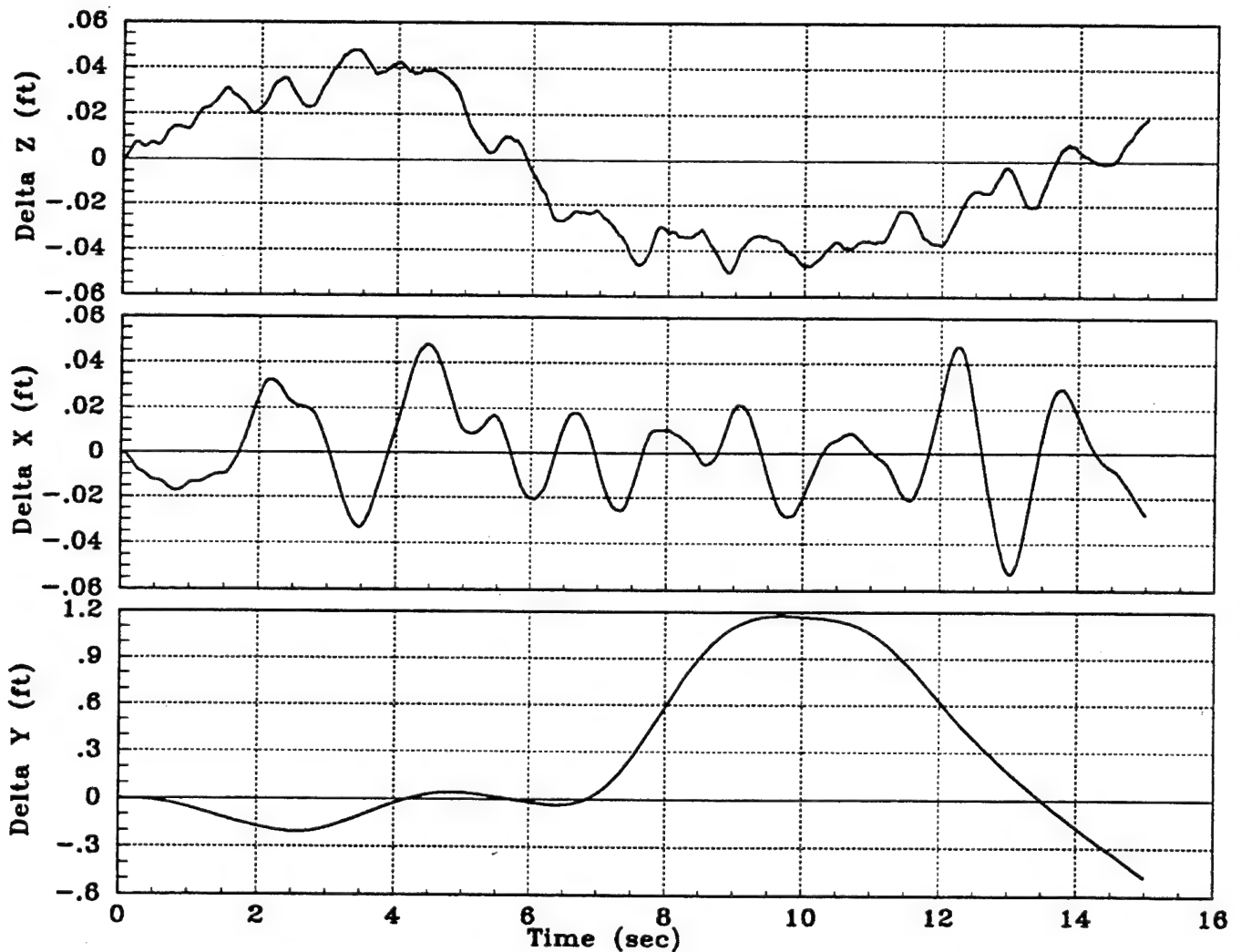


**Fig. VI.18 Nonlinear simulation - X, Y, Z position deflection, plant 1  $C_L = 0.2$ .**

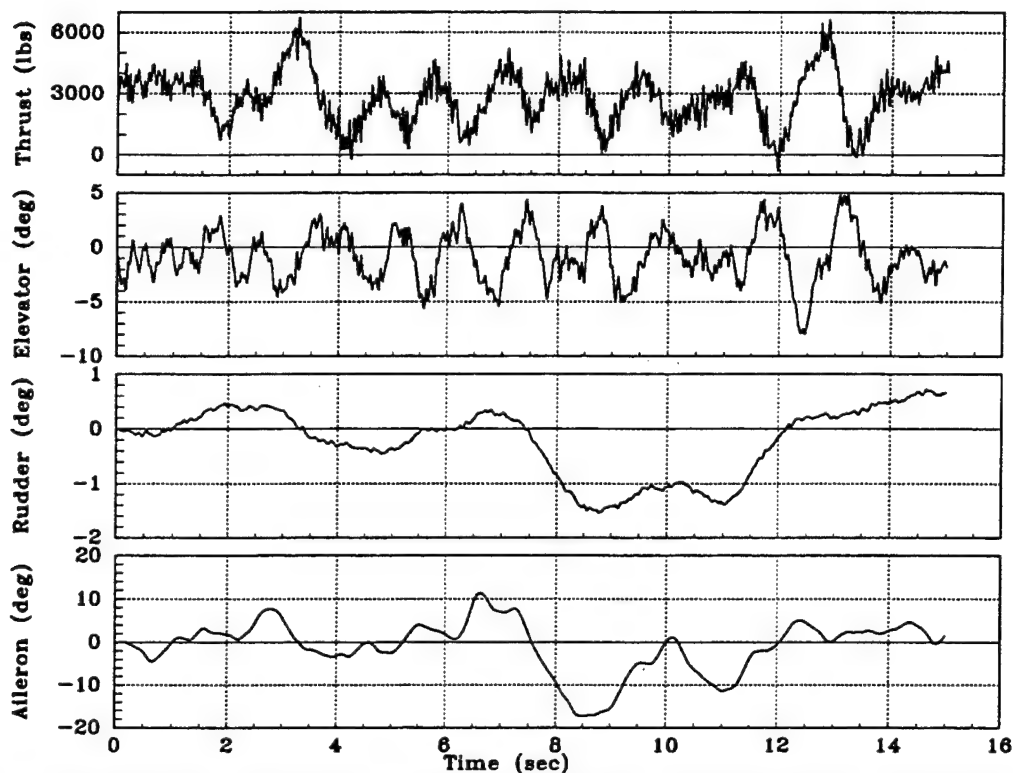


Fig. VI.19 Nonlinear simulation - control surface and throttle response, plant 1.

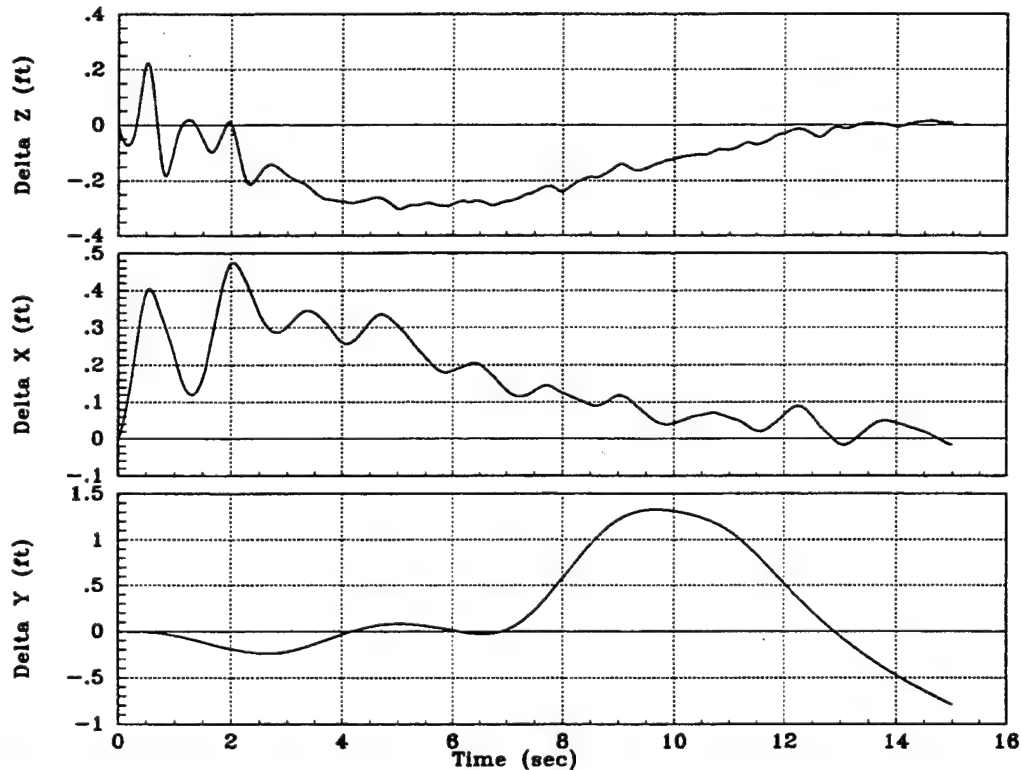
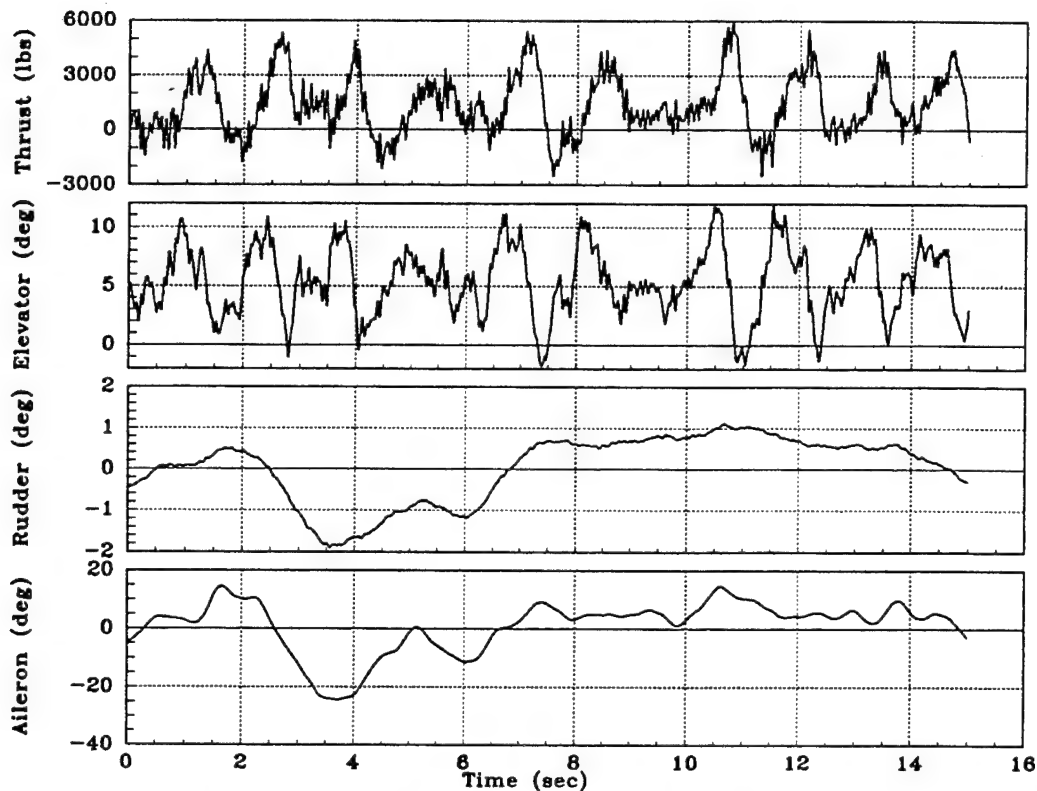


Fig. VI.20 Nonlinear simulation - X, Y, Z position deflection, plant 2  $C_L = 0.6$ .



**Fig. VI.21 Nonlinear simulation - control surface and throttle response, plant 2.**

## **VI.8 Summary**

This chapter presents the development of the improved QFT method to include the effects of external input disturbances on the system's outputs. Equations to calculate the new optimal bounds, which is the interaction bound for a pure regulator system for the improved method, are presented. This results of this development are applied to the design of a real-world problem: the AFCS. Each loop shaping is detailed, covering the particular difficulties in shaping the loops for each channel. Also the inherent nature of QFT's ability in handling large plant uncertainties is discussed. Finally the Lm of closed loop MISO system is shown, indicating a successful design given the tradeoffs made.

The compensators designed in this chapter are integrated into the air-to-air refueling AFCS. Linear and nonlinear simulations are performed with excellent results. The system response is within design specification. The QFT design process worked extremely well in designing the AFCS in the presence of external output disturbance.

## Chapter VII    Now the "Practicing Engineer Takes Over"

### VII.1    Introduction

The scientific method uses mathematical methods to gain insights into, to generalize, and to expand the state-of-the-art, in many areas of science and technology. Quite often this requires the proof of theorems, corollaries, and lemmas. At this stage, in general, the researcher (1) is not concerned with whether his or her efforts will result in the solution of "real world problems," and (2) applies linear analysis and synthesis techniques, although most of the real world problems are nonlinear. The scientific method is necessary in order for the researcher to be able "to see the trees from the forest," and thus to be able to achieve positive results.

Once the scientific approach has successfully advanced the state-of-the-art, and where applicable, the engineer must take over and apply the new results to real world problems. The engineer is at the "interface" of the real world, and the body of knowledge and theoretical results available in the technical literature.

Isaac M. Horowitz applied the scientific method in the development of his Quantative Feedback Theory (QFT) approach to the engineering design of robust control systems (see articles in Reference R.1). Professors F. Bailey, O. D. I. Nwokah, et al (see articles in Reference R.2) have used the scientific method to enhance the mathematical rigor of the QFT technique, in order to help the engineer to bridge the "interface" gap. The goal of these researchers is to establish theorems, corollaries, and lemmas that can tell the designer at the onset whether, given the required performance specifications, and in the face of parametric uncertainty, is a QFT solution feasible. This body of knowledge must be coupled with "the body of engineering knowledge" pertaining to the application, when dealing with nonlinear systems and real world problems. This requires that the engineer have a good understanding of the physical characteristics of the plant to be controlled.

In conclusion, the control system design task is a multi-stage process which entails many steps, say from A to Z. Mathematics is most helpful in taking the engineer through some of these steps, say from P to S. It however behooves the engineer to make the required modelling assumptions, hypotheses, and simplifications that are needed for him or her to proceed from A to O, so that the mathematical problem is tractable and the existing theory can be applied. Finally, steps T to Z entail extensive simulations where the validity of the model is verified, the implementation issues are addressed, and the design is validated. In Reference 118 an honest rendition of a flight control system design using QFT is presented.

## VII.2 Transparency of QFT

The elements resulting from the application of the scientific method which provide the "transparency" of the QFT design technique and that enhance its ability to solve real world problems are:

1. Template -- The size of the template (width and height) tells the engineer at the onset of the design process whether a fixed compensator  $G$  can be synthesized that will yield the desired system performance in the face of the prevailing structured uncertainty. If only the template's height is the problem then the engineer needs to employ straight gain scheduling. When control effector failures need to be accommodated, the width of template can become excessive and a successful design won't be possible. In this situation the designer needs to eliminate the effector failure case(s), in order to reduce the width of the template. Section IX.5.4 provides an example of how an engineer utilizes his or her knowledge of plant parameters, and performance characteristics and specifications, to select a set of  $J$  plants that ensures a template shape which represents as accurately as possible the extent of plant parameter uncertainty.

2. Phase margin frequency -- In order to ensure that the value of the specified phase margin frequency  $\omega_\phi$  is not exceeded by any of the plants in the set then, when all  $J$  plants in  $\mathcal{P}$  are stable,

select the nominal plant  $p_i$  to be the plant lying at the "top" vertex of the template. This assumes that this plant always lies, for all template frequencies, at the top of the templates. In the event that one or more plants in the set  $\mathcal{P}$  are unstable, then the design engineer must select as the nominal plant the plant  $p_i$  that has the highest degree of instability (the plant whose unstable pole lies furthest to the right in the s-plane) as the "worst case plant." This rule for the selection of the nominal plant will facilitate the achievement of the specified value of  $\omega_\phi$ . Also, see the discussion on page 86. It is advisable that one of the templates, for each loop, be obtained at the respective  $BW(L_i)$  frequency.

3. Signal flow graph (SFG) For  $y = P_e u = PWu$  -- Figure VII.1 represents a MIMO QFT control system structure. Having the SFG for the portion of Fig. VII.1 that represents  $P_e$  can be helpful in the initial selection of the values of  $w_{ij}$  and modifying some of these values during the simulation phase of the design process. This selection of values, etc, can be further enhanced by the engineer's firm understanding of the interrelationship of the plant outputs with the inputs to the  $W$  matrix.

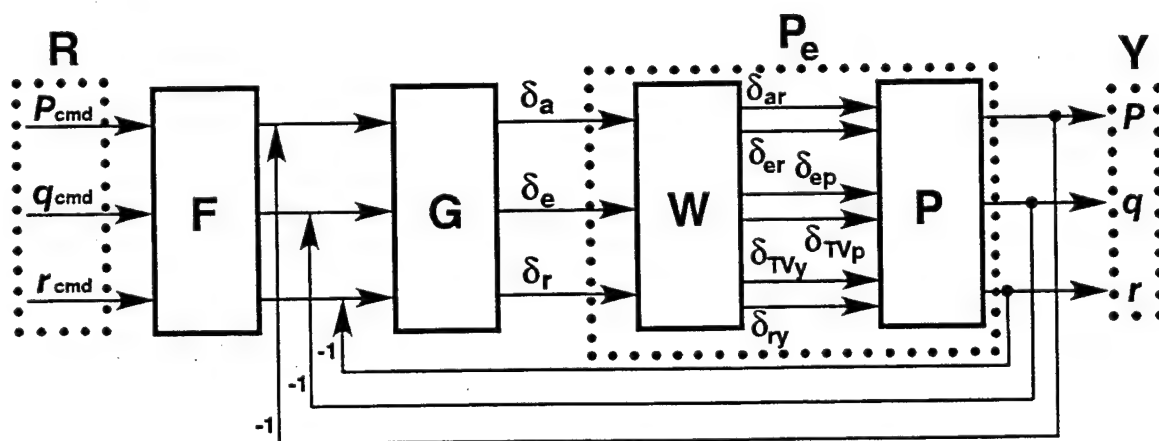


Fig. VII.1 MIMO QFT Control Structure, Block Diagram.

4. Minimum order compensator (controller) G -- Why are high-order compensators unacceptable? The implementation of an  $m$ -order compensator in a digital flight control system (FCS) yields an  $m$ -

order discrete-time dynamical system. The latter is equivalent to a first order dynamical system with  $m$ -time delays. Hence, during the first  $m-1$  time instants the input has a somewhat limited effect on the output, for the output is partially determined by the  $m$  initial conditions. Thus, the control action is delayed.

Example --- Consider a 60 Hz FCS sampling rate and a 20th order  $H_\infty$  compensator. The FCS's time delay is  $20/60 = 1/3$  s which is unacceptable. In general, the time delay caused by an  $m$ -order controller is  $m/60$  s.

Another factor that must be considered in maintaining low-order controllers is that on board flight control computers have limited capacity due to other non-control related computing requirements. As a rule, about 30% of the computer capacity is allocated to the FCS and 70% for non FCS requirements.

To achieve this desideratum some designers, or design methods, have recourse to plant  $P$ , and in-turn  $P_c$ , "doctoring" or "padding" by inserting additional poles and/or zeros into  $P$ . This results in an "augmented" plant matrix  $P_{cs}$  which these designers base their design on in order to achieve a so-called "minimum-order"  $G$ .

In QFT, in order to achieve the minimum size compensator  $G$ , during loop shaping, the poles and zeros of the nominal plant  $q_{iio}$  are put to good use in synthesizing a satisfactory loop shaping transfer function  $L_{iio}$ . Doing so yields the minimum-order compensator  $g_i = L_{iio}/q_{iio}$ .

Some or all of these elements, or comparable ones, are not available in other, optimization based, multivariable control system design techniques. This minimizes their ability to achieve, in a relatively "short design time," a design that meets all the performance specifications that are specified at the onset of the initial design effort.

### VII.3 Body of Engineering QFT Knowledge

Through the many years of applying the QFT robust control design

technique to many real world nonlinear problems, the following Engineering Lemmas have evolved:

**E.L.-1 Weighting Matrix** -- When a weighting matrix  $W = \{w_{ij}\}$  is required to achieve a square equivalent plant, it is desired to know at the onset if it is possible to achieve m.p.  $q_{ii}$ 's by the proper selection of the  $w_{ij}$  elements. Now, m.p.  $q_{ii}$  plants are most desirable for they allow the full exploitation of the "benefits of feedback," i.e., high gain. It turns out that one can apply the Binet-Cauchy theorem (see Chap V) to determine if m.p.  $q_{ii}$ 's are possible. Also, it may be desirable to obtain complete decoupling for the nominal plant case, i.e.,

$$P_{e_{diag}} = \begin{bmatrix} p_{11} & 0 & \dots & 0 \\ 0 & p_{22} & \dots & 0 \\ \vdots & \vdots & \dots & \vdots \\ 0 & 0 & \dots & p_{mm} \end{bmatrix} = PW \quad (\text{VII.1})$$

Although for the non-nominal plants complete decoupling, in general, will not occur, the degree of decoupling will have been enhanced. This greatly facilitates the QFT design process, for less attention needs to be given to cross-coupling effects ( $c_{ij}$ ) rejection. Method 1 is then more readily applicable, with the additional benefit of reduced closed-loop BW.

**E.L.2 n.m.p.  $q_{ii}$ 's** -- For  $q_{ii}$ 's that are n.m.p. one must determine if the location of the RHP zero(s) is in a region which will not present a problem for the real-world design problem being considered. For manual flight control systems,, if a RHP zero happens to be "close" to the origin, this is not necessary deleterious since the pilot inputs a new command before its effect is noticeable; in other words, it is assumed that the unstable pole is outside the closed loop system's lower bandwidth. If this RHP zero is "far out" to the right, it is outside the bandwidth of concern in manual control and it does not present a problem. For these cases a satisfactory QFT design may be achievable.



**E.L.3    Templates**    -- The adage "a picture is worth a thousand words" applies to the preliminary task of determining if a robust control solution exists, bearing in mind the need to satisfy tracking specifications, external disturbance and cross-coupling effects rejection, and satisfying the stability bounds. If the theorems, corollaries, and/or lemmas pertaining to these bounds, obtained by the scientific method, reveal that no loop shaping solution exists then one must be attuned to stepping back and doing a "trade-off" in which some specifications are relaxed in order to achieve a solution, or one must be willing to live with a degree of gain scheduling. Thus, a graphical analysis can reveal the following:

(a) The maximum template height, in dB, is too large, forcing one or more (tracking, cross-coupling rejection, external disturbance rejection, or stability) bound or the composite bound violation. One can then decide if gain scheduling is required and is feasible in order to yield a design that satisfies all the bounds.

(b) The situation where the templates are too "wide" (the magnitude of phase angle width) thus prohibiting a QFT solution or a solution by any other multivariable design technique (see Sec. V.3). This is especially true for real-world control problems that involve control effector failures accommodation. In these design problems, generally, the worst failure case is the culprit in generating this large "angle width." Thus, in order to achieve a solution one needs to relax the requirement that the "worst failure case" be accommodated. Naturally, when this situation arises, it is necessary to stipulate for what failure case or cases a successful design is achievable. In determining "reasonable failure cases" that can be accommodated by robust (not adaptive) control -- one must consider if 10%, 25%, 50%, 80% failure still permits enough control authority! This % of failure can only be determined by a person who is knowledgeable of the physical plant to be controlled. In general, knowledge of the plant (application) "is king" when it comes to the design of

a feedback compensator or controller for the said plant.

(c) In Sec. IX.5.4 it is shown how the engineer's insight into the plant's physics helps to efficiently determine the boundary of the template (where the parametric uncertainty is represented).

As stated in Sec. IV.6, if all the  $p_i$ 's of  $P$  do not have the same value of  $\lambda$  (excess of poles over zeros) then as  $\omega \rightarrow \infty$  the templates may not become straight lines. A possible method of reducing the size of the templates is given by E.L.8.

**E.L.4 Design Techniques** -- No matter what design method one uses, performance specifications must be realistic and commensurate with the real world plant being controlled. Situations have occurred where the conclusion was reached that no acceptable design was possible. For these situations when one "stepped back" and asked the pertinent question "was something demanded that this plant physically cannot deliver regardless of the control design technique?", it was determined that some or all of the prescribed performance specifications were unrealistic.

**E.L.5 OFT Method 2** -- By arbitrarily picking the wrong order of the loops to be designed (loop closures) by Method Two, can result in the nonexistence of a solution due to the chosen order of closures. This may occur if the solution process is based on satisfying an upper limit of the phase margin frequency  $\omega_\phi$  for each loop. The proper order of the loops to be designed by Method Two, entails picking the loops in the order of increasing values of the desired  $\omega_\phi$ ; i.e., first close loop 1, then loop 2, etc where  $\angle\phi_1 < \angle\phi_2 < \angle\phi_3 < \dots$ . Indeed, by Method Two it is known that the  $\omega_\phi$  of the succeeding designed loop is larger than the previously designed loops.

**E.L.6 Minimum order Compensator (Controller)** -- In order to ensure the smallest possible order compensator/controller, one starts the loop shaping process by using the loop's nominal plant  $L_{oi} = q_{i10}$ , and then zeros and poles are successively added in order to obtain the

required loop shape, resulting in:

$$L_o = \frac{L_{o_1}(s - z_1) \dots (s - z_w)}{(s - p_1) \dots (s - p_v)} \quad (\text{VII.2})$$

Finally, the compensator is obtained from  $g_1 = L_o/q_{110}$ . Thus, the nominal plant's poles and zeros are being used to shape the loop. This insures that the ensuing compensator/controller is of the lowest order, which is highly desirable.

**E.L.7 Minimum Compensator Gain** -- To minimize the effects of noise, saturation, etc., it is desirable to minimize the amount of gain required in each loop  $i$ , while at the same time meet the performance specifications in the face of the given structured uncertainty. To achieve this goal, a control system designer, with a good understanding of the Nichols Chart and a good interactive QFT CAD package, can use his "engineering talent" to make use of the "dips" in the composite  $B_{oi}(j\omega_i)$ . The designer by shaping  $L_{oi}$  to pass through these dips, where feasible, can ensure achieving the minimum compensator gain that is realistically possible. To achieve this by an automatic loop shaping routine may be difficult.

**E.L.8 Basic mxm Plant P Preconditioning** -- When appropriate, utilize unity feedback loops for the mxm MIMO plant  $P$  which will yield an mxm preconditioned plant matrix  $P_p$ . The templates  $\mathcal{S}P_p(j\omega_i)$ , in general can be smaller in size than the templates  $\mathcal{S}P(j\omega_i)$ . This template reduction size is predicted by performing a sensitivity analysis (see Sec. 14.2 of Ref. 15). The QFT design is performed utilizing the preconditioned matrix  $P_p$ . This concept has been used in a number of MIMO QFT designs<sup>56,77,78,121</sup> (see Sec. VI.2.1).

**E.L.9 Nominal Plant Determination** -- It is easy to determine the phase margin angle  $\gamma$ , the gain margin, and the phase margin frequency  $\omega_\phi$  of a feedback control system using the NC. Thus, QFT affords the robust establishment of these FOM. Indeed, by choosing the nominal plant: (a) to correspond to the maximum dB plant on the  $\omega_{\phi i} = BW(L_i)$  template ensures that  $\omega_{\phi i} < BW(L_i)$  for all plants; (b) for

the achievement of a robustly guaranteed gain margin is easily accomplished provided the nominal plant is uniformly the maximum dB plant for all templates; and (c) which is the "left-most" plant on all templates ensures that the desired  $\gamma$  is robustly achieved.

**E.L. 10 Simulation Run Time** -- In many real-world manual feedback linear or nonlinear control problems, the goodness of the design is judged on a prespecified planning time horizon beyond which the performance is less important since the human operator will inject new inputs to the system. For example, in manual flight control the time horizon is determined by the aircraft's short period dynamics, e.g., 5 seconds and there is no interest in the long time intervals commensurate with the slow phugoid dynamics.

**E.L. 11 Asymptotic Results** -- Asymptotic results by mathematical analysis are not as useful as they seem to be. Consider the manual control disturbance rejection case where fast disturbance attenuation is more desirable than total disturbance rejection which entails a very long "settling time."

#### **VII.4 Nonlinearities -- The Engineering Approach**

All the current robust control design methods, including QFT, yield linear compensators for linear, but uncertain, plants. Hence, the achieved robust performance applies to "small signals" only. The intrinsic scalability property which is afforded by linearity breaks down in the face of nonlinearity. The worst offenders are saturation type nonlinearities. The latter are encountered in actuators, which, unfortunately, are invariably located at the plant inputs. Both displacement and rate saturations significantly reduce the achievable benefits of (high gain) feedback. Thus, consider the extreme case of zero inputs to linear plants: the output will always be zero, irrespective of the (linear) plant, and so infinite robustness is achieved. The lack of robustness becomes evident when the plant is being driven hard (with a large input signal -- it is "slewed") and nonzero inputs are applied. This is also generally true in robust feedback control systems once significant slewing is attempted, and is due to nonlinearity and saturation. Fur-

thermore, nonlinearity and saturation need to be addressed when feedback control is used to stabilize open-loop unstable plants. Indeed, from a "small signal" point of view saturation is equivalent to opening the feedback loop. This will have catastrophic consequences, for it will cause instability and departure.

Hence, when saturation is encountered during simulations of the designed feedback control system, actuator "anti-windup" schemes must be employed. One might want to relax the robustness requirements and subsequently employ a limited degree of gain scheduling. Another possibility is to somewhat relax the tracking performance specifications and reduce the BW of the prefilter. This results in the tracking not being as tight as initially desired. However the error signal will be ramped into the compensator, thus delaying or eliminating the onset of actuator saturation.

### VII.5 Plant Inversion

Given an  $m$ -output vector  $y$ , an  $m$ -input vector  $u$ , the LTI plant transform equations can be written in the form (see Sec. III.1)

$$D(s)y = N(s)u \quad (\text{VII.3})$$

with  $D(s) = [d_{ij}(s)]$  and  $N(s) = [n_{ij}(s)]$  being  $m \times m$  polynomial matrices<sup>9</sup> in  $s$ . The resulting plant matrix  $P$  ( $y = Pu$ ) is

$$P = D^{-1}N = \frac{(\text{Adj } D)N}{\det D} = [p_{ij}(s)] \quad (\text{VII.4})$$

Suppose that the inverse plant

$$P^{-1} = [p_{ij}^*] = [1/q_{ij}] \quad (\text{VII.5})$$

is needed, for example, as in some of the QFT techniques. The designer can obtain it either from Eq. (VII.3), i.e., since  $u = P^{-1}y$ ,

$$P^{-1} = N^{-1}D = \frac{(\text{Adj } N)D}{\det N} \quad (\text{VII.6})$$

or from the state equations i.e.:

$$\dot{X} = AX + Bu \quad (a) \quad y = Cx \quad (b) \quad (\text{VII.7})$$

that describe the  $n$ th-order plant, where the matrices  $A$ ,  $B$ ,  $C$  are  $n \times n$ ,

$n \times m$ , and  $m \times n$ , respectively, and which, in turn, yields the following expressions:

$$y = C [sI - A]^{-1} B u \quad (\text{VII.8})$$

In other words,

$$P = C [sI - A]^{-1} B = \left\{ \frac{n_{ij}}{d} \right\} \quad (\text{VII.9})$$

where  $n_{ij}$  and  $d$  are polynomials of degree  $\ell$  and  $n$ , respectively, in  $s$ ;  $\ell \leq n$  and  $d$  is the characteristic polynomial of  $A$ .

For the numerical calculation of  $P^{-1}$  it is much better to use Eq. (VII.6) rather than Eq. (VII.9). The reason why is best illustrated by considering a  $2 \times 2$  ( $m = 2$ ) plant utilizing the second approach. Thus, from Eq. (VII.9):

$$P^{-1} = \frac{\text{Adj} \left\{ \frac{n_{ij}}{d} \right\}}{\det \{n_{ij}\}/d^2} = \frac{\text{Adj} \{n_{ij}\}/d}{\det \{n_{ij}\}/d^2} = \frac{d^2 \text{Adj} \{n_{ij}\}}{d \det \{n_{ij}\}} \quad (\text{VII.10})$$

In general, for the  $m \times m$  control system:

$$P^{-1} = \frac{d^m \text{Adj} \{n_{ij}\}}{d^{m-1} \det \{n_{ij}\}} \quad (\text{VII.11})$$

Thus, if  $P^{-1}$  is obtained from Eq. (VII.11), rather than directly from Eq. (VII.6), then  $m - 1$  cancellations of polynomials from the numerator in Eq. (VII.9) with the  $m - 1$  polynomials in its denominator is required. The numerical poles/zeros cancellations will of course not be exact, because of the inevitable computer round-off. Note that  $m - 1$  such cancellations of each zero of the numerator with the  $m - 1$  poles of the denominator must occur. Thus, in order to recover numerical accuracy one must factor all the numerator and denominator polynomials of  $P^{-1}$  and then check out the inevitable inexact cancellations.

Conclusion -- Evaluate  $\det P$  and  $P^{-1}$  directly from Eq. (VII.3). To do this, one needs the plant equations in the form of Eq. (VII.3),

which may not be readily available from the state space form. Therefore, the designer is very strongly advised at the very onset of the design process to obtain the data in the form of Eq. (VII.3).

### VII.6 Invertibility

The question is often asked: "How does one know that  $P(s)$  is invertible?" Obviously, the plant needs to be square, i.e.,  $P$  is  $m \times m$ . Then, bearing in mind that the entries of  $P$  are not real numbers but instead are (rational) functions in the dummy variable  $s$ , formal invertibility is almost guaranteed. Indeed, the following holds:

Theorem -- The  $m \times m$  matrix  $P(s)$  in Eq. (VII.9) is invertible iff the system  $(A, B, C)$  is controllable and observable. Moreover, in the formulation of Eq. (VII.10) no "pole/zero" cancellations occur iff the above system is controllable and observable.

Proof outline -- If the plant is not controllable and observable then even a formal inversion of  $P$  won't be possible because some of the rows and/or columns of  $P$  will be linearly dependent over the real field.

Finally, controllability and observability of the control system are "a given" in the real world.

### VII.7 Psuedo-Continuous-Time (PCT) System

In Chap. I an overview of the QFT design method applied to MISO sampled-data (S-D) control systems<sup>47</sup> is presented. As pointed out in this chapter, a m.p. s-domain plant becomes a n.m.p. plant in the w-domain. Also, as is well known, in converting an analog system whose stability, in general, is determined by the value of the open-loop gain  $K$ , to a S-D system, its stability is now determined not only by the value of  $K$  but is also a function of the sampling-time  $T$ . In general, in converting an analog system to a S-D system the degree of system stability is decreased. Because of this w-domain n.m.p. characteristic, as noted in Figs. I.15 and I.16, there is a "restricted" frequency band

$\Delta\omega = \omega_K - \omega_i$ ,  $\omega_K > \omega_i$  (or  $v_K > v_i$ ), in which loop shaping must be accomplished while satisfying all the bounds. Such a "restricted" frequency band does not exist for analog systems. Thus, for S-D systems this "restricted" frequency band makes loop shaping a little more difficult to accomplish. Finally, systems which are strictly proper in the s-domain are proper, but not strictly proper in the w-domain.

A technique for "by-passing" the restricted frequency band problem for a w-domain QFT S-D system design is to convert this S-D system to a psuedo-continuous-time (PCT) system.<sup>47</sup> The criteria<sup>47</sup> for converting a given S-D system to a PCT system must be satisfied in order to accomplish a satisfactory QFT design. The QFT design is then accomplished in the s-domain for the PCT system. The resulting s-domain controllers and prefilters are then transformed into the z-domain by use of the Tustin transformation.<sup>47</sup> The PCT QFT design approach was used to design a MIMO digital flight control system for an unmanned research vehicle<sup>120</sup> (see Chap. IX). This approach was also used to design a MIMO digital robotic control system.<sup>113</sup> Both designs were successful and met all desired performance specifications.

## VII.8 Summary

Engineers are applying the results of the scientific method to achieving solutions for real world problems. As an example, British Aerospace Ltd has stated to Professor M. Grimble, University of Strathclyde, the following: "The QFT approach has the obvious advantage that it is close to engineers' existing experience on classical design methods. However, it provides facilities to deal with uncertainty which are not available in traditional methods. More recent tools such as  $H^\infty$  design also show promise but are very different to the existing procedures used in parts of the Aerospace industry. The QFT approach therefore appears to have the attractive features of providing a link with existing techniques whilst at the same time providing many of the advanced features needed for the 90's high performance systems. What might be needed are tools for the future which combine the attractive features of QFT and  $H^\infty$  approaches. In this chapter guidelines are provided to the control engineer on how to interface between the scientific method and engineering. In conclusion, an attempt is made to bridge the often lamented about gap between theory and practice.



### VIII.1 Introduction

This chapter presents the up-dating of Version 2 of the MIMO/QFT CAD package. This updating entails the implementation of algorithms for the design of a robust multivariable control system that, in addition, rejects external disturbance signals. Both analog- and discrete-time MIMO tracking control systems are considered. Version 3 of the CAD package is capable of carrying through a robust control design from problem setup, through the design process, to a frequency domain analysis of the compensated MIMO system. For analog control problems, the design process is performed in the  $s$ -plane, while for discrete control problems the plants are discretized and the design process proceeds in the  $w'$ -plane. The package automates: the selection of the weighting matrix; the discretization of the plants; the formation of the square effective plants; the polynomial matrix inverse required to form the equivalent plants; the generation of templates; the selection of a nominal plant; the generation of stability, tracking, cross-coupling disturbance, external disturbance rejection,  $\gamma$ , and composite bounds; the loop shaping; and the design of the prefilter elements. This is followed by a frequency-domain analysis of the completed design, and export of this design to the MATLAB SIMULINK<sup>R</sup> toolbox in order to validate the frequency domain design by time-domain simulations. The bound generation routines and graphics have been enhanced. The allocation of the degree of the cross-coupling effects rejection is automatically performed, while in the process of generating the tracking bounds. Gain scheduling may be included in the weighting matrix. The improved (second) method may be applied for the general case of an  $m \times m$  effective plant for both external disturbance rejection and tracking control problems. The MIMO QFT CAD package is implemented using Mathematica and is hosted on Sun Work- station platforms. The CAD package can also be used to perform a QFT design for the special case of a MISO control system. A PC version of this CAD package is available.

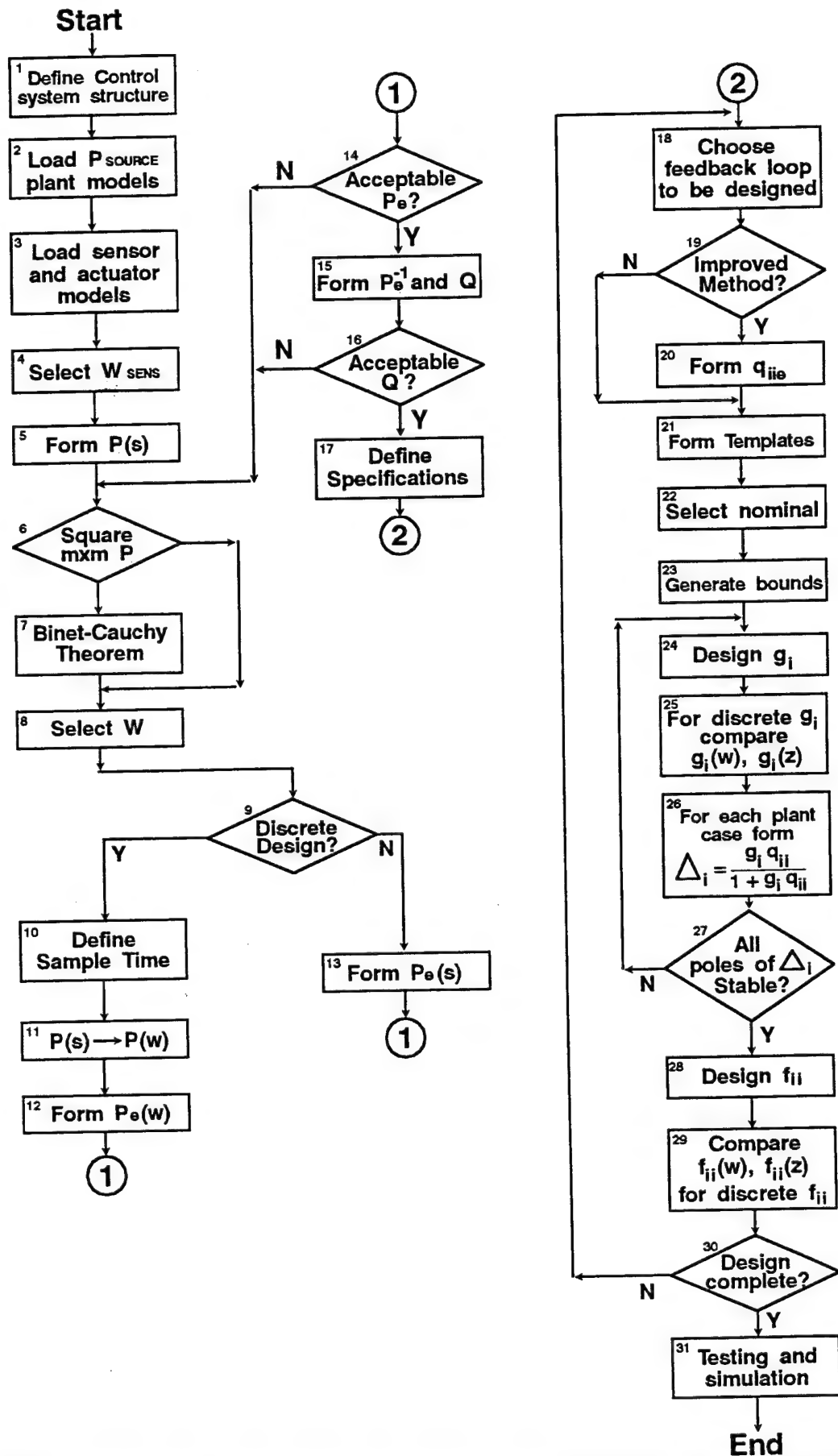
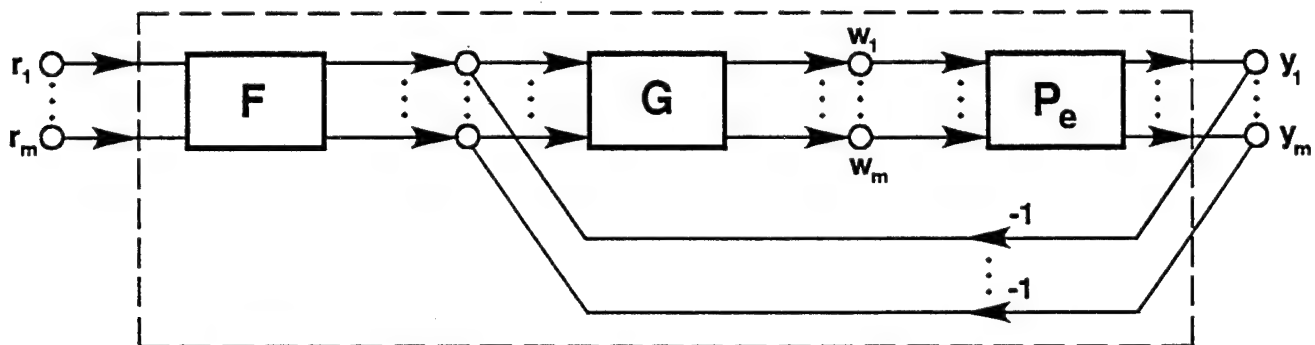


Fig. VIII.1 MIMO/QFT flow chart for analog and discrete control systems.

## VIII.2 Introduction: Overview of Multivariable Control

The CAD package (Version 3), as outlined in Fig. VIII.1, is a design tool for applying the Quantitative Feedback Theory (QFT) technique to analog and digital multivariable tracking control and external disturbance rejection design problems involving MIMO plants having structured plant parameter uncertainty. For tracking control problems, a MIMO square effective plant  $P_e$  with  $m$  inputs and  $m$  outputs is to be controlled by use of a diagonal compensator  $G$  and a diagonal prefilter  $F$  in the feedback structure shown in Fig. VIII.2. For external disturbance rejection problems, see Fig. VIII.3, a diagonal compensator  $G$  is designed such that the system rejects outside disturbances which are projected to the outputs of  $P_e$  through the disturbance plant model  $P_d$ , as shown in Fig. VIII.4. The system structure of Fig. VIII.3 can be used for a control problem specifying both tracking and external disturbance rejection requirements. For both classes of control problems the closed-loop system is required to meet appropriate stability and performance (tracking or external disturbance rejection) specifications.



**Fig. VIII.2 MIMO QFT controller block diagram.**

### VIII.3 Continuous-Time vs. Discrete-Time Design (see blocks 9 and 10 in Fig. VIII.1)

The design for a continuous-time system is done in the  $s$ -domain by the well defined analog QFT design process. These same procedures, as shown in Fig. VIII.1, are utilized for discrete-time systems that are described in the  $w'$ -domain (referred to in this sequel as the  $w$ -domain).

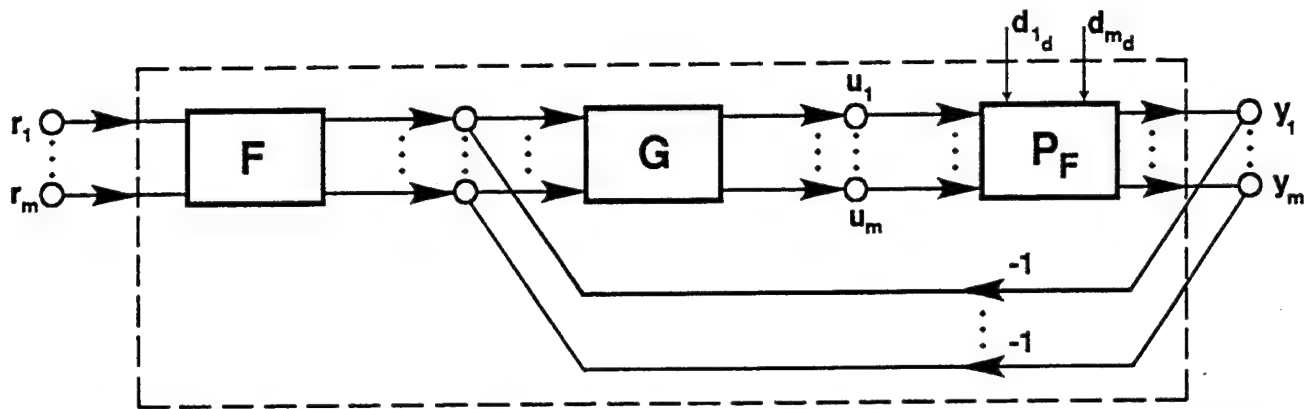


Fig. VIII.3 MIMO QFT controller block diagram. ( $r = 0$ )

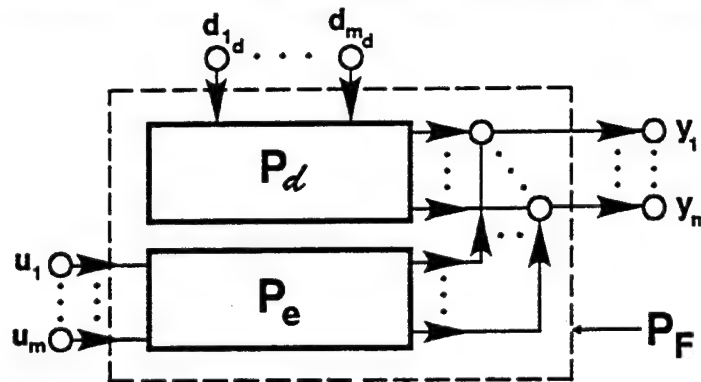


Fig. VIII.4 Partitioning of  $P_F$ .

As indicated in Block 9, the user selects the analog or discrete design CAD package route. Once  $F(w)$  and  $G(w)$  are synthesized, they are transformed into the  $z$ -domain for implementation by a digital computer. Thus, the following sections, although they refer to the  $s$ -domain design, apply equally well to a  $w$ -domain design.

#### VIII.4 Overview of the Multivariable External Disturbance Rejection Problem

Using the QFT design technique, external disturbances applied to the uncertain MIMO plant  $P_F$  are to be rejected by use of a diagonal compensator  $G$  in the feedback structure shown in Fig. VIII.3 such that the closed loop system meets stability and performance specifications. Obviously, a prefilter  $F$  is not required for pure external disturbance rejection problems in which it is assumed that the tracking command input is zero in Fig. VIII.3. Thus the  $m_d \times m$  SISO equivalents of the  $m_d \times m$  MIMO external disturbance rejection system are shown in Fig. VIII.5 for

the case in which  $m_d = m = 3$ . The plant model  $P_F$  is partitioned into two distinct plant models  $P_e$  and  $P_d$  as shown in Fig. VIII.4 for the QFT design process. The plant  $P_d$  models the transmission from the external disturbance inputs to the outputs of  $P_F$  and features only the external disturbance rejection problems.  $P_d$  does not affect the closed-loop stability of the  $m$  feedback loops in Fig. VIII.3. The plant  $P_e$  models the open-loop transmission of  $P_F$  in the feedback loop;  $P_e$  takes the place of  $P_F$  in pure tracking control problems.

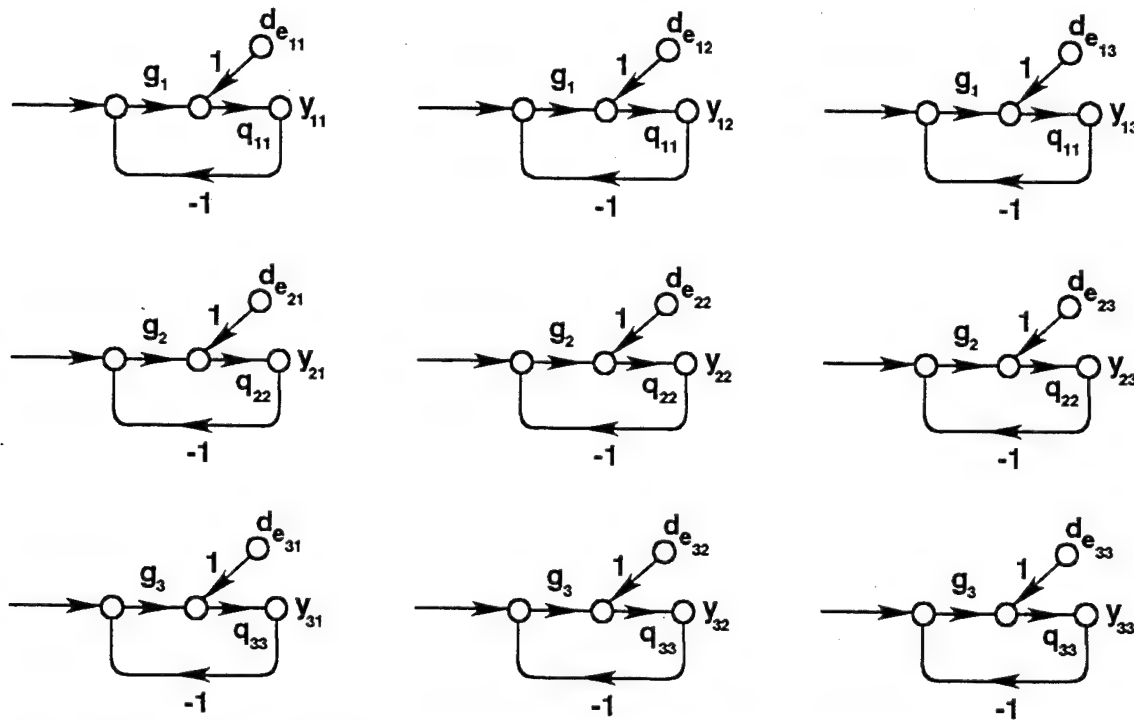


Fig. VIII.5 3x3 MISO Equivalent Loops for External Output Disturbance ( $r = 0$ ).

#### VIII.5 Open-loop Structure

When the plant matrix  $P$  is not square, then a square  $m \times m$  plant  $P_e$  is formed from the  $m \times l$  plant  $P$  by use of the  $l \times m$  weighting matrix  $W$  as shown in the block diagram in Fig. VIII.6 for analog designs, and Fig. VIII.7 for discrete designs. Even if  $m = l$  one may still use the weighting matrix  $W$  for the purpose of gain scheduling if needed. Thus:

$$P_e = PW \quad (\text{VIII.1})$$

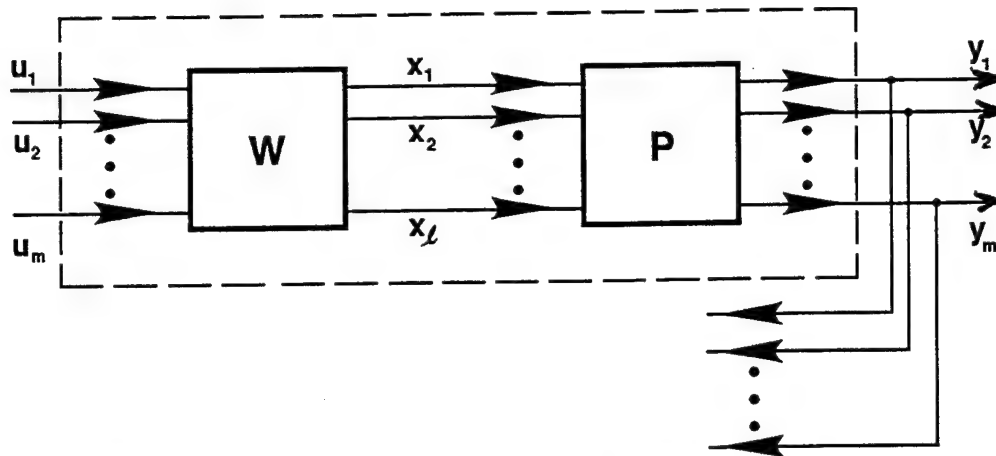


Fig. VIII.6 Formation of analog effective plant  $P_e$ .

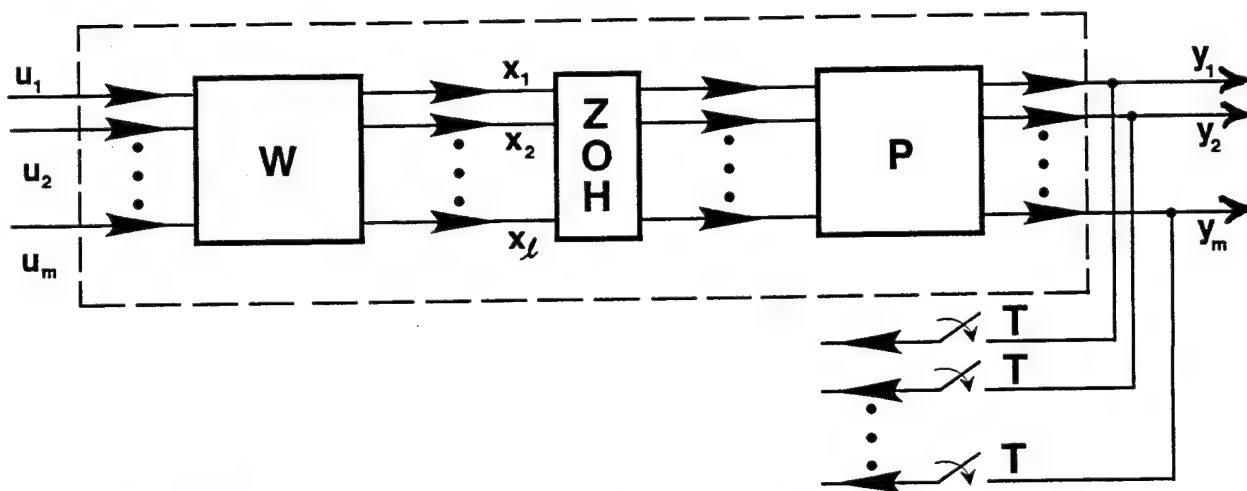


Fig. VIII.7 Formation of discrete effective plant  $P_e$ .

The open-loop plant  $P$  is in general constituted by four component parts. A block diagram showing the placement of the loaded plant model  $P_L$ , the actuator dynamics  $T_{ACT}$ , the sensor dynamics  $T_{SEN}$ , and the sensor gain matrix  $W_{SEN}$  is shown in Fig. VIII.8. The expression for the plant matrix  $P$ , of dimension  $m \times l$ , which in general is not square, is:

$$P = T_{SEN} W_{SEN} P_L W \quad (\text{VIII.2})$$

The disturbance plant model  $P_d$  is in general constituted by three component parts. A block diagram showing the placement of the loaded model  $P_{dL}$ , the sensor dynamics  $T_{SEN}$ , and the sensor gain matrix  $W_{SEN}$  is

shown in Fig. VIII.9. The plant  $P_d$  of dimension  $m \times m_d$  is, in general, not square. The expression for  $P_d$  is therefore:

$$P_d = T_{SEN} W_{SEN} P_{d_L} \quad (\text{VIII.3})$$

According to the partitioning of the disturbance rejection system in Figs. VIII.3 through VIII.9, the bare plant is composed of two transfer function models  $P_L$  and  $P_{dL}$  as shown in Fig. VIII.10. These transfer function matrices, which may not be square, are loaded by the designer

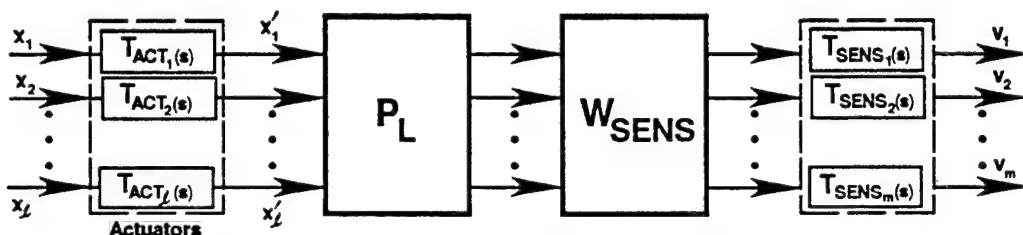


Fig. VIII.8 Components of the Plant P.

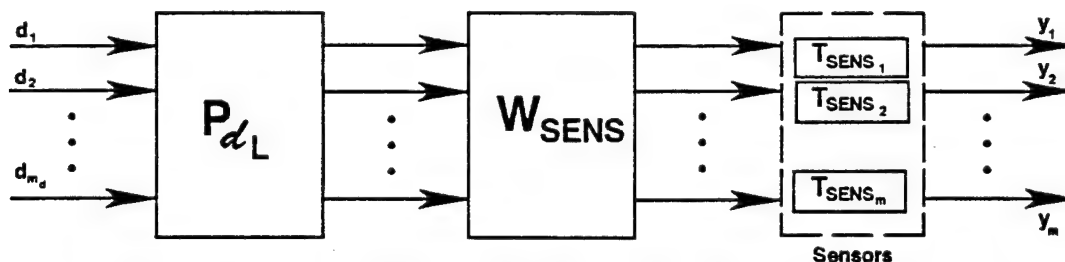


Fig. VIII.9 Components of the Plant  $P_D$ .

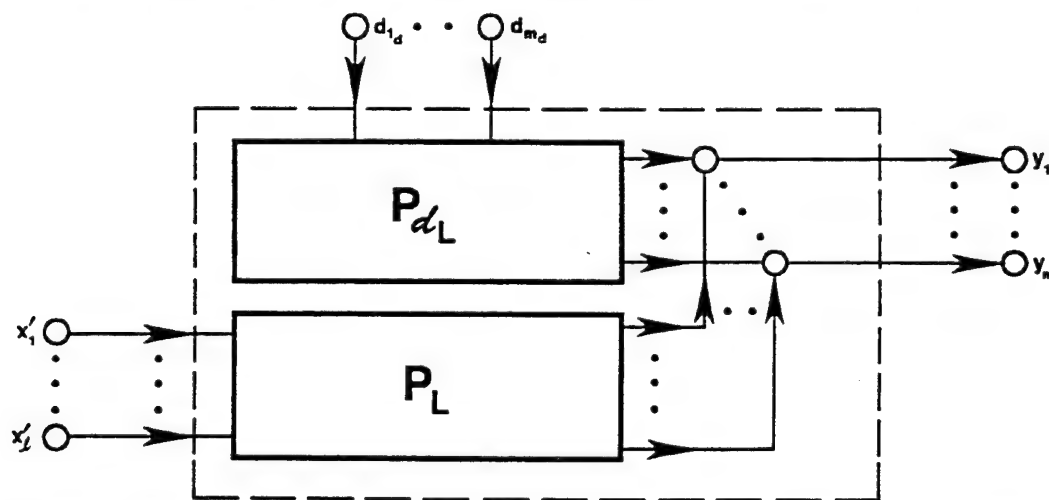


Fig. VIII.10 Partitioning of bare plant model.

and placed into the control system structures used by the CAD package shown in Figs. VIII.8 and VIII.9, respectively.

#### VIII.6 Formation of Plant Models for Tracking Control Problems (see blocks 4-13 in Fig. VIII.1)

For both analog and discrete control problems the plant model  $P$  to be controlled (see Fig. VIII.1) is in general constituted by the four analog component parts: the loaded plant model  $P_L$ , actuator dynamics  $T_{ACT}(s)$ , sensor dynamics  $T_{SENS}(s)$ , and the sensor gain matrix  $W_{SENS}(s)$ . The plant  $P(s)$  for the  $J$  plant cases  $i = 1, 2, \dots, J$  is therefore formed as follows:

$$P_i(s) = W_{SENS} T_{SENS}(s) P_{L_i}(s) T_{ACT}(s) \quad (\text{VIII.4})$$

For a discrete-time control problem, the analog plant  $P$  is embedded in the digital control system by placing a zero-order-hold before the inputs of the plant  $P$  and by sampling the feedback signal of the plant outputs.

The plant  $P$  of dimension  $m \times l$  is, in general, not square. Since QFT requires a square plant then the square  $m \times m$  effective plant  $P_e$  is formed from the non-square  $m \times l$  plant  $P$  by use of the  $l \times m$  weighting matrix  $W$ . It is desirable to select elements of  $W$  such that the determinant of  $P_e(s)$  is m.p.. For continuous-time designs, the Binet-Cauchy theorem (see Sec. V.8) is applied to  $P_e(s)$  in order to determine whether a m.p.  $\det P_e(s)$  is achievable by an appropriate  $W$ . If so, it will result in all  $(q_{ii})_i$  being m.p. For discrete-time designs one can apply the Binet-Cauchy theorem to  $P_e(s)$  in order to minimize the number of RHP zeros of  $\det P_e$  in the  $w$ -plane by an appropriate  $W$ . In some multivariable control problems, the degree of uncertainty in the plant  $P$  may render impossible a successful robust design. Thus, for these cases, (minimal) gain scheduling of  $W$  may be required to affect a QFT design by allowing a different weighting matrix  $W$ , for each plant case  $i$ .  $P_{e_i}$  for plant case  $i$  is formed from  $P_i$  and  $W_i$  as follows:



$$\mathbf{P}_e = [p_{ij}]_i = \mathbf{P}_i \mathbf{W}_i \quad (\text{VIII.5})$$

For discrete-time control problems, each plant  $\mathbf{P}_i(s)$  is discretized as each  $\mathbf{P}_{ei}$  is formed. To discretize  $\mathbf{P}_i(s)$  an exact z-transform is performed, followed by the z- to w- transformation resulting in w-plane transfer functions, i.e.:

$$\mathbf{P}_i(z) \rightarrow \mathbf{P}_i(w) \quad (\text{VIII.6})$$

The QFT design process then proceeds in the s-domain for a continuous design or in the w-domain for a discrete design using exactly the same design steps unless stated otherwise.

The effective plant matrix  $\mathbf{P}_e$  must have full rank, viz., controllability and observability are assumed, and have diagonal elements that have the same sign for all plant cases as  $\omega \rightarrow \infty$ . These are conditions that any of the usual LTI design techniques must satisfy (see Sec. V.8); they are not unique to QFT. The CAD package therefore allows the sign of the m diagonal plants to be examined for the J plant cases as  $\omega \rightarrow \infty$  in table form. The CAD package also allows the designer to list the determinant of  $\mathbf{P}_e$ , one plant case at a time.

A non-zero determinant is indicative of full rank. The numerator factors of the determinant, which are zeros of the  $q_{ij}$ , are examined as well. Thus, these determinants determine the m.p. or n.m.p. character of the effective plants  $(q_{ij})_i$ . If any  $\mathbf{P}_{ei}$  is unacceptable based on the above criteria, the weighting matrix is revised,  $\mathbf{P}_e$  is recomputed, and the tests are applied again.

#### VIII.7    Inverse of $\mathbf{P}_e$ (see blocks 14 and 15 in Fig. VIII.1)

The polynomial matrix inverse is performed using the Mathematica inverse function:

$$P_e^{-1} = \frac{\text{adj } P_e}{\det P_e} = \{p_{ij}^*\} \quad (\text{VIII.7})$$

The equivalent plants are then formed by inverting the elements  $p_{ij}^*$ , that is:

$$Q = \frac{\det P_e}{\text{adj } P_e} = \{q_{ij}\} = \left\{ \frac{1}{p_{ij}^*} \right\} \quad (\text{VIII.8})$$

The  $Q$  matrix elements become the equivalent plants of the MISO loops.

#### VIII.8 MISO Loops of the Tracking Control Problem

By the principle of superposition, each MISO loop transmission (see Fig. VIII.11) consists of both a tracking and a cross-coupling component. When using a diagonal prefilter, only the diagonal MISO loops have a transfer function component due to tracking:

$$t_{ii} = t_{r_{ii}} + t_{c_{ij}} \quad (\text{VIII.9})$$

Off-diagonal loops, with  $f_{ij} = 0$  and  $i \neq j$ , have a transfer function component due to cross-coupling only, i.e.:

$$t_{ij} = t_{c_{ij}} \quad \text{where } i \neq j \quad (\text{VIII.10})$$

Expressions for tracking and cross-coupling transfer function components of the  $(ij)$  MISO loop are explicitly given by:

$$(t_{r_{ij}})_i = f_{ij} \left[ \frac{g_i(q_{ii})_i}{1 + g_i(q_{ii})_i} \right] = f_{ij} \left[ \frac{(L_i)_i}{1 + (L_i)_i} \right] \quad (\text{VIII.11})$$

$$(t_{c_{ij}})_i = \frac{(c_{ij})_i (q_{ii})_i}{1 + g_i(q_{ii})_i} = \frac{(c_{ii})_i (q_{ii})_i}{1 + (L_i)_i} \quad (\text{VIII.12})$$

where the index  $i$  specifies one of the  $J$  LTI plants, i.e.,  $i = 1, 2, \dots, J$ , and where  $L_i = g_i q_{ii}$ . The cross-coupling effect input, a function of all other controlled outputs, can be expressed by the equation:

$$c_{ij} = - \sum_{k \neq i}^m \left[ \frac{t_{kj}}{q_{ik}} \right] \quad (\text{VIII.13})$$

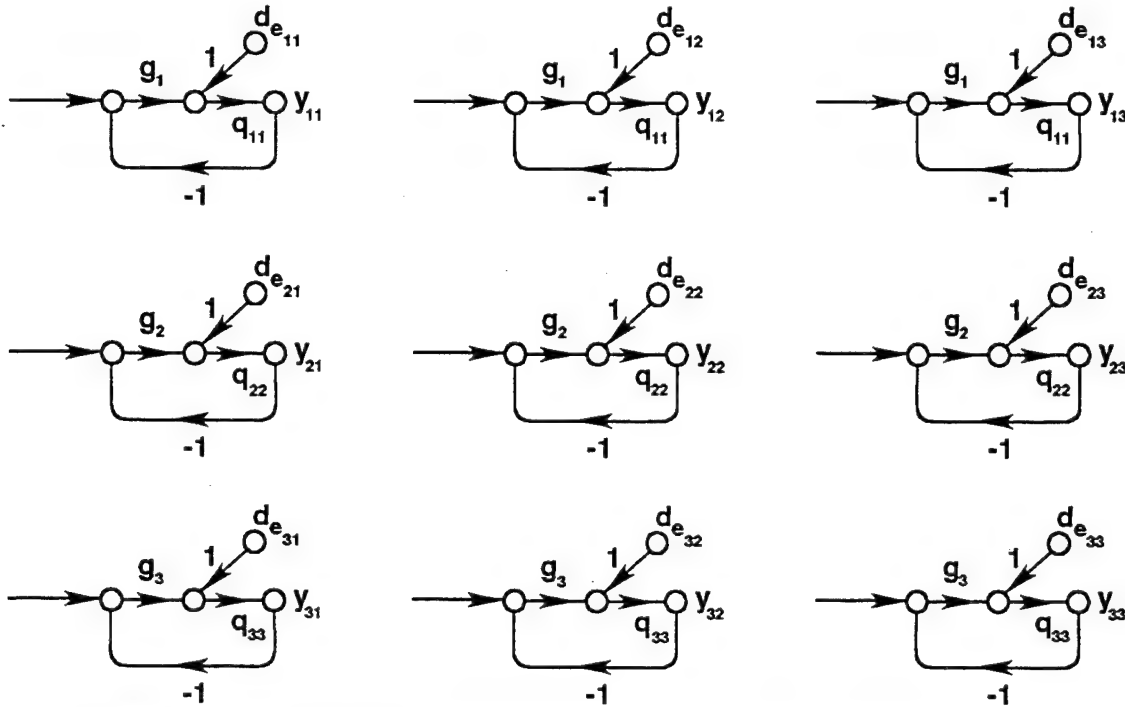


Fig. VIII.11 3x3 MISO Equivalent Loops for External Output Disturbance ( $r = 0$ ).

#### VIII.9 MISO Loops of External Disturbance Rejection Problem

For external disturbance rejection problems, each SISO loop transmission (see Fig. VIII.11) consists of only a disturbance component due to cross-coupling effects and the external disturbance forcing function:

$$t_{ij} = t_{d_{ij}} \quad (\text{VIII.14})$$

The transfer function  $T_d$  relating the disturbance input of the  $(i, j)$  SISO loop to its output, [see Eqs. (VI.27), (VI.30), and (VI.31)], is given by:

$$(t_{d_{ij}})_i = \frac{(d_{e_{ij}})_i (q_{ii})_i}{1 + g_i (q_{ii})_i} = \frac{(d_{e_{ij}})_i (q_{ii})_i}{1 + (L_i)_i} \quad (\text{VIII.15})$$

where the index  $i$  specifies which LTI plant is being considered, i.e.,  $i = 1, 2, \dots, J$ , and where  $L_i = g_i q_{ii}$ . In comparing Eq. (VIII.15) to Eqs. (VI.25) through (VI.27) the following relationship holds:

$$P = P_e = (\Lambda + B)^{-1}$$

The SISO loop disturbance input, a function of the external disturbance input and all other controlled outputs (cross-coupling), is expressed [see Eqs. (VI.31) and (VI.32)] by the equation:

$$d_{e_{ij}} = (d_{ext})_{ij} - c_{ij} = [P_e^{-1} P_d]_{ij} - \sum_{k \neq j}^m \left[ \frac{t_{kj}}{q_{ik}} \right] \quad (\text{VIII.16})$$

$$\text{where } [P_e^{-1} P_d]_{ij}$$

is the  $(ij)$  element of the transfer function matrix product  $P_e^{-1} P_d$ .

#### **VIII.10 Q Matrix Validation Checks (see block 16 in Fig. VIII.1)**

For analog and discrete tracking and external disturbance rejection problems, the  $Q$  matrix elements are tested to verify that the condition of diagonal dominance is satisfied. If diagonal dominance holds for all plant cases, then a QFT Method 1 design may be used. Otherwise, a QFT Method 2 (improved method) design must be used. If the results of this test are not satisfactory, then the weighting matrix  $W$  can be modified, and the  $Q$  matrix recomputed.

Additional tools for examining the equivalent plants  $q_{ii}$  of the  $Q$  matrix include a Bode plot function and a transfer function display subroutine. The Bode plot for a  $Q$  matrix element can be displayed for a specified set of plant cases or for all  $J$  plant cases together. The Bode plot for the set of  $J$  plant cases is useful for displaying

variation in equivalent plant transmission as an aid in selecting representative template frequencies. Also, the CAD package allows the  $Q$  matrix transfer function elements to be displayed in factored form for any selected plant case.

To reduce the order of the  $Q$  matrix transfer functions the package performs automatic pole/zero cancellation, canceling nearly identical pole-zero pairs based on a user specified ratio of the distance between the pole-zero pair to the distance of the zero from the origin in both the right-half and left-half plane.

#### **VIII.11 Improved Method (see blocks 19 and 20 in Fig. VIII.1)**

The improved QFT Method 2, takes into account any correlation between the uncertainty in the designed MISO loops and the next row of MISO loops for which a design is to be performed. The standard approach of QFT Method 1 assumes worst case conditions and does not take this design information into account. The improved method requires the derivation of the equivalent  $q$  plant transfer function for the next MISO loops yet to be designed. For both tracking and external disturbance rejection problems, the new set of transfer functions required by the improved method are generated using the equation:

$$Q_{ije(n+1)} = Q_{ije(n)} \left[ \frac{1 + L_k}{1 + L_k - \gamma_{ij(n)}} \right] \quad (\text{VIII.17})$$

where the compensator  $g_k$  for row  $k$  of the MISO loops has been designed ( $L_k$  is known), and where:

$$L_k = g_k q_{kke(n)} \quad (\text{VIII.18})$$

$$\gamma_{ij(n)} = \frac{q_{kke(n)} q_{ije(n)}}{q_{kje(n)} q_{ike(n)}} \quad (\text{VIII.19})$$

and  $q_{kke(0)} = q_{kk}$  are generated during the matrix inversion of  $P_e$ . The

number in parentheses in the subscript of the improved method plants indicates the number of times this method has been applied to generate the plant transfer function. For example, the plant  $q_{kke(1)}$  is obtained by applying the improved method once, and  $q_{ije(n)}$  in Eq. (VIII.17) is obtained after applying the improved method  $n$  times. (i.e.,  $n$  compensator elements of the matrix  $G$  were designed, and the improved method was applied after each design is completed.) Improved method plants are generated for all plant cases and for each row of MISO loops for which the compensator has not yet been designed. The notation  $k$  on  $L_k$  is not to be confused with the standard notation  $i$  on  $L_i$ . The notation  $k$ , as used here, denotes the index of the loop most previously designed, i.e.,  $k = i-1$  if loops are designed sequentially.

## **VIII.12 Specifications (see blocks 17 in Fig. VIII.1)**

### **VIII.12.1 Stability Specifications**

A stability margin is specified for each row of MISO loops. The stability margin may be specified in terms of the gain margin  $gm$ , the phase margin angle  $\gamma$  or the corresponding  $M_L$  contour. The two remaining specifications are calculated from the one specification that has been entered. Only the  $M_L$  contour stability specification is stored in memory.

### **VIII.12.2 Tracking Performance Specifications**

Frequency domain performance specifications are defined in the form of LTI transfer functions. For the diagonal MISO loops upper and lower bounds are specified as follows:

$$a_{ii} \leq |t_{ii}| \leq b_{ii} \quad \text{for } i = 1, 2, \dots, J \quad (\text{VIII.20})$$

For the off-diagonal MISO loops the following upper bound is specified:

$$|t_{ij}|_1 \leq b_{ij} \quad \text{for } i = 1, 2, \dots, J \quad (\text{VIII.21})$$

### VIII.12.3 External Disturbance Rejection Performance Specifications

For all MISO loops the following upper bound is specified:

$$|t_{ij}|_1 \leq b_{ij} \quad \text{for } i \neq j, \quad i = 1, 2, \dots, J \quad (\text{VIII.22})$$

This upper bound is determined based upon Eqs. (VI.46) and (VI.47) in Chapter 6. (Note that upper case letters for the bounds are used therein.)

For analog design problems, all performance specifications are defined as s-domain transfer functions. In the case of a digital control problem, the performance specifications are approximated in the bandwidth of interest by making the substitution  $s \rightarrow w$ . If the sampling rate is not sufficiently high for the above assumption to hold, the s-domain transfer functions yielding the desired performance specifications, are transformed to the z-domain and then transformed into the w-domain.

### VIII.12.4 Gamma Bound Specifications

The improved method requires the derivation of the effective  $q$  plant transfer function, i.e. Eq. (VIII.17). By proper design of each compensator  $g_k$ , new RHP poles will not be introduced in  $q_{iic}$ . By requiring the magnitude of the denominator of Eq. (VIII.17) be larger than a small value  $\epsilon_k$ , sign changes in the denominator are prevented and new RHP poles are not introduced. This constraint is given by:

$$\epsilon_k \leq |1 + L_k - \gamma_{ij}| \quad (\text{VIII.23})$$

A unique minimum value  $\epsilon_k$  is specified by the designer for each of the  $k = 1, 2, \dots, m$  channels.

### VIII.13    Bounds on the NC (see block 23 in Fig. VIII.1)

For a given row  $i$  of MISO loops, and for a template frequency  $\omega = \omega_i$ , several bounds may be included in the set plotted on the NC. These bounds include a stability bound, an allocated tracking bound, cross-coupling bounds, external disturbance bounds, and gamma bounds when using the improved method. The allocated tracking and cross-coupling bounds are generated such that the proper reduction in overdesign is achieved when using the improved method. This set of bounds can be replaced by a single composite bound before beginning a design.

#### VIII.13.1    Stability Bounds

A stability bound is generated for each template. The stability bounds constrain the maximum closed-loop transmission of the MISO loop with unity gain prefilter to have a bounded magnitude of:

$$\left[ \frac{g_i(q_{ii})_1}{1 + g_i(q_{ii})_1} \right] \leq M_L \quad (\text{VIII.24})$$

The bound is plotted for a given frequency by plotting the path of the nominal point while traversing the  $M_L$  contour with the template generated for that frequency.

#### VIII.13.2    Cross-Coupling Bounds

For tracking problems, cross-coupling bounds are generated for each template, one for each off-diagonal MISO loop in the row of MISO loops for which the compensator is to be designed. Each bound is generated based on the constraint:

$$|t_{ij}| = \left| c_{ij} \left[ \frac{q_{ii}}{1 + L_i} \right] \right| \leq b_{ij} \quad \text{for } i \neq j \quad (\text{VIII.25})$$



which is a function of all other cross-coupling controlled outputs. The specifications dictate that  $c_{ij}$  is less than an upper bound for each plant case  $i$ :

$$(|c_{ij}|_{\max})_i = \sum_{k \neq j}^m \left[ \frac{|b_{kj}|}{|q_{jk}|_i} \right] \quad (\text{VIII.26})$$

When the improved method has been applied, overdiseign is substantially reduced by modifying Eq. (VIII.26) as follows:

$$(|c_{ij}|_i)_{\max} = \sum_{\substack{k \neq i \text{ for} \\ L_k, f_{kj} \text{ unknown}}} \left[ \frac{|b_{kj}|}{|q_{ik(n)}|_i} \right] + \sum_{\substack{k \neq i \text{ for} \\ L_k, f_{kj} \text{ unknown}}} \left[ \frac{|f_{kj}|}{|q_{ik(n)}|_i} \right] \quad (\text{VIII.27})$$

where  $f_{kj} = 0$  when  $k \neq j$  for the case of a diagonal prefilter  $F$  required by the MIMO QFT CAD package.

Based on Eqs. (VIII.25) - (VIII.27), a lower bound is placed on  $|1 + L_i|$  as follows:

$$|1 + L_i| \geq \frac{|c_{ij}|_{\max} |q_{ii}|}{|b_{ij}|} \quad (\text{VIII.28})$$

By substituting  $L_i = 1/m$  into Eq. (VIII.28), the latter is transformed such that the bound is plotted on the inverse NC, i.e.,

$$\left| \frac{m}{1 + m} \right| \leq \frac{|b_{ij}|}{(|c_{ij}|_{\max})_i |q_{ii}|_i} \quad (\text{VIII.29})$$

Equation (VIII.29) is the basis upon which the cross-coupling bounds on  $L_{io}$  are generated. The bounds are generated such that the correlation between  $m$  and  $q_{ii}$  in Eq. (VIII.29) is properly taken into account over the range of the plant parameter uncertainty which is outlined by the template when the nominal loop transmission does not violate these bounds.

### VIII.13.3 Gamma Bounds

Gamma bounds are generated for each template, where the compensator for row  $j$  is to be designed after the compensator for row  $i$  of the MISO loops is designed. It is desired that the magnitude of the denominator of the effective plant  $q_{22c}$  calculated using Eq. (VIII.17) for an improved method design, not be smaller than a specified minimum value despite plant uncertainty. Thus, the gamma bound is generated based upon satisfying:

$$|1 + L_k - \gamma_{ij}| \geq \epsilon_k \quad (\text{VIII.30})$$

where  $L_k$  and  $\gamma_{ij}$  are given, respectively, by Eqs. (VIII.18) and (VIII.19).

Satisfying the constraint in Eq. (VIII.30) prevents a sign change (preventing the introduction of RHP poles) in the characteristic equation of the improved method plants' of Eq. (VIII.17). This enhances the ability to design a stabilizing compensator for each successive feedback loop. Given the range of plant uncertainty defined by the templates and variation of  $\gamma_{ij}$  among the plant cases, each gamma bound is generated such that Eq. (VIII.30) is satisfied when the nominal loop transmission  $L_{i0}$  does not violate the gamma bound.

### VIII.13.4 Allocated Tracking Bounds

For tracking problems, allocated tracking bounds are used to insure that variation in closed loop frequency domain transmission  $t_{ii}$  of the diagonal MISO loop does not exceed the variation  $\delta_R$  permitted by the performance specifications. Variation in the closed loop transmission of the diagonal MISO loop results from both uncertainty in the response due to tracking and from the presence of the cross-coupling effects:

$$t_{ii} = t_{i_{ii}} + t_{c_{ij}} \quad (\text{VIII.31})$$

where  $t_{ii}$  and  $t_{dij}$  are given, respectively, by Eqs. (VIII.11) and (VIII.12). The constraint on  $L_i$  used to determine a point on the

tracking bound is:

$$Lm(T_{R_{max}} + t_{c_{iimax}}) - Lm(T_{R_{min}} - t_{c_{iimax}}) \leq \delta_R \quad (\text{VIII.32})$$

where the transmission  $T_R$ , with unity gain prefilter, is:

$$T_R = \frac{L_i}{1 + L_i} \quad (\text{VIII.33})$$

and the most extreme transmission due to cross-coupling effects is:

$$t_{c_{iimax}} = \frac{|C_{iimax}| |T_{R_{max}}|}{|g_i|} \quad (\text{VIII.34})$$

Because points on the cross-coupling bound (if generated) are identical to those on the allocated tracking bound for the value of  $c_{iimax}$  in Eq. (VIII.34), only an allocated tracking bound is generated for diagonal MISO loops. By constraining  $L_i$  to be above the bound, the actual variation in  $t_{ii}$  is less than  $t_{c_{iimax}}$ .

#### **VIII.13.5 External Disturbance Rejection Bounds**

External disturbance bounds are plotted for each template, one for each MISO loop in the row of MISO loops for which the compensator is to be designed [see Eqs. (VIII.14) and (VIII.15)]. The disturbance entering the (ij) MISO loop resulting from the external disturbance entering through  $P_d$  and from the cross-coupling transmissions is given by Eq. (VIII.16). The specifications dictate that  $d_{e_{ij}}$  is less than an upper bound for each plant case  $i$  in the set of  $J$  plants; i.e.:

$$|d_{e_{ij}}|_i \leq |[P_e^{-1} P_d]|_i + \sum_{k \neq i}^m \left[ \frac{|t_{kj}|}{|q_{ik}|} \right] \quad (\text{VIII.35})$$

For a Method 2 design in which the improved method has already been applied, (say  $n$  times so far) the calculation of

$$(|d_{e_{ij}}|_{\max})_i$$

is modified as follows: by replacing the term  $|t_{kj}|/|q_{ik}|$  in the summation above (a) with  $|b_{kj}|/|q_{ik(n)}|$ , which is utilized when the improved method has not yet been applied, and (b) with

$$\frac{|g_k^{-1}[P_e^{-1}]_{kj}|}{|q_{ik(n)}|_1} \quad (\text{VIII.36})$$

when the improved method has been applied to take into account the designed open loop transmission  $L_k$ .

#### VIII.13.6 Composite Bounds

A set of composite bounds is formed based on any or all of the tracking, stability, cross-coupling effects, external disturbance rejection, and gamma bounds. The composite bound for a given frequency is formed by retaining the most restrictive portion of the bounds for the given frequency for which the composite bound is formed.

#### VIII.14 Compensator Design (see blocks 24-25 in Fig. VIII.1)

The compensator for an analog system (a controller for a discrete system) is designed to satisfy design specifications for the entire row of MISO loops in which the compensator is used. Since  $L_{i_0} = g_i q_{iio}$  is the same for all MISO loops in a given row, bounds for all MISO loops are plotted together on the NC. The compensator design may thus be performed for an entire row of MISO loops using a single design iteration based on composite bounds plotted on the NC.

The open-loop transmission is shaped by adding, deleting, or modifying the poles and zeros of the compensator and by allowing adjustment of the gain until an acceptable loop shape is obtained. Stability is checked during loop shaping by examining the nominal closed-loop MISO transmission in factored form. All closed-loop s- or w-domain

poles should be in the left-half-plane. For a discrete design,  $g_i(w)$  is transformed by a bilinear transformation to  $g_i(z)$ . As a validation check, the Bode plots of  $g_i(w)$  and  $g_i(z)$  are compared for  $0 < \omega < 2/3(\omega_s/2)$ . If very close, then one can proceed, since robustness will be maintained in the  $z$ -domain. Next, proceed with the formation of  $\Delta_i(z) = L_i(z)/[1 + L_i(z)]$  in order to ensure that all the poles of  $\Delta_i(z)$  are inside the unit circle (see block 26 in Fig. VIII.1). If not,  $g_i$  needs to be modified in order to achieve a stable system for all cases.

#### **VIII.15 Prefilter Design (see block 28 in Fig. VIII.1)**

The proper design of the compensator guarantees that the variation in closed loop transmission due to uncertainty for  $t_{ii}$  is acceptable, but does not guarantee that the transmission is within the upper and lower performance tolerances  $a_{ii}$  and  $b_{ii}$ . The prefilter is therefore required to translate the closed loop transmission  $t_{ii}$  such that it satisfies the upper and lower performance tolerances.

The prefilter design begins with the determination of  $T_{Rmax}$  and  $T_{Rmin}$ , the maximum and minimum closed loop transmission due to tracking  $T_R$  with unity gain prefilter, respectively, at each template frequency  $\omega_i$  using Eq. (VIII.33). As is the case for tracking bounds on the NC, a portion of the permitted range of variation of  $t_{ii}$  is allocated to the cross-coupling effects. Thus, restricted tolerances are placed on  $t_{ii}$

$$b'_{ii} = b_{ii} - |t_{c_{iimax}}| \quad (\text{VIII.37})$$

$$a'_{ii} = a_{ii} + |t_{c_{iimax}}| \quad (\text{VIII.38})$$

and the filter bounds on the nominal  $t_{ii}$  are as follows:

$$Lm(b'_{ii}) - Lm(T_{Rmax}) \quad (\text{VIII.39})$$

$$Lm(a'_{ii}) - Lm(T_{Rmin}) \quad (\text{VIII.40})$$

Once the filter bounds are generated, a prefilter is synthesized such that the Bode plot of the nominal  $t_n$  lies between the two filter bounds and satisfies  $t_n(s) = 1$  in the limit as  $s \rightarrow 0$ . For a discrete design,  $F(w)$  is transformed by a bilinear transformation to  $F(z)$ . As a validation check, the Bode plots of  $F(w)$  and  $F(z)$  are compared for  $0 < \omega < 2/3(\omega_s/2)$  (see block 29 in Fig. VIII.1). If very close, then one can proceed, since robustness will be maintained in the  $z$ -domain.

#### VIII.16 Design Validation (see blocks 25-31 in Fig. VIII.1)

The CAD package provides a number of tests to validate that the completed MIMO design meets the stability and performance specifications for the  $J$  plant cases. First (block 27), poles of  $\Delta_i$  for each feedback loop  $i$  are checked to validate that all poles of the characteristic equation are stable. If some plants are n.m.p., one cannot rely on the loop shapes on the N.C.

For the second test (block 31), an array of the  $J$  open-loop MISO loop transmissions  $(L_i)_i = g_i(q_{ii})_i$  for all plant cases  $i = 1, 2, \dots, J$  are plotted on the NC along with the  $M_L$  contour to validate that the stability requirements are satisfied for each feedback loop  $i$ . If no open loop transmission violates the  $M_L$  contour, then the stability specifications are satisfied.

For tracking control problems an  $m \times m$  array of Bode magnitude plots is generated for the  $m \times m$  matrix of elements  $t_{ij}$  of the closed-loop transfer function matrix  $T$ , where:

$$T = [I + P_o G]^{-1} P_o G F \quad (\text{VIII.41})$$

where  $I$  is the identity matrix, and  $P_o$ ,  $F$ , and  $G$  are the  $m \times m$  plant matrix, the  $m \times m$  diagonal prefilter matrix, and the  $m \times m$  diagonal compensator matrix, respectively.

Each Bode plot illustrates the frequency domain transmission  $t_{ij}$ , for the set of  $J$  plant cases along with the tracking performance

specifications, to allow the designer to validate that performance specifications placed on the closed-loop system have been met over the frequency range of interest. For each diagonal  $t_{ii}$ ,  $J$  Bode magnitude plots are plotted along with the performance bounds  $a_{ii}$  and  $b_{ii}$ . For each off-diagonal  $t_{ij}$ ,  $J$  Bode magnitude plots are plotted along with the performance bound  $b_{ij}$ .

For external disturbance rejection problems, a set of  $J$  Bode magnitude plots are plotted for each  $t_{ij}$ , along with the external disturbance rejection specifications  $b_{ij}$ . The  $m \times m$  closed-loop transfer function matrix  $T$ , whose elements  $t_{ij}$  are the transmissions plotted on the Bode plots, is formed for the  $J$  plant cases based on the equation:

$$T = [I + P_e G]^{-1} P_d \quad (\text{VIII.42})$$

where  $I$  is the identity matrix, and  $P_d$ ,  $P_e$ , and  $G$  are the  $m \times m_d$  external disturbance plant matrix, the  $m \times m$  effective plant matrix, and the  $m \times m$  diagonal compensator matrix, respectively.

For the final validation, MATLAB SIMULAB models are generated based on the completed design, one for each of the  $J$  plant cases. The designer can then insert nonlinear elements such as saturation or rate limits, and add anti-windup protection. The model is then simulated to verify that the time domain figures of merit specifications are satisfied. For a continuous control problem, an analog simulation is performed. For a discrete control problem, a hybrid simulation is performed based on the  $s$ -domain effective plants  $P_e(s)$ , and the  $z$ -domain compensator  $G(z)$ , and prefilter  $F(z)$ .

#### VIII.17      Summary

Version 3 of the MIMO/QFT CAD package has been developed for both analog- and discrete-time control system design based on Mathematica. The design procedure is automated. This includes problem setup, equivalent plant formation, compensator and prefilter design and design validation for  $m \times m$  MIMO systems. Bound generation routines have been

optimized to reduce overdesign. The package has been extended to handle in a unified way external disturbance rejection problems as well as tracking control problems.



## Chapter IX Development, Implementation & Flight Test Of A Mimo Digital Flight Control System For An Unmanned Research Vehicle

### IX.1 Introduction

The intent of this chapter is to provide the reader with an insight into the development of a QFT FCS and into the trials and tribulations in achieving successful flight tests. In this respect, this chapter is different from most papers that concentrate only on the theoretical aspects of a flight control system design. Thus, a discussion of the development, implementation, and successful flight test of a flight control system, designed using QFT techniques, is presented in this chapter. The flight control system was designed for and flown on the Lambda Unmanned Research Vehicle (URV), Fig. IX.1. It is a remotely piloted aircraft with a wingspan of 14 feet. It is operated by Wright Laboratory for research in flight control technology .

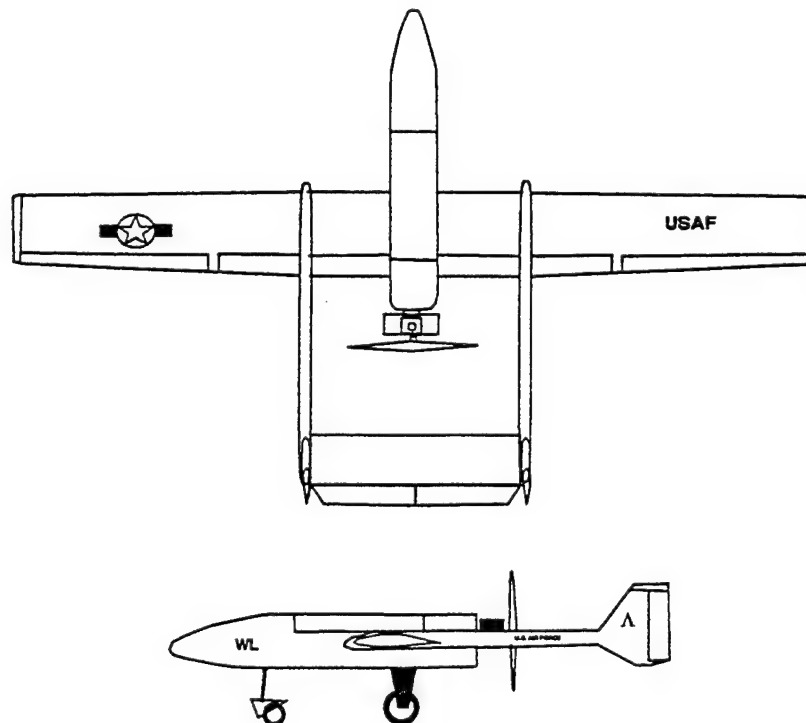


Fig. IX.1 Lambda unmanned research vehicle.

## IX.2 Objective

The objective of the project was twofold. First, develop a robust flight control system using QFT, and take the design through flight test. Second, implement an inner loop FCS on the Lambda URV that would be part of an autonomous flight control system. During the project the first objective was accomplished and then, because of hardware improvements, a second design was developed and flight tested. This second design was accomplished to better meet the requirements of the second objective. The FCS design process used is shown in Fig. IX.2. As indicated by the heavy dashed line one complete FCS design cycle covers the process through the flight test and then back to the redesign stage. During this project there were four cycles around this loop. Two of the cycles produced unsuccessful flight tests and two produced successful flight tests.

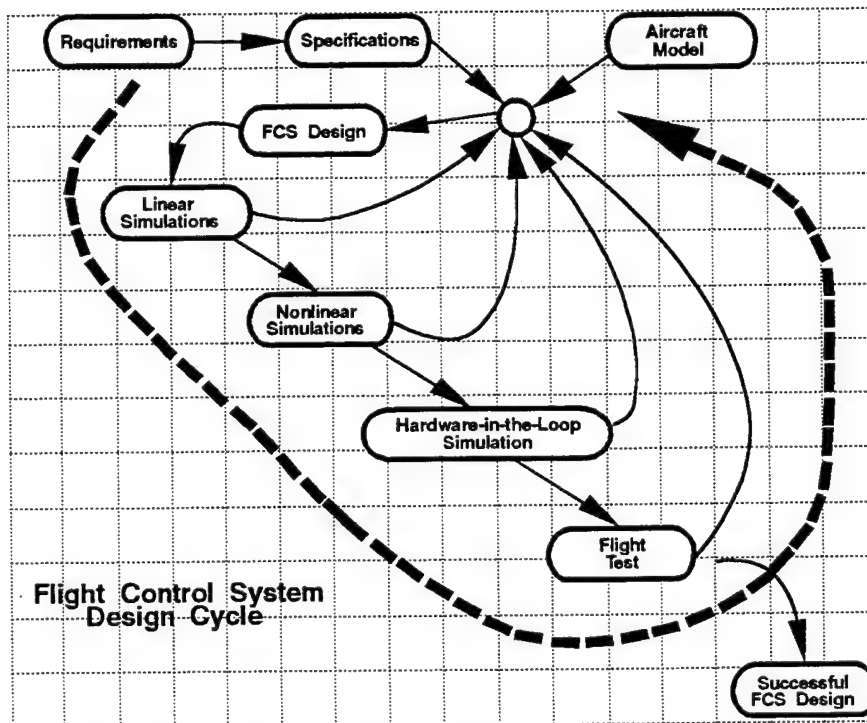


Fig. IX.2 Flight control system design process.

### IX.3 First Design Cycle

#### IX.3.1 Requirements

There were two major design requirements for this project. The first was a desire to develop a robust flight control system using QFT, and take the design through flight test. The second was a need for an inner loop FCS on Lambda that would interface with a autonomous waypoint directed autopilot.

#### IX.3.2 Specifications

The time response specifications were selected base on the open loop response of Lambda. The pitch rate is an underdamped response that settles fairly quickly. Overshoot and settling time were chosen to be 25% and one second for pitch rate response. Roll rate is an over-damped response that settles quickly, and the settling time was chosen to be one second. Yaw rate is also underdamped, but it doesn't reach steady state as fast as the other two. Yaw rate overshoot and settling time were chosen to be 15% and two seconds, respectively. These specifications were transformed into thumbprints.

#### IX.3.3 Aircraft Model

The aircraft model developmental process began with the use of Digital Datcom, a computer program which predicts stability and control derivatives for aerospace vehicles based on the physical characteristics of the vehicle. Datcom information formed the baseline model of the aircraft. This baseline model was refined by using system identification software to estimate the aerodynamic derivatives from actual flight test data<sup>74</sup>. Maximum likelihood identification was used to identify the natural frequency and damping ratios of the short period and roll modes. This information combined with the Datcom information provided a working model for the flight control system design.

#### IX.3.4 FCS Design

Much of the preliminary QFT design work was accomplished at the Air Force Institute of Technology<sup>56,78</sup>. The first<sup>56</sup> was based on the DATCOM model of lambda alone. The second<sup>78</sup> design was based on the DATCOM model with the refinements made with system identification. The latter design used linearized transfer functions to represent Lambda in various flight conditions, covering the entire proposed flight envelope, to accomplish the design and for linear simulations.

#### IX.3.5 Linear Simulations

All FCS designs were simulated using MATRIX<sub>x</sub> and linear time invariant state space models representing the full flight envelope of Lambda. After successful linear simulations, nonlinearities such as control surface travel limits were introduced into the linear simulation.

#### IX.3.6 Nonlinear Simulations

During the same period, a nonlinear simulation was developed at Wright Laboratory. This simulation incorporated a six degree of freedom simulation, automatic trim calculation, air vehicle kinematics, and control surface saturation. While this design produced the desired responses in the linear simulation, when implemented in the nonlinear simulation, the original control system exhibited undesirable behavior. The assumptions about allowable gain had been made that were not valid and had to be corrected. Thus, the allowable gain was modified to obtain the redesigned controller.

#### IX.3.7 Hardware-in-the-Loop Simulation

Software from the nonlinear simulation was used to develop a hardware-in-the-loop simulation<sup>65</sup>. This simulation allowed the implemented FCS, which was programmed on a EPROM chip, to be tested in the aircraft. When the FCS was implemented in this simulation, it was discovered that the angular rate sensors had high levels of noise, on

the order of 0.5 deg/sec. The FCS amplified this noise and this effectively masked any control command signal. The noise was recorded and incorporated into the nonlinear simulation. By this time, a new QFT computer-aided-design program was developed by AFIT for designing control systems which allowed for a rapid redesign to minimize the noise problem. The FCS was redesigned, tested in all three simulations and then test flown.

### **IX.3.8 Flight Test**

Two major difficulties caused the first flight test to fail, the first was reversed polarity on an angle sensor and the second was a integrator wind-up limiter scheme that did not work. Since the inner loop FCS was to be implemented as a part of an autonomous system, turn coordination logic was implemented around the inner loop FCS that relied on the roll angle. Post flight analysis of the flight test video and data showed that the polarity of the roll angle sensor was backward, thus, when the aircraft was commanded to bank, the rudder was commanded to deflect in the wrong direction. The FCS was turned off and testing involving the lateral control channel was terminated. Later, during the same flight test, when the FCS pitch channel was turned on, the aircraft developed a high pitch rate. This test was terminated and post analysis revealed that the scheme used to limit integrator wind-up had caused a numerical instability.

## **IX.4 Second Design Cycle**

### **IX.4.1 Requirements**

The requirements for the second design cycle did not change from the original requirements. An additional requirement involved the design of an improved integrator wind-up limiter.

### **IX.4.2 Specifications**

The specifications for the second design cycle did not change from the original requirements.

### IX.4.3 Aircraft Model

The aircraft model for the second design cycle did not change from the original requirements.

### IX.4.4 FCS Design

Since the problems encountered in the first test didn't have anything to do with the QFT designed FCS, the FCS remained unchanged for the second flight test. During the second flight test, there was no attempt to use a turn coordination algorithm. The implementation involved a major change in the FCS design. The integrator wind-up limiter involved a different form of implementation for the second design cycle. In this cycle the FCS's controller was implemented by factoring the s-domain compensator  $G_c(s)$  into poles and zeros, i.e., grouping individual poles with zeros to form w first- or second-order cascaded compensators, which are then transformed individually into the z-domain (see Fig. IX.3). The individual z-domain transfer functions were each then implemented to obtain the complete FCS transfer functions. This implementation allowed limitations to be placed only on those pieces of the FCS that contained pure integrators. Also, it provides a higher degree of accuracy in the software implementation.

### IX.4.5 Linear, Nonlinear, Hardware-in-the-Loop Simulation

All simulations consisted of checking out the new implementation of the FCS. There were no problems encountered during any of these simulations.

### IX.4.6 Flight Test

On 20 Nov 92, the temperature was in the 60s with winds at five to seven mph. Lambda was flown stick to surface for take-off, setup, and landing. Due to problems with the first flight test the FCS was engaged only during the test maneuvers and disengaged. The maneuvers performed consisted of unit step commands in all three axes. This set of

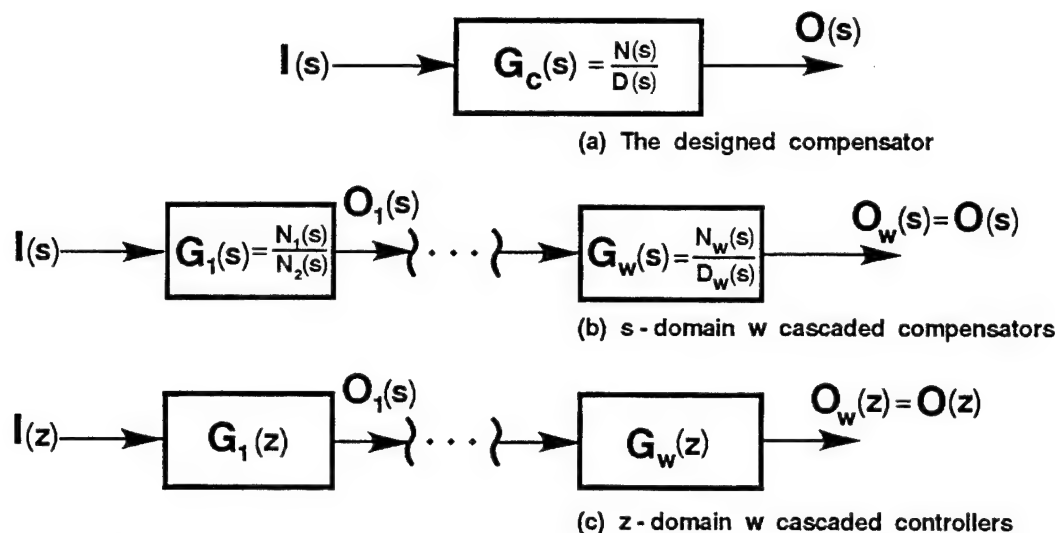


Fig. IX.3 s-domain to z-domain formulation for implementation of the  $G(z)$  controller.

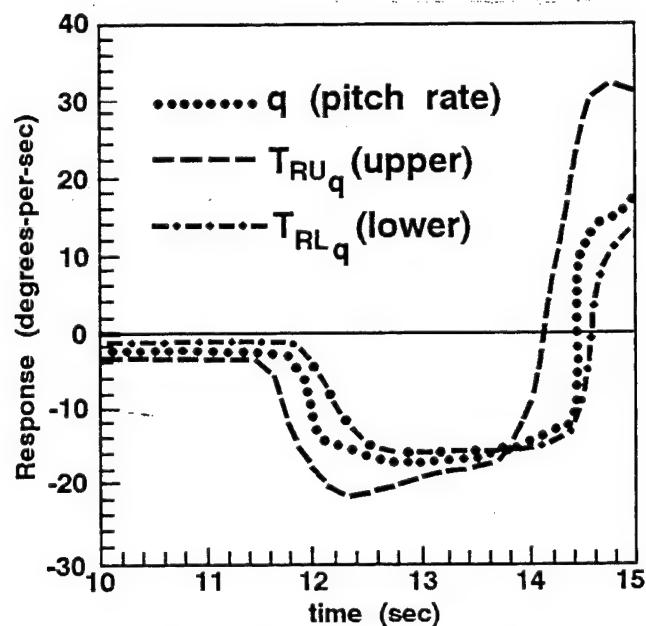


Fig. IX.4 Response to pitch-down command.

maneuvers was first performed with the QFT FCS and then with the open loop aircraft. The response of the controller was very good in that it performed as it was designed. Figure IX.4 represents the response of Lambda to a step pitch down command. The dotted lines in the plot represent the specified response thumbprint. It is important to note that during this maneuver the aircraft covered most of its flight envelope by varying in forward airspeed from 75 kts to 110 kts.

## **IX.5 THIRD DESIGN CYCLE**

### **IX.5.1 Requirements**

The requirements for the third design cycle had not changed from the original requirements. This cycle involved the design of an inner loop FCS that had intrinsic turn coordination. After the second flight test, the sensor noise problem had been reduced by an order of magnitude by the addition of a hardware noise filter on the output of the sensors. This allowed a redesign of the FCS to improve the system performance.

### **IX.5.2 Specifications**

#### **Sideslip Command**

For this iteration of the design a sideslip angle command was incorporated as part of the inner loop controller. Since Lambda has a sideslip sensor, a sideslip command was used to cause the aircraft to intrinsically fly coordinated turns. That is, the goal of turn coordination is to reduce the amount of sideslip angle during a turn by using the proper amount of rudder deflection during the turn.

#### **Yaw Damper**

Changing to sideslip command allowed the use of the yaw rate sensor to implement a yaw damper to reduced the phugoid mode oscillations. This yaw damper was implemented by adding a washout filter, designed through the use of a root locus plot. The yaw damper was designed and then incorporated in the aircraft model for a FCS design.

#### **Specification Change**

During the second flight test the pilot felt that the aircraft's roll rate response was too slow. Therefore, the roll rate response was change to match that of the pitch rate.

### **IX.5.3 Aircraft Model**

#### **Sensor Improvement**

After the second flight test, the problem of sensor noise was



fixed, reducing the noise by an order of magnitude.

#### **Model Refinement**

During the system identification work for the second aircraft model, some of the parameters had been scaled incorrectly. This caused some modeling errors. After the second flight test these errors were corrected through the use of system identification applied to flight test data.

#### **IX.5.4 FCS Design**

MATRIX<sub>x</sub> was used to develop linearized plant models about flight conditions in the flight envelope. An attempt was made to choose flight conditions in such a way as to fully describe the flight envelope with the templates. To do this a nominal flight condition was chosen to be 50 kts forward velocity, 1,000 feet altitude, 205 pounds, and center of gravity at 29.9% of the mean aerodynamic cord. From this nominal trim flight condition, each parameter was varied, in steps, through maximum and minimum values, while holding the other parameters at their nominal trim values. These variations produced a initial set of templates. On these templates variation corresponding to each parameter was identified. Each variation when translated, on the template, identified an expanded template area of the flight envelope that required more plants for better definition, see Fig IX.5.

#### **IX.5.5 Linear, Nonlinear, and Hardware-in-the-Loop Simulations**

The refined Lambda model was implemented in all three simulations. The FCS was implemented in cascaded method outlines previously. All simulations produced the desired responses to given stimulus.

#### **IX.5.6 Flight Test**

During the third flight test, when the FCS was engaged, the aircraft exhibited an uncontrolled pitching, or porpoising, behavior. While the post flight test analysis was inconclusive, a longitudinal bending mode at 13.2 radians/second seemed to be the likely cause.

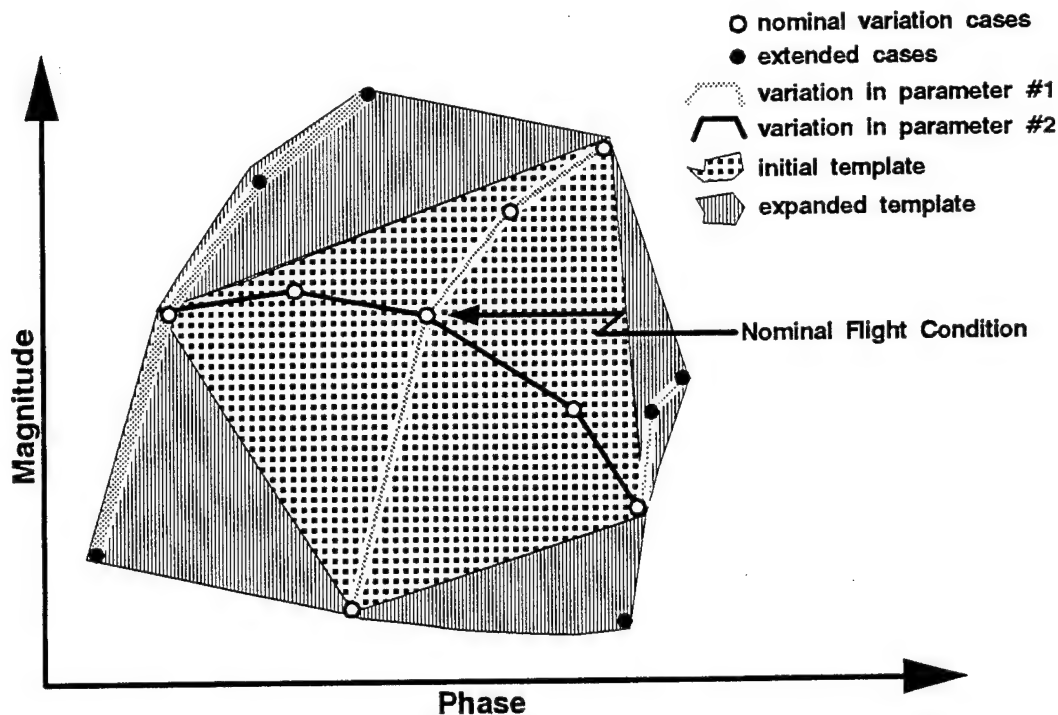


Fig. IX.5 Template expansion process.

## IX.6 FOURTH DESIGN CYCLE

### IX.6.1 Requirements

The requirements for the Second flight test had not changed from the original requirements, but involved a refinement in the aircraft model to incorporate a bending mode.

### IX.6.2 Specifications

The specifications for the fourth design cycle were the same as those for the third.

### IX.6.3 Aircraft Model

A model of the porpoising behavior encountered in the third flight test was identified by assuming that the behavior was caused by an unmodeled effect. Various models were incorporated into the nonlinear model and simulated. This simulation used the flight test inputs as

simulation inputs and compared the simulated outputs to the flight test data. Using this procedure, a violation of the gain margin was ruled out by increasing the inner loop gain in the model and observing the response. Instability caused by actuator rate limiting was ruled out by inserting severe rate limited actuator models in the nonlinear simulation. When a bending mode, modeled as a lightly damped pair of poles, was inserted in the model, the simulated responses were very similar to the flight test results.

#### **IX.6.4 FCS Design**

MATRIX<sub>x</sub> was used to develop linearized plant models about the given flight conditions and the FCS was redesigned based on the model containing the bending mode. Note, when the FCS from design cycle three was inserted in the loop with the aircraft model with the bending mode, there were violations of stability criteria in the frequency domain.

#### **IX.6.5 Linear, Nonlinear, and Hardware-in-the-Loop Simulation**

The new model was implemented in all three simulations and tested. The new model was tested with both the FCS cycle 3 and the FCS cycle 4. As expected the porpoising behavior occurred with the FCS cycle 3. The FCS cycle 4 responded within specifications.

#### **IX.6.6 Flight Test**

The fourth flight test occurred in September 1993. The field conditions were a little gusty, but within acceptable limits for the experiment. During the flight the FCS was engaged and then left engaged for the entire series of tests. The FCS performed as designed. The intrinsic turn coordination scheme worked as designed. The pilot was pleased with the handling qualities and felt comfortable flying with the FCS engaged at all times. His one criticism was that the roll rate was too slow. Since our roll rate was limited by the maximum roll rate detectable by the rate sensors, the problem was unavoidable. When the data was examined, it was found that all of the 60 hz data had been

data showed that the FCS did cause Lambda to respond within the specified envelope, during onset of the command, but, in some cases, Lambda's response exhibited more overshoot and longer settling time than specified. These problems could be attributable to the gusty conditions, since no gust disturbance was specified during the design process. More flight testing of this FCS will be required to answer this question.

### IX.7 Conclusions

This series of FCS design cycles has highlighted many of the benefits of using a robust design technique, such as QFT, to design and implement FCSs. Some of those benefits are:

- a. The result is a robust design which is insensitive to plant variation.
- b. There is one design for the full envelope (no need to verify plants inside templates).
- c. Any design limitations are apparent up front.
- d. There is less development time for a full envelope design.
- e. One can determine what specifications are achievable up early in the design. One can redesign for changes in the specifications quickly.
- f. The structure of controller is determined up front.

The goals of this program were to reveal the benefits of QFT as a robust control technique, and to prove that a robust flight control system could be implemented. It is felt that these goals were successfully achieved.

## Appendix A Design Examples

### A.1 MISO Design Problem

Given the plant transfer function:

$$P(s) = \frac{k}{s + a} \quad \text{with the structured parameter uncertainty of}$$

$$1 \leq k \leq 100, \quad -3 \leq a \leq 3$$

Specifications on  $|T_R(j\omega)|$  is given in the following table:

$\omega$	0	0.5	1	2	5	10	20
Lm $b(j\omega)$	0	1	1	0	-4	-10	-20
Lm $a(j\omega)$	0	-2	-4	-8	-20	$\begin{smallmatrix} (-40) \\ \infty \end{smallmatrix}$	$\begin{smallmatrix} (-80) \\ \infty \end{smallmatrix}$

$$M_L < 3 \text{ dB} \quad \lambda > 3 \quad \text{No specifications on } T_D$$

Nominal Plant:  $P_0(s) = 1/s \quad (k = 1, a = 0)$

Problem: Design  $L_0(s)$  and  $F(s)$  to meet the specifications.

Solution:

A. Template Generation -- The set of  $J$  plant transfer functions  $P_i(a_i, k_i)$ , where  $P_i \in \mathcal{P}$  and  $i = 1, 2, \dots, J$ , used to obtain the templates are:

$$P_1(3,1), P_2(0,1), P_3(-3,1), P_4(-3,100), P_5(0,100), \text{ and } P_6(3,100)$$

The templates all have the shape shown in Fig. A.1 where  $V = 40$  dB and as  $\omega$  increases the templates become narrower. It is left to the reader to obtain the templates in order to verify the solution to this problem.

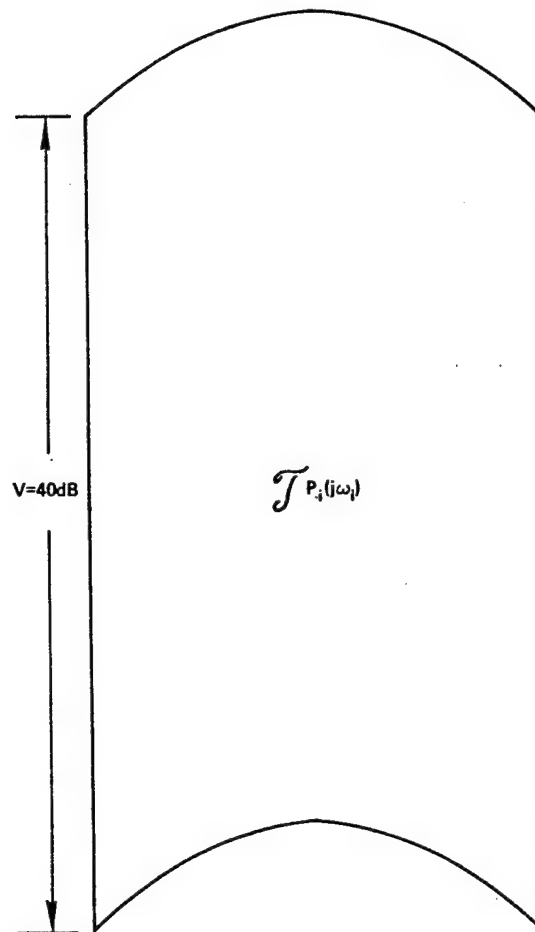


Fig. A.1 Template  $\mathcal{S}P_i(j\omega_i)$

B. Determination of Boundaries  $B_R(j\omega_i)$  -- The templates are used to determine the boundaries  $B_R(j\omega_i)$  and, along with the values of  $L_m$   $M_L$  and  $V$ , to determine the U-contour as shown in Fig. A.2.

C. Determination of  $L_o(s)$  --- The design of an optimum  $L_o(s)$  is not unique. Two possible designs of an  $L_o(s)$  are shown in Fig. A.2. The designs at the onset should be based upon a qualitative analysis of

$$L(s) = G(s)P(s) = \frac{kG(s)}{s + a} \quad (\text{A.1})$$

and

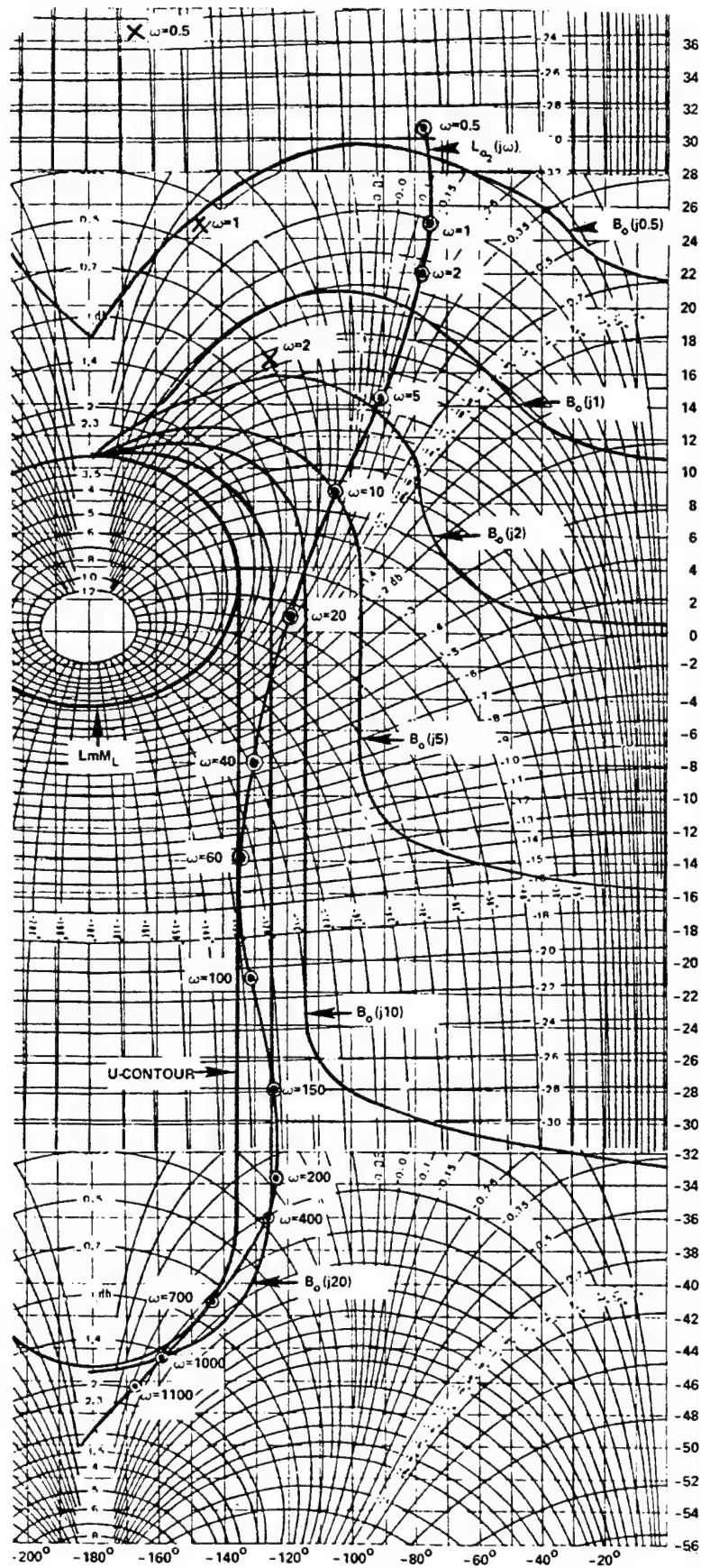


Fig. A.2 Plots of  $B_R(i\omega_l)$  and  $L_o(j\omega)$

$$L_o(s) = G(s) P_o(s) = \frac{kG(s)}{s} \quad (\text{A.2})$$

Trial 1 -- A type 0  $L_o(s)$  function requires the compensator to be of the format of:

$$G(s) = \frac{Ks( \quad ) \dots ( \quad )}{( \quad ) \dots ( \quad )} \quad (\text{A.3})$$

which from Eqs. (A.1) and (A.2) results in, respectively:

$$L(s) = \frac{kK( \quad ) \dots ( \quad )}{(s + a)( \quad ) \dots ( \quad )} \quad (\text{A.4})$$

and

$$L_{o_1}(s) = \frac{kK( \quad ) \dots ( \quad )}{( \quad ) \dots ( \quad )} \quad (\text{A.5})$$

When  $a \neq 0$ , Eq. (A.4) results in

$$T_{R_1}(s) = \frac{kKs( \quad ) \dots ( \quad )}{( \quad ) \dots ( \quad )} F(s) \quad (\text{A.6})$$

and  $Lm T_R(j\omega) = -\infty$  dB which is unacceptable.

Trial 2 -- A Type 1  $L_o(s)$  requires the compensator to be of the format:

$$G(s) = \frac{K( \quad ) \dots ( \quad )}{( \quad ) \dots ( \quad )} \quad (\text{A.7})$$

which from Eqs. (A.1) and (A.2) results in, respectively:

$$L(s) = \frac{kK( \quad ) \dots ( \quad )}{(s + a)( \quad ) \dots ( \quad )} \quad (\text{A.8})$$

and

$$L_{o_2}(s) = \frac{kK( \quad ) \dots ( \quad )}{s( \quad ) \dots ( \quad )} \quad (\text{A.9})$$

When  $a = 0$ ,  $T_R(s)$  corresponds to a Type 1 system and when  $a \neq 0$   $T_R(s)$  corresponds to a Type 0 system. Assuming this is acceptable an  $L_o(s)$  is synthesized, as shown in Fig. A.2, and results in



$$G(s) = \frac{8.504 \times 10^6 (s + 1) (s + 12) (s + 120)}{(s + 2) (s + 10) (s + 26.5) (s + 720 \pm j960)} \quad (\text{A.10})$$

In order to achieve the desired specification  $e(\infty) = r(\infty) - c(\infty) = 0$ , for  $r(t) = u_1(t)$ , then the compensator  $G(s)$  must be a Type 1 transfer function in order to yield a Type 1 system for  $a \neq 0$  and a Type 2 system for  $a = 0$ . The synthesized loop transmission function is

$$L_{o_3} = \frac{kK( \quad ) \cdots ( \quad )}{s^2( \quad ) \cdots ( \quad )} \quad (\text{A.11})$$

for which three points (denoted by X) are shown in Fig. A.2. It is left to the reader to complete the synthesis of an  $L_o(s)$ .

**D. Design of  $F(s)$**  --- Based upon the design procedure in Chap. I<sup>15</sup>, the following nonunique filter is obtained:

$$F(s) = \frac{1.5}{s + 1.5} \quad (\text{A.12})$$

**E. Simulation of Design** --- A simulation of the system for  $L_o(s)$  is made for each  $P_i(a_i, k_i)$ , where  $i = 1, \dots, 6$ , based upon Eqs. (A.10) and (A.12). The simulations indicate that all the specifications on  $|T_R(j\omega)|$  are met except, as expected, when  $a \neq 0$  and  $\omega = 0$ . The reader can simulate the system utilizing his  $L_{o_3}(s)$ .

## A.2 MIMO Design Problem

Given: A 2x2 plant where

$$Q(s) = \frac{1}{s} \begin{bmatrix} k_{11} & k_{12} \\ k_{21} & k_{22} \end{bmatrix} \quad (\text{A.13})$$

has the following independent structured plant parameter uncertainties:

$$\begin{aligned} 1 \leq k_{11} \leq 2 & \quad 0.5 \leq k_{12} \leq 2 \\ 5 \leq k_{21} \leq 10 & \quad 0.5 \leq k_{22} \leq 1 \end{aligned}$$

The diagonal dominance condition (Sec. III.7) requires, as  $\omega \rightarrow \infty$ , that

$$|q_{11}q_{22}| < |q_{12}q_{21}| \Rightarrow 2 < 2.5$$

### Specifications:

(a) There is only one command input:  $r_2(t)$

(b)  $|t_{12}| < -20$  dB for all  $\omega$

(c) For  $|t_{22}|$ :

Table A.1

$\omega$	0	0.5	1	2	5	10	20
$\text{Lm } b_{22}(j\omega)$	0	1	1	0	-4	-10	-20
$\text{Lm } a_{22}(j\omega)$	0	-2	-4	8	20	$-\infty$ (-40)	$-\infty$ (-80)

The values of  $a_{22}(j\omega)$  are considered to be zero for  $\omega > 5$ , and thus

$$\lim_{\omega > 5} [a_{22}(j\omega)] = -\infty$$

(d) For  $L_1 = g_1q_{11}$  and  $L_2 = g_2q_{22}$ , respectively:

$$Lm M_{L_1} \leq Lm \left[ \frac{L_1}{1 + L_1} \right] \leq 3 \text{ dB} \quad (\text{A.14})$$

$$Lm M_{L_2} \leq Lm \left[ \frac{L_2}{1 + L_2} \right] \leq 3 \text{ dB} \quad (\text{A.15})$$

Problem: Design  $L_1(s)$ ,  $L_2(s)$ , and  $f_{22}(s)$ .

A.  $L_1(s)$  Design --- For loop one design, see Fig. A.3, let  $f_{12} = 0$  (i.e., decouple output 1 from input 2). With  $f_{12} = 0$  then the loop 1 design becomes strictly a cross-coupling rejection problem (see Fig III.11).

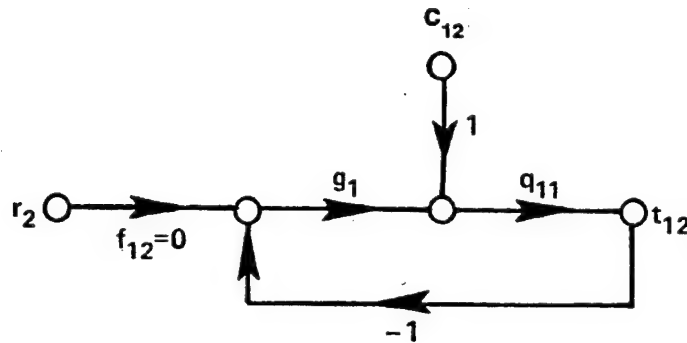


Fig. A.3 Loop one

Thus, from Eqs. (III.35) through (III.41) and Eqs. (III.50) through (III.53), where for an impulse input  $t_{ij} = y_{ij}$ :

$$t_{12} = \frac{q_{11}(g_1 \overset{0}{f_{12}} + c_{12})}{1 + g_1 q_{11}} = \frac{q_{11} c_{12}}{1 + g_1 q_{11}} \quad (\text{A.16})$$

Based upon the given disturbance rejection specification

$$|t_{12}| = \left| \frac{q_{11}c_{12}}{1 + g_1q_{11}} \right| \leq 0.1 \quad (\text{A.17})$$

which is rearranged to

$$|1 + g_1q_{11}| \geq \left| \frac{q_{11}c_{12}}{0.1} \right| \quad (\text{A.18})$$

Since

$$c_{12} = -t_{22}/q_{22} \quad (\text{A.19})$$

Equation (A.19) is substituted into Eq. (A.18) to yield

$$|1 + g_1q_{11}| \geq \left| \frac{10q_{11}t_{22}}{q_{12}} \right| \quad (\text{A.20})$$

Applying the maximum tracking specification value for  $|t_{22}|$  yields:

$$|1 + g_1q_{11}| \geq \left| \frac{10b_{22}q_{11}}{q_{12}} \right| \quad (\text{A.21})$$

Thus, this constraint imbeds the cross-coupling rejections bounds specifications on  $y_{12}(t)$ . As a consequence the cross-coupling bounds  $B_{c_i}(j\omega_i)$  become the composite bounds  $B_{c_i}(j\omega_i)$ . For the plant uncertainty a template can be generated for  $q_{11}$  which is good (for this particular design problem) for all  $\omega$ . The template is simply a 6 dB vertical line. Also, from the specification  $Lm M_L \leq 3$  dB and the uncertainty in  $q_{11}$  at  $\omega = \infty$ , the universal high frequency boundary can be drawn as shown in Fig. A.4. The nominal plant  $q_{11}$  is chosen to be the  $i$  which is at the bottom of the 6 dB template. Thus,

$$q_{11}(s) = \frac{1}{s} \quad (\text{A.22})$$

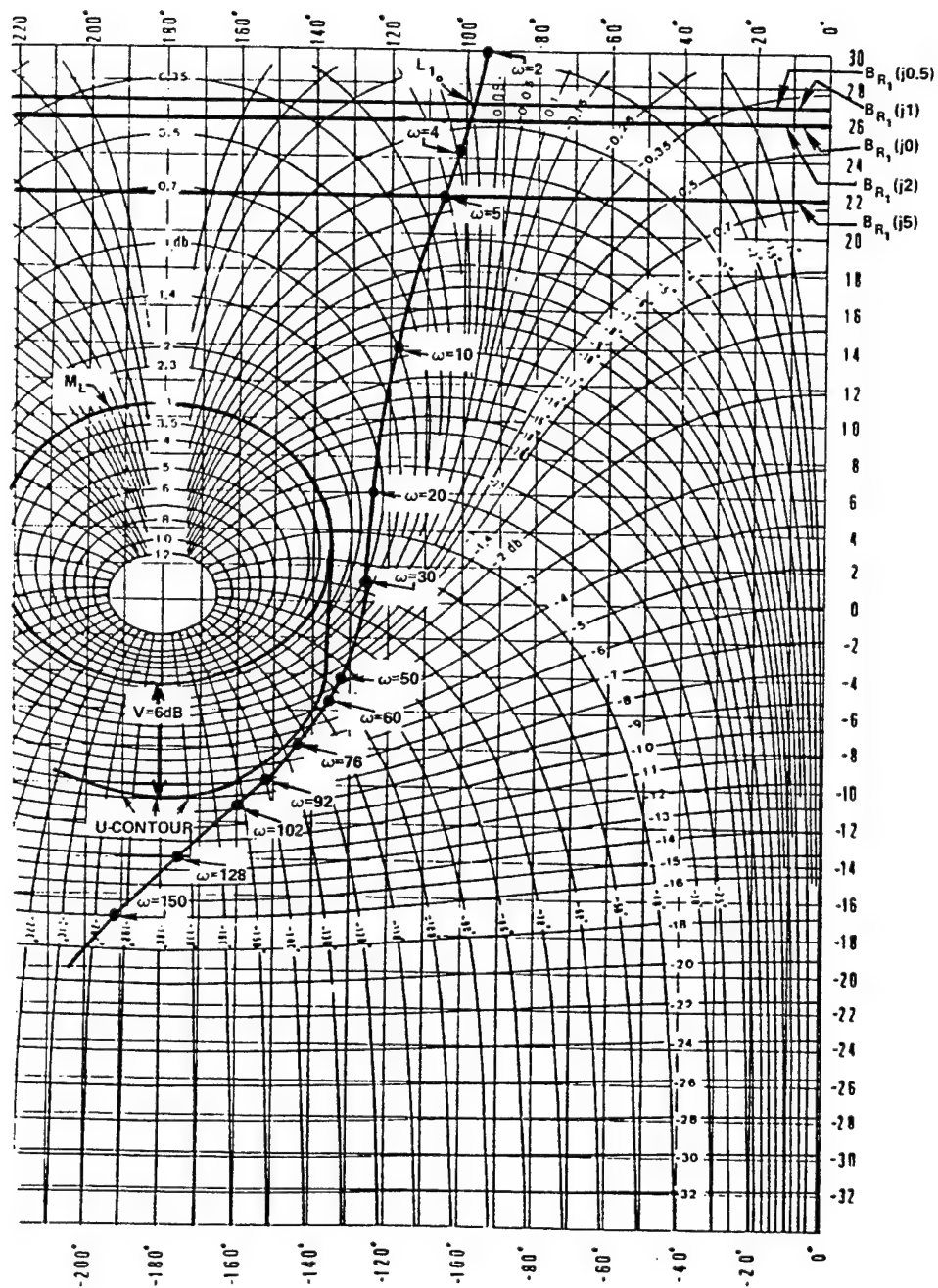


Fig. A.4  $L_1(s)$  design

Generally, for lower values of  $\omega$ , since  $|g_1 q_{11}| \gg 1$  then Eq. (A.21) can be simplified to:

$$|g_1| \geq \left| \frac{10b_{22}}{q_{12}} \right| \quad (\text{A.23})$$

Multiplying both sides of Eq. (A.23) by  $q_{11}$  yields:

$$|L_1| = |g_1 q_{11}| \geq \left| \frac{10b_{22} q_{11}}{q_{12}} \right| \quad (\text{A.24})$$

where  $L_1 = g_1 q_{11}$ . The worst case scenario must be chosen from the specifications in order to apply Eq. (A.24). Therefore, for

$$q_{12_{\min}} = \frac{0.5}{s} \quad \text{and} \quad q_{11} = \frac{1}{s}$$

Eq. (A.24) becomes

$$|L_1| \geq |20b_{22}| \quad (\text{A.25})$$

or

$$\text{Lm } L_1 \geq 26 + \text{Lm } b_{22} = B_{o_1}(j\omega_i) \quad (\text{A.26})$$

Thus Eq. (A.26) reveals that for this example the composite bounds  $B_{o_1}(j\omega)$  are straight lines whose magnitudes are a function of frequency. Based upon Eq. (A.26) and the given specifications on  $t_{22}$  in Table A.1 the bounds are:

Table A.2

$\omega_i$	1	0.5	1	2	5	10	20
$\text{Lm } B_{o_1}(j\omega_i)$	26	27	27	26	22	N/A	N/A

Since the value of  $b_{22}(j\omega)$  is very small for  $\omega > 5$ , the tracking frequency range is effectively  $0 < \omega < 5$ . The value  $\text{Lm } a_{22}(j\omega)$  yields

$\delta_R(j\omega) = \text{Lm } b_{22}(j\omega) - \text{Lm } a_{22}(j\omega) \rightarrow \infty \text{ dB}$  for  $\omega > 5$  and the tracking problem will always be satisfied in this frequency range. It is therefore necessary to shape the loop transmission  $L_1(j\omega)$  only for  $0 \leq \omega \leq 5$ . Only the cross-coupling rejection problem remains for  $\omega > 5$ .

Since the  $p_{ij}$  elements of  $P$ , and in turn all the elements of  $Q$ , and the nominal  $q_{11}$ , are Type 1 functions then  $L_1(s)$  should be chosen as a Type 1 or higher function. A Type 1 function is chosen for  $L_1(s)$ . An initial simple  $L_1(s)$  design containing only one pole at the origin, one complex-pole pair, and one zero resulted in  $\omega_\phi = 65 \text{ rps}$ . In order to reduce the value of the phase margin frequency the following  $L_1(s)$  is synthesized:

$$L_1(s) = \frac{54038(s + 25)}{s(s + 10)(s + 84 \pm j112)} \quad (\text{A.27})$$

where  $\omega_n = 140 \text{ rps}$  and is shown in Fig. A.4. Note that the approximation made in Eq. (A.24) is justified because all the values in Table A.2 are at least a magnitude above one. Since  $L_1 = g_1 q_{11}$ , then

$$g_1(s) = \frac{L_1(s)}{q_{11}(s)} = \frac{54038(s + 25)}{(s + 10)(s + 84 \pm j112)} \quad (\text{A.28})$$

B.  $L_2$  Design (Improved Method) --- The equations for loop 2, see Fig. A.5 and Eqs. (III.35) through (III.38) and Eq. (III.53), are

$$t_{22} = \frac{q_{22}(g_2 f_{22} + c_{22})}{1 + g_2 q_{22}} \quad (\text{A.29})$$

where  $c_{22} = -t_{12}/q_{21}$  and

$$t_{12} = \frac{q_{11} c_{12}}{1 + g_1 q_{11}} \quad (\text{A.30})$$

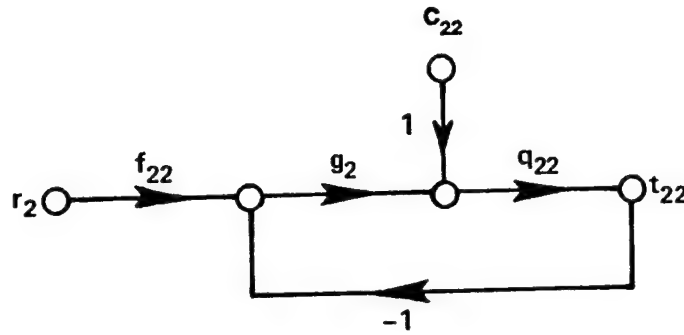


Fig. A.5 Loop 2

Instead of making the necessary substitutions and performing the associated algebra the following generalized loop 2 equations, see Eq. (V.4), are utilized in the design.

$$\gamma_{12} = \frac{q_{11}q_{22}}{q_{21}q_{12}} \quad (\text{A.31})$$

$$q_{22} = \frac{q_{22}(1 + L_1)}{1 + L_1 - \gamma_{12}} \quad (\text{A.32})$$

$$L_{2,} = g_2 q_{22,} \quad (\text{A.33})$$

and

$$c_{22,} = \frac{g_1 f_{12} p_{21}(1 - \gamma_{12})}{1 - \gamma_{12} + L_1} = 0 \quad (\text{A.34})$$

since  $f_{12} = 0$ . Thus loop 2 is only a tracking problem (see Fig. III.10).

Before generating the templates for  $q_{22}$ , it is necessary to ascertain whether all the poles and zeros of  $q_{22}$ , lie in the LHP  $s$ -plane over the region of uncertainty. The proper design of  $L_1(s)$  guarantees that the zeros of  $1 + L_1(s)$  are in the LHP. Since a m.p. plant is assumed, then  $q_{22}(s)$  will also be m.p. However, it is possible for



$1 + L_1(s) - \gamma_{12}(s)$  of Eq. (A.32) to have RHP zeros which become RHP poles of  $q_{22}(s)$  and therefore of  $L_2(s)$ . This possibility must be verified before proceeding with the design. The knowledge of the presence of RHP poles is necessary in order to correctly interpret the data for  $|q_{22}(j\omega_i)|$  and  $\angle q_{22}(j\omega_i)$  over the frequency range of interest (see Sec. 18.22 of Reference 15).

Plant uncertainty case 10 of Table A.3 represents an unstable plant. At low frequencies the templates are rectangles 6 dB in height

Table A.3

Combinations using plant maximums and minimums					
Case	$k_{11}$	$k_{12}$	$k_{21}$	$k_{22}$	Comments
1.	1	.5	5	.5	← unstable plant
2.	1	.5	5	1	
3.	1	.5	10	.5	
4.	1	.5	10	1	
5.	1	2	5	.5	
6.	1	2	5	1	
7.	1	2	10	.5	
8.	1	2	10	1	
9.	2	.5	5	.5	
10.	2	.5	5	1	
11.	2	.5	10	.5	
12.	2	.5	10	1	
13.	2	2	5	.5	
14.	2	2	5	1	
15.	2	2	10	.5	
16.	2	2	10	1	
<u>Random Points</u>					
17.	1.5	1	7	1	← nominal plant
18.	2	1.5	9	.75	
19.	1.75	.75	6	.75	
20.	1.25	1.25	8	.5	

and essentially  $360^\circ$  wide. That is, the template for  $\omega = 0.5$  is essentially 6 dB in height and  $360^\circ$  wide, and for  $\omega = 20$  rps it is 6 dB in height,  $345^\circ$  wide at the top and  $352^\circ$  wide at the bottom. The templates for  $\omega = 130$  rps and  $\omega = 150$  rps are approximately  $180^\circ$  and  $138^\circ$  wide respectively. It is thus apparent, in order to have a negative phase angle at all frequencies for  $L_2(j\omega)$ , templates must be generated for high enough frequencies such that they shrink in width sufficiently in order to allow a gap on the right side of the U-contour for  $L_2(j\omega)$  to "squeeze" through and achieve the desired value of  $\gamma = 45^\circ$  (for this example). This analysis of the plant template data reveals: (1) that the width (change in angle) of the templates is the crucial factor in the shaping of  $L_2$  of the template, and (2) that the template shapes go from being "very wide" (essentially rectangular), as shown in Fig. A.6, at "low" frequencies to the shape shown by the shaded area in Fig. A.6 at "high" frequencies. As shown in Fig. A.6, that in going from  $\omega = 0.5$  to  $\omega = 300$  rps the templates start to "droop" down to the right. This droop becomes more exaggerated if more template points are plotted from other unstable plants within  $Q$ . These unstable plants occur for this example, when the condition

$$\gamma_{12} = \frac{k_{11}k_{22}}{k_{21}k_{12}} > 0.5 \quad (\text{A.35})$$

is satisfied. This can be seen by partitioning the characteristic equation of Eq. (A.32) to yield  $L_1/(1 - \gamma_{12}) = -1$  for which a root-locus analysis can be made as the value of  $\gamma_{12}$  is varied. The "very wide" characteristics of some of these templates can best be appreciated by the reader by plotting a positive and negative real pole ( $a$  and  $-a$ ) in the  $s$ -plane. The reader is then urged to analyze the angular contribution of  $\angle[1 + j(\omega/a)]$  and  $\angle[1 + j(\omega/-a)]$  as the frequency is varied from zero to infinity.

In order to simplify the process of generating the bounds rectangular (solid curve) templates are used as shown in Fig. A.6. Although making this assumption yields an overdesign.

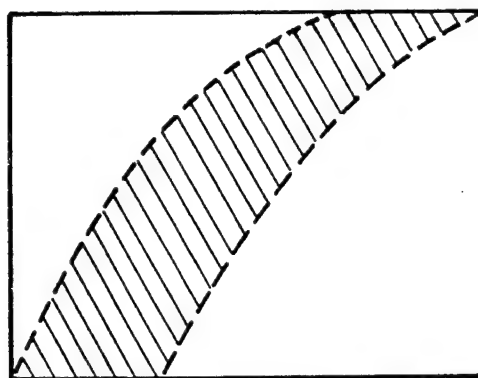


Fig. A.6 Template shape

The data for the templates (see Fig. A.7) that play the key role in achieving the desired value of  $\gamma$  is given in Table A.4. Note that at  $\omega = 500$  the template is 20 dB in height which the value of  $V(\text{UHFB})$  used to obtain the U-contour.

Table A.4

$\omega$	$\Delta$ dB	$\Delta\theta^\circ$
150	14.5	138
170	15.8	81
180	15	61
200	16.6	37
300	18	10
500	20	$\sim 0$

The templates are used to obtain the  $B_R(j\omega_i) = B_o(j\omega_i)$  bounds of Fig. A.8 for the loop 2 design. Note that for  $\omega < 150$  rps the bounds are considered to be essentially straight lines. That is, these bounds are represented by the straight line tangent to the top of the  $L_m M_L$  contour since all the templates for  $\omega < 150$  rps are greater than  $135^\circ$  in

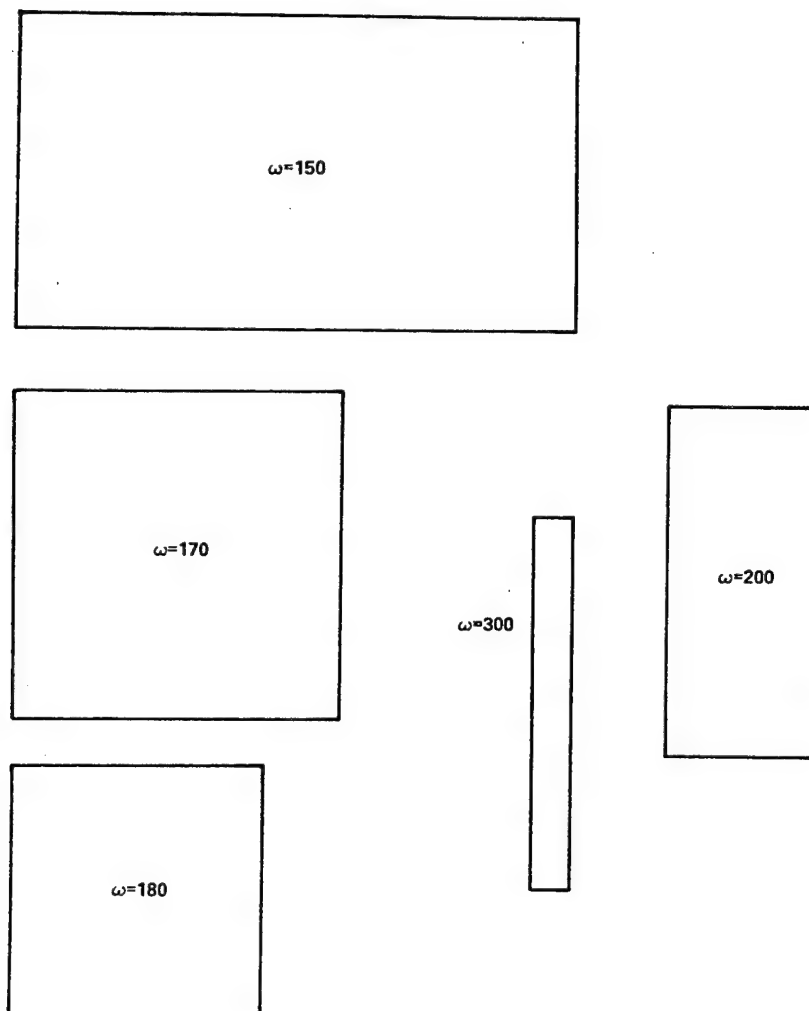


**Fig. A.7 Tracking Templates for Loop 2  
(using a rectangular approximation)**

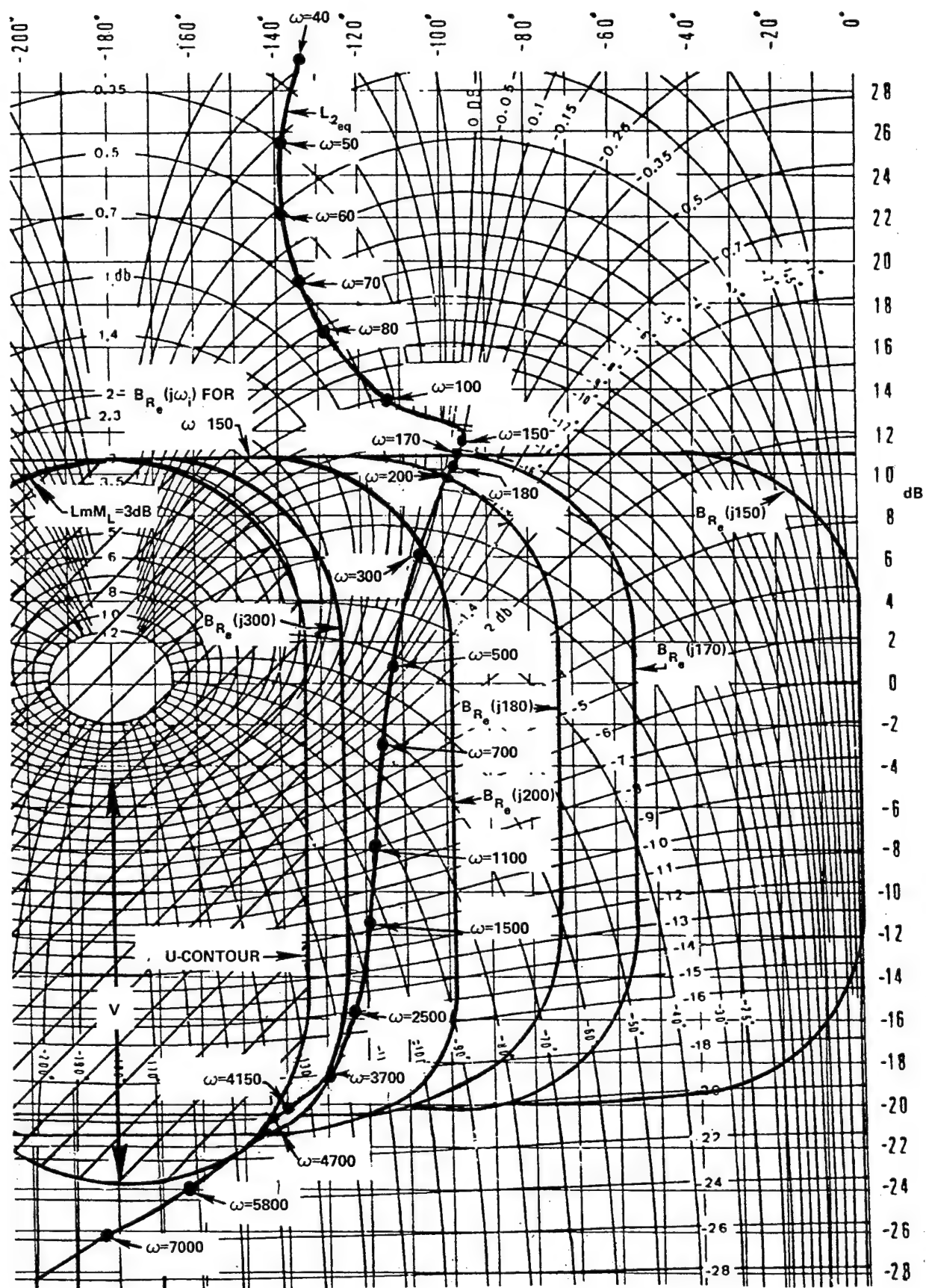


Fig. A.8  $B_{R_e}(j\omega)$  and  $L_{2eq}(j\omega)$  plots.

width. A stable plant is chosen to be the nominal plant, see Table A.3, and is located at the lower right-hand corner of the templates. Thus the plant gain values,  $k_{ij}$ , for the nominal plant are:  $k_{11} = 2$ ,  $k_{12} = 2$ ,  $k_{21} = 10$ , and  $k_{22} = 0.5$ . For these nominal values, where  $\gamma_{12} = 0.05$ , let

$$\alpha = 1 - \gamma_{12} = 0.95 \quad (\text{A.36})$$

thus from Eqs. (A.27), (A.31) through (A.34), and (A.36) obtain

$$\begin{aligned} q_{22} &= \frac{k_{22}[s^4 + 178s^3 + 21280s^2 + (196000 + 540838k_{11})s + 13520950k_{11}]}{s[\alpha s^4 + 178\alpha s^3 + 21280\alpha s^2 + (196000\alpha + 540838k_{11})s + 13520.95k_{11}]} \\ &= \frac{0.5263158(s^4 + 178s^3 + 21280s^2 + 1277676s + 27041900)}{s^5 + 178s^4 + 21280s^3 + 667303.1579s^2 + 14232578.955s} \\ &= \frac{0.5263158(s + 49.2349 \pm j6.0882)(s + 39.7651 \pm j96.9859)}{s(s + 17.3915 \pm j24.9674)(s + 71.6085 \pm j101.2169)} \quad (\text{A.37}) \end{aligned}$$

In order to make  $g_2(s)$  "fairly simple" the nominal plant is used in Eq. (A.33) which results in a nonunique  $g_2$  being designed rather than  $L_2$  where

$$L_2(s) = g_2(s)q_{22}(s) \quad (\text{A.38})$$

A synthesized (nonunique)  $L_2(s)$  is shown in Fig. A.8. The hump in  $L_2$  in the vicinity of  $\omega = 150$  rps is caused by the complex zeros ( $\omega_n = 104.8$  rps) of the nominal plant. These zeros have a low damping ratio ( $\zeta \approx 0.38$ ) which causes the "rapid" change in the phase angle. Usually a complicated  $g_2(s)$  results when adjusting  $L_2(j\omega)$  so that it crosses the  $B_o(j150)$  bound near the right side of the NC with  $L_2(j\omega)$  being on the corresponding  $B_o(j\omega_i)$  bound. However, in order to obtain a simpler  $g_2(s)$ , the approach in this example is to design  $g_2(s)$  so that  $L_2(s)$  crosses the first few bounds at a phase angle of approximately  $-90^\circ$ . As it turns

out, for this example,  $g_2(s)$  does not contribute very much to the phase angle at the  $B_o(j\omega_i)$  crossing for  $\omega \leq 150$  rps; i.e., the phase angle is due essentially to the nominal plant. The resultant  $g_2(s)$  is:

$$g_2(s) = \frac{3.3155 \times 10^{10}(s + 1000)}{(s + 500)(s + 3500 \pm j6062.1778)} \quad (\text{A.39})$$

where  $\omega_n = 7000$  and  $\zeta = 0.5$ . A second design for  $g_2(s)$  can be made by choosing smaller values for the real pole and zero of Eq. (A.39) in order to have  $L_2(s)$  track down the right side of the U-contour more closely. In general, a more complicated  $g_2(s)$  may be synthesized that approaches the optimal loop transmission function

$$L_2(j\omega_i)_{opt} = O(j\omega) = |O(j\omega)| \angle O(j\omega) \quad (\text{A.40})$$

whose magnitude lies on  $B_o(j\omega_i)$ , for each value of  $\omega_i$ , and whose phase

angle  $\angle O(j\omega_i)$  lies on the right side of the U-contour.

**C. Prefilter  $f_{22}(s)$  Design** --- The prefilter design procedure of Chap. I<sup>15</sup> requires the use of the templates to obtain the values of  $Lm t_{2_{\infty}}$  and  $Lm t_{2_{\omega}}$  where  $t_2 = L_2/(1 + L_2)$  over the frequency range  $0 < \omega < 20$  rps. In this frequency range, for this example, the templates are between  $345^\circ$  and  $360^\circ$  wide. As a consequence, the location on the NC where these templates are placed result in small positive values for  $Lm t_2$  ( $\leq 0.1$  dB). Thus, small variations exist for  $Lm t_2$ , i.e.,  $\Delta t_2 = Lm t_{2_{\infty}} - Lm t_{2_{\omega}}$  will be a very small number in the range  $0 < \omega < 20$  rps. For example, the bottom of the template, for  $\omega = 20$ , would be placed on the  $Lm L_2$  curve at the  $Lm L_2(j20) = 38.2$  dB point to yield  $Lm t_{2_{\infty}} \approx 0.1$  dB and a value for  $Lm t_{2_{\omega}}$  something less than 0.1 dB. Thus for  $\omega < 20$   $\Delta t_2$  is a very small number and  $|t_2| \approx 1$  for  $\mathcal{P} = \{P\}$ . Therefore, the corresponding figures of Fig. I.13, for this example, are obtained by plotting the data from Table B.1, i.e.,



$$Lm T_{R_v} - Lm T_{\max} = Lm b_{22} \text{ and } Lm T_{R_L} - Lm T_{\min} = Lm a_{22}$$

The filter chosen is:

$$f_{22}(s) = \frac{1}{s + 1} \quad (\text{A.41})$$

Note: care must be taken in determining the location of the pole of Eq. (A.41) since it may be necessary to lower the value of  $|f_{22}|$  at large values of  $\omega$  ( $\geq 10$ ), where  $a_{22} = 0$ , since this affects the value of  $|t_{12}|$ , etc. [(see Eqs. (A.19) through (A.21)].

D. Simulation --- The computer data for  $y_{22}$  for a number of plants from  $\mathcal{P}$  resulted in  $|t_2| \approx 1$  for  $0 \leq \omega \leq 20$ . Table A.5 presents the time response characteristics of  $y_{22}(t)$ , for a unit step forcing function, for three cases from Table A.3. These cases are chosen on the following basis:

Table A.5

Case	M	$t_p, s$	$t_r, s$	Final Value	Figure
10 (unstable plant)	1.000	3.91574	2.19709	1.000	A.10
15 (nominal)	1.000	3.91276	2.19726	1.000	A.9
16 (high gain)	1.000	3.91276	2.19722	1.000	A.11

(1) Nominal plant --- The loop transmission is obtained based upon the nominal plant.

(2) Unstable plant --- A "worst" case situation representative of the unstable plant region of  $\mathcal{P}$ .

(3) High gain plant --- A high gain plant is chosen because it is representative of the top of the templates on the "nominal plant side."

Since all the other cases of Table A.3 are extremely similar to one of the three cases of Table A.5 they are not simulated.

The frequency domain specifications, as demonstrated by the simulation, are met for loop 2. Although time response specifications are not prescribed,  $y_{22}(t)$  exhibits respectable rise and settling times. Because of the gross over design any other plant from the plant parameter space P should meet the specifications.

In designing loop one the cross-coupling rejections bounds are dropped to an arbitrary low value for the shaping of  $L_1$ . The synthesized

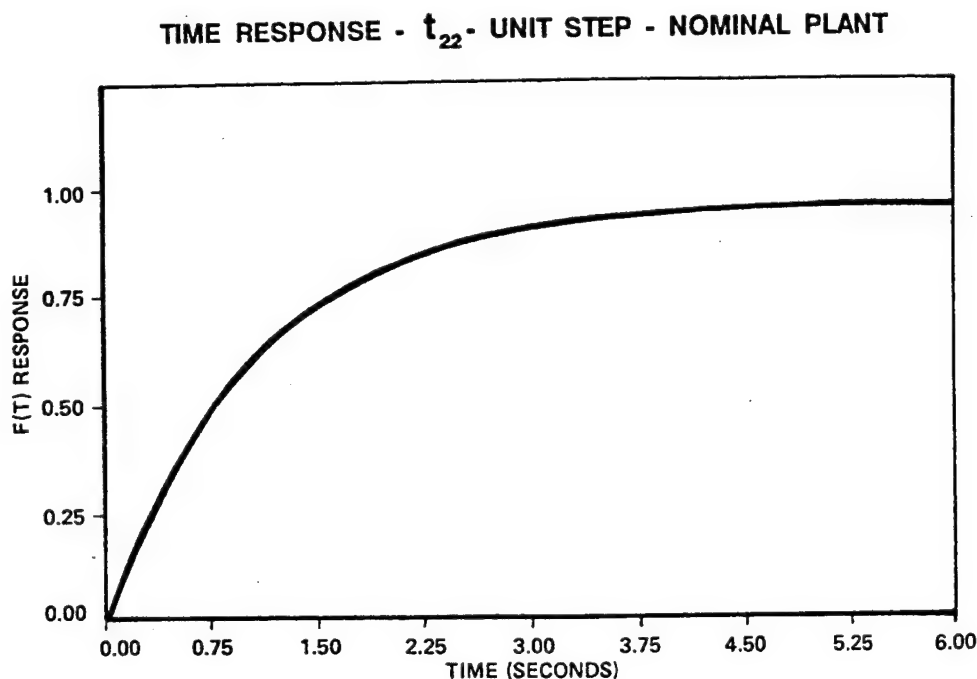


Fig. A.9 Time response  $y_{22}(t)$  for  $r_2(t) = u_{.1}(t)$ : nominal plant case.

TIME RESPONSE -  $t_{22}$  - UNIT STEP - UNSTABLE PLANT

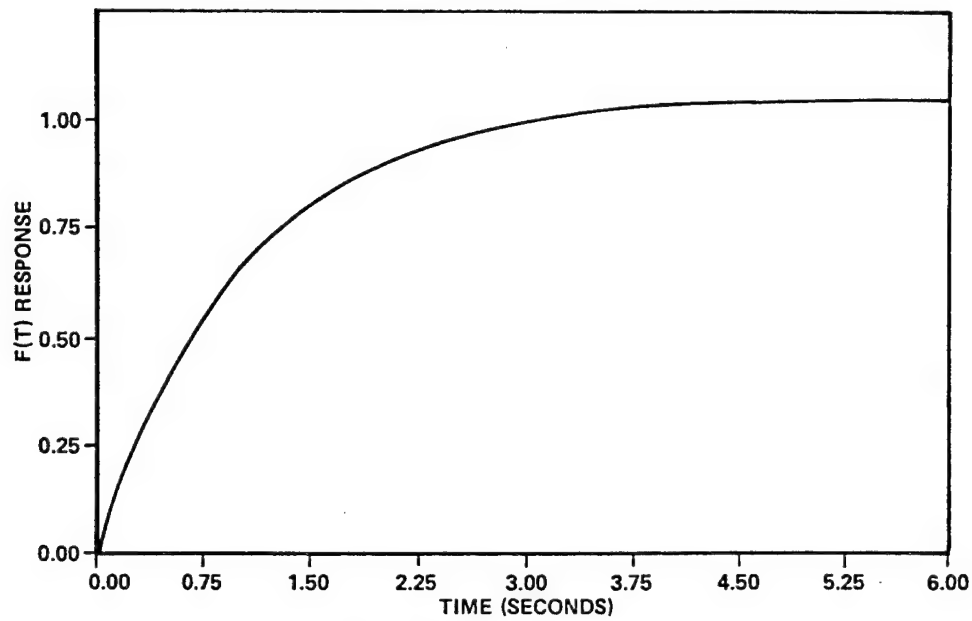


Fig. A.10 Time response  $y_{22}(t)$  for  $r_2(t) = u_{-1}(t)$ : unstable plant case.

TIME RESPONSE -  $t_{22}$  - UNIT STEP - CASE 16

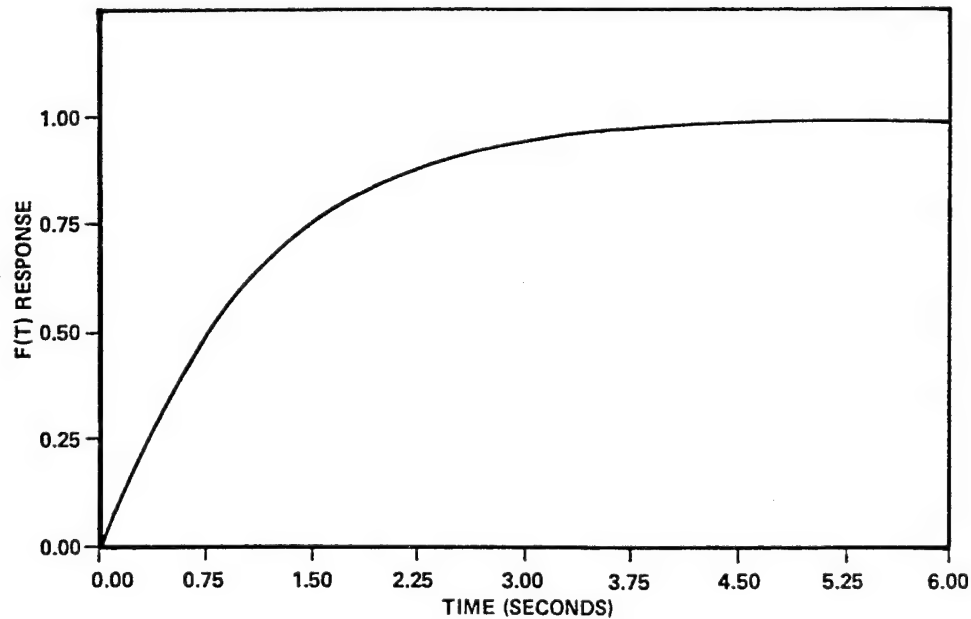


Fig. A.11 Time response  $y_{22}(t)$  for  $r_2(t) = u_{-1}(t)$ : high gain case.

$L_1$  for  $w = 20$  lies on  $B_{\phi}(j20) = 6$  dB but for  $\omega = 10$   $\text{Im } L_1(j10) \approx 14.5$  dB  $< B_{\phi}(j10) = 16$  dB. Thus, a check on the cross-coupling rejection  $t_{12}(j\omega)$  performance for loop one is made. From Eqs. (A.16) and (A.19) obtain:

$$t_{12} = \frac{-t_{22}}{q_{12}} \left[ \frac{q_{11}}{1 + L_1} \right] = -\frac{st_{22}}{k_{12}} \left[ \frac{q_{11}}{1 + L_1} \right] \quad (\text{A.42})$$

where  $q_{12} = k_{12}/s$ ,  $c_{22} = 0$ , and

$$t_{22} = \frac{q_{22}(g_2 f_{22} - c_{22})}{1 + L_2} = \frac{f_{22} L_2}{1 + L_2} \quad (\text{A.43})$$

Substituting Eq. (A.43) into Eq. (A.42) yields

$$t_{12} = - \left[ \frac{f_{22} L_2}{1 + L_2} \right] \left[ \frac{s}{k_{12}} \right] \left[ \frac{q_{11}}{1 + L_1} \right] \quad (\text{A.44})$$

Only the plant parameters associated with the unstable  $q_{22}$  plant (case 10) are used in Eq. (A.43) for a simulation. No other plants are simulated to determine if the cross-coupling rejection specification are met. The frequency response plot for Eq. (A.44) using the parameters for the unstable plant is shown in Fig. A.12. As seen from this figure the -20 dB specification is met. The simulation yields  $t_{12}(t_p) = -0.0579$  at  $t_p \approx 0.026$  s,  $|t_{12}(t_s)| = 0.002$  (2% of the specified maximum magnitude of 0.1) at  $t_s = 2.61$  s, and  $t_{12}(\infty) = 0$ .

E. Summary --- In some problems  $\gamma_{12} \ll 1$  and therefore  $q_{22} \approx q_{22}$  [see Eq. (A.32)] which simplifies the design. For the example of this appendix  $\gamma_{12\max} = 0.8$ . Thus for  $0.5 < \gamma_{12} < 0.8$  there will exist an unstable  $q_{22}$ , i.e.,  $q_{22}$  will have RHP poles. An unstable plant with a pole  $p_1 > 0$  requires a loop transmission with a crossover frequency

$\omega_\phi \cong > 2p^{15}$ . Therefore,  $L_2$  has to have a large crossover frequency. In order for  $L_2$  to have a lower value for its  $\omega_\phi$  it is necessary to design  $L_1$  so that  $1 + L_1 - \gamma_{12}$  does not have RHP zeros. This makes  $L_1$  costlier, the benefit going to  $L_2$  (or  $g_2$ ). This freedom can be used as a trade-off feature to be used according to the relative sensor noises, etc.

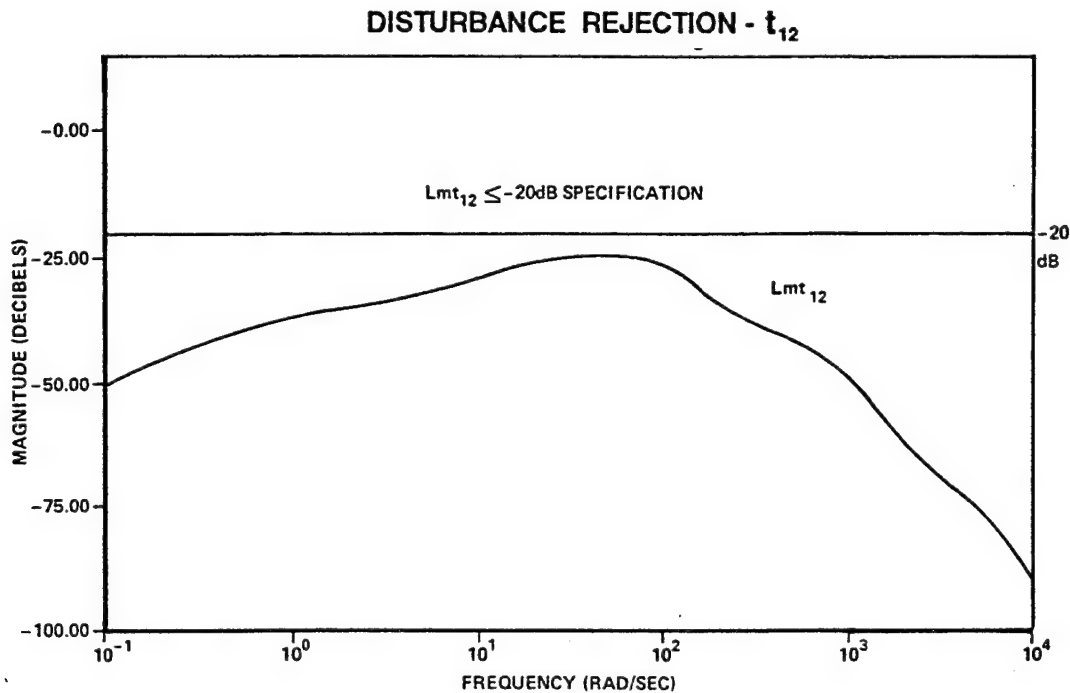


Fig. A.12 Frequency response  
 $t_{12}(j\omega)$ : an unstable case.

## Appendix B Longitudinal Handling Qualities Approximations & Bandwidth Minimization<sup>115</sup>

### B.1 Introduction

In designing automatic flight control systems for modern aircraft several concerns confront the design engineer. How to include MIL-STD-1797A specifications in the design? Will the design be robust enough to handle the uncertainties, not only in the approximations used to realize a design, but also in the conditions the system will see once placed into the "real" world? How large will the required system bandwidths be, and what are the chances of exciting spurious modes (unmodelled high frequency dynamics)?

One of the areas of interest that faces these issues is the design of fixed-compensation controllers for reconfigurable flight control systems<sup>13,14</sup>. A desired design will stabilize the aircraft (A/C) in case of failure until the source can be determined and corrected for. The salient features of this control law are:

Robust Fixed Compensation  
MIL-STD-1971A HQ for Healthy Aircraft  
Stability for Large Failure Set

Satisfaction of these requirements can lead to large system bandwidths, leading to noise corruption, actuator saturation, and spurious mode excitation, any of which can be serious for reduced static stability aircraft.

This appendix addresses the factoring of handling qualities (HQ) and bandwidth (BW) considerations into the QFT design method to formulate a more reasonable point to start off practical design work.

### B.2 Background

QFT relies on shaping the loop transmission  $L$  to meet certain

restrictions(bounds) placed upon it by desired system responses and cross-coupling effects rejection levels. QFT is used extensively for investigations into robust automatic flight control system (AFCS) design resulting in fixed compensation without extensive failure detection/identification (FDI) routines. From the flying qualities specifications<sup>12,60</sup> Level 1 A/C are the "good" planes that all designers desire, Level 2 have deficiencies which should be corrected, and Level 3 are barely controllable. In this presentation the term "flying qualities" (FQ) is assumed the same as HQ. This isn't quite true since FQ is a subset of HQ but it suffices for the design presented in this appendix. During AFCS synthesis using the m.p. QFT design technique it is hard to guarantee Level 1 (MIL-STD-1797A) HQ for healthy A/C while trying to control the same A/C with failures within reasonable loop bandwidths. This stems from two basic assumptions/steps in design. The inclusion of the no-fail plant into the same set as all the failed plants, and assuming the output(s) are controllable, but not Level 1 (it is normal to relax the tracking specifications a bit for failures to reduce actuator demands). The design becomes concerned with the response of the set rather than that one individual plant lost in its midst. Some of those plants may meet the stricter Level 1 demands, or they may not. Reducing the size of the plant set will decrease the "distance" (in a frequency response sense) between plants, but it also reduces the total number of situations the controller can handle. The acceptable outputs could be limited a priori Level 1; however, this would lead to controllers having unrealistic gains and bandwidths trying to force a crippled A/C to fly like a healthy one. Compensation could be scheduled, but now some sort of FDI routine is required (which is the reason for fixed compensation in the first place). For Reduced Static Stability aircraft (RSS) the problem is compounded further since any actuator rate/position saturation resulting from over zealous compensation can lead to loss of control.<sup>5,6,58</sup>

What is required is a logical method by which the designer can factor in HQ criteria while loop shaping and at the same time keep loop bandwidths reasonable. From an engineering standpoint it should be simple as possible and provide "feedback" to the designer during

synthesis. Some way should be devised such that the particular military specifications can be included into the design process to begin with, thus avoiding control "kluges" when the design fails to work properly. Closed-loop checks of the actuator states can provide insight into saturation.

### B.3 Desired Handling Qualities

In order to set the proper frequency responses for control synthesis they must first be defined from the requisite specifications. A typical desired longitudinal short-period response to a pilot stick input is a second-order system with a closed-loop transfer function of

$$TF(s) = \frac{\omega_{sp}^2}{s^2 + 2\zeta_{sp}\omega_{sp}s + \omega_{sp}^2} \quad \text{(B.1)}$$

$\omega_{sp}$  is the short period natural frequency

$\zeta_{sp}$  is the short period damping ratio

The damping ratio and natural frequency vary for the type of A/C, type of task, and the  $n/\alpha$  factor. It is assumed that the A/C is an advanced fighter configuration in a landing scenario, with  $n/\alpha$  as the independent variable. With the task, aircraft, and  $n/\alpha$  fixed, an approximate range of  $\omega_{sp}$  and  $\zeta_{sp}$  can be determined from MIL-STD-1797A. Background documents to the spec give actual experimental data on ranges of  $\omega_{sp}$  and  $\zeta_{sp}$  from various A/C simulations and test flights. Figure B.1 shows such a chart. The points A-H denote the boundary of Level 1 flight. The  $\omega_{sp}$  and  $\zeta_{sp}$  for these points are averaged over numerous charts of similar A/C doing similar tasks. The result is a representative group of short-period frequencies and damping ratios which denote the borders of Level 1 flight. From these a representative group of transfer functions are developed. The set of transfer functions developed for the conditions



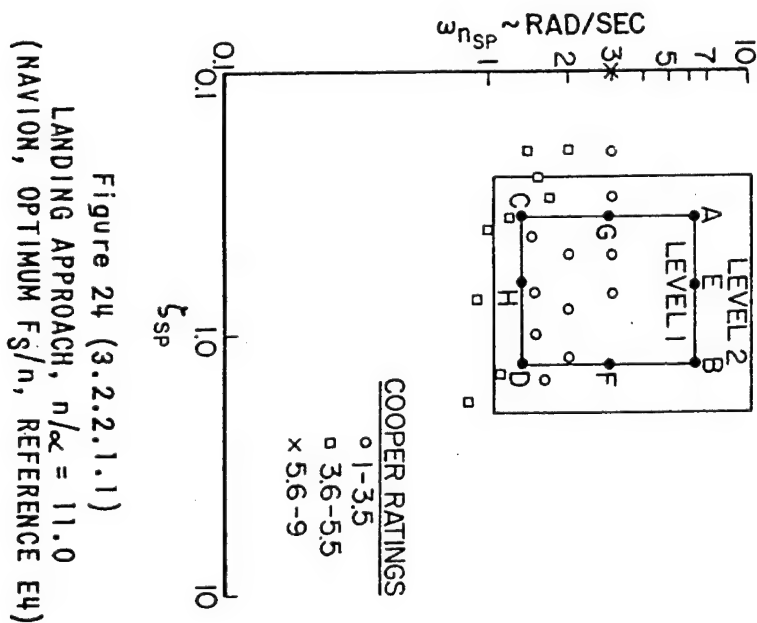
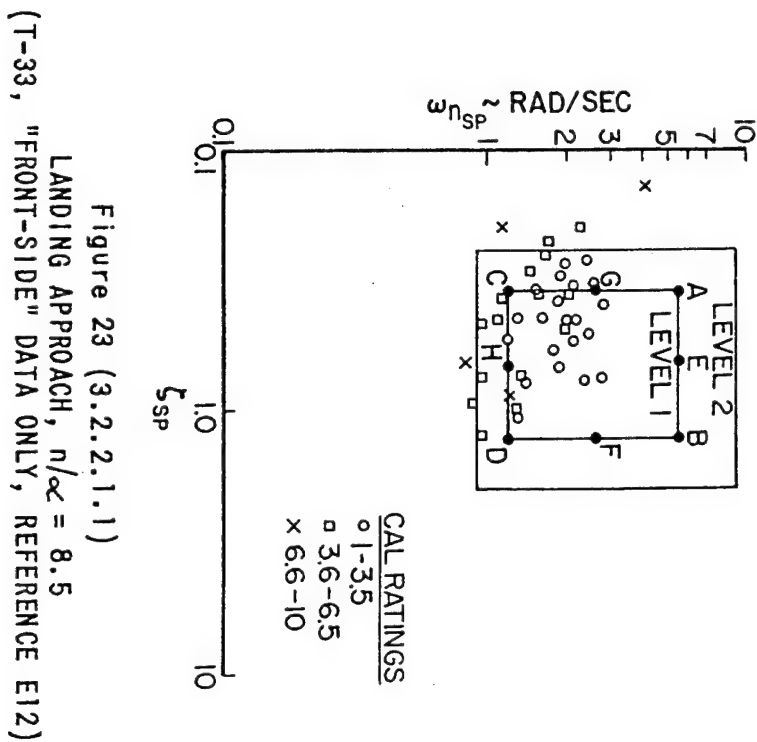
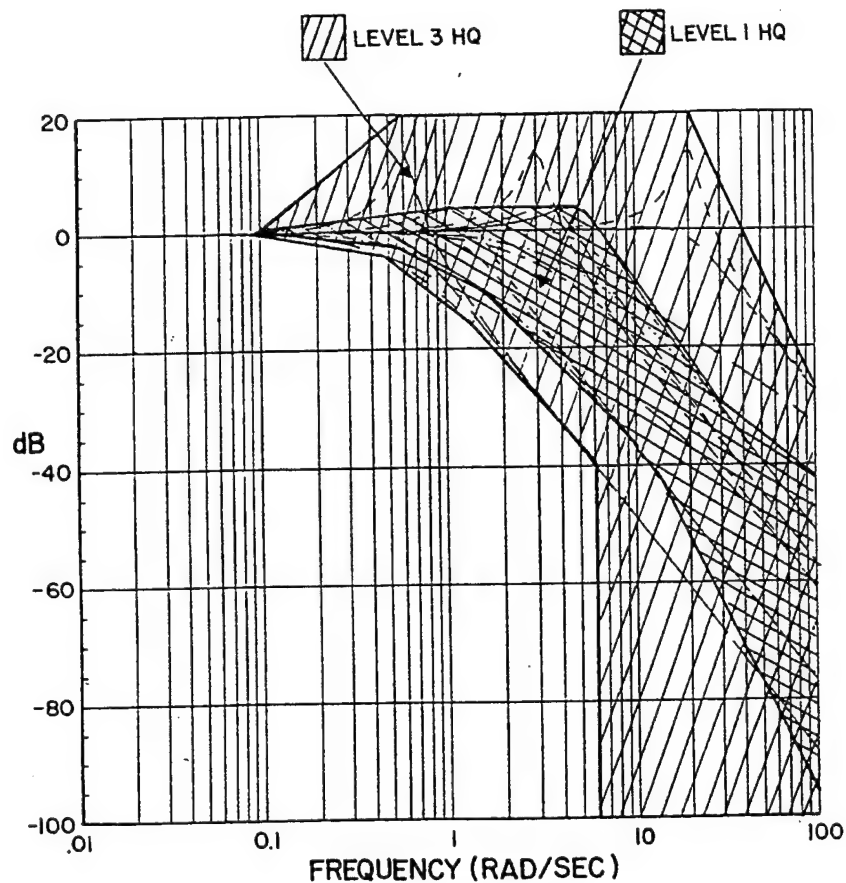


Fig. B.1 Example of ranges of short period frequency and damping ratio used to develop the acceptable set of closed loop transfer functions. (MIL - F - 8785C).

above are in Table B.1. From these transfer functions, and from those developed for Level 3 flying qualities, frequency bound can be plotted to define the range of each. Figure B.2 shows a magnitude versus frequency plot of these bounds for Level 1 and Level 3 HQ. This plot is required later on when the synthesis procedure is modified.



**Fig. B.2 Frequency bounds (approximate) on Level 1 and Level 3 HQ for fighter A/C landing task.**

**Table B.1 Closed-loop Transfer Functions Representing The Boundaries For Level 1 HQ.**

<i>Point</i>	<i>Transfer Function</i>
<i>A</i>	$\frac{27}{s^2 + 3.54s + 27}$
<i>B</i>	$\frac{27}{s^2 + 12.5s + 27}$
<i>C</i>	$\frac{1.44}{s^2 + 0.82s + 1.44}$
<i>D</i>	$\frac{1.44}{s^2 + 2.88s + 1.44}$
<i>E</i>	$\frac{27}{s^2 + 6.76s + 27}$
<i>F</i>	$\frac{14.4}{s^2 + 2.56s + 14.4}$
<i>G</i>	$\frac{14.4}{s^2 + 9.12s + 14.4}$
<i>H</i>	$\frac{1.44}{s^2 + 1.56s + 1.44}$

#### **B.4 Modification of the QFT Design Procedure**

This section addresses the problem of insuring handling qualities for a given subset of the total plant set, where this subset is assumed as a small part of the plant set. To do this, the QFT design process is slightly altered to take advantage of the difference in stability and tracking criteria for the plant set in question. Before this is done, however, the whole concept of robust control for reconfigurable flight control systems requires examination so the "task" of the controller is well defined.

What are the causes of unrealistic, high bandwidths in the QFT design process? Large plant uncertainty and tight tracking/cross-coupling rejection tolerances. Does that uncertainty in the plant lead to large plant templates even at "high" frequencies? Does the strict tolerances place too much of a burden on compensation for a plant with failures? Normally, given a problem with strict tolerances and large plant uncertainty one would expect "healthy" loop bandwidths. To get around this one could limit the amount of uncertainty dealt with, leaving some situations uncontrollable. Or, the system specifications could be relaxed for the total plant set, ending up with a sluggish and/or noisy system. The goal is to do a little of both, compromising to insure stability and tracking performance.

Obviously, a pilot wants to fly a Level 1 A/C all the time, but most pilots are practical and will accept HQ degradation for failures as a fact of life. To take advantage of this in the design process relax the idea of initial acceptable tracking responses from Level 1 to Level 2 or minimum control conditions, Level 3. This meets one of the goals:

FOR ROBUST CONTROL IN THE FACE OF SURFACE FAILURES IT IS DESIRED TO SIMPLY KEEP THE PLANE IN THE AIR LONG ENOUGH FOR THE FDI SYSTEM TO EFFECT AN OPTIMAL SOLUTION (or get the pilot out)!

For this Level 1 HQ is not required, Level 3 qualities are acceptable. Relaxing tracking requirements as shown in Fig. B.3 can significantly increase the area of acceptable tracking responses, likewise pushing the tracking bounds lower on the NC, reducing loop BW. Now the reader is saying at this point, "Sure you've lowered the loop BW (ignoring cross-coupling effects), but the tracking response could be terrible for healthy plants." True; however, the desired tracking response for those plants in the subset of interest will be recovered later in the design process, the loop compensation is insuring stability while the prefiltering will give the required tracking response. In addition to using the lowest acceptable HQ for failed A/C as initial tracking bounds the cross-coupling rejection should be moved from "desired" to "acceptable" levels to arrive at the lowest practical cross-coupling bounds.

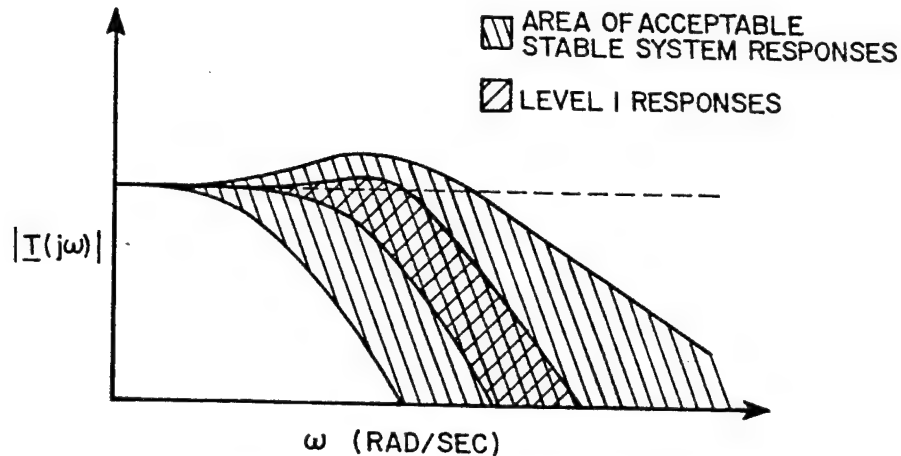


Fig. B.3 Acceptable frequency response areas for flight stability and controllability, and Level 1 flying qualities.

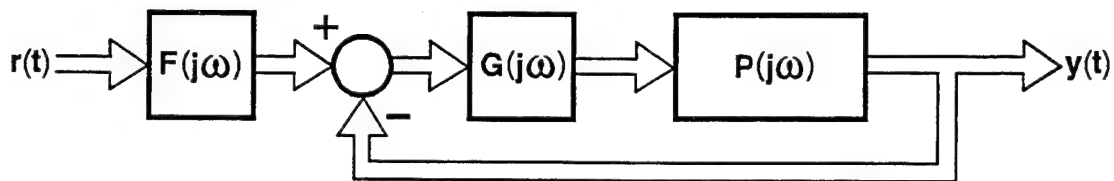


Fig. B.4 QFT system configuration

The approach taken here is to use QFT almost exactly as before, but relaxing a few tolerances, and making others stricter. Figure B.4 shows the system configuration used in the QFT design process.  $P$  is the plant to be controlled,  $G$  is the loop compensator, and  $F$  is the prefilter. The input and output dimensions are assumed the same, the plant being observable and controllable.

The first step is to break the entire plant set  $\mathcal{P}$  into two subsets, the plants which should fly Level 1,  $\mathcal{P}'$ , and those that can fly a worse HQ level,  $\mathcal{P}^-$ . Two sets of plant templates are required, those for  $\mathcal{P}$ , and those for  $\mathcal{P}'$ . Using the tracking specifications for Level 3 and the required cross-coupling rejection, develop loop bounds on the NC with the templates for  $\mathcal{P}$ . Once the bounds are on the NC a loop transfer is shaped in the normal way. The nominal plant used to plot the bounds and to shape the loop is a member of  $\mathcal{P}'$ , preferably the plant which flies

the most. Calculate  $G$  in the normal manner. Note that the loop has been designed for stability: the compensator  $G$  has now resulted in a range of stable plants that may, or may not, meet the tracking requirements for Level 1 - no guarantees, all that is known is that they are stable and, if the design process is continued, they will fly Level 3. Normally at this point in the design, the prefilter is derived from the original tracking bounds. All this does is guarantee possible bad responses for  $P'$ , stable, but not Level 1. Going back to the original premise, only Level 1 responses are desired for the plants in  $P'$  (not caring much about  $P^-$  as long as it's stable and controllable). Thus the prefilter is synthesized for just that, agreeing to accept whatever responses for the other (non  $P'$ ) plants arise.

One has to insure that the prefilter modifies the system such that a chosen subset of the original plant set have closed-loop responses within a specified range on a Bode plot. The modification results in Level 1 HQ for the chosen set, but can't guarantee good HQ for the rest of the plant set (but it is reasonable to assume some performance degradation for A/C with failures). This method insures stability and a level of controllability with failures (which is what is desired for a damaged A/C). Since the prefilter is placed ahead of the closed loop, the problem now is a simple cascade compensation, or how best to pick the prefilter. The prefilter is chosen using just the data from  $P'$  recognizing that only the loop transfers of  $P'$  are of concern. So working just with those plants:

- a. Derive templates using only the plants in  $P'$ . These templates have a smaller area than the templates for the entire plant set, and thus contain less uncertainty.

- b. "Run" the new templates along  $L_o(jw)$ , noting the maximum and minimum values (as would be done normally with the entire plant template for the set  $\mathcal{P}$ ). Use the stricter Level 1 boundaries (Fig. B.2) to calculate the prefilter limits.

- c. Shape the prefilter the normal way.

The prefilter(s) thus designed insure that the particular plants of interest  $P'$  have Level 1 HQ while at the same time the loop compensator(s)  $G$  guarantee stability for the entire plant set. Note that the(se) prefilter(s) have larger bandwidth(s) than ones designed using QFT and the original, looser tracking bounds for Level 3. This increase should not cause problems since all uncertainty, instability, and cross-coupling effects are contained in the compensated loop previously designed, besides they are lower in BW than prefilters designed assuming Level 1 for all plants in  $\mathcal{P}$ . The actual time responses for the non- $P'$  plants can not be predicted, but then again they are not of concern as long as they are stable and controllable.

#### **B.5 Remarks by Dr. I. M. Horowitz**

I. The idea of using Level 3 performance specifications is certainly sound and worth pursuing in any tough problem where physical limitations such as when practical sampling frequency  $\omega_s^{47}$  and loop bandwidths are in conflict. A priori, one can (at the very onset) define several sets of bounds on  $|T(j\omega)|$  (or even more). There are a variety of possibilities:

1. Determine only one set of bounds on  $L_0$ , i.e., such that for any set  $\mathcal{P}_1$  bounds  $B_1$  [on  $|T(j\omega)|$ ] are satisfied and for set  $\mathcal{P}_2$  bounds  $B_2$  [on  $|T(j\omega)|$ ] are satisfied.
2. For all  $\mathcal{P}$  (i.e.,  $\mathcal{P}_1 \cup \mathcal{P}_2$ ) the bounds  $B_1$  are satisfied giving one set of bounds on  $L_0$ . Likewise, for all  $\mathcal{P}$ ,  $B_2$  are satisfied, etc.

Possibility 1 appears to be more reasonable.

It is a good idea to see the templates before spending a great deal of time on formulating  $B_1$  and  $B_2$ . The templates pretty well push you in a certain direction in formulating the lesser desirable  $B_i$ .

For difficult problems, one should economize as much as possible on the bounds  $B(j\omega)$  on  $|T(j\omega)|$  as follows:

(a) For any  $T(j\omega)$   $[t_{ii}, t_{ij} (i \neq j)]$  consider the actual typical time response characteristics (see MIL specifications). For example, a pitch-rate response usually allows for large overshoot with a reasonable settling time, i.e., Fig. B.5(a) is okay but not Fig. B.5(b). A second-order  $T_{ii}(s)$  results in the  $q_3(t)$  response which is not satisfactory for a  $q_1(t)$  time response. A pole-zero pattern for an acceptable  $T_{ii}(s)$  is shown in Fig. B.6. If the constraints on the parameters of Fig. B.7 are specified, then synthesize a pole-zero pattern which will yield this desired response and use it to  $|T_{ij}(j\omega)|$  bounds. Thus, the  $|T(j\omega)|$  bounds are being tuned to the natural system response which can result in a maximum economy in bandwidth.<sup>18</sup>

(b) In loop shaping there is often a dominant bound, e.g.,  $B_L(j2)$  in Fig. B.8 (solid lines) dominates. By analyzing the plant templates and the bounds on  $|T(j\omega)|$ , shown in Fig. B.9 (a), an improvement in BW may be achieved, if it is possible, by widening the bounds at  $\omega = 2$  and narrowing them at  $\omega = 4$  as shown in Fig. B.9 (b). What is the resulting effect on the time response range? The time-frequency relation is via an integral. If Fig. B.9(b) gives the dashed bounds in Fig. B.8 then an improvement has been achieved. This approach is worth trying where an improvement in BW is desired.

II. The possibility of scheduling the high-frequency gain factor through air data measurements (aerodynamic data for each flight condition mach vs altitude, which is apparently quite reliable, should be considered. Even if the air data measurements are quite inaccurate, say  $1 \pm 0.25$ , then the uncertainty factor (which is the length of the UHFB) is now only  $1.25/0.75$  ( $< 6$  dB) instead of possibly 30 dB. However, this scheduling is the same as for the failure cases (see Reference 3).

III. More advanced approaches should be considered such as:

1. Using a n.m.p. MIMO plant and allowing one row of  $t_{ij}$  to suffer. If available, select an output variable which can be sacrificed in order that the others are m.p.



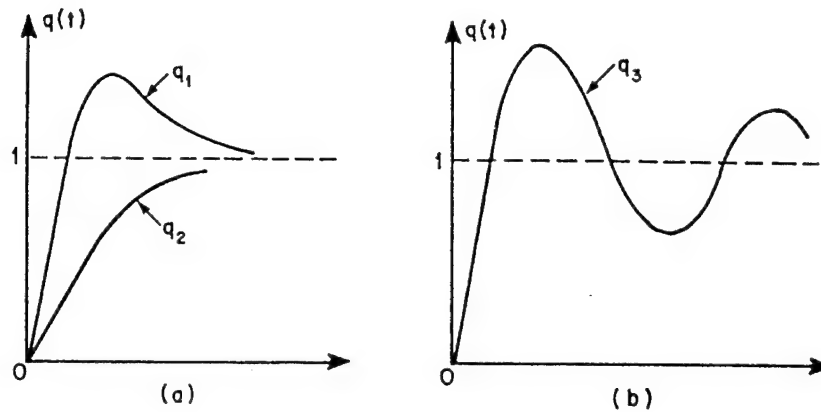


Fig. B.5 Pitch-rate time responses: (a) acceptable; (b) unacceptable

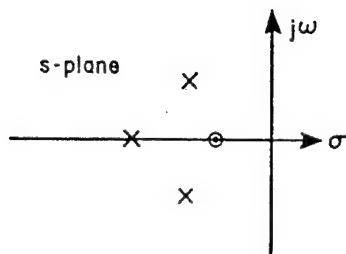


Fig. B.6 Pole-zero pattern for an acceptable  $T$ 's

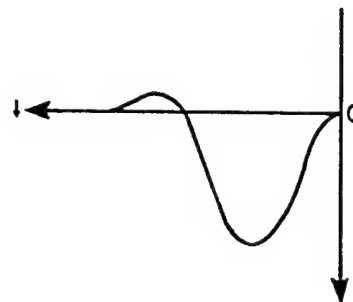


Fig. B.7 An interaction response

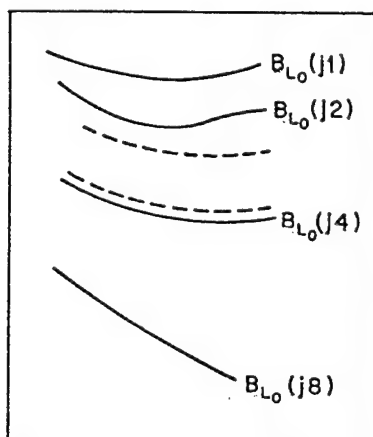


Fig. B.8  $L_o$  bounds

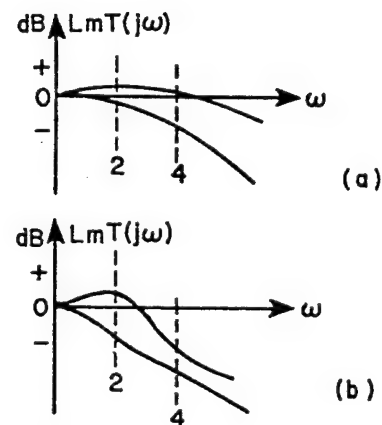


Fig. B.9 Upper and lower bounds on  $T(j\omega)$

2. Doing a preliminary design with smaller BW, which only stabilizes the system, i.e., the bounds on only  $L_m [L/(1 + L)] < 3$  or 4 dB. Then doing a second design with the resulting new effective plant (which includes the compensation of the preliminary design) for achieving the desired performance.

3. An oscillating adaptive system was used by Minneapolis-Honeywell on the X-15 but they never developed an analytic design technique. This was done by some PHD students at Weizmann Institute of Science.<sup>115</sup>

4. Nonlinear compensation (non-identification -- strictly passive nonlinear compensation) for loop BW economization should be investigated.

#### B.6 Summary

This appendix has presented a method by which compensation that guarantees specific (Level 1) HQ for a subset of a larger plant set containing both healthy and failed plants can be derived using QFT. Since only a few plants must exhibit good HQ, the BW penalties for forcing A/C with failed actuators to fly the same as healthy A/C are diminished, leading to more realistic compensation (or a larger amount of plant uncertainty being controllable given a specific BW and actuation). Thus, healthy A/C can be included into the design as before, but now with the guarantee that they will fly Level 1, while at the same time insuring robust behavior of the control system. The modifications to QFT are minimal: relax the initial acceptable tracking and cross-coupling responses to the bare minimum for controllable flight, use the loop compensation to guarantee stability, and develop the prefilter to give Level 1 HQ for the specific plants chosen. This method has yet (1985<sup>115</sup>) to be tried out in earnest, but synthesis-simulation work needs to be undertaken to verify the approach taken in this design.

## References

### R.1 References for the TR

1. Abrams, C. R., "A Design Criterion for Highly Augmented Fly-by-Wire Aircraft," U. S. Naval Air Dev. Centre, Warminster, PA., 1982.
2. Arnold, P. B., "Flight Control System Reconfiguration Using Quantitative Feedback Theory," M.S. Thesis, AFIT/GE/ENG/84D-15, Graduate School of Engineering, Air Force Institute of Technology, 1994.
3. Arnold, P. B., I. M. Horowitz, and C. H. Houppis, "YF16CCV Flight Control System Reconfiguration Design Using Quantitative Feedback Theory," Proceedings of the IEEE 1985 National Aerospace and Electronics Conference (NAECON), Vol. 1, pgs 578-585, 1985.
4. Astrom, K. J. and B. Wittenmark, Adaptive Control, 2nd Ed., Addison Wesley, 1995.
5. Beaufriere, H., "Limitations of Statically Unstable Aircraft Due to the Effects of Sensor Noise, Turbulence, and Structural Dynamics," AIAA, Aug. 1986.
6. Beaufriere, H. and S. Soeder, "Longitudinal Control Requirements for Statically Unstable Aircraft," NAECON Proceedings, May 1986.
7. Belsley, D. A., et al, Regression Diagnostics, Wiley, 1980.
8. Betzold, R. W., "Multiple Input-Multiple Output Flight Control Design with Highly Uncertain Parameters, Application to the C-135 Aircraft," M.S. Thesis, AFIT/GE/EE (83D-11), Graduate School of Engineering, Air Force Institute of Technology, Wright-Patterson Air Force Base, OH, Dec. 1983.
9. Blakelock H. John, Automatic Control of Aircraft and Missiles 2nd Ed., Wiley-Interscience, 1991.
10. Bode, H. W., Network Analysis and Feedback Amplifier Design, Van Nostrand, 1945
11. Brogan, W. L., Modern Control Theory, Quantum Publishers, Inc., pp 48-49, 1974.
12. Chalk, C. R., et al. Background Information and User Guide for MIL-F-8785B (ASG), "Military Specification-Flying Qualities of Piloted Airplanes", AFFDL-TR-69-72, Aug. 1969.
13. Chandler, P. R., "Self-Repairing Flight Control System Reliability and Maintainability Program Plan," Air Force Wright Aeronautical Laboratories, Wright-Patterson AFB OH, Feb. 1984.

14. Chandler, P. R. and D. W. Potts, "Shortcomings of Modern Control as Applied to Fighter Flight Control Design," Control and Decision Conference, 1983.
15. D'Azzo, J. J. and C. H. Houpis, Linear Control System Analysis and Design, McGraw-Hill Book Co., 4th Ed., 1995.
16. East, D. J., "A New Approach to Optimum Loop Synthesis," Int. J. Control, Vol. 34, pp 731-748, 1981.
17. Horowitz, I.M., "Advanced Control Theory and Applications," The Weizmann Institute of Science, Rehovot, Israel, unpublished notes, 1982.
18. *ibid*, Synthesis of Feedback Systems, Academic Press, 1963.
19. *ibid*, "Optimum Loop Transfer Function in Single-Loop Minimum Phase Feedback Systems," Int. J. Control, Vol. 22, pp 97-113, 1973.
20. *ibid*, "Synthesis of Feedback Systems with Non-Linear Time Uncertain Plants to Satisfy Quantitative Performance Specifications," IEEE Proc., Vol. 64, pp 123-130, 1976.
21. *ibid*, "Quantitative Synthesis of Uncertain Multiple Input-Output Feedback Systems," Int. J. Control, Vol. 30, pp 81-106, 1979.
22. *ibid*, "Improved Design Technique for Uncertain Multiple Input-Output Feedback Systems," Int. J. Control, Vol. 36, pp 977-988, 1982.
23. *ibid*, "A Synthesis Theory for Linear Time-Varying Feedback Systems with Plant Uncertainty," IEEE Trans, AC-20, pp 454-463, 1975.
24. *ibid*, "Improvement in Quantitative Nonlinear Feedback Design by Cancellation," Int. J. Control, Vol 34, pp 547-560, 1981.
25. *ibid*, "Feedback Systems with Nonlinear Uncertain Plants," Int. J. Control, Vol 36, pp 155-172, 1982.
26. *ibid*, "A Quantitative Inherent Reconfiguration Theory for a Class of Systems," Int. J. Sys. Sci., Vol 16, pp 1377-1390, 1985.
27. *ibid*, "The Singular-G Method in Unstable Nonminimum-phase Feedback Systems," Int. J. Control, Vol 44, pp 533-541, 1986.
28. Horowitz, I. M. and M. Breiner, "Quantitative Synthesis of Feedback Systems with Uncertain Nonlinear Multivariable Plants," Int. J. Sys. Sci., Vol 12, pp 593-563, 1981.
29. Horowitz, I. M. and T. Kopelman, "Multivariable Flight Control Design with Uncertain Parameters," The Weizmann Institute of Science, Rehovot, Israel, Final Report, Oct. 1981.

30. Horowitz, I. M., and Y. K. Liao, "Limitations of Nonminimum Phase Feedback Systems," Int. J. Control, Vol. 40, pp 1003-1013, 1984.
31. *ibid*, "Quantitative Feedback Design for Sampled-Data System," Int. J. Control, Vol. 44, pp 65-675, 1986.
32. Horowitz, I. M. and C. Loecher, "Design of a 3x3 Multivariable Feedback System with Large Plant Uncertainty," Int. J. Control, Vol. 33, pp 677-699, 1981.
33. Horowitz, I. M., and P. Rosenbaum, "Nonlinear Design for Cost of Feedback Reduction in Systems with Large Plant Uncertainty," Int. J. Control, Vol 21, pp 977-1001, 1975.
34. Horowitz, I. M. and U. Shaked, "Superiority of Transfer Function Over State-Variable Methods in Linear, Time Invariant Feedback System Design," IEEE Trans., AC-20, pp 84-97, 1975.
35. Horowitz, I. M. and D. Shur, "Control of a Highly Uncertain Van der Pol Plant," Int. J. Control, Vol 32, pp 199-219, 1980.
36. Horowitz, I.M., and M. Sidi, "Synthesis of Feedback Systems with Large Plant Ignorance for Prescribed Time Domain Tolerance," Int. J. Control, Vol. 16, pp 287-309, 1972.
37. *ibid*, "Optimum Synthesis of Nonminimum-Phase Feedback Systems with Parameter Uncertainty," Int. J. Control, Vol. 27, pp 361-386, 1978.
38. *ibid*, "Synthesis of Cascaded Multiple-Loop Feedback Systems with Large Plant Parameter Ignorance," Automatica, Vol 9, pp 589-600, 1973.
39. Horowitz, I. M. and T. S. Wang, "Quantitative Synthesis of Multiple-Loop Feedback Systems with Large Uncertainty," Int. J. Sys. Science, Vol 10, pp 1235-1268, 1979.
40. *ibid*, "Quantitative Synthesis of Uncertain Cascade Feedback System with Plant Modification," Int. J. Control, Vol 30, pp 837-862, 1979.
41. Horowitz, I. M., B. Golubev, and T. Kopelman, "Flight Control Design Based on Nonlinear Model with Uncertain Parameters," AIAA J. Guidance and Control, 3, No. 2, pp 113-118, March-April, 1980.
42. Horowitz, I. M., S. Oldak, and O. Yaniv, "Important Property of Nonminimum Phase MIMO Feedback Systems," Int. J. Control, Vol. 44, pp 677-688, 1986.
43. Horowitz, I. M., et al., "Research in Advanced Flight Control Design," AFFDL-TR-79-3120, Air Force Wright Aeronautical Laboratories, Wright-Patterson Air Force Base, OH., 1979.

44. Horowitz, I. M., et al, "Multivariable Flight Control Design with Uncertain Parameters (YF16CCV)," AFWAL-TR-83-3036, Air Force Wright Aeronautical Laboratories, Wright-Patterson Air Force Base, OH, 1982.
45. Horowitz, I. M., et al, "A Synthesis Technique for Highly Uncertain and Interacting Multivariable Flight Control Systems," Proceeding of NAECON Conference, pp 1276-1283, 1981.
46. Houppis, C. H. and P. R. Chandler, "Quantitative Feedback Theory Symposium Proceedings," WL-TR-92-3063, Wright Laboratories, Wright-Patterson AFB OH, 1992.
47. Houppis, C. H., and G. Lamont, Digital Control Systems: Theory, Hardware, Software, 2nd Edition, 1992
48. Houppis, C. H., R. R. Sating, S. Rasmussen, and S. Sheldon, "Quantitative Feedback Theory Technique and Applications," Int. J. of Control, 59, pp 39-70, 1994.
49. ibid, "Design of Feedback Systems with Nonminimum-Phase Unstable Plants," Int. J. Sys. Science, Vol 10, pp 1025-1040, 1979.
50. ibid, "Nonlinear Uncertain Feedback Systems with Initial State Values," Int. J. Control, Vol 34, pp 749-764, 1981.
51. ibid, "Quantitative Synthesis of Uncertain Nonlinear Feedback Systems with Nonminimum-Phase Inputs," Int. J. Sys. Sci., Vol 12, pp 55-76, 1981.
52. ibid, "Synthesis of a Class of Uncertain Multiple-Loop Feedback Systems," Int. J. Control, Vol 29, pp 645-668, 1979.
53. Kochenburger, R. J., "Limiting in Feedback Central Systems," Trans. AIEE, pt II. Appl. Ind., p 180, 1972.
54. Krishnan, K. and A. Cruickshanks, "Frequency Domain Design Feedback Systems for Specified Insensitivity of Time-Domain Response to Parameter Variation," Int. J. Control, Vol 25, pp 609-620, 1977.
55. Laban, M., "Feedback System with Uncertain Nonlinear Plant," M.Sc. Thesis, The Weizmann Institute of Science, Rehovot, Israel, 1981.
56. Lacey, D. J. Jr., "A Robust Digital Flight Control System for an Unmanned Research Vehicle Using Discrete Quantitative Feedback Theory," MS Thesis, AFIT/GE/ENG/91D, Graduate School of Engineering, Air Force Institute of Technology, Wright-Patterson AFB, OH, Dec. 1991.
57. Lancaster, P., Theory of Matrices, Academic Press, 1969.

58. Lapins, M., et al, "Control Definition Study for Advanced Vehicles," NASA Contractor Report 3738, Nov. 1983.
59. Migyanko, B. S., "Design of Integrated Flight/Propulsion Control Laws of a STOL Aircraft During Approach and Landing Using Quantitative Feedback Theory," M.S. Thesis, AFIT/GE/ENG/86D-33, Graduate School of Engineering, Air Force Institute of Technology, 1986.
60. Military Specification-Flying Qualities of Piloted Airplanes. MIL-F-8785C.
61. Pachter, M., and P. R. Chandler, "Universal Linearization Concept for Extended Kalman Filters," IEEE Trans. On Aerospace and Electronic Systems, Vol. 29, pp 946-961, July 1993.
62. Pachter, M., P. R. Chandler, and M. J. Mears, "On Line Optimizing Networks for Reconfigurable Control," Proceedings of the American Control Conference, San Francisco, CA, pp 3141-3144, June 1993.
63. *ibid*, "Constrained Linear Regression for Flight Control System Failure Identification," Proceedings of the American Control Conference, San Francisco, CA, pp 3141-3144, June 1993.
64. *ibid*, "A Hopfield Neural Network for Adaptive Control," Proceedings of the 1993 AIAA Conference on Guidance, Navigation and Control, Monterey, CA, pp 276-284, Aug. 1993.
65. Ramage, J. K., C. R. Abrams, and J. H. Watson, "AFTI/F-16 Digital Flight Control Systems Development Status," presented at 4th AIAA/IEEE Digital Avionics Systems Conf., St. Louis, MO., Nov. 17-19, 1981.
66. Robertson, S. D., "A Real-Time Hardware-in-the-Loop Simulation of an Unmanned Aerial Research Vehicle," Technical Report WL-TR-93-9005, Wright Laboratory, Wright-Patterson AFB, OH, Aug. 1992.
67. Rosenbaum, P., "Reduction in the Cost of Feedback in Systems with Large Parameter Uncertainties," D. E. E. Thesis, The Weizmann Institute of Science, Rehovot, Israel, 1977.
68. Rosenbrock, H. H., Computer-Aided Control System Design, Academic Press, 1974.
69. Sating, R. R., "Development of an Analog MIMO Quantitative Feedback Theory (QFT) CAD Package," MS Thesis, AFIT/GE/ENG/92J-04, Graduate School of Engineering, Air Force Institute of Technology, Wright-Patterson AFB OH, June, 1992.
70. *ibid*, "Development of an Analog MIMO QFT CAD Package," Quantitative Feedback Theory Symposium Proceedings, WL-TR-92-3063, Dayton, OH, WL/FIGS, Aug. 1992.

71. Sating, R. R., I. M. Horowitz, and C. H. Houppis, "Development of a MIMO QFT CAD package (Version 2)," Air Force Institute of Technology (AU), Wright-Patterson AFB OH, USA, Proceedings of the American Control Conference, Vol. 3, pp 3081-3084, San Francisco CA, June, 1993.
72. Schneider, D. L., QFT Digital Flight Control Design as Applied to the AFTI/F-16, M.S. Thesis, AFIT/GE/ENG(86D-4), Graduate School of Engineering, Air Force Institute of Technology, Wright-Patterson Air Force Base, OH, Dec. 1986.
73. Sidi, M., "Synthesis of Feedback Systems with Large Plant Uncertainty," Ph.D. Thesis, The Weizmann Institute of Science, Rehovot, Israel 1972.
74. Swift, G. A., "Model Identification and Control System Design for the Lambda Unmanned Research Vehicle," MS Thesis, AFIT/GAE/ENG/91S, Graduate School of Engineering, Air Force Institute of Technology, Wright-Patterson AFB, OH, Sept. 1991.
75. The Boeing Company, "Summary of the Stability, Control and Flying Qualities Information for All the -135 Series Airplanes," Technical Report D3-9090 REV LTR A, Wichita KS, Oct. 1973.
76. Thompson, D. F. and O. D. I. Nwokah, "Optimal Loop Synthesis in Quantitative Feedback Theory," Proceed. of the American Control Conference, San Diego, CA, pp 626-631, 1990.
77. Trosen, D. W., "Development of an Prototype Refueling Automatic Flight Control System Using Quantitative Feedback Theory," MS Thesis, AFIT/GE/ENG/93-J-03, Graduate School of Engineering, Air Force Institute of Technology, Wright-Patterson AFB OH, Jan. 1993.
78. Wheaton, D. G., "Automatic Flight Control System for an Unmanned Research Vechicle Using Discrete Quantitative Feedback Theory," MS Thesis, AFIT/GE/ENG/90D, Graduate School of Engineering, Air Force Institute of Technology, Wright-Patterson AFB, OH, Dec. 1990.
79. Yaniv, O. and I. M. Horowitz, "A Quantitative Design Method for MIMO Linear Feedback Systems Having Uncertain Plants," Int. J. Control, Vol 43, pp 401-421, 1986.
80. Zames, G. and D. Bensoussan, "Multivariable Feedback Sensitivity and Optimal Robustness," IEEE Trans, AC-28, pp 1030-1035, 1983.
81. Zeevi, G., "Design and Simulation of a Nonlinear Feedback System," M. Sc. Thesis, The Weizmann Institute of Science, Rehovot, Israel, 1981.



## **R.2 References for Other Pertinent Articles**

82. Bailey, F. N., J. W. Helton and O. Merino, "Alternative Approaches in Frequency Domain Design of Single Loop Feedback Systems with Plant Uncertainty," Proceedings of the American Control Conference, Baltimore, MD, June 1994.
83. Bailey, F. N., D. Panzer and G. Gu, "Two Algorithms for Frequency Domain Design of Robust Control Systems," Int. J. of Control, Vol. 48, No. 5, pp 1787-1806, 1988.
84. Bailey, F.N. and C. H. Hui, "A Fast Algorithm for Computing Parametric Rational Functions," IEEE Transactions on Automatic Control, Vol. 34, No. 11, pp 1209-1212, 1989.
85. Freudenburg, J. S. and D. P. Looze, "Frequency Domain Properties of Scalar and Multivariable Feedback Systems," Springer Verlag, NY, 1987.
86. Gallagher, J. E., "Quantitative Feedback Design of a Robust Control System for an Aircraft Engine," MS Thesis, Purdue University, West Lafayette, IN, May 1992.
87. Gera, A. and I. Horowitz, "Optimization of the Loop Transfer Function," Int. J. of Control, 31(2):389-398, 1980.
88. Horowitz, I. M., "Survey of Quantitative Feedback Theory," Int. J. of Control, 53:255-291, 1991.
89. Jayasuriya S. and Y. Zhao, "Stability of Quantitative Feedback Designs and the Existence of Robust QFT Controllers," In C. H. Houpis and P. R. Chandler, editors, Quantitative Feedback Theory Symposium, pp 503-541, Wright-Patterson AFB, OH, Aug. 1992. USAF.
90. *ibid*, "Stability of Quantitative Feedback Designs and the Existence of Robust QFT Controllers," Int. J. of Robust and Nonlinear Control, 1993.
91. Kharitonov, V. L., "Asymptotic Stability of Equilibrium Position of a Family of Linear Differential Equations," Differential Equations, 14:1483-1485, 1979.
92. Kidd, P. T., "Design of a Controller for a Multivariable System with Varying Parameters Using the Extended Direct Nyquist Array," Int. J. of Control, 43(3):901-920, 1986.
93. Kouvaritakis B. and J. M. Edmunds, "The Characteristic Frequency and Characteristic Gain Design Method for Multivariable Feedback systems," In M. K. Sain, J. L. Peczkowski and J. L. Melsa, editors, Alternatives for Linear Multivariable Control, pp 229-246, National Engineering Consortium, Chicago, 1978.

94. MacFarlane A. G. J. and J. J. Belletrutti, "The Characteristic Locus Design Method," *Automatica*, 9:575-588, 1973.
95. Nordgren, R. E., O. D. I. Nwokah and M. A. Franchek, "New Formulations for Quantitative Feedback Theory," *Int. J. of Robust and Nonlinear Control*, 4:47-64, 1994. Also in *Proceedings of the American Control Conference*, San Francisco, CA, pp 1716-1720, 1993.
96. Nwokah, O. D. I., "Synthesis of Controllers for Uncertain Multivariable Plants for Described Time Domain Tolerances," *Int. J. of Control*, 40:1189-1206, 1984.
97. *ibid*, "Strong Robustness in Uncertain Multivariable Systems," *IEEE Conference on Decision and Control*, Austin, TX, Dec. 1988.
98. Nwokah, O. D. I., S. Jayasuriya and Y. Chait, "Parametric Robust Control by Quantitative Feedback Theory," *AIAA J. of Guidance, Control and Dynamics*, 15(1):207-214, 1992.
99. Nwokah, O. D. I., R. E. Nordgren and G. S. Grewal, "Optimal Loop Transmission Functions in SISO Quantitative Feedback Theory," *Proceedings of the American Control Conference*, Baltimore, MD, June 1994.
100. Nwokah O. D. I and D. F. Thompson, "Algebraic and Topological Aspects of Quantitative Feedback Theory," *Int. J. of Control*, 50:1057-1069, 1989.
101. Nyquist, H., "Regeneration Theory," *Bell Systems Technical Journal*, 11:126-147, 1932.
102. Ostrowski, A., "Uber Die Determinanten Uberwiegender Hauptdiagonale," *Comment. Math. Helv.*, 10:69-96, 1937.
103. Perez, R. A., and O. D. I. Nwokah, "Full Envelope Multivariable Control of a Gas Turbine Engine," *Proceedings of the American Control Conference*, pp 735-740, Boston, MA, June 1991.
104. Punyko, A. J. and F. N. Bailey, "A Delta Transform Approach to Loop Gain-Phase Shaping Design of Robust Digital Control Systems," In C. H. Houpsis and P. R. Chandler, editors. *Quantitative Feedback Theory Symposium*, pp 49-73, Wright-Patterson AFB, OH, Aug. 1992. USAF.
105. Rosenbrock, H. H., State-Space and Multivariable Theory, Wiley, New York, 1970.
106. Skelton, R. E., Dynamic Systems Analysis, Academic Press, New York, 1979.
107. Skira, C. A. and M. Agnello, "Control Systems for the Next Century's Fighter Engines," *ASME J. of Engineering for Gas Turbines and Power*, 114:749-754, 1992.

108. Skira, C. A. and R. L. DeHoff, "A Practical Approach to Linear Model Analysis for Multivariable Turbine Engine Control Design," International Forum on Alternatives for Multivariable Control, pp 29-44, National Engineering Consortium, 1977.
109. Stevens, A. L. and J. N. Ridley, "An Efficient Method for Calculating Plant Uncertainty Templates in QFT," Int. J. of Control (under review), 1995.
110. Thompson, D. F., "Optimal and Sub-Optimal Loop Shaping in Quantitative Feedback Theory," PhD Thesis, Purdue University, West Lafayette, IN, Aug. 1990.
111. Yau, C. H. and O. D. I. Nwokah, "Almost Decoupling of Uncertain Multivariable Systems," Int. J. of Control, 58(6):1385-1408, 1994.
112. Yau, C. H., J. E. Gallagher and O. D. I. Nwokah, "A Model Reference Quantitative Feedback Design Theory with Application to Turbomachinery," Int. J. of Robust and Nonlinear Control, 4:181-210, 1994.

### **R.3 Additional References**

113. Bossert, D. E., "Design of Pseudo-Continuous-Time Quantitative Feedback Theory Robot Controllers," MS Thesis, AFIT/GE/ENG/89D-2, Graduate School of Engineering, Air Force Institute of Technology, Wright-Patterson AFB, OH, Dec. 1989.
114. Boyum, K. E., M. Pachter, and C. H. Houppis, "Evaluation of Moderate Angle of Attack Roll of a Dual Engine Thrust Vectoring Aircraft Using Quantitative Feedback Theory," 13th IFAC Symposium Automatic Control in Aerospace-Aerospace Control 1994, Palo Alto, CA, Sept. 1994.
115. Clough, B. T., "Reconfigurable Flight Control System for a STOL Aircraft Using Quantitative Feedback Theory," MS Thesis, AFIT/GE/ENG/85D-8, Graduate School of Engineering, Air Force Institute of Technology, Wright-Patterson AFB, OH, Dec. 1985.
116. Horowitz, I. M., "Quantitative Feedback Theory," Proceedings of the IEEE, Vol. 129D, No. 6, Nov. 1982.
117. *ibid*, "Design of Feedback Systems With Nonminimum-Phase Unstable Plants," Int. J. Sys. Sciences, Vol. 10, pp 1025-1040, 1979.
118. Kang, F. H., "Electro-Hydrostatic Actuator Controller Design Using Quantitative Feedback Theory," MS Thesis, AFIT/GE/ENG/94D-18, Graduate School of Engineering, Air Force Institute of Technology, Wright-Patterson AFB, OH, Dec. 1994.
119. Keating, M. S., "Design of a Flight Controller for an Unmanned Research Vehicle Using Quantitative Feedback Theory," MS Thesis,

AFIT/GE/ENG/93D-18, Graduate School of Engineering, Air Force Institute of Technology, Wright-Patterson AFB, OH, Dec. 1993.

120. Rasmussen, S. J. and C. H. Houppis, "Development, Implementation & Flight Test of a MIMO Digital Flight Control System for an Unmanned Research Vehicle Using Quantitative Feedback Theory," Proceedings of the ASME Dynamic Systems & Control, Winter Annual Meeting of ASME, Chicago, IL., Nov. 1994.
121. Reynolds, O. R., M. Pachter, and C. H. Houppis, "Full Envelope Flight Control System Design Using QFT," Proceedings of the American Control Conference, Baltimore, MD, pp 350-354, June 1994.
121. Robertson, S. D., "A Real-Time Hardware-in-the-Loop Simulation of an Unmanned Aerial Research Vehicle," Technical Report WL-TR-93-9005, Wright Laboratory, Aug. 1992.